# INFORMATION TO USERS

This manuscript has been reproduced from the microfilm master. UMI films the text directly from the original or copy submitted. Thus, some thesis and dissertation copies are in typewriter face, while others may be from any type of computer printer.

**The quality of this reproduction is dependent upon the quality of the copy submitted.** Broken or indistinct print, colored or poor quality illustrations and photographs, print bleedthrough, substandard margins, and improper alignment can adversely affect reproduction.

In the unlikely event that the author did not send UMI a complete manuscript and there are missing pages, these will be noted. Also, if unauthorized copyright material had to be removed, a note will indicate the deletion.

Oversize materials (e.g., maps, drawings, charts) are reproduced by sectioning the original, beginning at the upper left-hand corner and continuing from left to right in equal sections with small overlaps.

ProQuest Information and Learning
300 North Zeeb Road, Ann Arbor, MI 48106-1346 USA
800-521-0600

# THERMAL ERROR MODELLING AND COMPENSATION FOR A COORDINATE MEASURING MACHINE

by

Nael Barakat, B.Eng., M.A.Sc., P. Eng.

A Thesis submitted to the School of Graduate Studies

in partial fulfilment of the requirements for the degree of

Doctorate of Philosophy

McMaster University

DOCTORATE OF PHILOSOPHY (2000) McMaster University

(Mechanical Engineering) Hamilton, Ontario, Canada

Title: Thermal error Modelling and compensation for a Coordinate Measuring Machine

Author: Nael Barakat, P. Eng., B.Eng.(Kuwait University, 1989), M.A.Sc. (Concordia University, 1996).

Supervisor: Dr. M. A. Elbestawi

Dr. A. D. Spence

Number of pages: xx, 229

## Abstract

Thermal Error Modelling and Compensation

for a Coordinate Measuring Machine

by: Nael Barakat

A methodology for quasi-static error correction by compensation for an intrinsic Coordinate Measuring Machine (CMM) is proposed and tested in this thesis. It consists of three major parts.

The first part includes a systematic approach to machine kinematic modelling. Using this approach results in an analytically based, forward kinematics model of the machine including its errors.

In the second part, the model error functions are identified, at the constant thermal state. At a later stage of the research, error functions identification at varying thermal states is carried out.

The third part of the proposed methodology includes the actual utilization of the model in a compensation strategy to correct for the machine errors.

To visualize the effect of the proposed methodology, the performance of the CMM is evaluated using the standard ASME B.89 test before and after compensation for its errors in the constant thermal state. Dramatic improvements are obtained reducing the machine error in measurement by 93%.

A modified version of the B.89 standard incorporating the thermal state of the machine is used to test the machine performance at varying thermal states. Improvement of

the CMM performance by reducing the volumetric error by 97% is obtained.

The research was expanded by applying the proposed methodology to CMM contouring. Regression analysis was proposed for the models. Thermal sensors were used to provide information to update the models. The CMM behavior was tested through simulation in tracking the diagonals of its work volume. Remarkable improvement in the tracking errors reduction is observed. Results obtained show an improvement in the CMM performance to a level close to machine resolution.

## Dedication

The very first verses that were revealed from Allah (SWT) "God" to the prophet Mohammed (PBUH) were:

*In the name of Allah, Most Gracious, Most Merciful.*

*Proclaim (Read), In the name of thy Lord and cherisher who created.*

*Created man, out of a leech-like clot.*

*Proclaim, and thy Lord is the most bountiful.*

*He who taught (the use of) the pen.*

***Taught man that which he know not.***

The Holy Quran.

To My Parents, who were the first to teach me these verses.

## Acknowledgement

Before all, Praise and gratitude be to Allah (God) the cherisher and sustainer of the world, the bountiful Lord of all, by the grace of whom, this work was completed.

I would like to extend my sincere thanks and appreciation to my research supervisor, Dr. M. A. Elbestawi, for his guidance, continuous encouragement, and moral and financial support throughout the course of this work. Thanks are also due to Dr. A. D. Spence, my co-supervisor, for his help and encouragement. I would like to also acknowledge the rest of my supervisory committee, Dr. Sklad and Dr. Capson for their time and help in this work.

I wish to thank the staff and colleagues in the Department of Mechanical Engineering, and the Intelligent Machines and Manufacturing Research Center (IMMRC), for their assistance in all forms, D. Schick, R. Lodewyks, J. Varhaeghe, and J. McLaren, as well as the secretarial staff. Working with these teams made my stay at McMaster University pleasant and fruitful, particularly: Dr. R. Teltz, Dr. M. Hassan, Dr. H. Kishawy, and Dr. R. Fleisig, and many others that I did not have enough space to mention in this limited page.

The author would like to thank OMNI-TECH CMM Services Inc. (Canada), for their assistance in providing measurement equipment necessary to carry out this work. This work was made possible by financial assistance of "Fonds Pour la Formation de Chercheurs et l'Aide a la Recherche" (FCAR), Quebec, Canada in the form of a Ph.D. Scholarship granted to the author during two thirds of the period of this work.

A word of appreciation and gratitude goes to Tom Charlton Jr., Director of Research and Development at Brown and Sharpe Manufacturing company. Tom's technical and moral help, encouragement and mostly tolerance to finish this work at the last stage, was vitally

important and effective.

Finally, I would like to thank my parents and family members, who sowed in me the first and early seeds of respect and eagerness to knowledge, and kept me focussed all the way.

Table of Contents

## List of Figures

## List of Tables

Chapter One

# Introduction

Global advancement in manufacturing technology coupled with the severe competition towards cost reduction of a superior product, have focussed attention on precision engineering as a key factor for surviving this competition. Precision engineering now is indispensable for the automated manufacturing processes of many technologically advanced and highly precise strategic products. Molds, dies, aircraft propellers, and jet engines components are examples of the overwhelmingly expensive and extremely accurate components handled by industry. As modern industry moves towards more strict and unified standards, while trying to reduce production costs, precision engineering climbs rapidly to the top of the priority list in research and development.

Precision engineering is defined by McKeown (1987) as manufacturing to tolerances smaller than 1 part in 10000 or perhaps $10^5$. Higher precision manufacturing is known as micro-engineering and following would be nano-technology, which is working with 'atomic

bit' engineering. Precision engineering promotes more strict limitations in quality control and metrology standards, which consequently redefines production accuracy and conformance to specifications.

## 1.1 Motivation

This research is motivated by the high accuracy needs expressed among contemporary industries. For many years, the research community has concentrated on improving aspects of accuracy in manufacturing. Higher accuracy in manufacturing results in the following:

a. Quality control improvement to reduce rework and rejection rate of produced parts.

b. More automatic assembly as opposed to fitting.

c. Improvement of components life against wear and fatigue.

d. Increase of interchangeability of components.

Accuracy is pertinent, in particular, to both the machining and inspection stages. To achieve better accuracy at the machining stage, improved design concepts and working conditions have been studied and introduced to the machining process (Veldhuis, 1998). At the inspection stage, quality inspection and assessment are usually carried out using the most accurate instruments available, which are Coordinate Measuring Machines (CMM's). CMMs are usually utilized for inspecting dimensions and forms of products to be compared to the design specifications, and help carry out the quality control of the process. CMM's should to be 10 times more accurate than the machine tools in the same production line (Sartory, 1995). Therefore, detailed knowledge and correction of errors occurring in their

results is imperative to the level of accuracy of the entire manufacturing system. The factors affecting the accuracy of both machine tools and CMMs are similar in principle. The difference between them is dependent on the functionality and particulars of each machine. CMMs find applications in different industries from tiny parts to complete vehicles (Danzer and Kunzmann, 1987). Figure 1 represents a schematic of the CMM under investigation.

## 1.2 Problem definition and description

Errors affecting a multi-axis machine are defined as the difference between the real and measured position of the end effector. These errors cause a deterioration of the machine performance, which in turn directly influences both the process output and the final product specifications. To maintain high quality performance for a CMM, these errors have to be detected and eliminated. The effect of these errors on the machine performance can be considered as twofold; Contouring inaccuracy of a machine affects the dimensional tolerances of the final product, particularly in machine tool cutting or in CMM scanning processes, while the measurement and probing inaccuracy affects the product quality verification, and accordingly, the process rate of material rejection. A CMM can perform both measuring and contouring and therefore, makes an ideal experimental test bed for the purpose of this thesis. For this work, a DEA-IOTA 1102 CMM, with a retrofitted computer based motion controller, was used to study both measuring and contouring performance. Figure 2 shows a picture of the CMM under investigation. This CMM represents an intrinsic machine which is a kinematic sequence, by convention, where body one supports the

workpiece and X is the direction of the guide connecting it to the adjacent body; Z is the direction of the guide connecting the body supporting the end effector to its neighbour. CMMs are the instruments that define the final product accuracy. In spite of the care taken in manufacturing these instruments, errors still occur in their measurements and cause their performance to deteriorate. Errors in a CMM reading can originate from different sources. They can be quasi-static like the thermal error, dynamic like the controller errors, or from other sources such as software induced errors. Some of these errors are indirectly sensed and

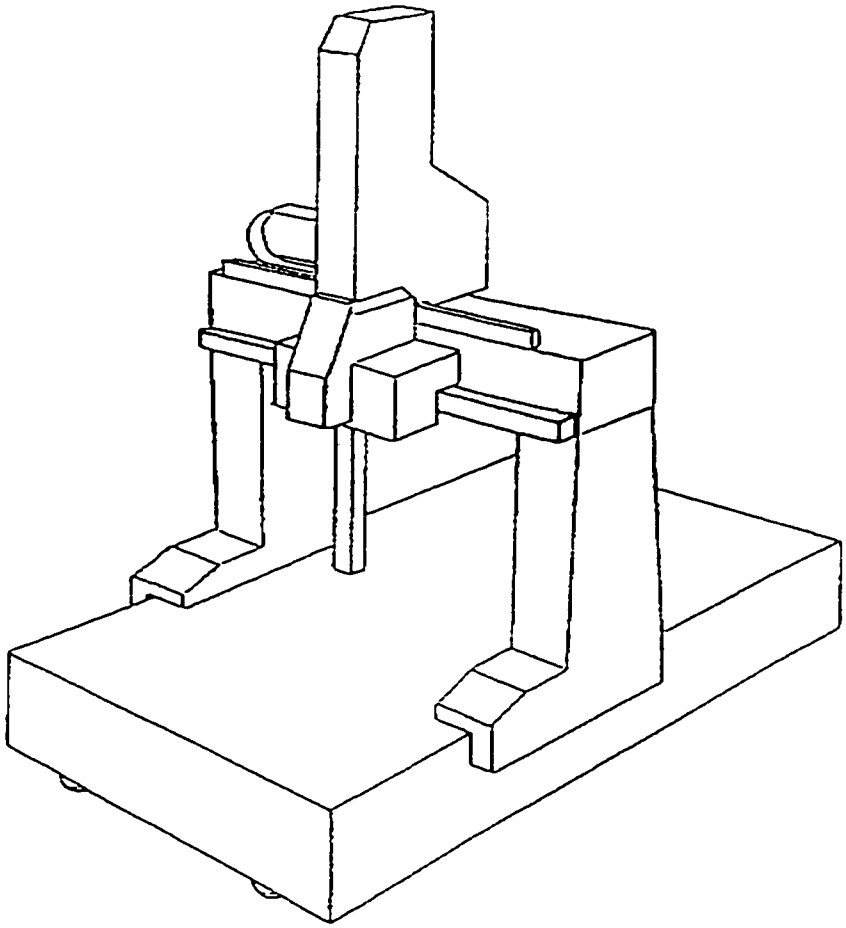

**Figure 1** Schematics of the CMM under investigation.

have effects and traces that show as quasi-static errors. Quasi-static errors contribute by more than 70 % to the total CMM measurement error (Sartori, 1995; Eman et al., 1987). These are errors in the relative position of the end effector which are slowly varying with time. They are related to the structure of the machine. Figure 3 represents an exaggerated picture of the final deteriorated shape of the CMM under the influence of the above mentioned errors (Bosch 1995). Some of these errors can be avoided and corrected at the design and manufacturing stages of the CMM. Others can be reduced by choosing a more restricted environment. On the other hand, the effect of wear and tear, environmental changes, and errors left after proper design and manufacturing procedures have been followed, will eminently affect the machine performance. One way that is currently followed to reduce the effects of environmental changes is to preserve the CMM in a thermally controlled room. However, this introduces a barrier between the CMM and the production line resulting in production inefficiency caused by measures like time delay, especially while waiting for products to soak out in the CMM environment, and general increase of production costs.

## 1.3 Solution Criteria

In a survey conducted by Brown and Sharpe, which is a major manufacturer of CMM's, requesting customers opinions and initiatives in regards to CMMs improvement, metrology, and quality issues (Garcia, 1999), the customers had a lot to suggest. Among the top ten customer initiatives were the following:

a. To move metrology closer to shop floor production.

b. To re-use the capital equipment.

c. To continually improve key quality characteristics.

Based on these premises, including the problem description mentioned above, correction of errors occurring in a CMM becomes of vital importance. This correction should be cost effective and make use of the available resources while improving the CMM performance.

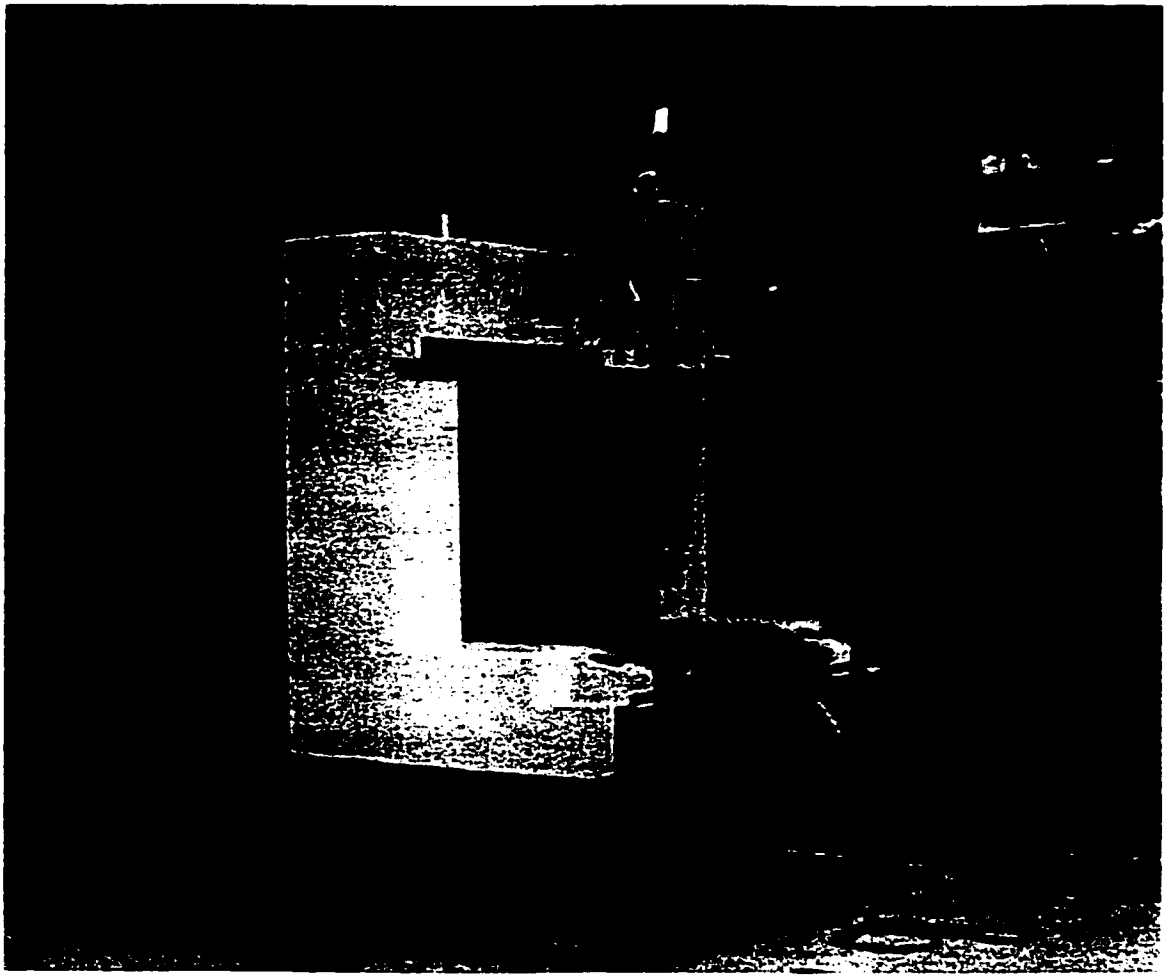

**Figure 2** The DEA-IOTA 1102 CMM under investigation.

As was mentioned above, the major error causing the CMM performance deterioration is the quasi-static error. In particular, thermally induced errors are still the focus of research because of their complex nature and remarkable contribution to CMM performance degradation. Therefore, major CMM performance enhancement can be achieved by reducing this source of error.

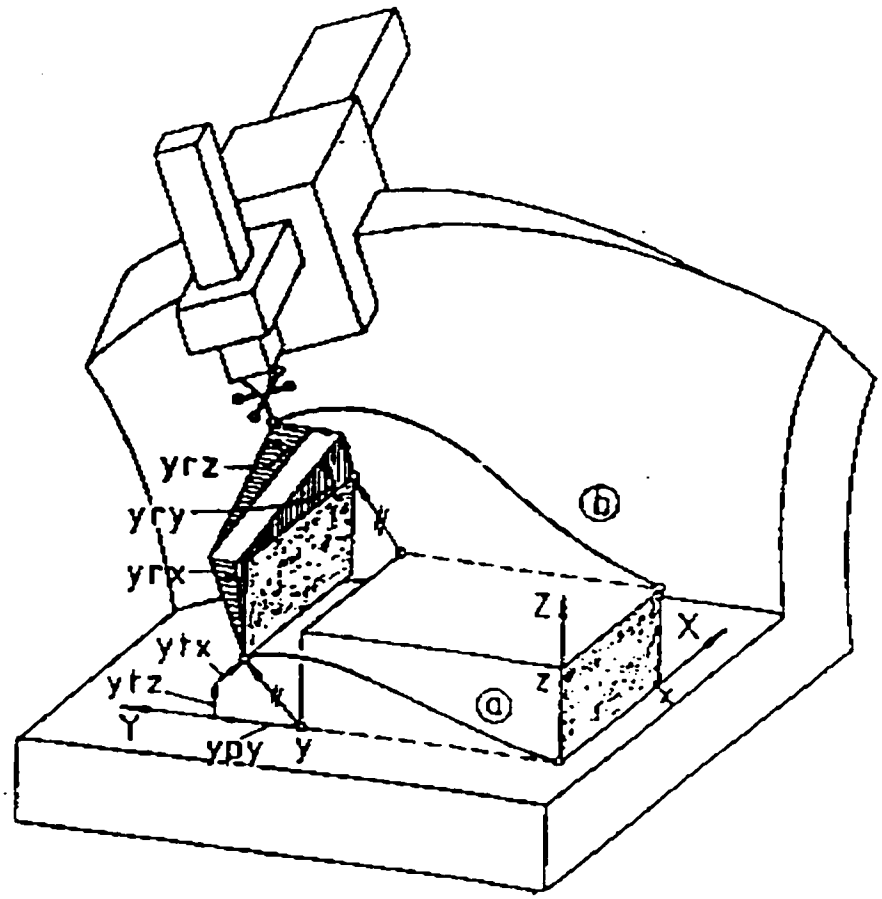


**Figure 3** Exaggerated picture of the different errors influence on the CMM.

## 1.4 Scope of thesis

The objective of this thesis was the development of a cost effective and systematic method for CMM quasi-static error identification and compensation. The focus was on quasi-static errors because of their major accountability to CMM performance degradation. Thermal error component is the first major error contributor on the list of error characterization and correction. Knowing that the traces of the thermal effect show as other quasi-static errors, specifically geometric, makes the geometric, kinematic, and thermal errors, collectively, the target of this study. There are other types of errors that also contribute to the CMM inaccuracy, but have a minor role, such as the stiffness error (Weekers and Shellekens, 1995) or have a high frequency response, like the dynamics and drive controller errors. These errors are outside the scope of this thesis.

Compensation for the CMM errors was the candidate solution that satisfied the required criteria. Although compensation for the CMM errors is a reasonable and cost effective solution, it only works for a small error range. This is because it is based on a model, which is not completely perfect, and it is not a replacement for design major considerations (Veldhuis and Elbestawi, 1995, Barakat et al., 1999). However, compensation is considered an effective solution to the machine gradual performance deterioration by time and use, as well as the smaller errors left after proper design and manufacturing procedures have been followed. It also can be customized for usage with old machines and to incorporate the changing environmental conditions. The scope of this thesis includes the detection of major CMM errors using a practical and cost effective methods. It also includes

the characterization and correction of the CMM quasi-static errors in both measurement and contouring operations. This is carried out systematically through modelling, model error functions identification, and compensation. Figure 4 represents a flow diagram summarizing the scope of the thesis.

## 1.5 Thesis layout

This thesis is divided into four major parts. The first part contains an introduction, a general background, a definition of the problem and objective, a criteria for the solution sought, and the scope of thesis. This is included in chapter one. In this same part, chapter

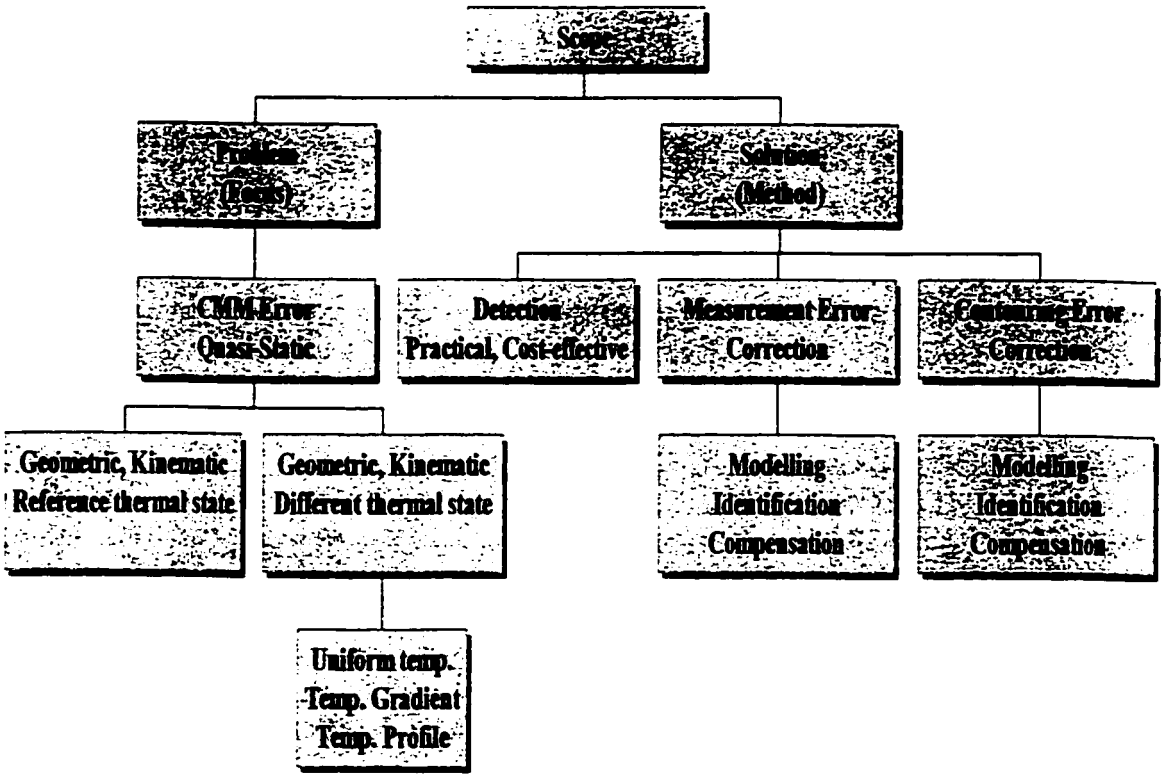


**Figure 4** Flow diagram detailing the scope of thesis.

2 includes a recent literature survey with more insight into the relevant issues to the defined problem and the suggested solutions from the literature. It also touches upon relevant topics to bring the current work in context with the global efforts to toggle the problem at hand.

In the second part, the CMM is being investigated as an example for an intrinsic, and multi- axis machine. A general and systematic modelling of the CMM quasi-static errors is carried out in two steps. First, the CMM errors are physically modelled at a constant reference thermal state, to arrive at a basic model with acceptable accuracy. The model effectiveness is tested using the standard ASME B.89 test for CMM performance evaluation (Barakat and Elbestawi, 1998). The effect of ambient thermal changes is then incorporated through analytical modelling based on statistical regression. The final form of the models becomes a hybrid of analytical and physical modelling. To quantify and model the environmental changes, thermo-mechanical models of material reaction to thermal changes are used and then the principle of superposition is applied to find the final error at the end effector. In addition, experimental measurements are carried out to obtain the error functions values at different thermal conditions using laser measurements and the Effective Coefficient of Thermal Expansion (ECTE) of the machine material. A compensation and control strategy is proposed to correct for the machine quasi-static errors in contouring, applying feed forward and state observer techniques. To study the effect of the proposed methodology in measurement errors prediction and correction, the compensation strategy is applied to the performance evaluation tests at both stages. To visualize the effect of the proposed methodology in contouring error correction, the CMM contouring performance is tested and

simulated by attempting to track straight diagonal lines in the work volume, for the two previously mentioned modelling stages. A direct method is proposed to obtain the inverse kinematics model of the machine by applying nonlinear regression analysis based on the least squares errors principle. The basic inverse kinematics model of the CMM is obtained from the forward kinematics modelling first stage. Consequently, the dynamic effect of thermal changes is incorporated in the model starting with theoretical separate models for the individual error functions and coefficients. On-line model update of the thermal state is carried out using the state observer technique. The fitted model validity is confirmed using two statistically based tests based on the Analysis of Variance (ANOVA) technique. Finally, the full model is tested for its contouring performance through simulations. A novel performance evaluation using a modified version of the standard ASME B.89 test is carried out at randomly varying ambient thermal states to demonstrate the machine improvement.

## 1.6 Summary

This chapter described some of the major issues facing industry today. It also provided an idea of how precision engineering has become an important factor in deciding the success of engineering products in a competent atmosphere. Precision engineering influence can be seen in tighter limitations on quality control and the advancement of metrology standards.

In brief, the motivation of this thesis lies in the high accuracy needs expressed by industry combined with the fact that CMMs are the focal point of production accuracy. As

a consequence, the knowledge of CMMs errors and their correction is imperative to acquire high standards of accuracy in the production system as a whole.

The problem to be addressed has also been defined in this chapter. Errors occurring in a multi axis machine causes deteriorations in its performance. The major source for these errors is known as the quasi static errors and a big part of it is the thermal error. Thermal errors and accordingly quasi static errors affect both the production and inspection of quality stages. A CMM can perform both measurement and contouring and therefore is chosen as a test bed. The solution criteria proposed is to use compensation based on error modelling to correct for these errors and enhance the CMM performance. However, it is important to know that compensation works only for a small range of errors and that a proper design is vital to the reduction of errors that could result in the machine. The solution concentrates on a systematic and a cost effective compensation methodology.

The thesis in general is composed of parts in accordance with the solution steps. The first part includes the introduction and literature. The second part describes the theory and modelling procedure followed. The third part details the compensation strategy for both the measurement and contouring stages. The final part includes experimental results and real time recorded outcomes of error functions identification and compensation in action for the measurement and contouring stages.

Chapter Two

# Literature Survey

Quality control and high accuracy demands require strict standards of production and inspection. This is where CMM's stand out, as the instruments capable of inspecting dimensions and forms of products to be compared to the design specifications. CMMs are the most accurate instruments used for precession inspection in industry. Although they should be 10 times more accurate than the machine tools, they still encounter errors in their readings for different reasons. Part of these errors can be identified and avoided by calibration of the CMM. Special artifacts like ball bars are made for the purpose of CMM calibration and error inspection. The literature provides various practical methods to carry out CMM calibration. Nevertheless, the error in a CMM reading can originate from different sources. Special attention is paid by the research community to the thermal error. Different solutions have been suggested for the thermal error in particular and for the total CMM error in general. This chapter presents issues relevant to CMMs history, development, role in industry, and error inspection. It also

deals with the sources and types of errors occurring in a CMM, with a concentration on the quasi-static errors. Efforts to monitor, model, and statistically obtain the errors in CMMs as found in the literature are also summarized in this chapter. Literature suggestions and methodologies to correct the errors, with a concentration on compensation for CMMs, as well as other related research issues are also presented.

## 2.1 CMM history

Measurement standardization is directly related to the progress of mankind. To build a pyramid in ancient Egypt or south America, a wall in China, or measure land in Mesopotamia, means for measurement were needed and therefore, invented. Throughout the history of humanity, these measurement systems and relevant tools kept on developing and improving. The first measuring machine that can be considered as a CMM by present common knowledge, was introduced in 1956 by Ferranti, Ltd. of Dalkeith, Scotland (Bosch, 1995). This was a two dimensional machine of a classical kinematic design as opposed to a conventional machine tool design. The introduction of CMMs was a response to the automation and extreme reduction in production time at the machine tool compared to the hours consumed at the inspection stage. CMMs were introduced, coupled with the modern CNC machine tools, to perform a comparable task of inspection, in terms of speed and accuracy, and to ameliorate the production task in general. In the following years more industries introduced CMMs including Digital Electronic Automation (DEA) of Italy, which was the first company formed to produce CMMs. In 1985 Carl Zeiss of Germany and

Sheffield of the UK became the first to introduce a CMM with software error correction. Although each company introduced their product separately, together they brought a revolutionary idea to CMM performance enhancement.

Before CMMs were incorporated in the production line, parts inspection used to be performed manually and separately. This inspection included measurements for part dimensions, form, surface characteristics and position of geometrical elements. The incorporation of CMMs in the production line allowed for a complete metrological description of the workpiece in a fully coordinated manner. It also accomplished a giant step in bringing up the production line to the automated flexible manufacturing system (FMS) level (Peggs and McKeown, 1989). Kunzmann and Waldele, (1988) described the future factory as including CMMs with automatic feeders. With the incorporation of different robotics, a 24 hour flexible manufacturing system can be built including automatic inspection. An automatic inspection system similar to the one just described has been installed since 1986 for turbine parts inspection. The market growth in CMMs utilization as a part of the FMS is 10 to 15 % per year (Kunzmann and Waldele, 1988). This shows the value of CMMs for industry as the most accurate means for products inspection. Nowadays, CMMs find applications in different industries from tiny parts to complete vehicles (Danzer and Kunzmann, 1987).

## 2.2 CMMs types

There are four types of CMMs if they are to be divided according to their mechanical

systems configuration. Table 1 shows the different types applications and specifications. The selection of the CMM is dependent on the type of product to be handled. In some cases a CMM is complemented by a rotary table or a fourth axis. This increases flexibility of the CMM without losses in accuracy (Kunzmann and Waldele, 1988).

Another division of CMM types based on the sequence order of their base is provided by Balsamo (1995). He reported the existence of an intrinsic axis order in a CMM which is referred to as CMM kinematic sequence. This is based on the fact that each CMM is made up of four rigid bodies, three carriages, and a base. These components are linked together in a sequence from the workpiece to the probe. This concept is used in modelling CMMs.

**Table 1** Types and specifications of CMMs.

| CMM Type | Specifications | Applications |
|---|---|---|
| 1. Column | - High accuracy<br>- Convenient access for the operator. | - Universal applications<br>- Small measuring volume |
| 2. Cantilever | - Lower accuracy compared to type 1.<br>- Has relatively low movable masses.<br>- Very Fast.<br>- Allows excellent access to the measuring area. | - Big measuring ranges.<br>- Called a measuring robot. |
| 3. Bridge | - Mostly used machine.<br>- High accuracy.<br>- Limited access to the measuring volume. This can be solved using an automatic feeder. | - Medium & small size measuring volumes(1 $M^3$ ) |
| 4. Gantry | - Reasonable accuracy. | - Very large parts handling. (Up to 10 M Horizontally) |

of the mechanical system. This is if the calibration is to be effectively employed in machine error correction. This model describes the interaction between the system parts and is the base for error propagation computation and overall accuracy description of the task. Calibration of a CMM with a rotary table has also been reported in the literature (Kunzmann and Waldele, 1988). Zhang et al. (1991) developed a calibration method using a ball bar and employing a laser interferometer. They aimed at a system which can be inexpensive and simple enough to be used in a shop floor. They provided simple formulae for errors calculation. Table 2 summarizes the methods suggested in the literature to obtain the different machine errors components experimentally (Zhang et al., 1991).

**Table 2** Measuring methods for different error components of a CMM (Zhang et al., 1991).

| **Error Component** | **Measuring Method** |
|---|---|
| Rectangularity | Straightness measurement in two rectangular lines, test bodies. |
| Straightness | Reversal method with straight edge. |
| Positioning | Laser interferometer or Capacitive probe. |
| Squareness | Along diagonals displacement errors. |
| Pitch, Yaw | Laser interferometer with angular reflector |
| Roll of X and Y axes | Level |
| Roll of Z - axes | Straightness measurement in two parallel distant lines. |

Ball plates are very popular in CMM calibration as an artifact. The centre lines of the balls are coordinates that have to be measured by the CMM in different orientations. On the other hand, ball plates were reported to suffer instability during transfer from one location to another. To preserve these plates, an added cost has to be considered which is normally

of high value. This adds up to the cost of making them which is considerably high. Gauge blocks and end bars are also used for CMM calibration. Peggs and McKeown, (1989) described different ways of utilizing step gauges in CMM calibration. In addition, they elaborated on the calibration of one, two and three dimensional artifacts and its importance and uses. Kunzmann et al., (1995) presented a comparison of calibration between commercially available CMMs using ball plates. They also discussed a methodology to follow in calibration and error analysis to find the sources.

In a comparison between standard artifacts of calibration, it was found that ball beams proved to be excellent in stability and efficiency compared to gauge blocks and ball plates. They are less possible to have problems of hysteresis and directional error characteristics of the probing process.

A cost effective, multi-purpose, and quick method is required for CMM calibration and machine accuracy inspection. According to literature reports, the ideal method for CMM calibration and inspection should have the following properties :

a. Traceability according to standards for stable reference objects.

b. Accuracy which is similar to CMMs global standards.

c. A uniform approach in concept, allowing the use of the same hardware and software for calibration and inspection.

d. Quality parameters should be the same for all inspection, periodic tests, and calibrations to allow for the deduction of applications measurement uncertainty.

e. Compatibility with existing standards.

f. Affordable by CMM users.

Among the most recent trends in calibration of a CMM employing a laser interferometer, is the straightness measurement suggested by Tani et al., (1995). This measurement was aimed at finding the degree of flatness of the granite base of the CMM. They reported high speed and accuracy achievement using this method.

In general, Calibration methods of CMMs can be gathered in three categories:

a. Methods based on measuring the 21 source errors. These methods require the use of expensive instruments including laser interferometers.

b. Methods based on measuring certain artifacts, which are used as references for calibration. These methods do not give the source errors directly and so can not be used for direct compensation. This is in addition to the cost of building and preserving the accurate artifacts.

c. Methods based on kinematic references (e.g. the magnetic ball bar). These also have the problem of not defining the source errors and therefore can not be very useful in direct compensation.

Choosing any of the methods above would involve a compromise which has to be considered by the user. Moreover, combinations of these methods might be more useful to achieve direct error compensation.

### 2.3.2 Performance evaluation

For some time, the research community have been concentrating on a measuring

standard to evaluate machining and measuring accuracies. This is useful in the precision evaluation of both the machining center and the CMM performing the inspection on the workpiece. CMM error inspection works with methods similar to those used for CMM calibration (Kunzmann et al., 1990). Inspection methods include the use of gauge blocks, ball plates, and ball bars, which are the same standards used for calibration. Moriwaki et al., (1982) listed some of the CMM disadvantages in measuring functional items like cam profiles and waviness. He suggested a modular-type measuring system for the evaluation of the machining accuracy using "the part family" concept to classify the required measurements. The rotary table was a major part in his suggested module. Other investigations on these types of errors have been reported in the literature by Nawara and Kowalski, (1981), and Kunzmann and Waldele (1983). In the eighties, modular type recognition of measured parts was an appealing solution compared to expensive laser instruments and computations equipment. Nowadays, laser based measurements are widely available, easier to perform, and comparatively less time consuming.

It is to be mentioned here that some research has been produced to standardize errors inspection using the Abbe principle which is known as the first principle in metrology (Zhang, 1989). Since CMMs are presently used in contouring mode, where two or more axes move simultaneously, positioning accuracy is not enough as an acceptance test of a CMM (Knapp, 1988). In general, volumetric accuracy is described by systematic deviations in the relative location of the probe for two arbitrary positions of the machines carriages. A considerable amount of geometrical and thermal quantities have to be measured to determine

the volumetric accuracy of a CMM. Teeuwsen et al. (1989) summarized the specifications according to which measurements should be carried out as follows:

a. Spacing between measured positions should be sufficiently small. This is to obtain information about the periodic terms in the measuring system.

b. The measured positions have to be approached from two opposite directions. This is to find backlash effects.

c. Multiple measurements have to be carried out to obtain good estimation of the measurements, especially in the case of random vibrations occurrence.

They also suggested a method to perform automated and fast inspection of a CMM employing laser interferometers.

One main objective of CMM performance evaluation is to quantify the operational status of the CMM and obtain a distinctive quantified definition of each individual CMM. An important remark here is the fact that none of the standards used for performance evaluation uses the word calibration in their title. This is because calibration by definition means that these performance evaluation standards are capable of accurately predicting the CMM measurement uncertainty, which is still a widely open investigation topic.

Another objective of CMM performance evaluation is to avoid confusion in CMMs description and comparison. This also extends to the method of specifying the performance evaluation method test results. In general, any of the performance evaluation methods used would finally produce an estimate of the error that a CMM is likely to produce for an

individual test. If this evaluation indicates that actual results produced are within the manufacturers specifications, then the CMM is fit to be used for the particular production situation. In other words, the performance evaluation results would set the upper limit on any test results performed by the CMM (Bosch, 1995).

At present, there are standard performance evaluation tests set for the industry to provide a practical standard quantification for the CMM performance. The ANSI / ASME B.89 also known as the American National Standard provides a practical method for CMM performance evaluation. The philosophy behind the B.89 test is to quantify different categories of CMM uncertainty sources. It also includes a section discussing the thermal environment and an index to be calculated (Thermal Error Index TEI) for an estimation of the CMM performance degradation accordingly. However, it does not fully account for the degradation in measuring capability due to poor thermal environment. The volumetric performance test described by this standard is the one that was used for performance evaluation throughout this thesis. This test requires the use of a standard ball bar in different locations and orientations in the work volume of the CMM. The number and setup of these locations and orientations differ based on the machine dimensions and are given in details by the standard (ASME / ANSI B.89). For the CMM at hand, the test setup selected and applied is given in Appendix A.

Another known standard is the VDI / VDE 2617 test. This is a standard test that is used to specify performance of most CMMs used and sold in Europe. This is not a national standard but rather a standard of the society of professional engineers. Many similarities

exist between the B.89 and the VDI/VDE although the underlying philosophies are somehow different. Other tests exist like the CMMA and the British Standard BS6808. The main item that all of the available tests miss is a comprehensive and detailed performance evaluation procedure for a CMM in a thermally varying environment.

## 2.4 Probing

The first touch trigger probe was introduced in 1972 in the Rolls-Royce Aero Engine Division, England. Later on, Renishaw followed with a commercial probe in 1973. Since then, touch trigger probing introduced a revolution to CMM performance.

CMMs utilize commercially available touch trigger probes. The use of probes is beneficial in the automation of the measurement process because touch trigger probes are self guiding feedback control sensors for part search and measurement data collection (Jie-Chi et al., 1982). Using a touch trigger probe for measurements and sensing is a standard practice in industry. A touch trigger probe is a digital device that changes a signal state upon physical establishment or loss of contact with another object. It consists of a probe stylus connected to a deflection sensor that switches between the "0" and "1" states. Upon receipt of a change of signal of the probe from "0" to "1" the controller can activate an interrupt routine to read the coordinates of the null origin of the probe. In a CMM, all axes position coordinates are read simultaneously. Figure 5 presents the details of a typical touch trigger probe.

Several probe path generation algorithms can be traced in the literature. It is to be

mentioned here that the probing process contains errors in the order of microns. Nawara and Kowalski, (1984) studied the static and dynamic forces affecting the probe. Moreover, they reported some results regarding the effect of speed of probing and data transfer from the probe on the results collected. The probe was modeled and the deflections were calculated and compensated for in tests conducted. Results reported suggest more deflection to occur than calculated due to dynamic forces. Chan (1997) studied the probe lobing errors as a function of the approach vector and presented a compensation for the error involved.

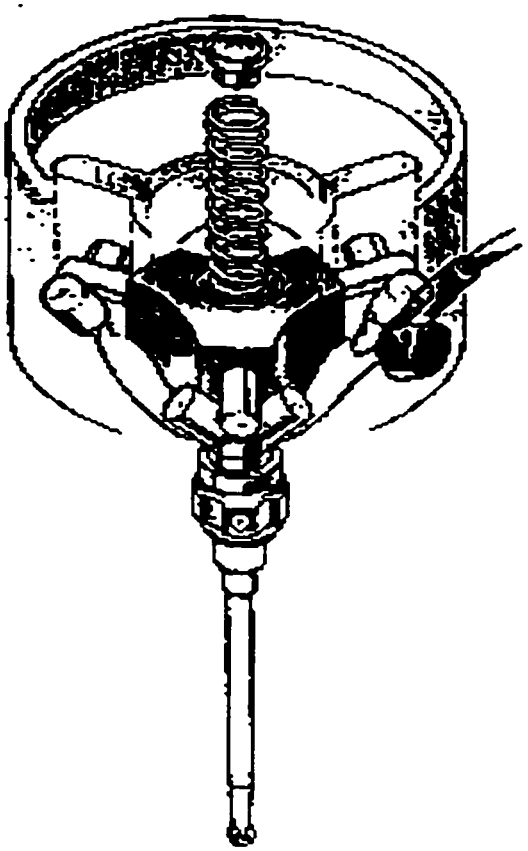

**Figure 5** Details of a typical touch trigger probe.

Nowadays, CMMs are used to perform scan probing which introduces a whole new range of factors that need to be investigated. Scan probing is relatively new and the literature available on it is quite scarce. One remarkable fact about scan probing is the fact that it involves pre-calculated motion guidance and positioning points to be fed to the CMM controller.

## 2.5 CMM errors

Measurement inaccuracy occurs when an error in the relative position between the measured point and the probe exists. In different words, measurement error is the difference between the true value and the observed value of a variable (Eman et al., 1987, Shen and Duffie, 1991).

### 2.5.1 Types and sources of errors

Every error affecting a CMM has a systematic and a random component. An example of systematic errors is link geometry related errors which are time invariant and repeatable. This part can be calculated using error models developed for the machine (Treib, 1987). An example of the random errors component is link motion related errors because it is non-repeatable. This is known in some literature as the precession error. Eman et al., (1987) suggested the use of average values of the random error to calculate the CMM accuracy. Nawara and Kowalski, (1987) analyzed the random component in a CMM position error. They suggested statistical methods to obtain the random error and calculate their distribution

and standard deviation. They also proved experimentally the inverse proportional relation between the random error component and the number of data points collected for a circular profile. This supported the use of statistical methods to handle the random error component which is quite popular in the literature. On the other hand, the idea of random errors being statistically treated, introduces a more recent topic for investigation, which is uncertainty in measurement. In general, the new trend in handling measurement errors tries to minimize the acceptance of the randomness idea. The premises of such trend is the fact that every error has a source which might not be known to us. Therefore, it should be included as a source of uncertainty in measurement, which should be attached to every number produced by a measuring machine.

Errors can generate from different sources. Some researchers reported the reduction in measurement accuracy by the increase of measuring speed (Knapp, 1988). Others developed methods to calculate the uncertainty in the use of HTM (Shen and Duffie, 1991). Errors, in general, can be divided into categories based on different criteria (Lau and Hocken, 1984). The following list of errors is divided according to the difference in its physical cause (Weekers and Schellekens, 1995). Figure 6 shows these different errors affecting a CMM.

### 2.5.2 Quasi-static errors

These are defined as errors of the relative position that are varying slowly in time and are related to the structure of the machine. These errors contribute to more than 70 % of the machine errors. Figure 7 presents the components of this category of errors (Barakat et al.,

2000). Quasi-static errors include the following components:

### 2.5.2.1 Geometric error

This error is inherent in the manufacture of the machine and can be found by the measurement of squareness, straightness, flatness, and angular motion errors. A practical way of performing these measurements can be found in the literature (Kunzmann et al., 1995) and Table 2 of section 2.3.1. This error is caused mainly by the structural elements. Sources of geometric errors are :

a. Accuracy of Components (Manufacturing errors).

b. Accuracy of components adjustment and alignment (Maintenance and Installation).

c. Measuring systems errors.

Knapp (1983) demonstrated that a CMM can be tested using a circular profile for

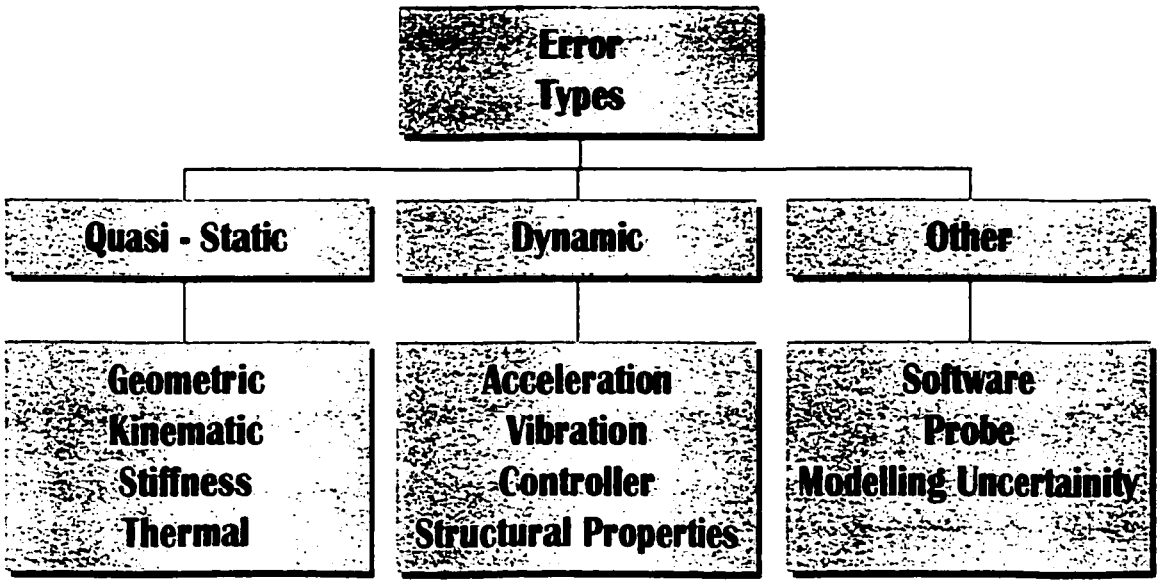


**Figure 6** Errors in a CMM.

geometric errors. The recorded data can be analyzed and some logical combinations can be used to find the main sources of geometric errors in the structure of the machine. The geometric error affects the machine repeatability and kinematic accuracy. It also is the direct measured error produced partially by other sources such as the thermal error.

### 2.5.2.2 Stiffness error

Although this error has a relatively minor effect on the machine, the literature reports tests and results relating to it. This error can originate from the following sources :

a. Assumptions of finite stiffness, which is not a fully correct assumption. This error has been investigated and a finite stiffness of some machines components have been

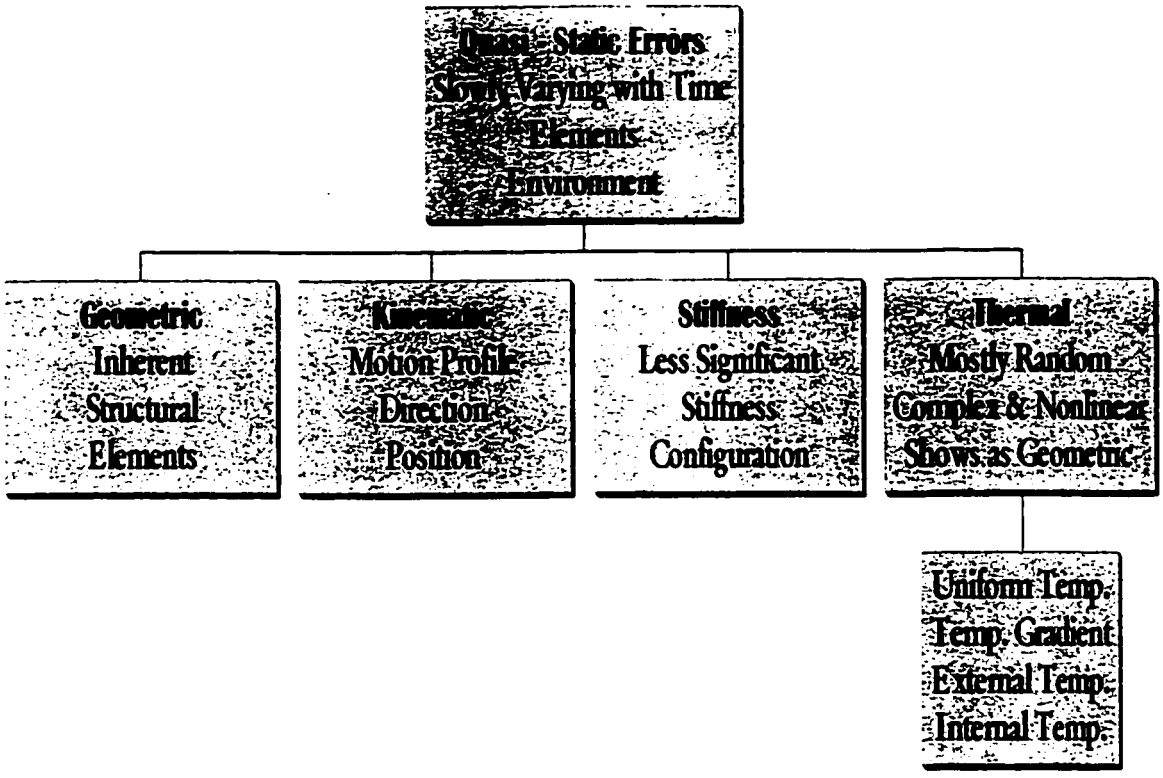


**Figure 7** Quasi-Static errors.

reported which causes a limitation and an error to the modelling methodology of that machines error (Weekers and Schellekens, 1995).

b. Weight of components in the structure, especially moving components.

c. Configuration of Components.

#### 2.5.2.3 Kinematic error

Some literature reports consider this category as part of the geometric error. Others make a distinction between them. The kinematic error is the inability of the CMM to reach the exact specified position by the controller. It is related to the commanded motion of the machine. Nawara et al. (1989) studied kinematic error modelling and calculation in a CMM. They presented results showing the effect of change of position and measured profile on kinematic errors. They also discussed the effect of both systematic and random components of kinematic errors. Position of machine slides, gears, ball screws, couplers, motors, and controllers contribute to this error. In addition, hysteresis and backlash in these elements affect this error and consequently make it a function of motion direction (Veldhuis and Elbestawi, 1995).

#### 2.5.2.4 Thermal error

Thermal error is a major factor in machine performance deterioration. In addition, it is a major part of the scope of this work. Therefore, a separate section is devoted for the wide literature related to this error. This is explained in section 2.6 to follow.

### 2.5.3 Dynamic errors

This is the collection of errors that cause dynamic instability of the CMM (Weekers and Schellekens, 1995). It is caused by factors like excessive play or pre-load in the joints and gears, structural flexibility, and external excitation forces. Medium to high frequency vibrations of relatively high amplitudes are the signs of this error group. These vibrations are often at well defined frequencies (Lau and Hocken, 1984). This group is outside the scope of this thesis. Dynamic errors include the following subgroup of error types and sources:

#### 2.5.3.1 Acceleration of motion errors

Which is due to parts movement and consequently developing forces.

#### 2.5.3.2 Vibration errors

This can be of two types; self induced and/or forced. Nijs et al., (1988) suggested that the amplitude of vibrations by CMMs in response to excitations have to be kept low because substantial amplitude of resonance vibrations can cause severe loss of accuracy. He proposed a method to estimate the dynamic behavior of a CMM and henceforth optimize its dynamic response before constructing the prototype. On the other hand, he did not propose any solution to the problem, only a method for analysis prior to building. Numerical analysis methods and finite element methods can also be used for the same analysis purposes. Some recommendations are provided in the literature for the design specifications of a CMM.

Among those are higher drives stiffness, and a better balancing system than counterweight to avoid low natural frequencies.

#### 2.5.3.3 Control errors

Effects of errors related to the controller show mainly as quasi-static errors when measured, although the cause is classified as dynamic. An unstable controller design or changes in the CMM parameters (e.g. payload, speed of operation, extra hysteresis..etc.) which are not accounted for by the controller can cause such errors. Moreover, a defective device or sensor feeding the controller can also be the cause for this error. The signs for this error can be summarized by the motion overshoot, position drift, poor repeatability and errors in velocity and acceleration control.

#### 2.5.3.4 Distributing forces errors

Includes forces exerted by the measuring system on the measured piece and vice versa. Deformation resulting of these forces contributes to the total error of the machine (Zhang and Fang, 1991).

#### 2.5.3.5 CMM structural properties errors

This category is very much related to the quasi-static errors category, but contributes as well to the dynamic error. It include factors like mass distribution, component stiffness, and damping characteristics.

### 2.5.4 Other errors

This category includes errors that contribute to the deterioration of the CMM performance but do not result from the core CMM. They are normally introduced by auxiliary systems added to the CMM to complete its tasks. Software induced error is one of these errors. This error has been detected and reported in the literature using what is known as the "black box test". Peggs and McKeown, (1989) concluded that the black box testing technique is the only practical method of evaluating the performance of geometrical element assessment software. Testing available software in the market for CMMs, some results were not satisfactory in one or more aspects. The errors stemming from software become more evident as fitting and form testing is performed by the CMM. Different data fitting techniques produce differences in results of measuring the same dimension.

Another error is the probing error. This error is added to the CMM core errors and results from the probing unit and its system. This includes lobing and probing software errors. Any additional fixture, vision, or feeding system introduced to the CMM will arrive with its own errors that will finally add up to the total CMM error.

## 2.6 Thermal errors

Thermal errors effect in machining and measuring accuracy is one of the most addressed problems in precision engineering and machining accuracy literature. For many years, thermal effects have been the largest sources of dimensional errors and equipment non-repeatability. Thermal error variation has a complex nonlinear nature which makes it

difficult to handle. Bryan (1990) divided the overall thermal problem into two major categories:

a. The effect of uniform temperatures other than 20 deg. C.

b. The effect of non-uniform temperatures.

He also provided an illustration of the problem and the concepts. He suggested that every measuring and machining problem has three elements, the part, the machine frame, and the master (or scale), through which the thermal error propagates. Figure 8 presents his suggestion of the thermal error components interaction.

Thermal error effect on the CMM accuracy has been widely addressed. This error is considered as a component in the random part of the total error. It shows as a difference in the readings or positioning of the CMM, a geometrical, or a size difference in the workpiece for the case of machining. In the case of machining centers thermal errors have an essential effect and a major contribution to the total error. Attempts for correction of the thermal error can be found in many reports (Veldhuis and Elbestawi, 1995). The thermal error has a clear importance. The Abbe principle holds only if thermal error is neglected (Zhang, 1989). According to Bryan (1990), all the systematic solutions suggested for the thermal error problem fall into three categories:

a. Control of heat flows into the system.

b. Redesign of the frame and scale to reduce their sensitivity to heat flows.

c. Compensation through controlled relative motions among the frame or scale.

The components contributing to the development of thermal errors are as follows:

a. Uniform temperature changes.

b. Temperature gradients.

c. Machine structure and heat sources distribution.

d. Material of components of the machine and its thermal properties.

e. Temperature distribution of the machine influenced by :

   a. External sources: which is the environment effect including room temperature variation, exposure to sunlight, and use of coolant in

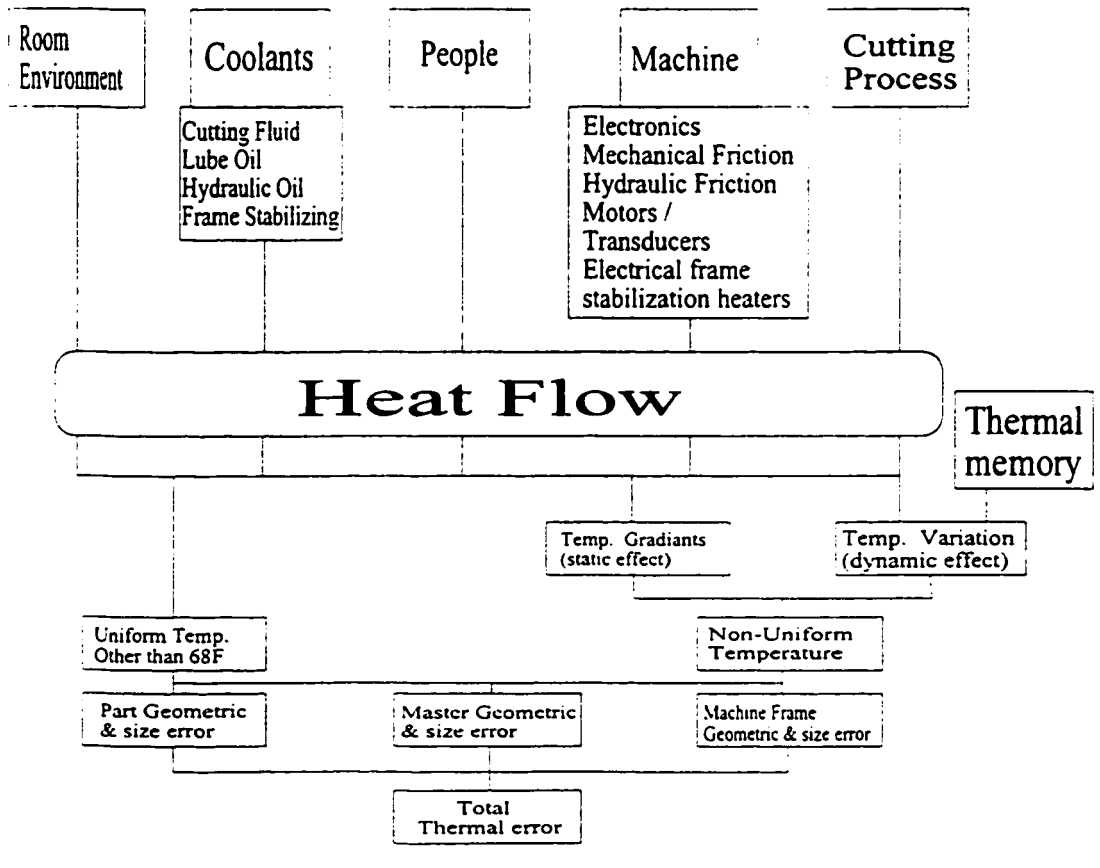


**Figure 8** Thermal Effect Diagram (Bryan, 1990).

machining...etc.

b. Internal sources: Which result from the drives and internal heat sources like motors, amplifiers, circuitry, and slide friction.

The most widely used sensors in measuring temperature variation are thermocouples. Veldhuis (1998) used type E thermocouples to measure temperature changes in a five axes machine, based on recommendations by Attia and Kops, (1993). The main qualities of type E thermocouples are its low thermal conductivity and having the highest output level. Many solutions have been suggested in the literature to treat and eliminate this error. These solutions are surveyed in the following sections.

## 2.7 CMM modelling and error description

Modelling a CMM is important to establish a generalized framework which facilitates a systematic approach to the analysis of errors. This leads to a better assessment of the influence of errors, individually and collectively, on the accuracy of a multi-axis machine. Furthermore, the individual sources of error originating from the CMM components and its motion can be related to the final error between the tool and workpiece through the model. Nevertheless, according to Ferreira and Liu, (1986), analytical and empirical models are generally difficult to obtain because of the large number of influencing variables and complex inter-dependencies. Therefore, they have to be built over restricted domains which are increased by periodic updating.

The most powerful modelling method under accuracy aspects is the one which

assumes that the components of the CMM are rigid bodies. The position error of a carriage can be described by three displacement errors and three rotational errors parallel to the axes and about the axes respectively (Slocum, 1992). These six errors can be measured separately for each of the three carriages as they are independent for one of the others. A total of 18 path dependent errors and three squareness errors can be measured and treated in the model (Barakat, 1998). A rotary table addition would add six more errors to be measured.

This modelling method has roots which can be traced in the literature of robotics. The CMM can be considered as an open chain mechanism where the Denavit - Harenburg (D-H) modelling methodology can be applied. This methodology is based on the Homogeneous Transformation Matrices (HTM) and the rigid kinematics assumption (Paul, 1982, Craig, 1989). This method has already been applied to CMM modelling in the literature and link geometry and motion errors have been identified (Slocum, 1992). Other modelling methods of CMMs different types of errors can be found in the literature. These methods include:

a. The application of analytic geometry to arrive at an expression for the geometric errors.

b. Vector representation utilization to obtain an expression for the vector error (Nawara and Kowalski, 1987).

c. Error matrices calculation where the error vector components at different locations in the machine's workpiece are stored for various loading and thermal conditions (Zhang et al., 1985).

Nevertheless, The first method described provides a simple error model formulation for an arbitrary machine configuration. The other methods also lead to an error model, but lack formalism (Eman et al., 1987). Other modelling methods are reported in the literature. Belforte et al. (1987) presented a general model of a CMM based on parametric functions and a simulation program of the model. This model is based on a combination of assumptions and hypotheses. The simulation output is an estimation of the CMM reading which is used to calculate the machine error and compensate for it.

However, the HTMs method proved to be very powerful and general compared to the rest of the methods. This method is based on assumptions which impose restrictions on the model accuracy. These assumptions are:

a. Rigid body kinematics.

b. Approximation of differential errors (e.g. Cos $\theta$= 1, Sin $\theta$=$\theta$, for very small $\theta$,.. etc).

c. First and second orders terms of errors equations are considered only and higher order terms are neglected.

Teeuwsen et al. (1989) incorporated a set of five stiffness parameters in the HTM based model to describe the static deformation effect on the CMM. This is a counter-measure to the first assumption above. They suggested the elimination of the stiffness parameters only if suitable measurements are performed. They also proved that for a specific machine these parameters are not negligible. On the other hand, some machines do have components with stiffness parameters that can be considered rigid (Zhang et al., 1985). In all cases, the model has to be reasonably simplified by means of suitable assumptions. This

results in having to compromise between cost and benefits required (i.e. the less complicated the model the faster it is in calculations without considerable loss in accuracy) (Balsamo et al., 1990).

Balsamo (1995) elaborated on some rules regarding the choice of parameters for error models. This is to avoid errors showing in the compensation especially when using a multiple stylus configuration.

Srivastava et al. (1995) used the HTM model combined with the small angle approach to model geometrical and thermal errors of a five axes milling machine. In a later work, a compensation strategy was based on this methodology (Barakat and Elbestawi, 1998). Modelling techniques can also be divided into direct modelling techniques like the HTM kinematic model or indirect modelling techniques like the linear regression estimation. Although both models provide good tools for relating the error between the end effector and the workpiece to the axes of motion, the later (indirect techniques) have more limitations and require more computational time.

## 2.8 Solutions for error elimination

Improvement in the accuracy of a machine can be achieved by two means: the first one is error avoidance which implies the elimination of the source of error at the design and assembly stage. The second solution is error compensation, which is defined as being a method of cancelling the effect of the error by means of predicting it using a model built for that purpose and correcting it through software and control schemes. As for the design

problem, better quality control in machines manufacturing reduces the geometric errors significantly. Improved quality of the machine components like gears and ball screws reduces their kinematic errors. The same goes for thermal errors when properly choosing the machine components materials and thermal sources distribution. Nevertheless, the effect of thermal errors, as well as the other errors remains inevitable. According to Kunzmann and Waldele (1988), the treatment of all measured errors can be of two types :

a. Improvement of the accuracy by numerical error correction.

b. Computation of measurement uncertainty.

In general, thermal error avoidance can be achieved by the following measures:

a. Improvement of structure design (McKeown et al., 1995).

b. Improvement of heat distribution by circulation of thermally-conditioned fluids (for machining centres) (Veldhuis and Elbestawi, 1995).

c. Improvement in external heat sources by placing the machine in a thermally controlled environment.

d. Real-time software compensation and correction for the rest of the errors.

Other issues affecting the machine accuracy like the trade-off between accuracy and speed in measurement modules has also been addressed in the literature (Weekers and Schellekens, 1995). Yonezawa et al., (1990) simulated and designed a high precision table to demonstrate this principle.

Methods of position measurement by means of laser interferometers based on distance data are proposed in the literature. Nakamura et al., (1991) developed a coordinate

measuring system based on this idea. Although their system gives more accurate figures than the regular available ones, it still needs more investigation to be error proof and applicable.

Weekers and Schellekens (1995) developed a method to assess the dynamic errors in a CMM due to carriage motion. The method includes measuring the major joint deflections due to accelerations with position sensors. The influence of these errors on the probe positioning is calculated by means of a kinematic model of the machine.

Laser interferometers are becoming popular in use. A calibration method using laser is reported by Lingard et al., (1991). This method is quick and minimizes thermal effects due to parts handling. Along the lines of recommended specifications to avoid the majority of the previously mentioned errors, a typical CMM should have specifications which can be summarized by the following:

a. High manufacturing and adjusting accuracy.

b. High component stiffness and low mass.

c. Temperature conditioned environment and small internal heat sources.

d. Vibration isolation and small movements during probing.

## 2.9 Compensation strategies

Software compensation for CMM errors is not a replacement to design major consideration related to errors, especially the thermal error (Balsamo et al., 1990). This is because for software correction to be effective, the following points have to be considered:

a. It is impossible to get a perfect model or a completely general one.

b. Correction can be achieved for a small range of error, The bigger correction comes from the machine proper design.

Nevertheless, compensation for errors gains its importance because design and operating specifications are either difficult to implement or contradicting. Moreover, dynamic errors are random and not systematic, so they are not easy to calculate always and account for. In summary, compensation for errors correction has the following advantages (Teeuwsen et al., 1989):

a. Cost reduction of error correction and avoidance.

b. Increase in machine accuracy to its level of resolution.

Another advantage of numerical correction of errors is that it is based on the models developed for describing the machines errors so it indirectly represents a test of the value of these models. Sartori (1995) used the term compensation to describe the procedure implemented after calibration applying corrections to the measurement system.

Focusing on thermal errors, attempts of compensation for errors by software are presented by Zhang et al. (1985) and Balsamo et al (1990). Zhang used an error matrix model to obtain thermal errors in different points of the work volume. In addition, the HTM model was used to compensate for geometric errors. A simple thermal model was developed and a factor called "effective coefficient of expansion" was used to find the error and compensate for it. This coefficient is discussed in detail by Bryan (1990).

Moriwaki (1988) presented a method for thermal error real time compensation in machines based on a feed forward controller. He used the difference method, which requires

a smaller memory and simpler calculations compared to the FEM, to model the errors and simulate the cutting process. The simulation parameters were obtained from external sources in the real process. The results of the simulation were fed forward for the real process controller to compensate for thermal errors. The results obtained were promising. On the other hand, this method had the problem of slow control of the real process because of the real time simulation data that had to be continuously fed to the controller. On the simulation side also, Belforte et al. (1987) used a simulation program to estimate a CMM error and numerically compensate for it focusing on geometric and kinematic errors.

Another strategy is to assume that a quadratic correlation between the error at a point and the coordinates of the point exist and build correlational models from observations.

Measuring position errors at discrete points in the working volume and storage of these errors in a three dimensional lattice which is called an error map, is the core of this strategy. The compensation is achieved using interpolation between measured errors at the lattice to obtain the required position error and modify the position command accordingly (Duffie and Malmberg, 1987).

Yonezawa et al. (1990) designed a high precesion table with a controller that can handle the errors resulting from high speed motion. The controller for this table switches between a PD controller to run the high speed positioning (course) part and a feed forward controller to run the (fine) part while compensating for errors based on the model.

Another way of looking at error correction is by combining volumetric error measurement with parametric error correction using equations fitting methods (e.g. least

square method). Real time error correction can be achieved since this strategy looks at the systematic part of the error (Teeuwsen et al., 1989, Duffie and Yang, 1985).

Mou and Liu (1993) presented a compensation strategy based on adaptive control of the machining process. Process parameters were fed to a kinematic error model and the error was calculated and compensated for, employing state observers. Statistical methods based analysis was performed to establish a base for the choice of the sensors locations and parameters to be fed to the model. The adaptive control method was chosen because of the uncertainties involved. These uncertainties originate from using statistical methods, model assumptions, and the constantly changing machine wear conditions. In summary, their model was a linear model handling a highly nonlinear relation, which is similar to linearizing about different thermal operating conditions.

Valdhuis (1998) implemented a neural network based controller in a compensation strategy for machining errors in a five axes machine. The focus was on geometric, kinematic and thermal errors together. Thermocouples were chosen and placed strategically on the machine to monitor thermal errors and feed a kinematic model to predict the error and compensate for it through the controller. Neural networks were chosen for their ability to handle non-linear, multi-variable systems. Moreover, they provide an in-out relation based on training. This is in addition to their excellent interpolation capabilities and noise tolerance. The neural networks training was achieved on two stages, simulation and experimentation. Dynamic errors were avoided using optimal cutting parameter selection. This is due to the low speed of this compensation strategy.

The choice of a compensation strategy depends to a great deal on the type of controller used or available on the machine and its flexibility.

## 2.10 Summary

This chapter presented the collection of research results history relating to the topic of thermal error correction in a CMM. A brief description of the history related to the topic as well as other topics that touch the scope of this thesis were given to place the thesis topic in its general context.

CMMs should be 10 times more accurate than the production machines in its manufacturing system. However, they still encounter some errors. Before CMMs were invented, manual quality control was in effect. CMMs brought quality control into automation. There are different types of CMMs available now. CMMs performance and error correction is one of the most addressed topics. Between calibration and performance evaluation, many reports can be found. The objective of CMM performance evaluation is to quantify the operational status of the CMM and compare the different available ones. One standard performance evaluation missing is the one that considers the changing thermal status of the CMM.

Different types and sources of errors affect the CMM performance. Thermal errors are reported by many researchers and described as having a noticeable and nonlinear influence. A systematic approach to error characterization and correction is achieved through modelling and error functions identification. Modelling is performed based on the HTMs

idea. Different solutions are presented by researchers including compensation. The choice of a compensation strategy is affected by the amount of errors to be corrected, the flexibility of the machine and its controller, and the comprehensibility of the correction methodology desired, especially when changing errors are present.

Chapter Three

# Theory and Modelling

Modelling of the CMM is the first of three essential steps constituting the systematic approach to error correction. A model allows a better assessment of the influence of individual errors, on the general accuracy of a multi-axis machine through relating them to the final error at the end effector.

CMMs belong to a group of multi-axis machines which are composed of a sequence of links connected through joints. These joints could be revolute or prismatic. These joints provide the rotational and translational motions of the links which, combined, produce the motion of the end effector of the machine commanded by the user through the control software. This group of multi-axis machines, belongs to a larger category which is the chain mechanisms. For the purpose of this research, a "DEA IOTA 1102" CMM with a retrofitted computer based motion controller, is used to study both measuring and contouring performance.

## 3.1 Solution criteria

Based on the previous information regarding the CMM structure, modelling can start from the rigid body kinematics modelling methodology, reported in the literature, and already used for such mechanisms. Figure 9 shows a schematic diagram of the CMM under investigation. This CMM represents an intrinsic machine which is a kinematic sequence, by convention, where body one supports the workpiece and X is the direction of the guide connecting it to the adjacent body; Z is the direction of the guide connecting the body supporting the end effector to its neighbor (Barakat, 1998). Physical modelling can be used to characterize the CMM behaviour as long as the bases for these models exist, and the cost of obtaining them is tolerable. When in a situation where physical modelling becomes short of proper description of the problem or extremely expensive to obtain, empirical modelling methods can be introduced to complete the task. This will result in models that are a hybrid between physical and theoretical approaches from one side and empirical and statistical based from the other side. This approach is followed in this thesis where the idea is to start with the theoretical base and expand throughout using the experimental results.

## 3.2 Forward kinematics model of the CMM

A systematic approach to the analysis of CMM errors and a representation of their influence is critical to the improvement of the CMM performance. The position error of a carriage can be described by three displacement errors and three rotational errors around its axis of motion (Slocum, 1992). For an intrinsic machine, this results in 18 separate and path

dependent errors, in addition to the three squareness errors. The final error model is based on the assumption of rigid body kinematics and involves the use of Homogeneous Transformation Matrices (HTM's). The machine individual errors can be found by two major methods (Sartori, 1995, Barakat et al., 2000). (i) direct measurement using laser interferometry, and (ii) indirect measurement through the use of a standard calibration artifact. Consequently, model coefficients can be found for a particular investigated machine based on these measurements, and a compensation strategy can be devised to correct its

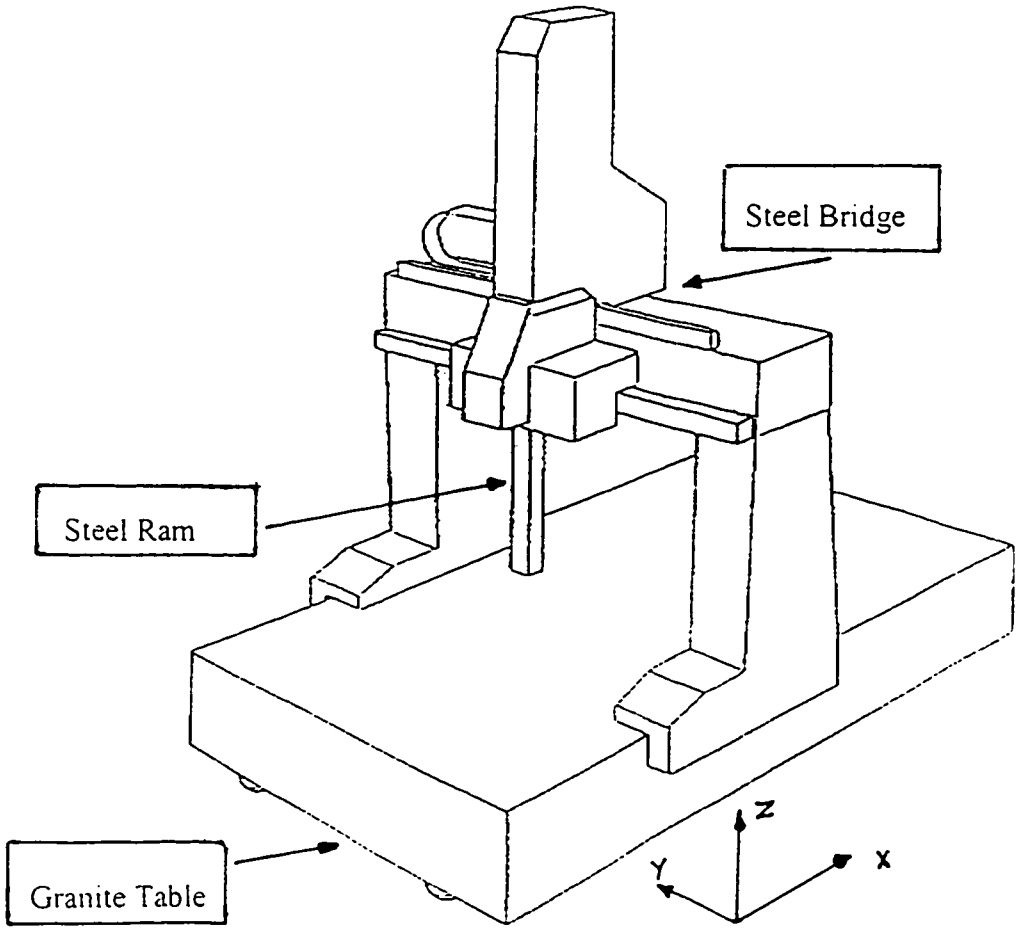


Figure 9 Schematic of the DEA IOTA 1102 CMM.

volumetric error (Barakat and Elbestawi, 1998).

The general forward kinematics model including the different errors of the machine parts, for any intrinsic machine, is based on the physical relationships of the machine parts and represented by equation (1):

$$[P_a] = [P_i] + [E] \tag{1}$$

where $[P_a]$ is the actual position (real), $[P_i]$ is the ideal (nominal) position of the end effector, and [E] is the collection of error terms that are added to the ideal model. For the CMM under investigation, $[P_a]$ and $[P_i]$ can be found using the method of Homogeneous Transformation Matrices (HTMs). The final error model for any intrinsic machine, including the CMM has the general form represented by equation (2).

$$\begin{bmatrix} Ex \\ Ey \\ Ez \end{bmatrix} = \sum_{i=x,y,z} \left[ \begin{bmatrix} \delta_x(i) \\ \delta_y(i) \\ \delta_z(i) \end{bmatrix} + \begin{bmatrix} \varepsilon_x(i) \\ \varepsilon_y(i) \\ \varepsilon_z(i) \end{bmatrix}^T * \begin{bmatrix} x \\ y \\ z \end{bmatrix} \right] + \begin{bmatrix} S_X(y) + S_x(z) \\ S_y(z) \\ 0 \end{bmatrix} \tag{2}$$

Equation (2) has the following terms:

$\delta_i$ (j): 9 Translational Errors where; i is the error direction, j is the moving axis and, when i=j, $\delta_i$ (j) implicitly includes the scale error;

$\varepsilon_j$ (i): 9 Rotational Errors where; rotation is around axis i, and [X, Y, Z] = end effector coordinates Vector;

$S_j$ (i): 3 squareness errors in the direction of j.

These 21 terms can be determined for the CMM at hand by methods like direct measurement using laser interferometry. This results in a model representing the machine errors as a function of position at any ambient thermal condition. Therefore, $[P_s]$ of equation (1) represents the machine forward kinematics model including its quasi static errors.

Based on the small angles approach to model errors and imperfections in the links and motion of the machine elements, the matrices $S_i$ and $J_i$ can be used to model link (i) and joint (i) respectively, (Slocum, 1992). The errors in the $S_i$ matrix, equation (3), are assumed position independent and treated as constants.

$$S_i = \begin{bmatrix} 1 & -\gamma_i & \beta_i & a_i + \Delta a_i \\ \gamma_i & 1 & -\alpha_i & b_i + \Delta b_i \\ -\beta_i & \alpha_i & 1 & c_i + \Delta c_i \\ 0 & 0 & 0 & 1 \end{bmatrix} \quad \textbf{(3)}$$

These errors are $\alpha_i$, $\beta_i$, and $\gamma_i$ which are the angular errors of the $i^{th}$ link and $\Delta a_i$, $\Delta b_i$, and $\Delta c_i$ which are the dimensional errors of the $i^{th}$ link as in figure 10. On the other hand, errors in the $J_i$ matrix, representing a joint, are treated as position dependent, as in equation (4).

$$J_i = \begin{bmatrix} 1 & -\gamma_{ix} & \beta_{ix} & x_i + \Delta x_i \\ \gamma_{ix} & 1 & -\alpha_{ix} & y_i + \Delta y_i \\ -\beta_{ix} & \alpha_{ix} & 1 & z_i + \Delta z_i \\ 0 & 0 & 0 & 1 \end{bmatrix} \quad \textbf{(4)}$$

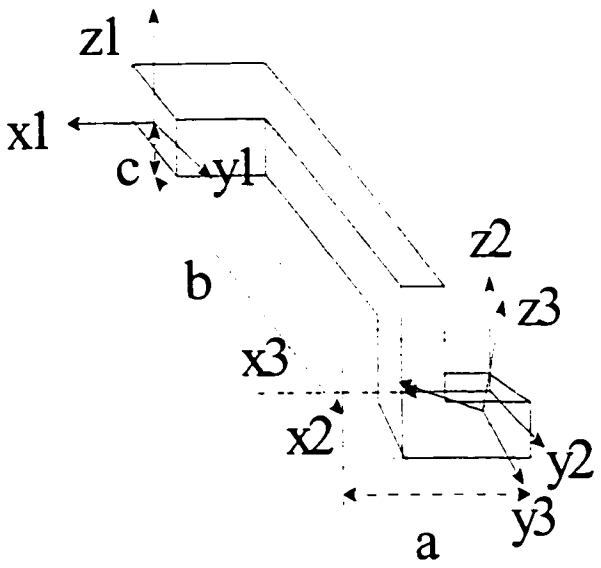


**Figure 10** Solid link with errors.

These need to be identified to derive the specific error model for this particular machine under investigation. They are $\alpha_{xi}$, $\beta_{xi}$, and $\gamma_{xi}$ which are the angular errors (roll, pitch, and yaw) along the $i^{th}$ joint, as well as, $\Delta x_i$, $\Delta y_i$, and $\Delta z_i$, which are errors in the desired displacements along the $i^{th}$ joint, as in figure 11.

The general HTM for an inaccurate positioning element is expressed by equation (5).

$$T_i = S_i * J_i \qquad \textbf{(5)}$$

The combination of all elements HTMs can be used to build a mathematical model,

which in turn helps in finding the error expression at the probe tip measurement. For the CMM at hand, this kinematic model, as well as the accompanying wire frame, are shown in figure 12. Individual matrices for each link and joint of the CMM and the final equations are given in Appendix B. For the error expression form, which is used as an essence for the compensation strategy, to be found, the final form of the model matrix is compared to the final form of the ideal kinematic model of the CMM with no errors included.

The relationship between actual and measured position of vectors of the probe of the CMM is expressed as

$$[P_{ideal}] = [P_{actual}] - [E] \tag{6}$$

$$[E] = [P_{actual}] - [P_{ideal}] \tag{7}$$

where every [P] can be expressed as :

$$[P] = [T_1] * [T_2] * [T_3] * \ldots * [T_n] \tag{8}$$

$T_i$ is the individual HTM related to the joint or member and [E] is the final error terms matrix. Notice that the ideal kinematic model matrix for the CMM can be obtained from the model including the errors by making all the error terms ($\alpha_i$, $\beta_i$, $\gamma_i$, $\alpha_{xi}$, $\beta_{xi}$, $\gamma_{xi}$, $\Delta x_i$, $\Delta y_i$, $\Delta z_i$, $\Delta a_i$, $\Delta b_i$, $\Delta c_i$) equal to zero. By following this approach the forward kinematic model can be used to predict the error vector at each point in the work volume of the CMM.

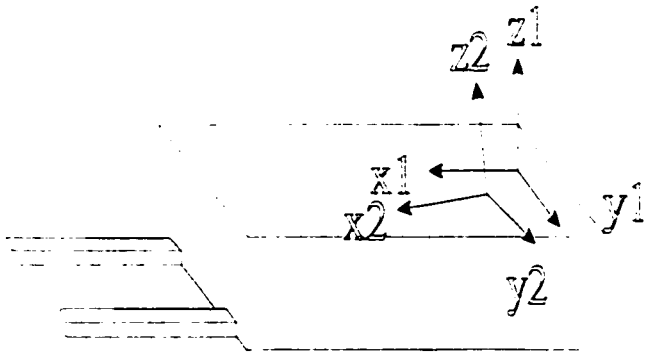


**Figure 11** Axis motion with errors.

## 3.3 The inverse kinematics model

To correct for the CMM contouring errors, a feed forward control strategy can be designed to modify the commanded positions based on the error model knowledge. This necessitates the existence of the inverse kinematics model of the CMM including its errors. The available machine forward kinematics model includes non continuous error functions which are found by different measurement techniques. This makes the inversion of the forward kinematics model extremely difficult and complicated. Therefore, multi nonlinear

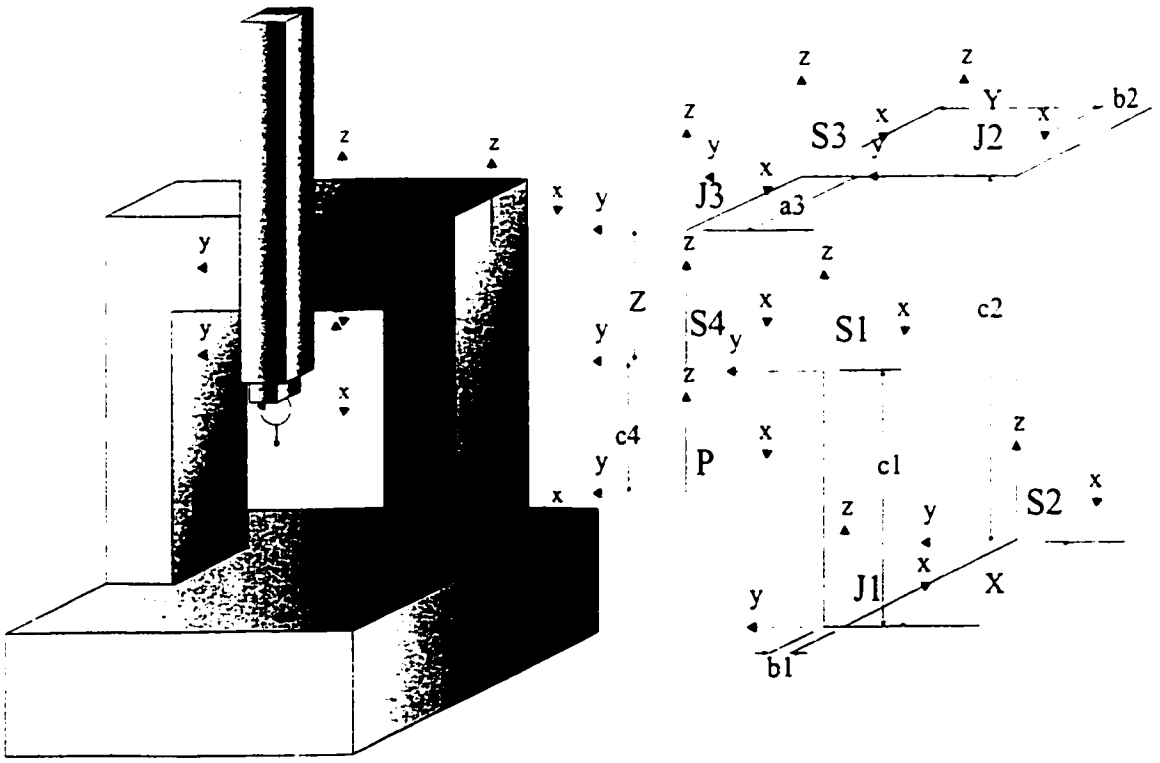


**Figure 12** Schematic of the CMM.

regression is proposed as a direct method to obtain the inverse kinematics relation by applying the least squares algorithm. The basic formula for this method is represented by equation (9):

$$Y(t) = \theta^T \phi(t) + e(t) \tag{9}$$

Where Y(t) is the dependent variable, $\phi(t)$ is the independent variable, and $e(t)$ is the equation error (Ljung, 1983). The least square estimate, which is in accord with the maximum-likelihood principles of statistics, for the coefficient $\theta$ is presented by equation (10):

$$\hat{\theta}(N) = \left[\sum_{t=1}^{N} \phi(t)\phi^T(t)\right]^{-1} \sum_{t=1}^{N} \phi(t)Y(t) \tag{10}$$

Where N is the number of observations. The final and simplified form of equation (10) can be written as in equation (11):

$$\hat{\theta} = \left[\phi^T \phi\right]^{-1}\left[\phi^T Y\right] \tag{11}$$

and the error in the estimation can be expressed by equation (12) (Brook and Arnold, 1985):

$$\hat{e} = Y - \hat{\theta}^T \phi \tag{12}$$

It is to be mentioned that this method is based on statistical analysis concepts. Therefore, the quality of the model produced using this method relies mainly on the number of data pairs that are used to build it. As a consequence, validation tests, including the ANOVA technique were used to test the resulting inverse kinematics model.

## 3.4 Thermal error models

Finally, the changes in the ambient thermal state can be incorporated in the kinematics and error models. Considering the thermal state as an independent variable affecting the machine behavior, the forward kinematics can be considered as a function of both the nominal position of the end effector and the ambient temperature and gradient as in equation (7):

$$[P] = f(P_i, T, G) \tag{13}$$

where T is the ambient temperatures vector and G is the ambient thermal gradients vector. The final volumetric error at the end effector is calculated through the error functions models

where the principle of superposition is applied.

The effect of thermal state changes from the reference temperature $T_{ref}$ to T or the effect of a temperature gradient on the dimensions of a part along the gradient direction can be calculated by assuming a macro element of dimension L, along the X-axis direction, and equipped with multiple temperature sensors to measure $T_i$ along the dimension L. Average change in the element temperature $\Delta T_{avg}$ from $T_{ref}$, at any point x, can be calculated as:

$$\Delta T_{avg} = \frac{\int_0^x \Delta T(x)dx}{\int_0^x dx} \tag{14}$$

where $\Delta T$ is the infinitesimal change of temperature from $T_{ref}$ at each measurement location. Considering the measurements to be along the full element length the integration would be carried to the length L, this gives the following equation:

$$\Delta T_{avg} = \frac{1}{L}\int_0^L \Delta T(x)dx \tag{15}$$

In the case of not having an expression for the temperature distribution along the measured element as a function of x, a numerical integration can be applied.

To calculate the deformation of the whole element tested in the direction of X excluding the gradient effect, the following equation can be used:

$$dL = \int \alpha \Delta T_{avg} dx \tag{16}$$

which has the general form of:

$$\left[\Delta L_i\right]_{(i=x,y,z)} = \alpha . \Delta T_{avg} . \left[L_i\right] \tag{17}$$

where $L_i$ is the dimension of the element along the axis i= {X, Y, Z}. $\Delta T$ is the temperature difference from the standard $T_{ref}$.

To account for the presence of thermal gradients, a second order model can be used to calculate the deformation of the CMM components affected (Appendix C). The final equation has the following form:

$$Z(x) = \tfrac{1}{2} . \alpha . x^2 . G(T_z) \tag{18}$$

where Z(x) is the deformation in the Z direction as motion is attempted along the X direction, and $G(T_Z)$ is the temperature gradient along the Z direction in the global spatial reference frame. The ECTE ($\alpha$) is determined experimentally. Different sets of volumetric errors result for different thermal states, which in turn will produce a new set of coefficients for the inverse kinematics model $\theta$ found by equation (5). Again nonlinear regression can be employed to find the relation between the elements of $\theta$ and the ambient thermal state of the environment, which forms the model of the state observer used in the feed forward control strategy. The previously obtained models for the error functions will be calibrated or

modified by laser measurements. Error functions of no direct relation to the thermal state will be incorporated by either regression modelling or piecewise bilinear interpolation.

## 3.5 Bilinear interpolation

Piecewise bilinear interpolation is based on the idea of data distribution in space and their connection through surface patches. It is a method which can be used to approximate values inside a three dimensional matrix of data, for which the corner values ($x_{ij}$, $y_{ij}$, $z_{ij}$, where { i, j = 0, 1}) are known. Each bilinear patch connects four corner points using parameterized linear segments. The parameters u and v are:

$$u = \frac{x - x_{00}}{x_{10} - x_{00}} \tag{19}$$

$$v = \frac{y - y_{00}}{y_{01} - y_{00}} \tag{20}$$

where x, y and z are the corresponding coordinates of the corners. The z coordinate of a point on the patch can be found using the final equation as follows:

$$z = \left[(1-u)z_{00} + z_{10}u\right](1-v) + \left[(1-u)z_{01} + z_{11}u\right]v \tag{21}$$

This equation can be written in matrix form as:

$$z = \begin{bmatrix} 1-u & u \end{bmatrix} \begin{bmatrix} z_{00} & z_{01} \\ z_{10} & z_{11} \end{bmatrix} \begin{bmatrix} 1-v \\ v \end{bmatrix} \tag{22}$$

Orientation information, which is required to calculate the final probe tip position, is obtained by constructing a vector between two closely spaced end effector positions.

## 3.6 Summary

In this chapter, the basis for the first step towards CMM error compensation were explained in detail. A general and systematic modelling of the CMM including its quasi-static errors was carried out. The CMM errors were physically modelled at a constant reference thermal state, to arrive at a basic model with acceptable accuracy. To quantify and model the environmental changes, thermo-mechanical models of material reaction to thermal changes are provided. To combine these models, the principle of superposition should be applied to determine the final error at the end effector. In addition, experimental measurements will be carried out to improve the models. The final form of the models will be a hybrid of analytical and physical modelling.

A direct method is proposed to obtain the inverse kinematics model of the machine by applying nonlinear regression analysis based on the least squares error principle. This is because of the difficulty in arriving at the inverse kinematics model by direct inversion of the forward model. The basic inverse kinematics model of the CMM will be obtained from the forward kinematics model output data. Consequently, the dynamic effect of thermal changes can be incorporated in the model starting with theoretical separate models for the individual error functions.

Chapter Four

# Methodology and Implementation

The methodology for CMM quasi-static error correction by compensation consists of three main steps. The first step is to model the machine behaviour and errors, which is explained in details in chapter 3. The second step includes the development of a strategy to compensate for these errors, which is explained in the present chapter. The third step is to identify the error functions in the model. This is carried out experimentally and explained in details in chapter 5.

## 4.1 Compensation and control strategy

Compensation for errors affecting the CMM, whether it is in measurement or in contouring, is a solution to improve the CMM performance. The compensation strategy

proposed for the measurement error correction in the CMM work volume is based on the error model equations (1) and (2) of chapter 3. The volumetric error associated with any position in the work space of the CMM is estimated using the error model. Consequently, the CMM reading is corrected in software to the actual position value of the machine. Figure 13 represents the details of this compensation strategy. For the case of changing thermal conditions, the model error functions are continuously modified to adapt to the machine thermal state changes.

In the case of contouring, adaptive response to these changes is achieved through the integration of a state observer. The state observer measures error function deviation from

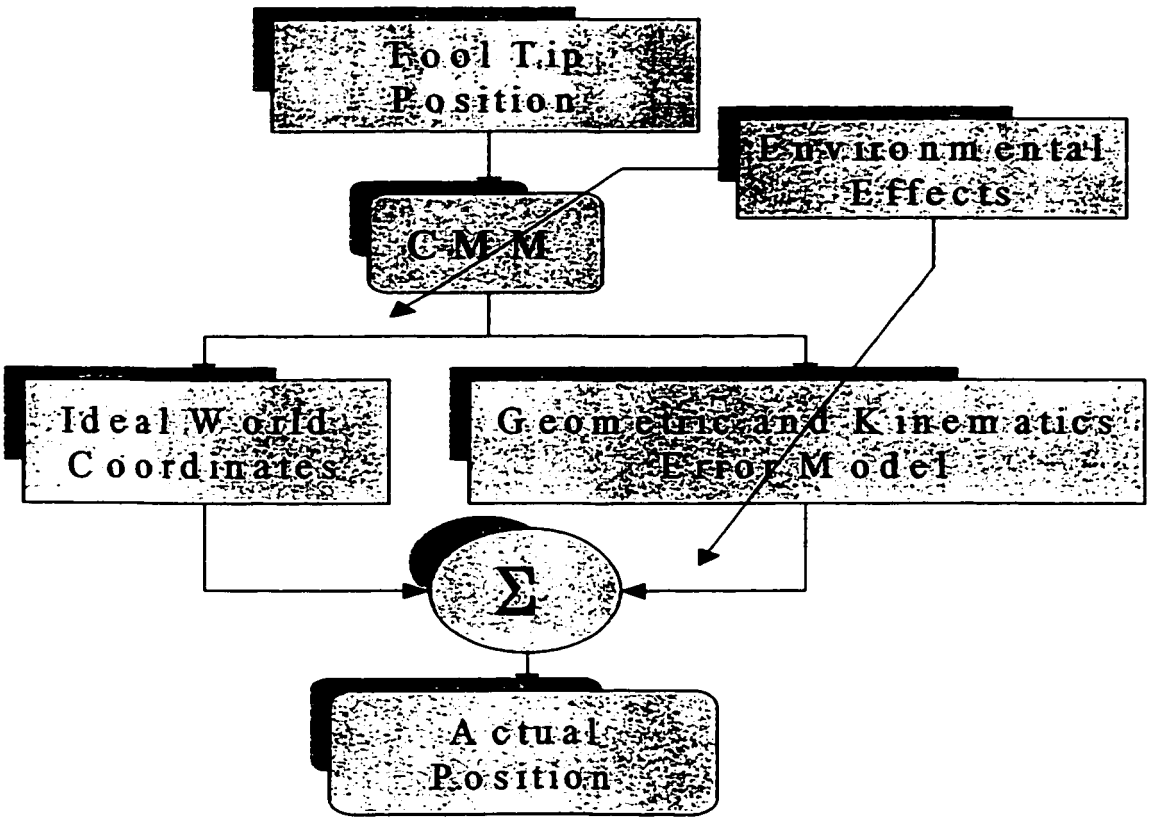


**Figure 13** Compensation strategy proposed for the CMM measurement error correction.

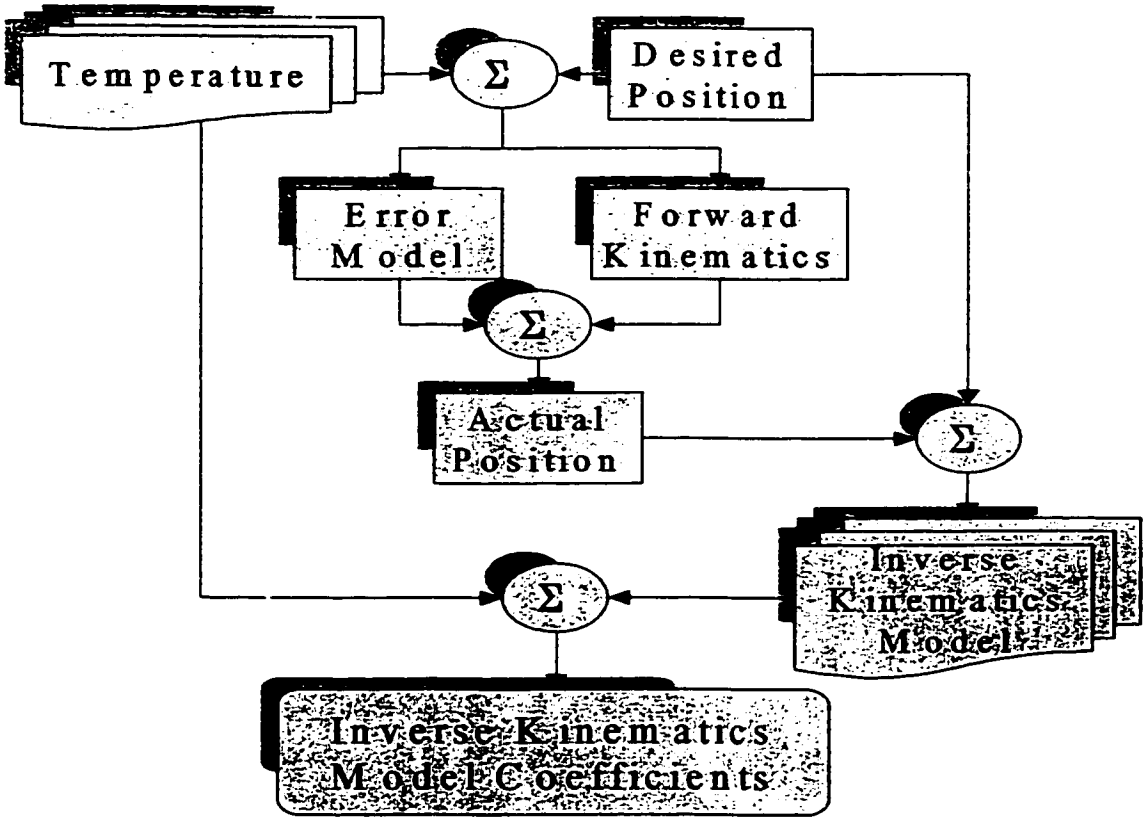


**Figure 14** Inverse kinematics model construction procedure.

the reference original state and calculates their new values. The primary experimental values of the error functions provide the observer original state. These calculations are based on error functions models combined with the CMM Effective Coefficient of Thermal Expansion (ECTE). Consequently, the new error functions values vector is fed back to the inverse kinematics model to modify its output. The inverse kinematics model is necessary for the contouring error correction procedure. The direct building procedure of the inverse kinematics model, based on the theoretical bases explained in chapter 3, is presented by figure 14. For this purpose, the forward kinematics based error model is used to produce error vectors corresponding to sets of input positions. The statistical regression procedure

is carried out to produce the inverse kinematics model and repeated for every thermal state change. Another modelling process is carried out for each error function individually to arrive at the final model and observer form. The feed forward adaptive compensation and control strategy proposed to eliminate the errors in contouring is presented by figure 15. The inverse kinematic model of the CMM accounting for the errors affecting the machine is used to calculate the error signals which, in turn, are combined with the commanded positions by the trajectory planner. The resulting modified signals are then provided to the servo controllers of the CMM. Dynamic changes of the system thermal state affecting the model can be modeled by state space equations. The thermal state of the model error functions at any instant can be represented as a function of the old state modified by the temperature change sensed as a disturbance to the system. To represent this interaction, equations (23) and (24) can be used:

$$C(k+1) = GC(k) + HT(k) \tag{23}$$

$$\hat{C}(k) = BC(k) \tag{24}$$

where C(k+1) is the vector of error functions values for the error model at state (k+1), and T(k) is the vector of temperature measurements from sensors surrounding the machine. $\hat{C}$(k) is the vector of estimated values of error functions. Only measurements of sensors and the output of equation (23) are required to update the inverse kinematics model.

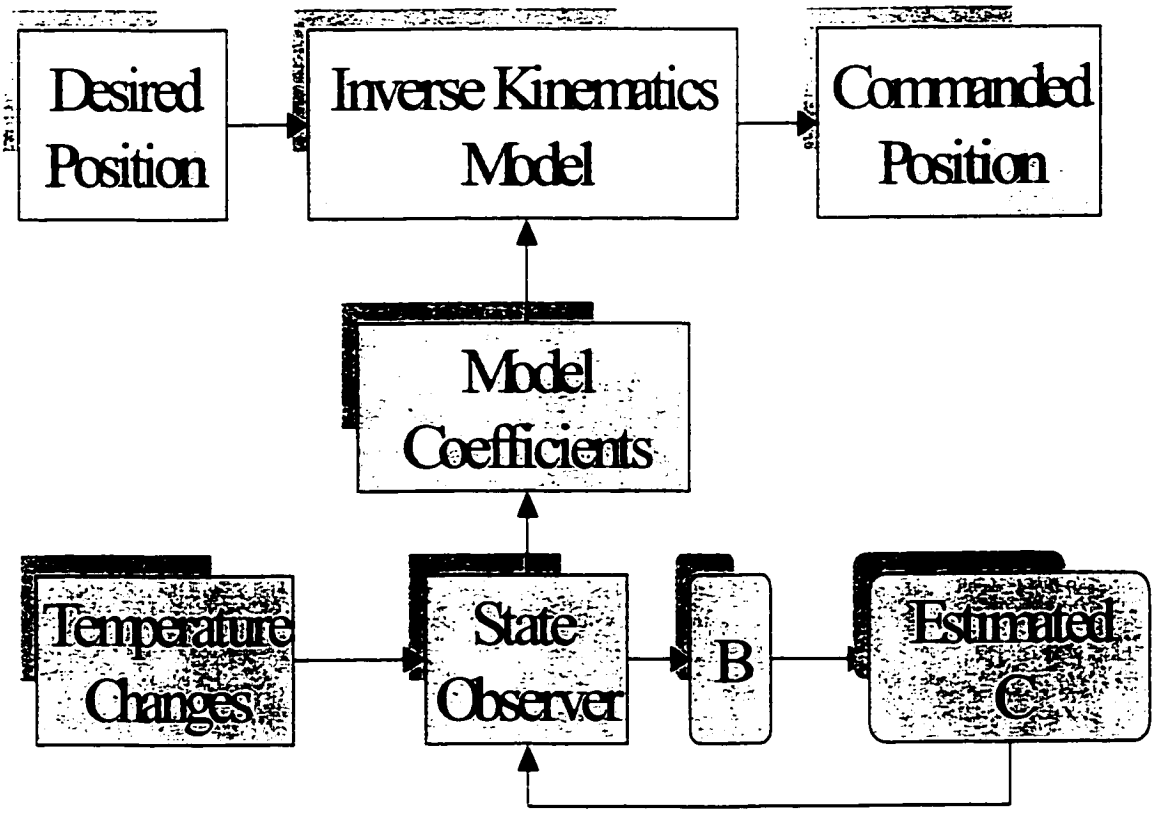


**Figure 15** Schematics of the state observer technique for model on-line update.

## 4.2 Modelling approach

The forward and inverse kinematics models were built in two stages. The first stage consisted of modelling for a constant reference thermal state and the second stage included ambient thermal state changes incorporation in the model. The final form of the error model is presented by equation (2) of chapter 3 for the general case and by equations (19, 20, and 21) for the CMM under investigation. The combination of these equations is the model of the volumetric error of the CMM. These equations refer to the frames represented by figure 12 in chapter 3.

$$E_x = \Delta x + \varepsilon_{xx} + \varepsilon_{zx} + \gamma_{1x} y - \beta_{1x} c_2 - (\beta_{2y} + \beta_{1z}) z + \gamma_{1x} b_2 + \sum \Delta_{ai} - (\beta_{1x} + \beta_{2y} + \beta_{3z}) c_4 \quad (25)$$

$$E_y = \Delta y + \varepsilon_{zy} + \varepsilon_{xy} - (\alpha_{2y} + \alpha_{1x}) z + \sum \Delta b_i - (\alpha_{1x} + \alpha_{2y} + \alpha_{3z}) c_4 + (\gamma_{1x} + \gamma_{2y}) a_3 - \alpha_{1x} c_2 \quad (26)$$

$$E_z = \Delta z + \varepsilon_{zz} + \varepsilon_{yz} + \alpha_{1x} y + \sum \Delta c_i - (\beta_{1x} + \beta_{2y}) a_3 + \alpha_{1x} b_2 \quad (27)$$

where $\Delta j$ is the linear error of axis j, $\varepsilon_{ij}$ is the straightness error of axis of motion j in the direction of axis i, $a_i$, $b_i$, and $c_i$ are lengths of elements of the CMM in the direction of axes X, Y, and Z respectively. The subscript number is the element reference frame number. The angular errors are represented by the roll, pitch, and yaw angles ($\alpha$, $\beta$, and $\gamma$) where $\alpha_{ij}$ is the effect of angular error in axis j caused by rotation of axis i. Angular errors also include the squareness errors.

Building the models in two stages allowed the inclusion of kinematic and geometric errors alone at one stage and then the thermal effects at a separate stage which in turn facilitated the detailed verification of the models. The models were tested at both stages experimentally using the ASME B.89 standard performance evaluation of the CMM. For the first stage, the ambient thermal state of the CMM was maintained constant. In the second stage, the ambient thermal state of the CMM was randomly disturbed during the test to verify

the model effectiveness. Results of these tests are presented and discussed in chapter 5.

## 4.3 Error functions identification

To fully utilize the model, the error functions had to be determined. These were obtained experimentally for both stages through the use of laser interferometry. For the reference thermal state, the laser measurements produce sets of data for each error function where the carriage position on the axis tested is the input to the model and the error is the output. To find the model coefficient values corresponding to the position of the end effector in the work space, piecewise linear interpolation is applied to the data sets obtained. For the stage of incorporating the thermal changes, the calibration procedure was repeated at different thermal states. Results collected in this process will be presented in chapter 5. Consequently, each error function becomes a function of both position and thermal state. Some error functions are direct functions of the temperature state while others are functions of the temperature gradients. Theoretical models of the error functions were verified and completed using the experimental results. The final general error models were then formulated for the compensation to be applied and tested.

## 4.4 Inverse kinematics model determination

The inverse of the kinematic model can be used to produce the commanded positions of the end effector for contouring. The ideal inverse kinematics model can be obtained by direct inversion of the ideal forward kinematics model. For the actual model, multi nonlinear

regression analysis was proposed as a solution for the inversion problem and carried out. At the first stage, the calibration positions and their associated error vectors at the reference thermal state were used to produce data to build the inverse kinematics. The input positions were taken as the calibration positions to reduce the errors resulting from interpolation and use actually measured values of the error functions. These combinations produced 7462 position vectors and their corresponding volumetric errors. In the second stage, repeating this procedure for each thermal state produced the corresponding matrix of error data. Using these sets, the regression procedure was applied to find a model representing the effect of thermal changes on each error function in the inverse kinematics model, and build the state observer. A partial group of data equivalent to 10 % of the calibration data and their corresponding errors were split randomly and taken into a new group as the verification set for each thermal state. This verification set did not contribute to the construction of the inverse kinematics model and were used after the model was built to independently verify the model. This is in accordance with the statistical principles to verify the model performance in the proper confidence intervals. The rest of the data were used for the nonlinear regression fit combined with the ANOVA technique to build the inverse kinematics model. The output of the inverse kinematic model were vectors of the commanded positions. To choose the proper order of the regression model, the principle of parsimony was followed. This is in spite of the fact that in polynomials regression the higher the degree of the polynomial the better representation and less error is present in the data. Until the optimum value is reached which is the degree n equals N-1 where n is the

polynomial order and N is the number of data sets available. This is the polynomial of exact match that contains all the data used for fitting. On the other hand, this will produce a high degree, computationally expensive, equation. The answer to proper choice of regression order was to use the statistics based analysis of variance (ANOVA). The degree of the fitting equation is increased gradually as long as there is a statistically significant decrease in the variance, $\sigma^2$, which is computed by equation (28). This indicates a decrease in the error of fitting:

$$\sigma^2 = \frac{\sum e_i^2}{N-n-1} \qquad \textbf{(28)}$$

The variance was calculated for each order throughout the tests. The fitted models were also tested using the verification set of data which was randomly selected and isolated and did not contribute to the construction of the model. These calculations for fitting were carried out to the $15^{th}$ order using a computer program. The results are represented in table 3. The volumetric error, which is the vector summation of the individual axes errors at the test point in space, was considered to be the variable of interest. Second order regression produced the most favourable of the results among the 15 orders of regression. The selection was based on the significant decrease in the variance value combined with the degree of complexity introduced by the selected fitting order will introduce. Once these tests were finished and the regression fit of the data proved to have minimum errors, the inverse kinematic model was built based on these results. The final inverse kinematics model has the following form:

$$[P_c] = \begin{bmatrix} a_1 & a_2 & a_3 \\ b_1 & b_2 & b_3 \\ c_1 & c_2 & c_3 \end{bmatrix} \left[ [P_a]^T [P_a] \right] + \begin{bmatrix} a_4 & a_5 & a_6 \\ b_4 & b_5 & b_6 \\ c_4 & c_5 & c_6 \end{bmatrix} [P_a] + \begin{bmatrix} a_7 \\ b_7 \\ c_7 \end{bmatrix} \quad \textbf{(29)}$$

In this equation, each [P] is as follows:

$$[P] = [x \quad y \quad z]^T \quad \textbf{(30)}$$

Where $[P_c]$ is the position that should be commanded or fed forward to the machine, $[P_a]$ is the position desired by the operator for the end effector to be at. The variables $\{a_i, b_i, \text{and } c_i\}$ are the coefficients of the model found by regression. To test the performance of this model, and its robustness, a contouring process of diagonal paths in the CMM work-space through simulation was carried out. Positions desired and produced by both the ideal and proposed inverse kinematics models, were fed to the machine forward kinematics model combined with the error model, at different temperatures ranging between 6° and 35° C. The resulting positions are the real ones that the end effector will be in. Volumetric errors between these positions and the desired positions were calculated and monitored. In the second stage, the inverse kinematic model was built based on the above mentioned procedure for each thermal state individually. Following, a regression analysis was performed for the coefficients {a, b, c} as a function of thermal state. The result is the state observer model.

The resulting functions compose the state observer model. Using the state observer, the model was tuned again through a set of simulations to arrive at the values of coefficients producing the best results.

Finally, thermal changes were incorporated in the general model and a new set of simulations was carried out. The use of computer software allowed the automation of this process. Further investigation and testing should be carried out to transfer the obtained models into the real system. Chapter 5 presents the numerical results of the previously mentioned processes. Favourable results were obtained reducing the contouring errors to less than 1 % of the original error values.

**Table 3** ANOVA technique application to the regression model using residual errors and a set of independent testing data.

| **Order of Regression** | **Fitting Residuals Volumetric Error Variance** | **Test Data Volumetric Error Variance** |
|---|---|---|
| 1 | 2.63e-07 | 4.30e-06 |
| 2 | 3.06e-07 | 4.28e-06 |
| 3 | 3.15e-07 | 4.57e-06 |

## 4.5 Rapid CMM error detection

A preliminary step in applying quasi-static error compensation for a CMM is to investigate the existence of errors. The size of the existing error can roughly indicate their

sources and accordingly a proper approach to correct these errors can be chosen. As an example, errors of a large magnitude indicate major problems in the machine parts and their mutual alignment. Errors of this type normally call for a major maintenance procedure to be applied for them to be corrected.

CMM errors can occur for different reasons. The circular contour test using a commercial ring gauge can be used to rapidly detect these errors, especially the geometric ones. This approach is useful for frequent CMM maintenance and performance verification. A ring gauge is made of hardened gauge steel and it normally has an inner circle ground and polished to a high degree of accuracy.

Assuming measurements of the gauge in the X-Y plane are carried out in the automated mode (direct computer control, DCC), this will guarantee measurements with an optimum constant speed and in a direction normal to the surface. For an error free machine, or if machine errors are in the range of the probe usual errors (i.e. lobing errors), the measured ring data would be identical to the original ring shape plus the these minor errors. If one of the axes (e.g. X-axis) moves a shorter distance than a perpendicular axis, the fitted measurements profile would form an ellipse with its longer axis in the direction of the longer machine moving axis (e.g. Y-axis). Figure 16 demonstrates this concept.

On the other hand, the squareness error between the two perpendicular axes causes the measurements profile to be shaped like an ellipse with its axes inclined by 45° from the two major axes (e.g. X, and Y). A simulation of a squareness error of less than 0.1° between the X and Y axes is shown by a polar plot in Figure 17. Combinations of these errors would

affect the form, location and inclination of the circle fitted to the measured points.

As an example, the "DEA IOTA 1102," which is under investigation was tested using a commercial ring gauge. The ring diameter is 71.1216 mm while the CMM measuring volume is 1000 x 500 x 500 $cm^3$. The lobing error of the probe used by this machine has been measured previously using a calibration sphere. Chan (1997) reported the three lobing patterns to have a maximum of 6 micrometers. With this data provided, points were measured in the automated mode from the inner circle of the ring and the form error in the X-Y plane was plotted against the simulation results in Figure 17. Similar measurements were carried out for the other two planes. From Figure 17 results, alone, it can be concluded

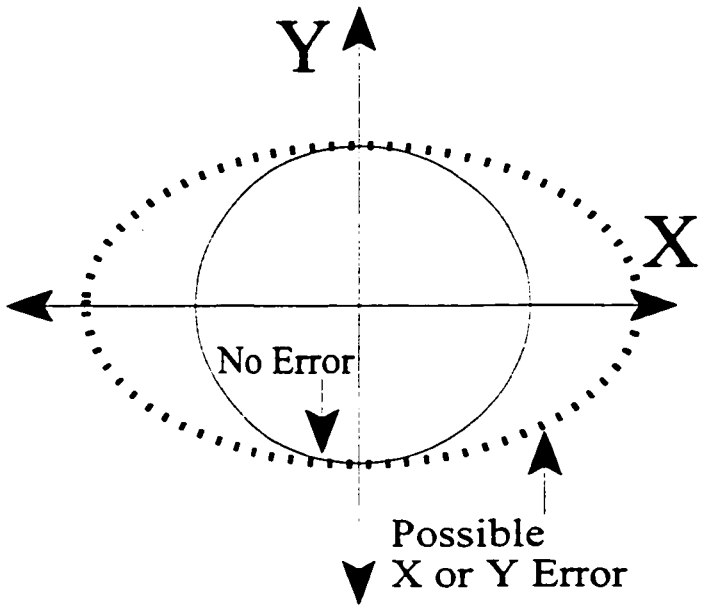


**Figure 16** Example of ring gauge measurements results in the case of an error existing in X or Y direction.

that the CMM investigated has a major error, which is easily detected by one measurement round of the relatively simple commercial ring gauge described. In addition, this reported detection was conducted only at one thermal state, other thermal states would provide different results. The magnitude of the measured data error is almost four times the lobing error. Moreover, this error is very likely to be a squareness error, and therefore, a simple re-calibration of the CMM will not be sufficient to correct for these errors. Assuming the physical parts of the CMM (e.g. bearings adjustments) to be free of defects, correction for these errors can be achieved through compensation.

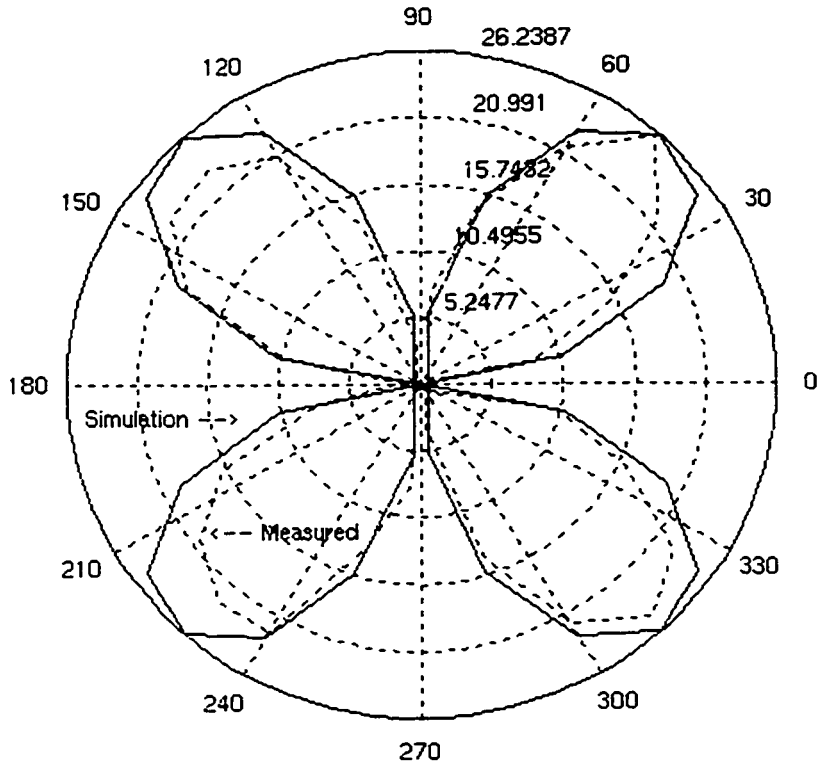


**Figure 17** Real measurements vs. Simulation of ring squareness error of less than 0.1°.

## 4.6 Experimental setup

To carry out the experimental part of this thesis, a special setup was prepared. The laboratory experiments served two purposes. The first purpose is to provide actual values of the model error functions at different thermal states. This was a necessary step to complete the models and employ the proposed compensation and control strategy to real situations. The second purpose was to verify and visualize the degree of effectiveness of the produced model and proposed compensation strategy.

To facilitate the control of the thermal state of the CMM environment, a special setup was introduced to the laboratory containing the CMM. An extra wall with proper insulation was built to separate the section containing the CMM. Moreover, an insulation board was installed over the window. Coupled with the ability to control exhaust and intake air to the laboratory, the CMM area was brought to a level were it can hold a certain thermal state for a period of time longer than usual and enough to do the testing.

Two external commercial heaters that have a power rating of 1500 Watt each were added into the lab and used in different combinations with the air exhaust system to introduce different thermal states to the testing area. The heaters control circuitry was modified to allow an external controller to be introduced. In addition, two de-humidifiers were also added to the testing area to keep the relative humidity at the desired level of 50%.

An external control box containing a thermal controller was built and used to control the heaters. The thermal controller was a precision temperature controller to the level of 0.1° C. Details of the circuit diagram and the schematics of the control box are provided in

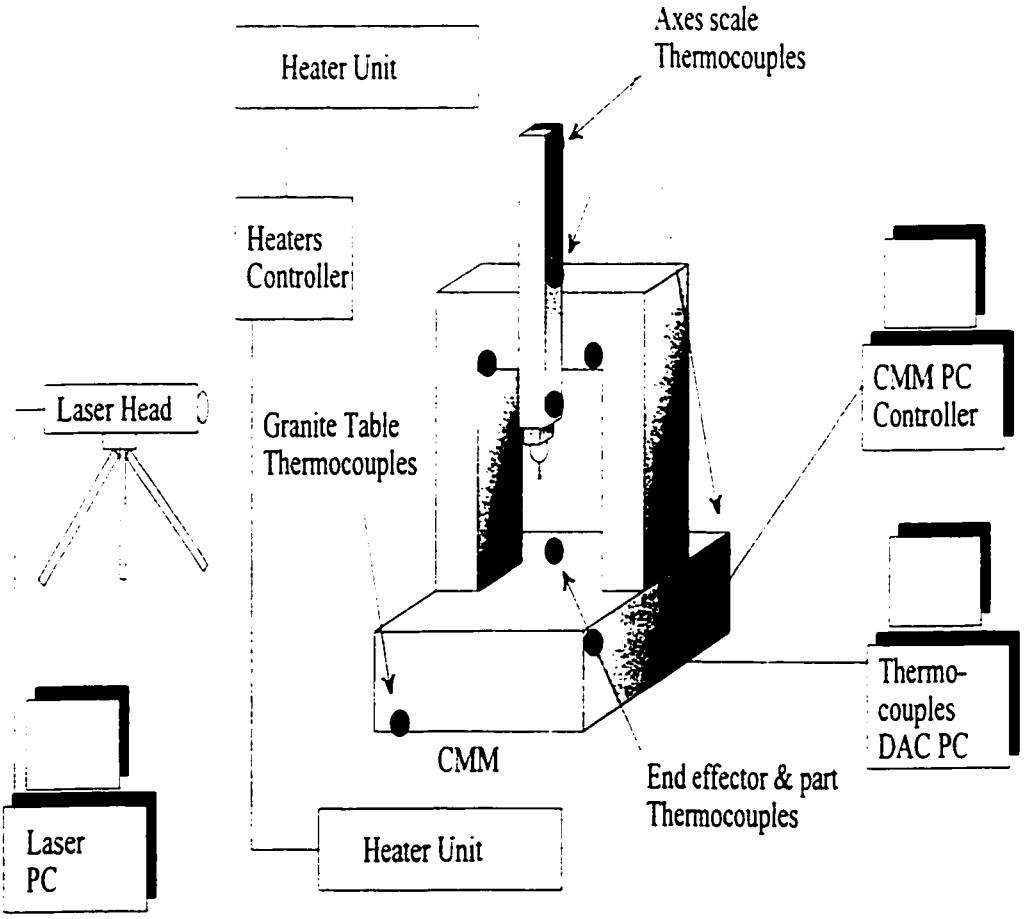


**Figure 18** Schematics of the experimental setup used to measure the error functions by laser and monitor the thermal state of the CMM using a set of sensors.

Appendix D.

To measure the temperature of the CMM, thermocouples were installed in strategic locations of the machine structure. These sensors were chosen of the "E" type thermocouples based on a recommendation by Veldhuis (1998). The locations of the sensors were selected based on the understanding of the physics of thermal behavior of the CMM. The basic criteria was to select sensor locations which are not redundant, while acquiring

most useful information. Moreover, this selection was guided by analogy to reported studies by Veldhuis and Elbestawi, (1998), and Bosch (1995). As a result, 12 sensors were distributed over the CMM as in figure 10. Each axis scale had three sensors, in addition to a sensor at the upper rear corner of the granite table and another one on the opposing corner. The last sensor was installed very close to the end effector and the point touched of the measured part. These sensors were connected to a data acquisition system (DAS) consisting of an electronic data board installed in a Personal Computer (PC). Schematics of the complete system are presented in figure 18. Laser interferometry was the main measuring device employed in the experimental stage. An HP laser was used to measure the position and angular changes. The laser was read through an interface setup to a PC involving the use of a standard GPIB card. The laser interferometer used had a built in capability to compensate for environmental changes effect on its wave length.

## 4.7 Summary

This chapter described the compensation strategy set to carry out the CMM error correction process. This strategy is based on the knowledge of the error model presented in the previous chapter. Using this error model, an estimation can be given for the measurement error associated with any position in the CMM work volume.

The error functions forming the model are continuously modified to account for the thermal state of the CMM. In case of contouring, a state observer is employed to update the model continuously based on the thermal state. Systematic modelling was approached in two

stages. The first stage included errors excluding the thermal state and resulting errors. The second stage incorporated the thermal errors and effects.

Rapid error detection of the CMM was also described and carried out to provide a practical approach for observing errors in the shop floor. The experimental setup necessary to carry out all the related measurements was also described in detail. This included the CMM and environment controlling equipment.

Chapter Five

# Implementation and Results Analysis (I):

## Constant Thermal State

The proposed solution for the CMM error correction consists of three main steps. These steps are: modelling, identification, and compensation for the machine errors. Chapters five and six present the details of the actual experimental steps that were carried out to achieve the CMM error compensation. They also include an analysis of the results of these experiments. Quasi-static errors compensation of the CMM was tested in two stages. The first stage included the kinematic and geometric errors of the machine excluding the thermal effects through having a constant thermal state. The results of this stage are presented and discussed in the present chapter. The second stage involved the incorporation of the thermal effects in the error modelling and compensation process. The following chapter presents the details of the experiments carried out for that stage as well as

the analysis of its results.

## 5.1 Experimentation plan

The plan for carrying out the experiments included two major goals to be achieved. The first goal was to measure and identify the error functions of the models. The second goal was to test and validate the proposed strategy for CMM error compensation in both measurement and contouring. A combination of simulations and experimental methods was carried out for verification, depending on equipment availability. Error functions of the CMM were measured by laser interferometry, in a constant thermal state. The performance of the CMM was evaluated based on the ASME B.89 standard test. This test involved the use of a ball bar as a testing artifact. For the contouring performance testing of the machine, a simulation of the machine in tracking selected trajectories in its work volume was carried out. This is because of the limitations in availability of the proper equipment for the CMM under investigation, to carry out the contouring tests.

## 5.2 Coefficient of thermal expansion determination

Incorporation of thermal changes in the models requires the knowledge of the Effective Coefficient of Thermal Expansion (ECTE) of the machine elements. The literature provides empirical values for the ECTE for different materials (Sydney, 66). For the CMM under investigation, two of its scales are mounted on the bridge, which is mainly made of a steel alloy, and one scale is mounted on the granite table. The ECTE of the bridge was

measured experimentally. This is to find out the realistic value of the ECTE for an element formed of more than one material, especially if the scale bonded to it, which is made of glass, is considered. The procedure consisted of changing the temperature by a known amount for a measurable part of the machine bridge and measuring the change in dimensions on that part, as read by the scale encoder. This experiment included using the CMM to carry out measurements in normal conditions and then in warm conditions, while the temperature was monitored throughout using thermocouples of the "E" type surrounding the element under testing. Geometric relations were used to analyse a unidirectional error and arrive at the ECTE of the CMM material. The thermo-mechanical model used was explained in equation (17) of chapter 3. The combination of the bridge and ram is made mainly of steel, with the two different material scales attached to each of them. From the literature, the reported ECTE of steel is 12 PPM/°K (Part per Million per degree Kelvin), while the ECTE for the granite is 4.5 PPM/°K (Sydney, 1966). Measurements were conducted for a 100.000 mm long gauge block at a room temperature of 22.0° C, by the CMM in the Z direction. The measurements were recorded at 25 different locations of the X and Y plane, forming a matrix covering a large portion of the measuring table of the machine. The ample of measurements was necessary to produce a reliable average value. Further, a monitored part of one arm of the CMM bridge was artificially heated by means of an electric blanket wrapped around the arm, while having thermocouples installed on the arm part investigated at carefully selected points and equally displaced to read the thermal state changes of the arm. Data were collected from the thermocouples through a data acquisition system (DAS) set up in a

separate PC. Interface was arranged for the PC to collect data from the sensors directly through the DAS every 5 minutes throughout the period of measurement in both normal and warm conditions. Heating was applied until the temperature settled and the final measurements were carried out while the machine arm is warm. The same 25 locations of the gauge block in X and Y were used to repeat the measurements of the Z direction reading of the machine at warm conditions for the gauge block length at room temperature of 22° C. The experimental setup is shown by figure 19. Figure 20 represents a sample of one thermocouple reading during both the normal conditions and the warm conditions. Figure 21 represents the results of the gauge block length measurements as a function of position change along the Y axis, where every data point is an average of all five measurements along the X axis at that particular Y position. Figure 22 represents the measurement errors between the two thermal states along the Y axis. This is the axis along which the bridge extends. Temperature of the part of the arm under investigation is measured by the thermocouples. The dimensional change of the arm was found by using the thermo-mechanical model presented in equation (17) from chapter 3. Calculating the average temperature for the arm along the affected length produced a value of 28.6° C. This results in a difference in temperature between the room temperature and the CMM column of 6.6° C. These results were used to back calculate the ECTE of the column material ($\alpha$). The affected length of the column is 840 mm. As in figure 19, and from the geometry of the machine, the relation between the measurement error of the gauge block and the expansion in the heated part can be approximated as follows:

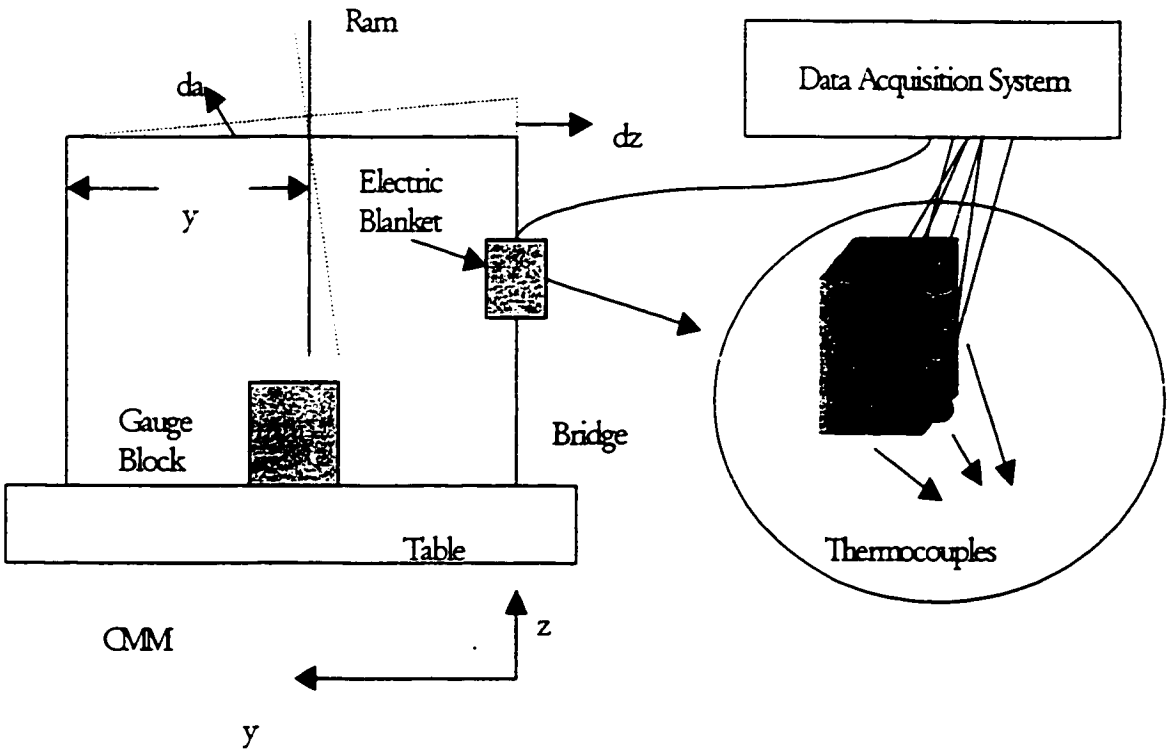


**Figure 19** Schematics of the experimental setup to find the ECTE.

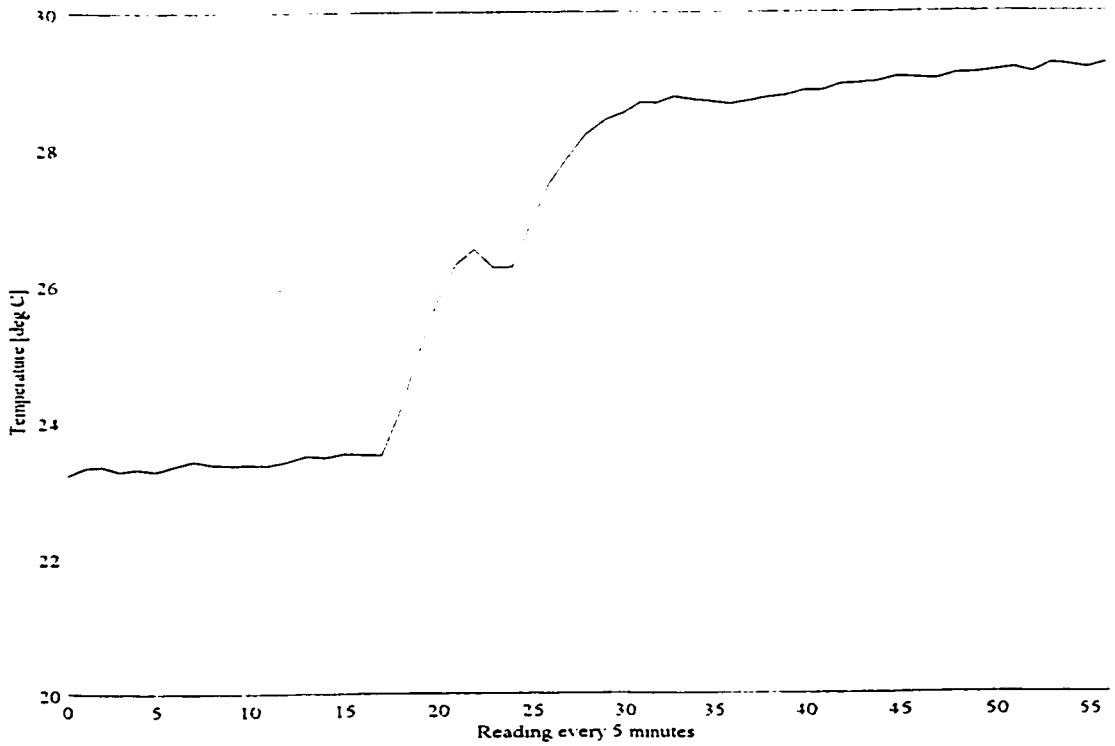


**Figure 20** Thermocouple data collected by the DAS.

$$dZ = Y.d\theta \tag{31}$$

For dZ in a constant thermal state, and Y=Y max - Y measured, $d\theta$ can be found by carrying out different measurements of Y measured and dZ. Using the data represented by figure 22, the relation becomes as in equation (28):

$$dZ = a + b.dY \tag{32}$$

where, by linear regression approximation, a = 0.0153576, b = 0.0000576, dY and dZ are in mm. This relation can be used to find the expansion in the column being tested. Substituting back in equation (13), a value of $\alpha$ = 9.5238 PPM/°K is determined. This value is close to the literature reported value of the steel coefficient of thermal expansion. The difference can be explained by the fact that the bridge of the CMM is a combination of materials in addition to steel, which is the major component, as well as the scales being glass, which has an ECTE of almost 6 PPM/°K. Some minor uncertainty in the calculated ECTE value can be explained by the fact that an approximation of linearity for this geometric relation was considered which is widely used when the swept angle is relatively very small !

## 5.3 Measurement errors correction

The forward kinematics model representing the CMM behaviour in equations (19, 20 and 21) and the final error model in equation (2) were formulated. The error functions of the forward kinematics model were evaluated using two different methods. The first was through analysis of measurement of a standard artifact and the second was through using

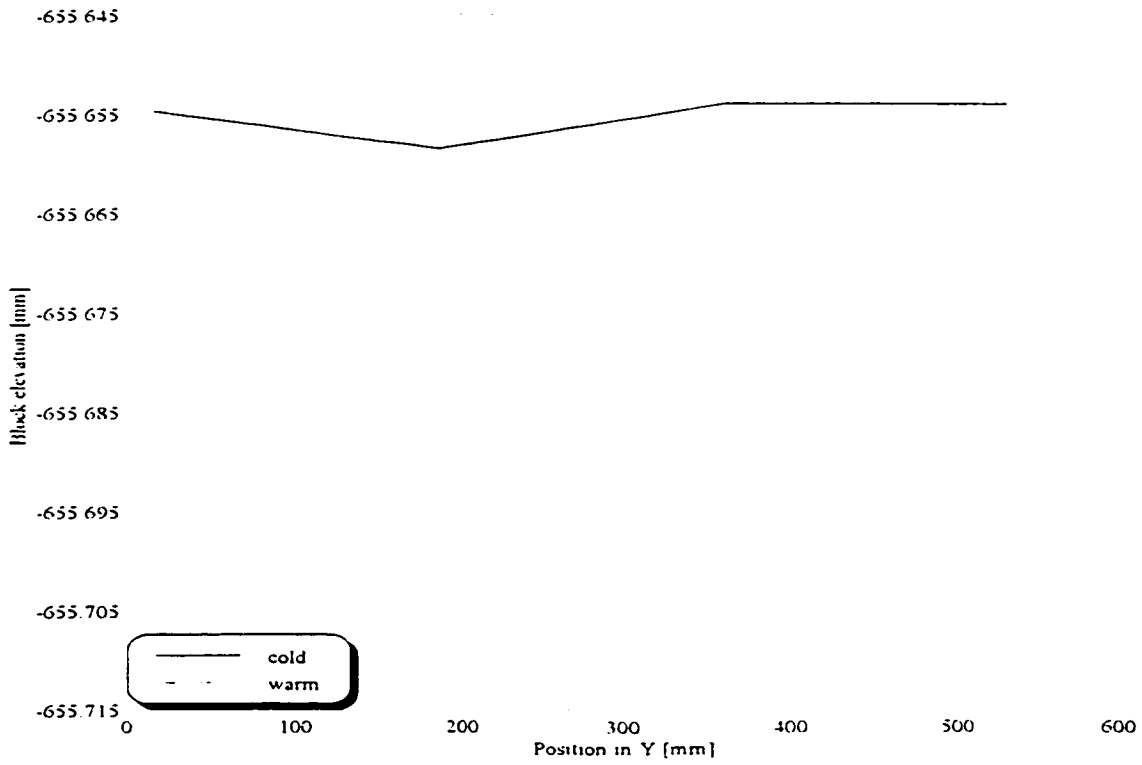


**Figure 21** Average block elevation measured in positions along the Y-axis.

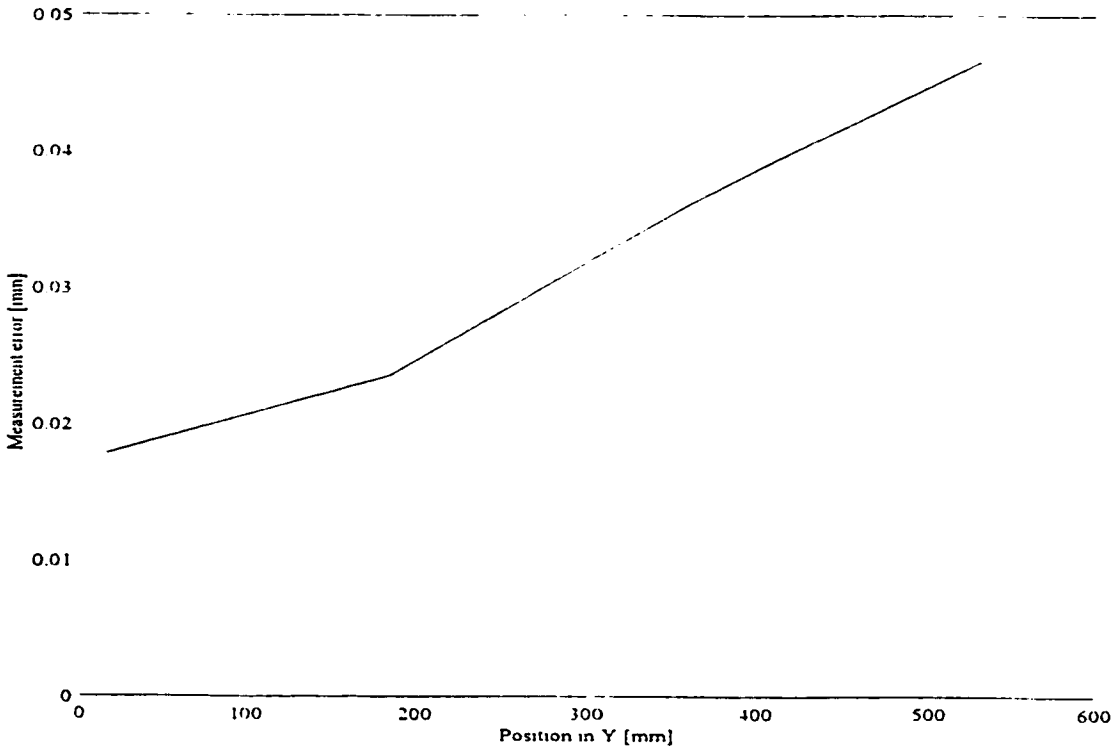


**Figure 22** Discrepancy in block elevation measurement, along the Y axis.

direct measurement by applying laser interferometry. Details of this evaluation are presented next. Following the error functions measurement, the error model was formulated and used for measurement error compensation. The standard ASME B.89 performance evaluation test was carried out for the CMM. Particulars of the test and the locations of the ball bar are presented in Appendix A. Results before and after application of the proposed compensation strategy, of the CMM performance, are presented next. Minimization of the thermal error factor was attempted by collecting the data during the most stable ambient conditions possible.

### 5.3.1 Error functions identification using a standard artifact

To evaluate the volumetric error as a function of position in the work space of the CMM, the model error functions were evaluated. The literature provides a variety of methods to carry out error functions evaluation. The first method incorporated the use of the error in measurements of a simple standard artifact in conjunction with statistical analysis methods. The error in each individual axis direction occurring when measuring a ring gauge radius was isolated and calculated by measuring the ring gauge radius at local positions in a structured lattice. This was achieved by repeating the process three times at each measuring position. Twice in the automated mode (DCC) in addition to the manual first measurement for each point. This was carried out in order to:

1. Reduce the possibility of errors occurring from manual measurement procedure.
2. Achieve repeatability in the results obtained.

3. Ensure measurements of the radius are in the axes directions which in turn results in the least cosine errors possible.

4. Locate the nominal centre of the ring gauge.

At each point, the ring gauge radius was measured four times in directions matching the major axes directions, and the average was compared to the original manufacturer specified diameter (2.80005"). The obtained results are averaged to give a local error value at the nominal centre point of the ring positions in all directions. According to Teeuwsen et al., (1989), multiple measurements have to be carried out to obtain good estimation of the error, which is in agreement with the principles of statistical analysis. To ensure environmental stability and reduce the thermal error effect, all the experiments were performed at a chosen time where the environment surrounding the CMM was stable and the ambient temperature is at 21° C throughout. The CMM was moved and in operation for enough time before the measurements were taken to ensure its temperature stability and resemblance to operating conditions. Figure 23 shows the measuring positions projection in the X-Y plane , and figure 24 shows the projection in the Y-Z plane. Results of the volumetric errors obtained are statistically sampled and averaged. In this method, the error in X direction at an X position is the average of all the error in X measurements positioned in the Y-Z plane corresponding to this X position, which makes the sample become an average of 20 data points. This applies also to the rest of the results. Errors as a function of Y position are averages of 36 data points and errors as a function of Z position are averages of 45 data points. A sample of the results obtained is presented in figure 25 which shows the error along the X-axis. This error

function is known as the linear or position error ($\Delta$ axis). The full set of results obtained for all axes is presented in Appendix E. Figure 26 presents another sample which is the error in X-direction as a function of position in Y-axis. The rate of change of the errors in figures 27 and the like are used to calculate the squareness errors between the relevant axes. They are also used to find the angular and straightness errors in the corresponding axes. These functions require processing of the obtained data, before they can be individually separated. This is because the observed and measured error is a localized and not a cumulative error. The same is applied to the rest of the obtained results.

As a result of these findings, the error model coefficients can be evaluated and applied to error compensation and correction. However, some of these error functions are a measurement of a combination of more than one error which could not be individually separated any further. Therefore, details about some of the individual errors affecting the CMM performance were impossible to obtain using this method.

Because of the localized nature of the error functions values obtained, the model coefficients were based on regression analysis of the error functions point values. Regression, as well as, interpolation were applied to this data to arrive at the best curve fit for purposes of continuation, automation, and comparison of results. Linear approximation and curvilinear approximation are referred to as $1^{st}$ order and $2^{nd}$ order in the figures. The final model based on these results is called the "artifact model" for the purpose of this thesis. The fitting of the data produced three types of the artifact model: a $1^{st}$ order model, a $2^{nd}$ order model, and an interpolation model.

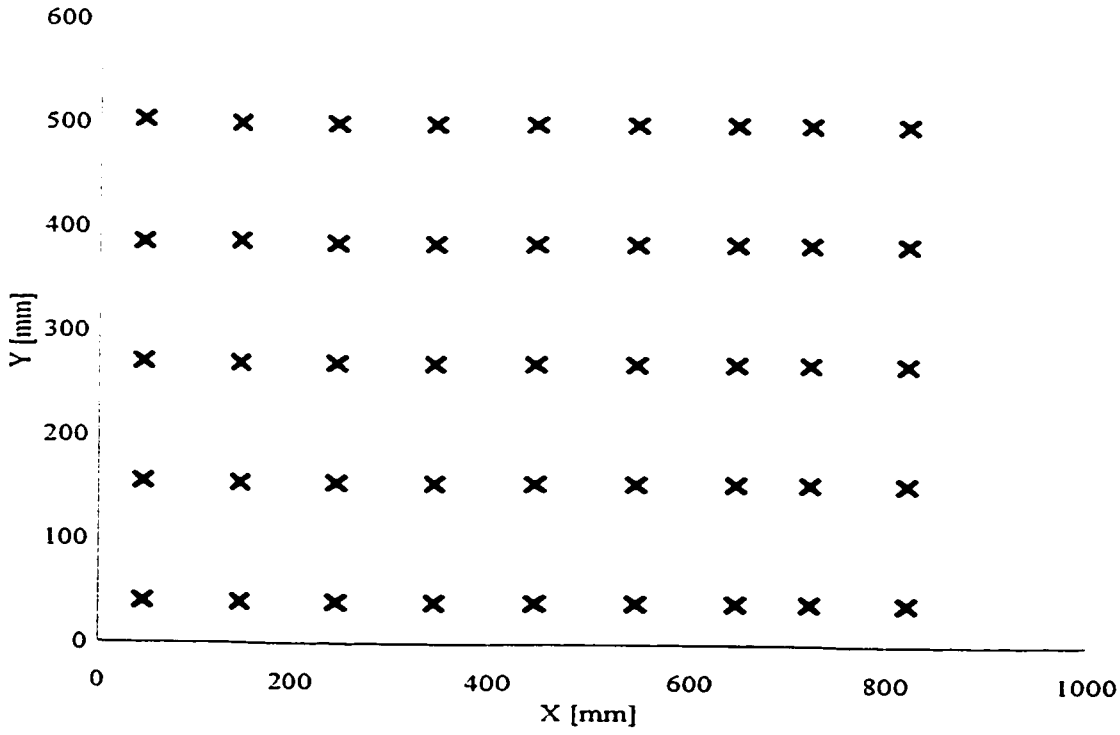


**Figure 23** Projections of the lattice measuring positions in the X-Y plane.

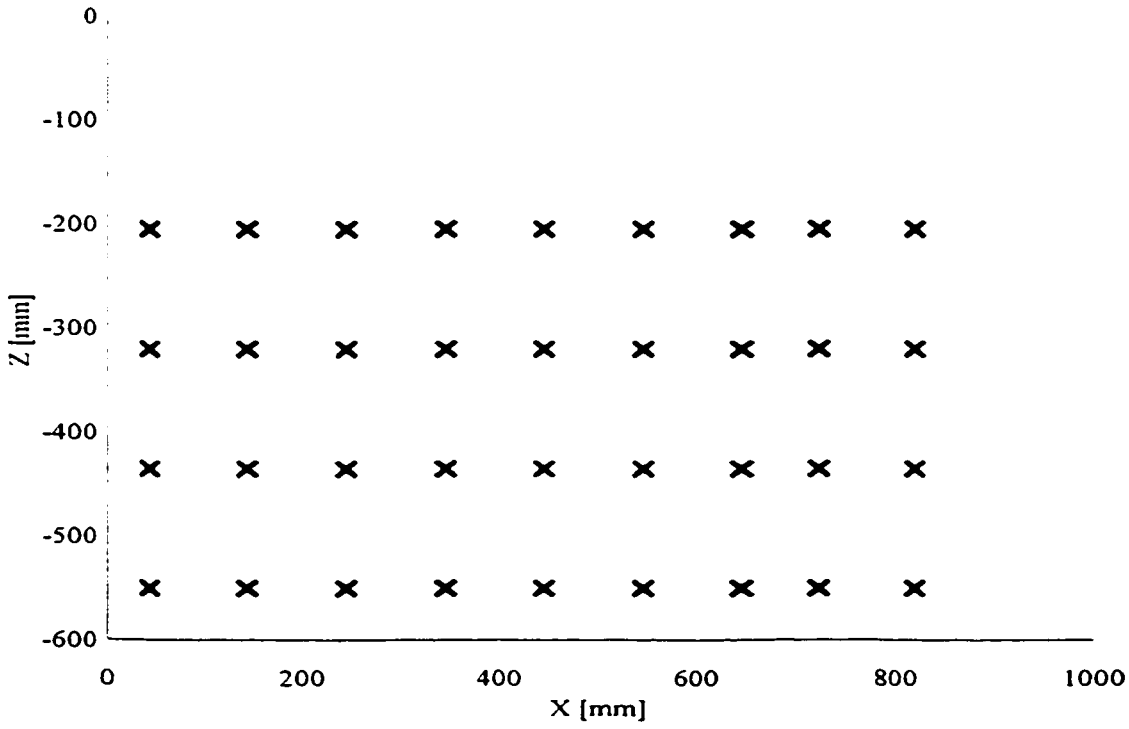


**Figure 24** Projection of the lattice measuring positions in the X-Z plane.

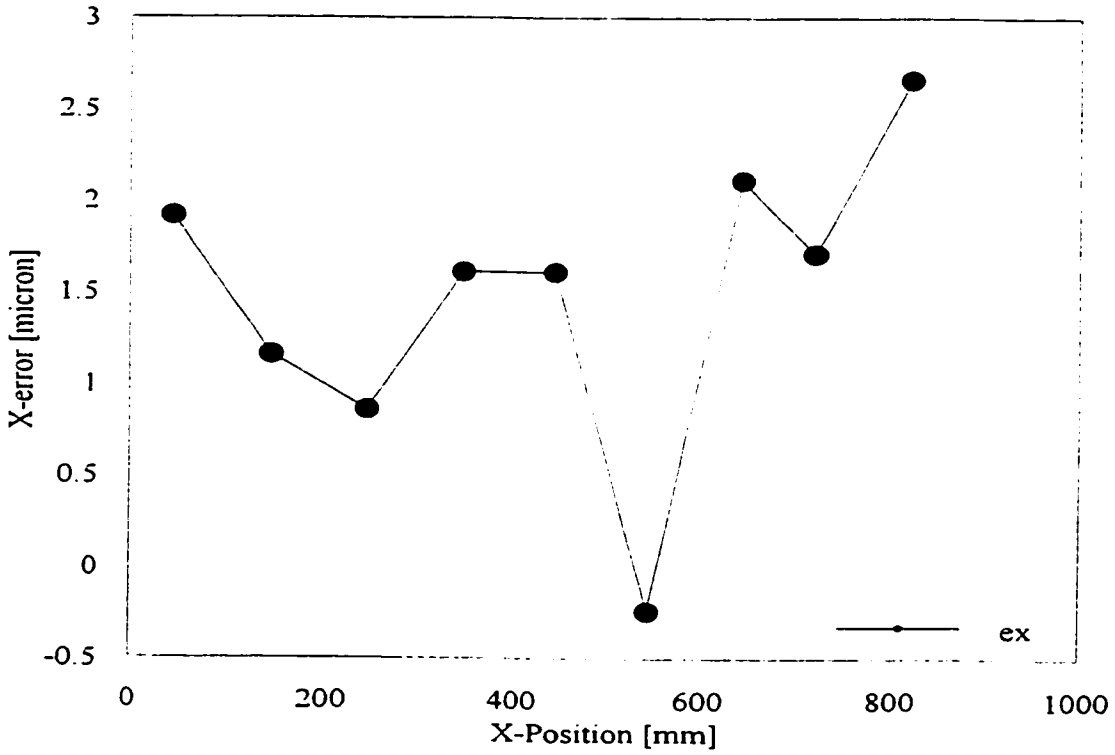


**Figure 25** Error in the X-axis measurement as a function of position in the X-axis.

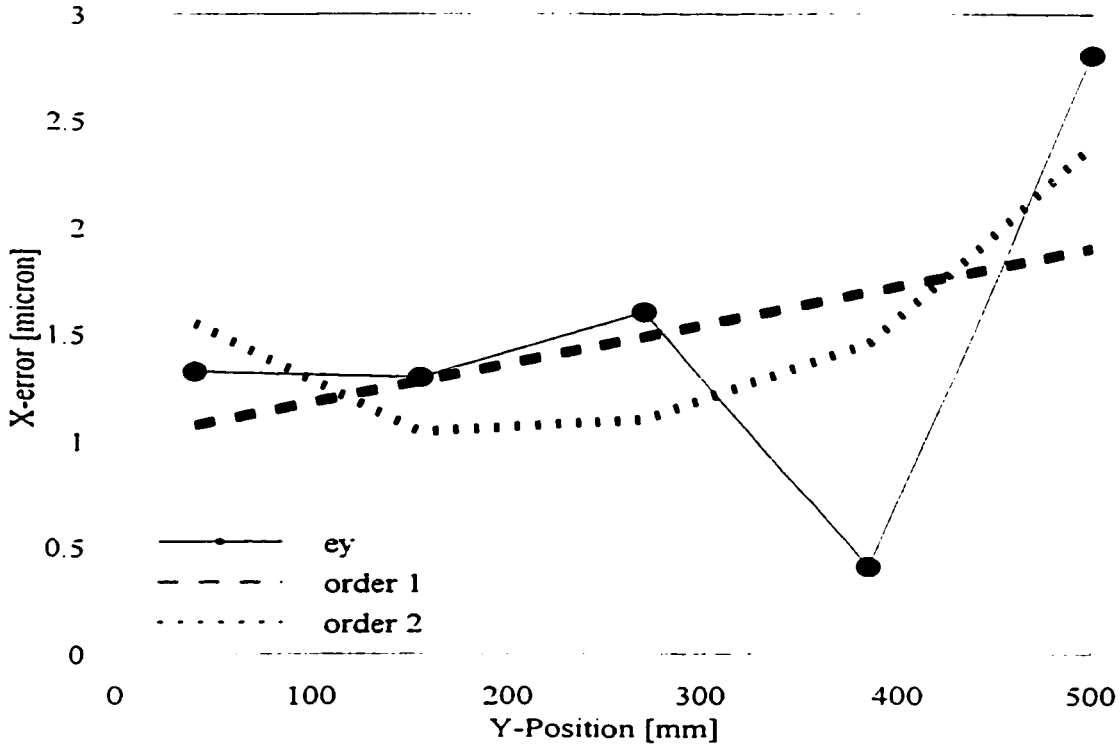


**Figure 26** Error in the X-axis measurement as a function of Position along the Y-axis.

These types are based on the regression polynomial used for the first two and on the idea of interpolation between known points for the third type. The results obtained suggest the existence of a squareness error, roll error (where the rate of change of error in one axis is a direct function of the position in another axis), and linear errors.

### 5.3.2 Error functions identification using laser measurements

A second method employing laser interferometry was also applied to evaluate the error functions of the machine. An H-P Helium-Neon laser with a set of optic lenses and mirrors is used to measure the individual error functions of the CMM as a function of the end effector position in the work volume. This method was suggested by the literature as being expensive but capable of providing values for each individual error function of the 21 errors that could exist in the CMM. Individual errors in the CMM were measured and the results obtained are presented in Appendix F. Figure 27 presents a sample of these results which is the position error in microns in the direction of the X-axis. Figure 28 presents another sample of the results which is the angular error of the X-Y plane roll. In addition, the squareness angles were measured using the ball bar and were found to be (297.7547 arcsec) for the X-Y angle, (39.3506 arcsec) for the Y-Z angle, and (-19.24 arcsec) for the Z-X angle. Remarkably, no roll angles along the axes were detected. Based on the information provided by these figures the model coefficient were obtained. It is worth mentioning here that no data processing is involved here since the laser measurements provide direct values for the individual errors in the relevant axes.

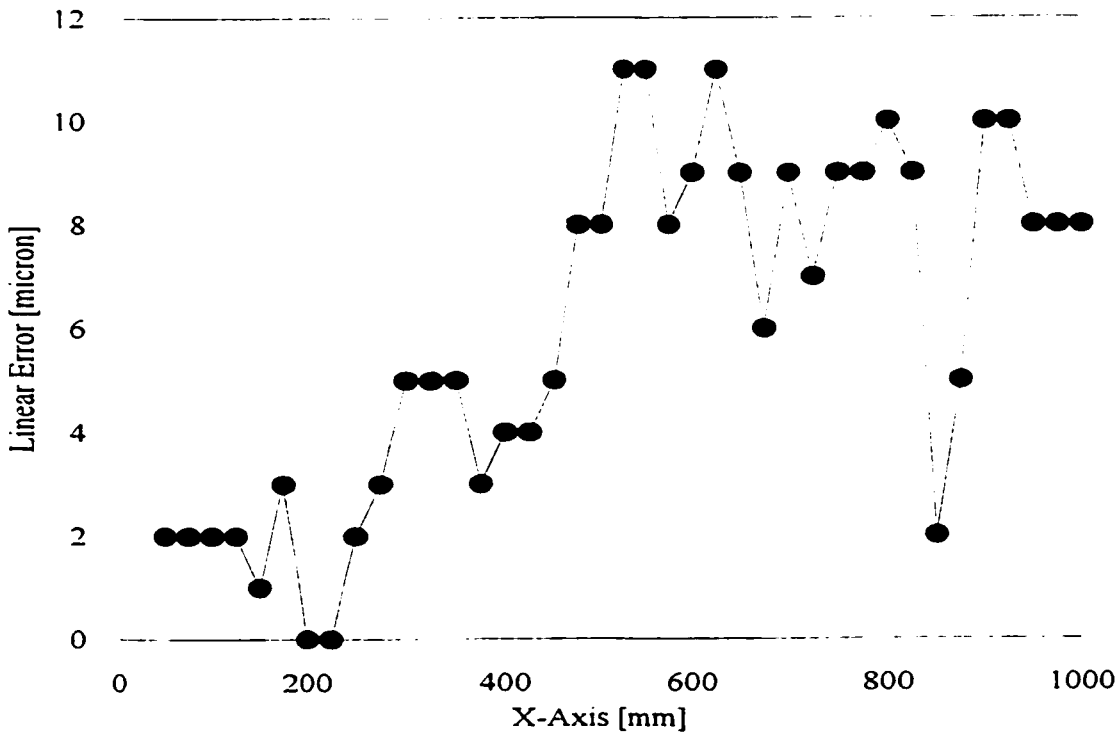


**Figure 27** Linear Error in X-axis Using Laser Measurements.

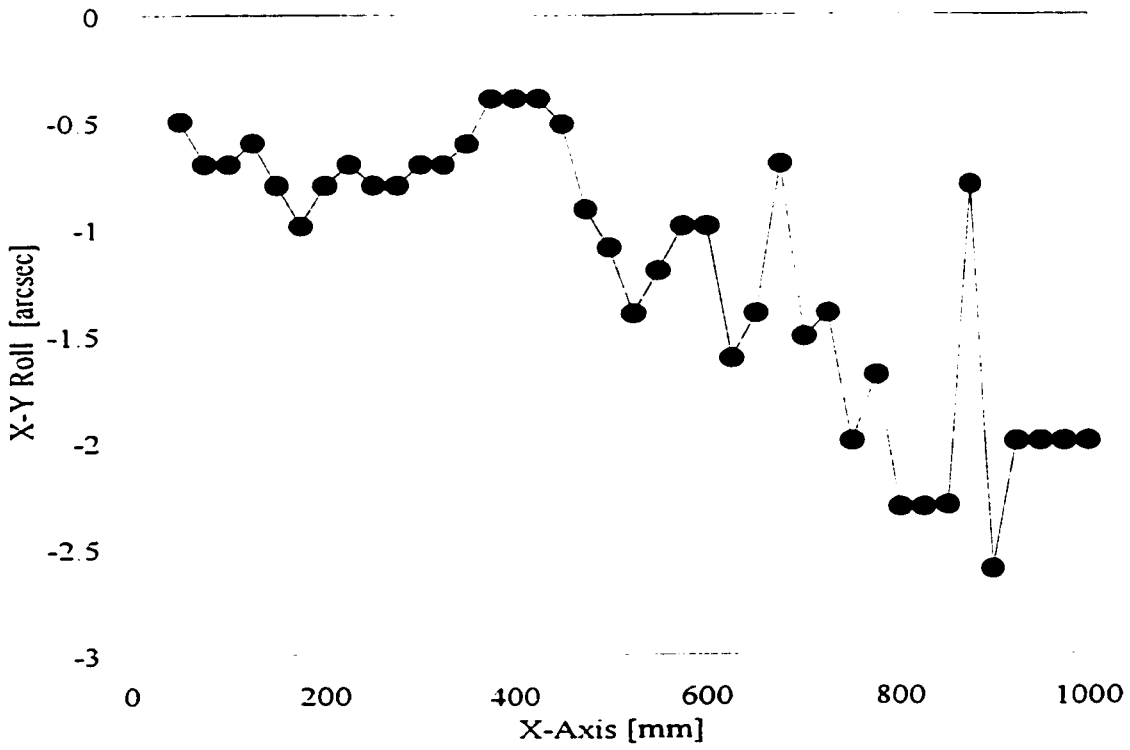


**Figure 28** X-Y Roll Angle Using Laser Measurements.

Laser measurements are automatically corrected for, because of the environmental influence on the wave length, in terms of temperature and humidity. The data obtained here also confirm the facts suggested by the previous method and provide more insight into their details. These facts include the major effect of squareness errors and the existence of angular and linear errors. The final error model based on these results is called the "laser model" for the purpose of this thesis.

### 5.3.3 Compensation using the artifact based model

The length of a standard ball-bar artifact was measured at different locations and orientations distributed in the work space of the CMM. These locations and orientations were chosen in full compliance with the standard provided by the ASME B.89, for the machine volumetric performance evaluation testing procedure. A reproduction of the ball bar locations and orientations is provided in Appendix A. The resulting data was used to apply and evaluate the compensation strategy suggested above. According to the standard, the obtained length measurements of the ball-bar were compared to its nominal length and the discrepancies are calculated as the residual errors at the measurement in the relevant positions. Figure 29 presents these findings as per the recommended presentation of results by the ASME B.89. Using the volumetric error model to compensate for the error in the CMM measurements, figures 30, 31, and 32 are obtained. Figure 30 represents the residual errors in the ball-bar length when the coefficients resulting from linear regression are used. Figure 31 represents the residual errors when using the set of coefficients obtained by

curvilinear regression. Figure 32 represents residual errors when using the model in conjunction with interpolation to arrive at the final error vector value. Investigating figures 29 - 32, it can be seen that the value obtained for error in position number 26 and corrected by the models proposed, presents an outlier data point. Outliers occur among data due to different reasons including errors in data collection or sampling procedure. To eliminate this data point it has to be investigated as if it stands as an outlier or not. Appendix G includes a full statistical analysis and verification of this procedure. It was found that considering 95.5 % significance level for the data collected, the point under investigation still stands insignificant. Figure 33 shows the results after removal of this data point and table 4 summarizes a comparison between the results obtained using the different coefficients sets and the original error values.

**Table 1** Comparison of Results Obtained.

| Method | Error | 1st Order | 2nd Order | Interpolation |
|---|---|---|---|---|
| Mean | $4e10^{-15}$ | $4e10^{-16}$ | $-7e10^{-16}$ | $-3.4e10^{-16}$ |
| Std. Div. | 147.787 | 36.0481 | 35.9731 | 35.8503 |
| Variance | 21841 | 1299.5 | 1294.1 | 1285.2 |
| Working Tolerance | 670.067 | 169.5761 | 167.9564 | 168.6417 |
| % red. | N/A | 74.69 | 74.93 | 74.83 |

Investigating figures 12 - 17, it can be seen clearly that the major error in the CMM measurement is a result of its axes being out of squareness. When evaluating the error functions using the artifact (section 5.3.1), the error was measured in directions perpendicular to the position change axis. The existence of changes in error values in a suggested. The straightness and angular errors are therefore minor compared to the regular fashion supports

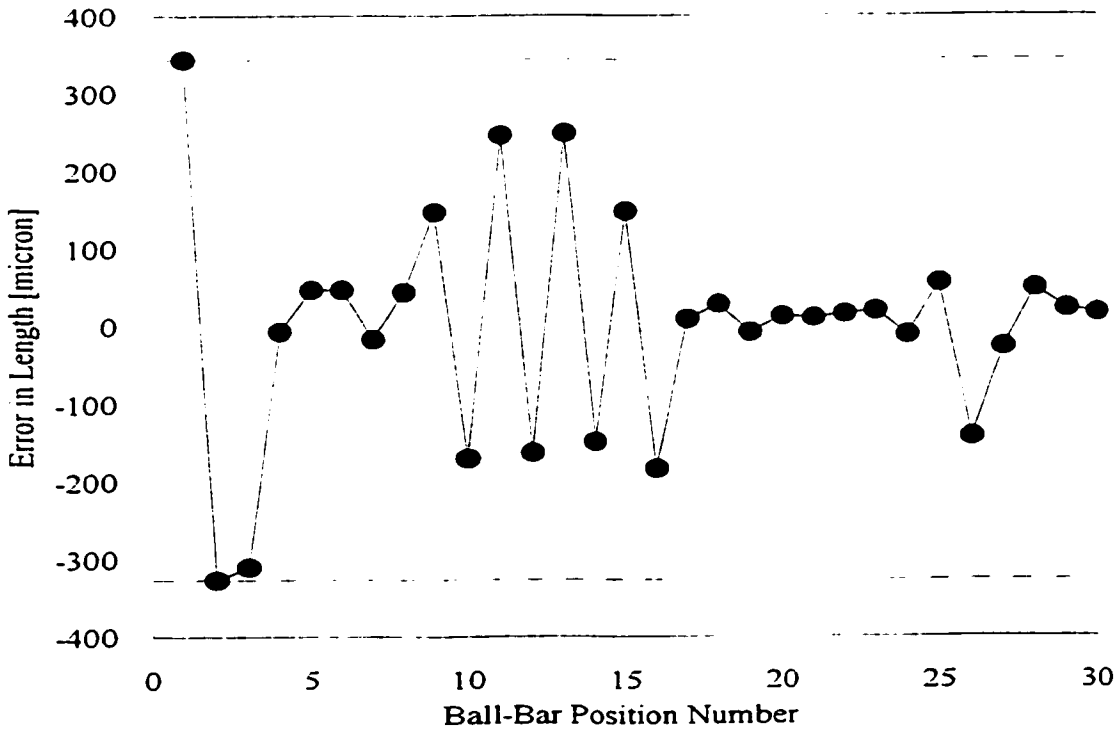


**Figure 29** Error in Ball Bar Length Measurement at ASME Standard Positions.

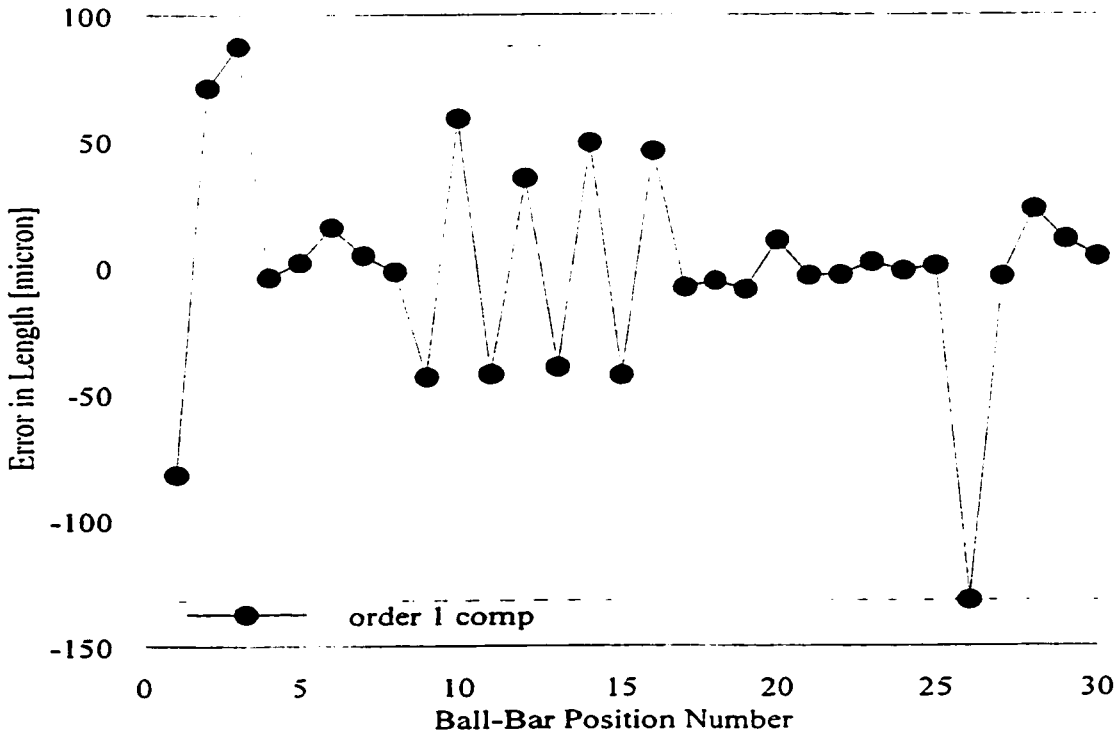


**Figure 30** Residual Errors After Compensation Using 1st Order Model.

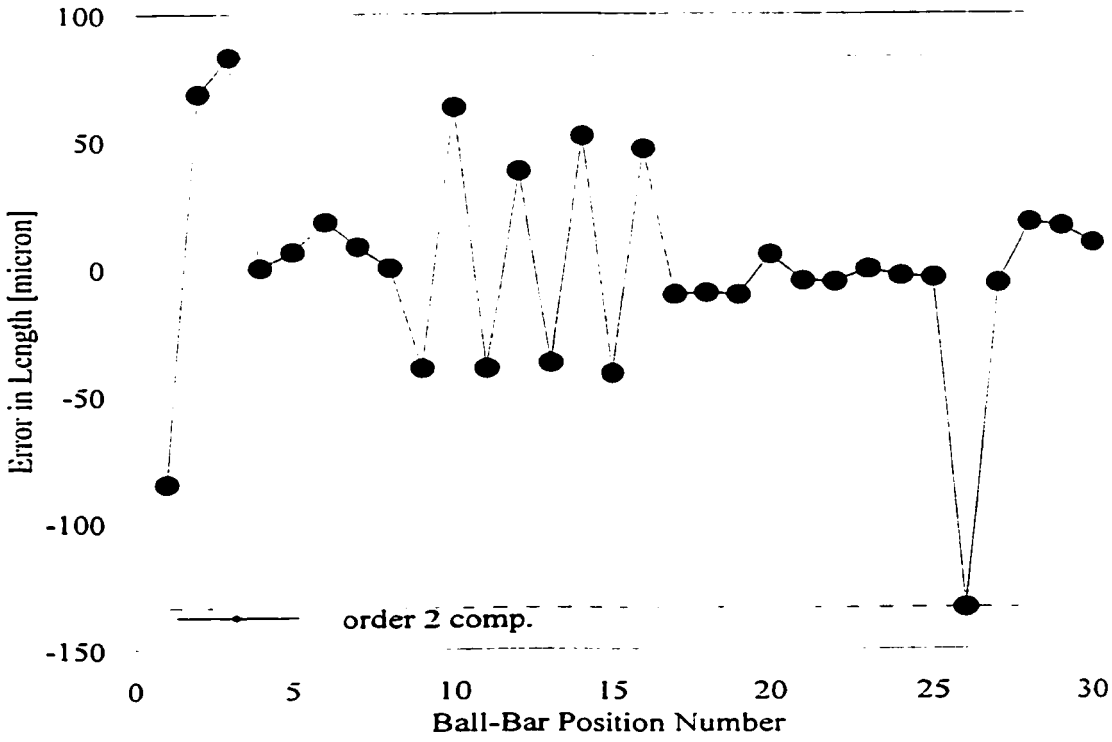


**Figure 31** Residual Errors After Compensation Using 2nd Order Model.

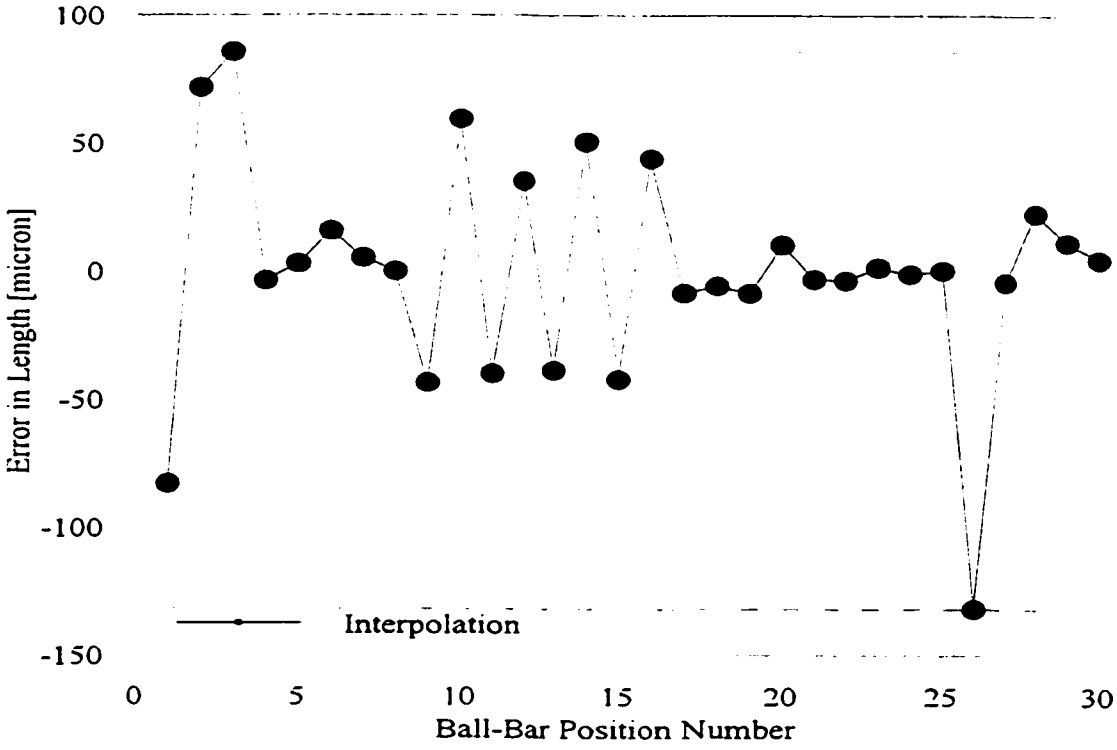


**Figure 32** Residual Errors After Compensation Using the Interpolation Based Model.

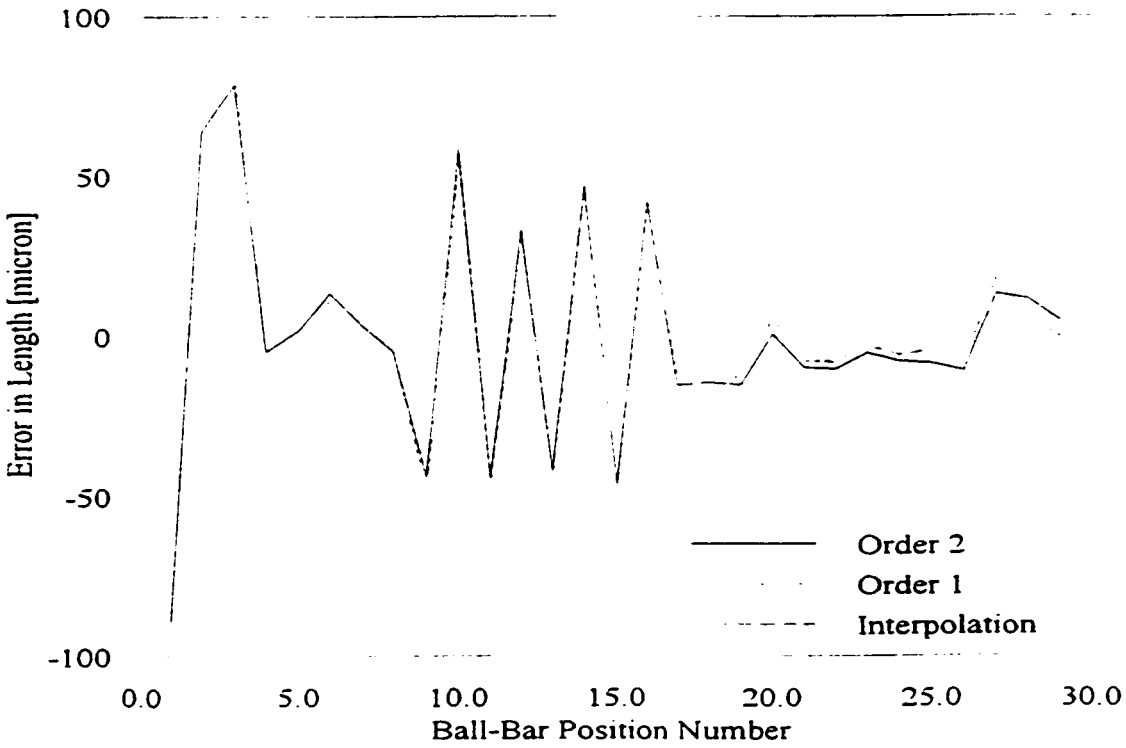


**Figure 33** Residual Errors After the Removal of The Outlier.

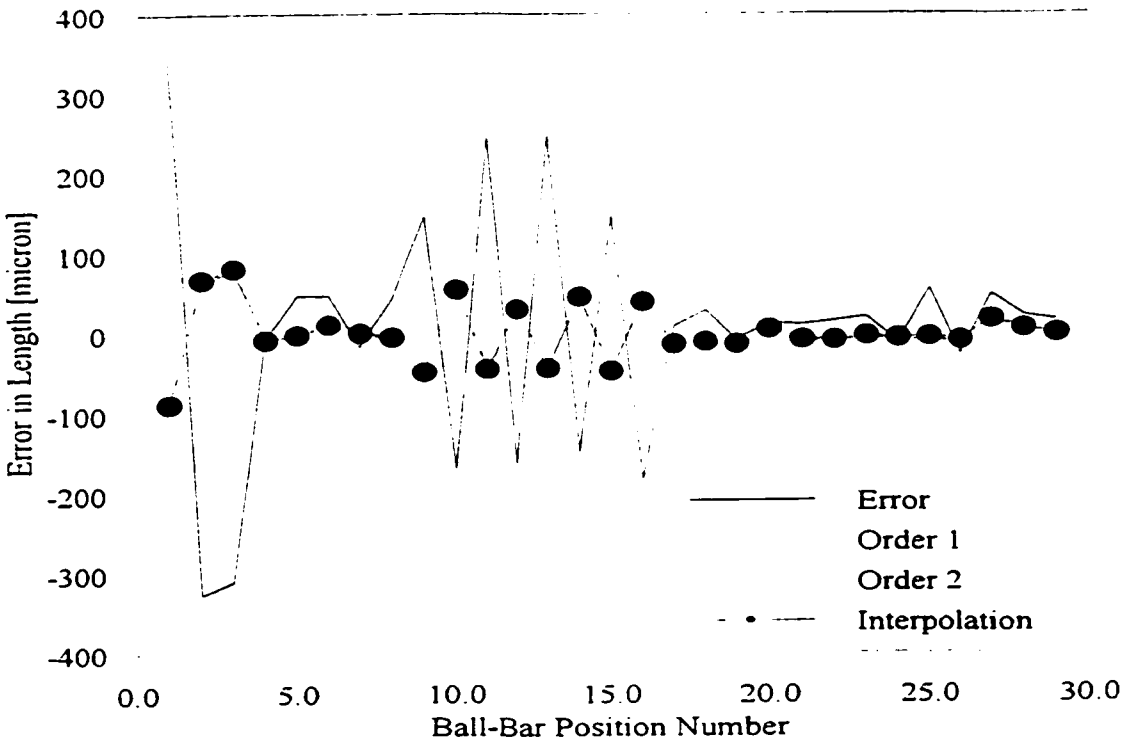


**Figure 34** Error Residuals Using Ring Gauge Measurements Model Compensation vs Original Error.

this observation. This was also confirmed using the laser based error model. The straightness and angular errors are therefore minor compared to the squareness error, but they still contribute to the final error. From table 1, it is clear that the compensation strategy used reduced the volumetric working tolerance of the CMM by almost 75 %. The difference in performance among the different model coefficients sets obtained is very minor. Superimposing the residual errors calculated using the three different methods figure 33 is obtained. Figure 34 presents the residual errors after compensation compared to the original error. Based on these findings, a considerable amount of the CMM error was compensated for. Nevertheless, the CMM performance can still be improved further. When working at the micrometer level, the involvement of manual operations, human factor, and data averaging, introduces noticeable errors. Moreover, the ring gauge used is chosen as the simplest and most available artifact of all. Henceforth, another error factor is introduced while trying to mathematically process the data obtained by measuring a small artifact to arrive at the model coefficients of the CMM work volume. Much better results can be obtained using an artifact like the ball plate. On the other hand, a compromise is considered between cost of the artifact and data processing in one side and the accuracy of the results obtained on the other side. The collection of the above mentioned error factors highly affected the accuracy of the results obtained.

### 5.3.4 Compensation using the laser measurements based model

The compensation strategy mentioned above was applied using the error model

coefficients obtained by laser measurements. The resulting error residuals are presented by figure 35. Results obtained are summarized in table 5 compared to the original error. Figure 36 presents the residual errors of compensation using the laser based model compared to the original errors.

**Table 5** Summary of Compensation Results Using Laser Measurements.

| Method | Error | Laser |
|---|---|---|
| Mean | $4e10^{-15}$ | $1.84e10^{-16}$ |
| Std. Div. | 147.7871 | 10.2191 |
| Variance | 21841 | 104.4291 |
| Working Tolerance | 670.0674 | 47.405 |
| % Reduction | N/A | 92.93 |

Laser measurement set of the error functions of the CMM confirms that the major error source in the CMM is the squareness error. It also confirms the fact that for this particular CMM, angular errors are the second major source of error. These findings are suggested by the model built in chapter 3. They are also confirmed by results in the previous section. As in table 5, the working tolerance of the CMM is reduced by almost 93 % using this method. Figure 34 compares all compensation models results. From this figure, it can be concluded that the laser based model results are more accurate. This can be attributed to many factors. Human error and manual operations in data sampling for this part are almost non-existing. In addition, data processing and averaging is also minimal. To explain the 7 % residual error left, the following facts have to be considered. Since individual CMM error measurements are in discrete points, interpolation is involved when compensation is applied for positions in between known points. Random errors still exist, in addition to the averaging process

environment as much as possible. Although minor, a gradient in temperature still exists in the laboratory. The collective of these factors explains the residual errors obtained using this method. On the other hand, laser data employment to evaluate the error model coefficients resulted in a remarkably effective compensation. In spite of the investment involved in the device itself, a great accuracy level is reached in addition to savings in computational time and efforts. More investigation should be carried out to improve measurement conditions and calculate the random CMM error average. This information can be modeled using the regression methods mentioned above to be added to the model. Finally, compensation can be applied to visualize a further improvement in the CMM volumetric performance.

The suggested compensation strategy was applied to the ring gauge measurement data. The corrected ring gauge measurements gave an error in the range of 7 microns compared to an original error of 46 microns. The results are presented by figures 37 and 38.

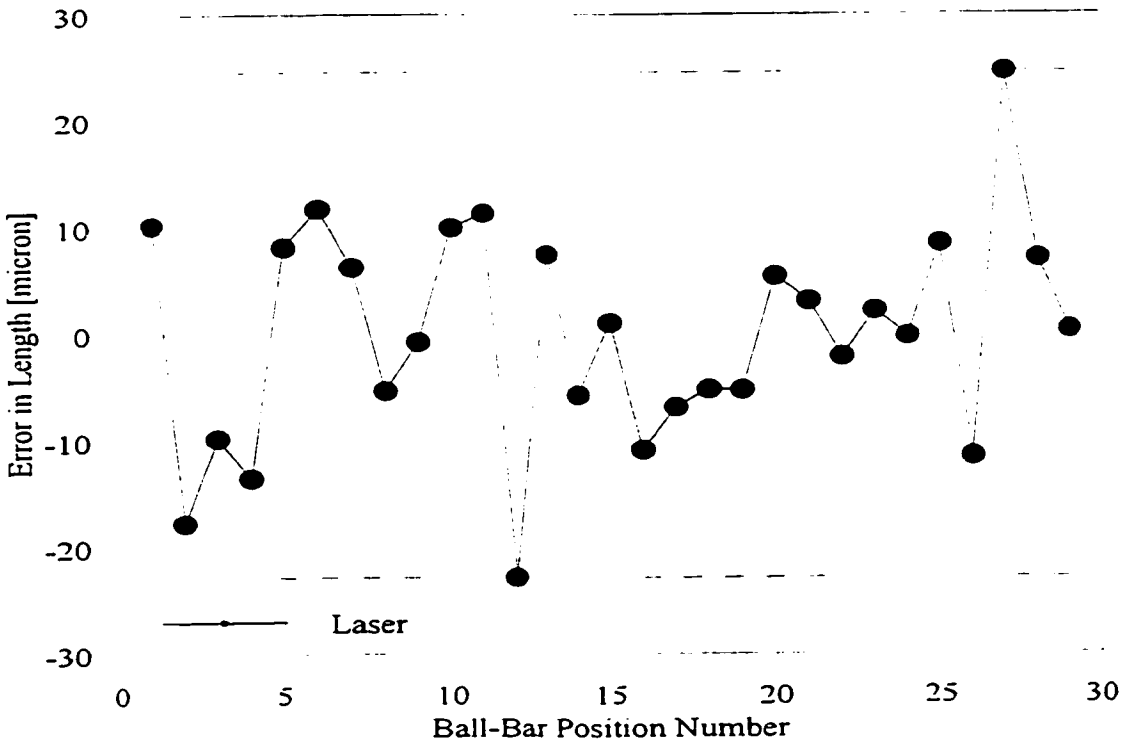


**Figure 35** Residual Errors After Compensation Using Laser Data.

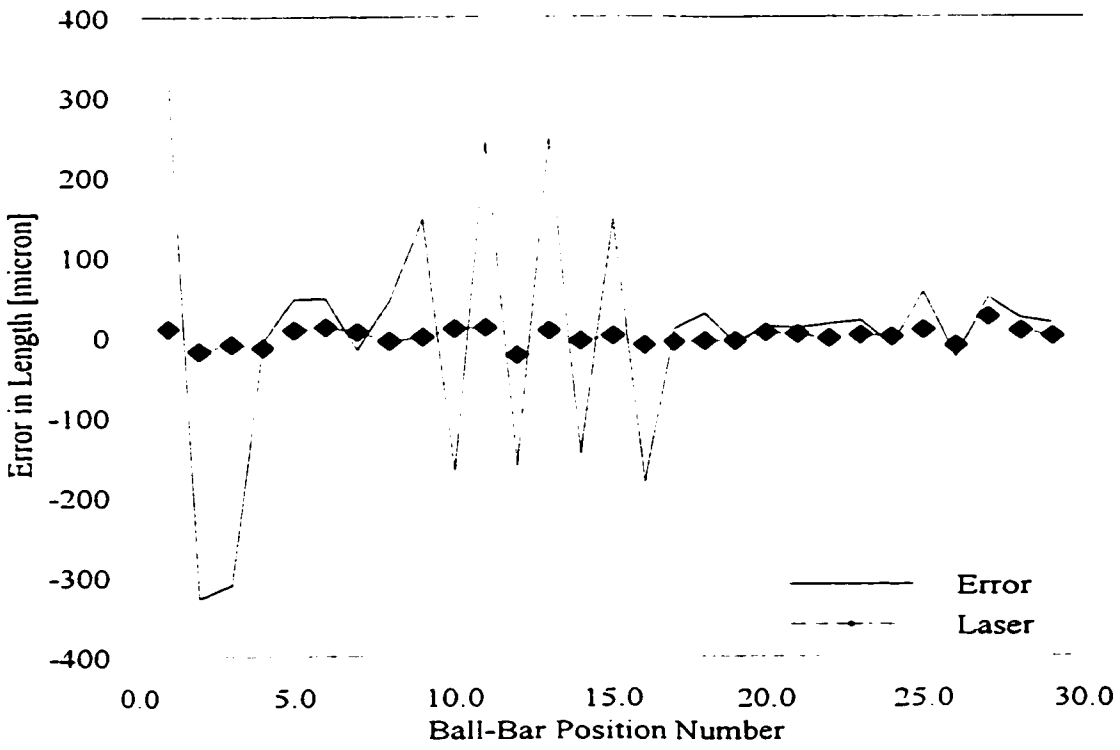


**Figure 36** Error Residuals Using Laser Measurements Model Compensation vs Original Error.

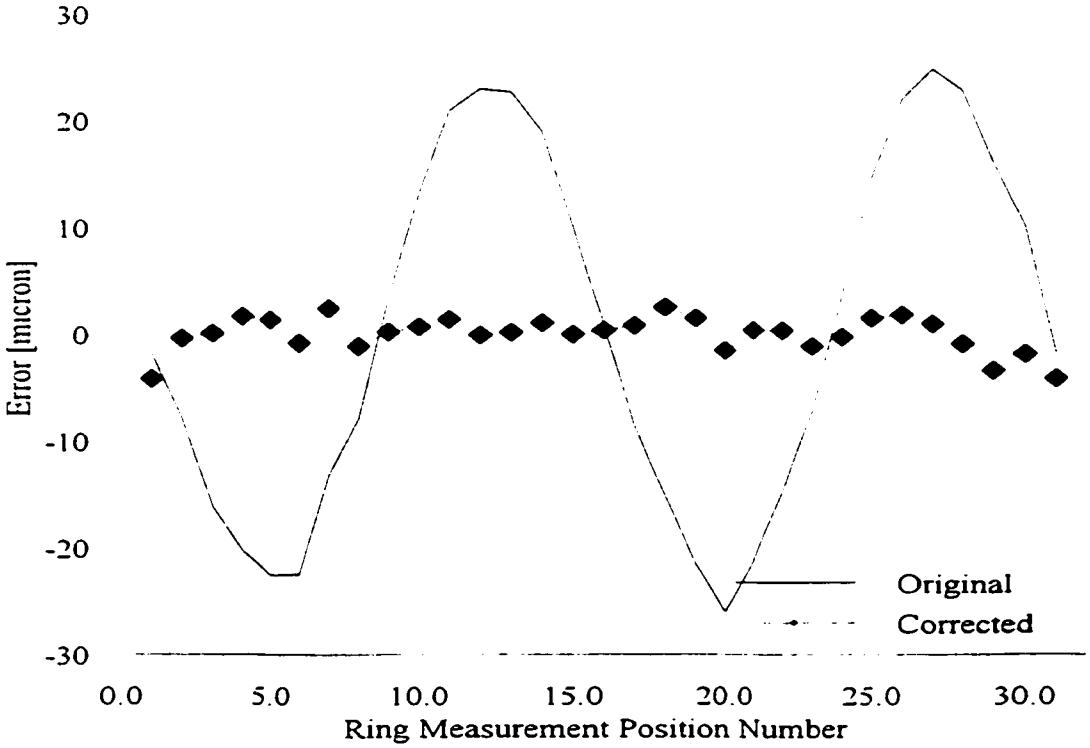


**Figure 37** Residual erors of the ring gauge measurement error before and after compensation.

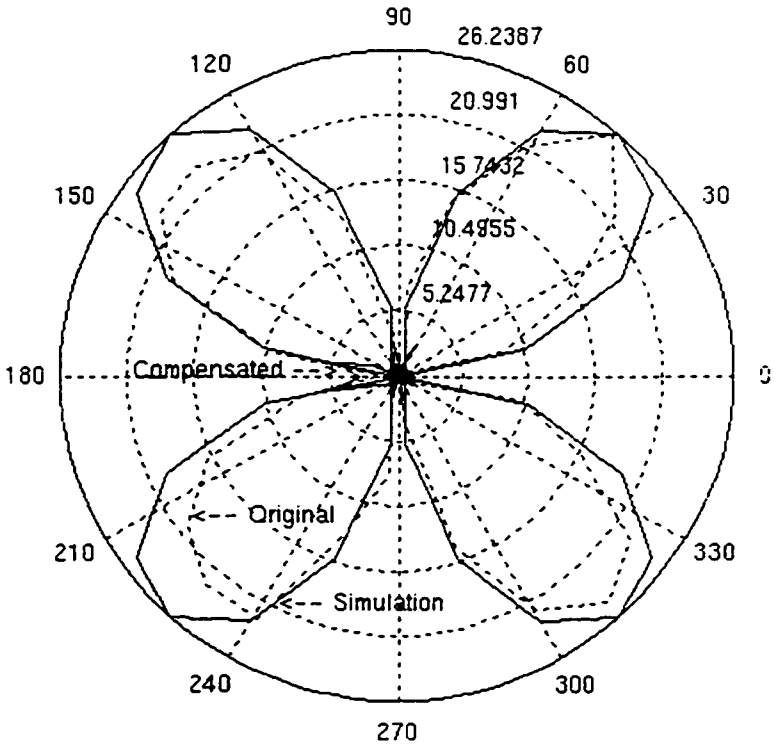


**Figure 38** Ring gauge measurements error after compensation compared to the original and simulated error.

## 5.4 Contouring errors correction

The inverse kinematics model resulting in equation (23) was formulated. Simulation of the CMM while in the process of tracking oblique trajectories in its work volume was carried out. This is employing the inverse kinematic model and at a constant reference thermal state. Figure 39 represents the oblique trajectories selected. These contours are chosen because they involve the interaction of most machine elements and cover a large part of the work volume. Each trajectory was given a reference number (e.g. Line 1 or L 1) as in the figure. The simulation steps are presented by the flow chart in figure 40.

Resolution of the trajectory planner is a user parameter that is input to the simulation program based on the fine details in dividing the trajectory segments desired by the user. Following, a trajectory is built and points to be followed are fed to the program, which, in this case, would be one of the lines suggested for testing. These points pass trough the inverse kinematic model to be modified in the feed forward stage, based on previous knowledge of the machine errors encountered in the work volume corresponding to the desired positions. The output of this module becomes the input to the actual CMM forward kinematics model which represents the CMM behaviour. The end effector position resulting from the forward kinematics of the CMM is compared to the desired trajectory and the resulting error is calculated. Figure 41 depicts the resulting volumetric errors of contouring these trajectories using the ideal CMM models without consideration of the CMM quasi-static error. This is the case of no error compensation. Figure 42 represents these errors calculated again when using the fitted inverse kinematic model, including the CMM

quasi-static errors, at the reference thermal state, in the feed forward path. The abscissa in the figures represent the corresponding location on the CMM X-axis of each point on the trajectory. As a result, the volumetric error have been reduced significantly. The maximum volumetric error before correction was 580 μm.

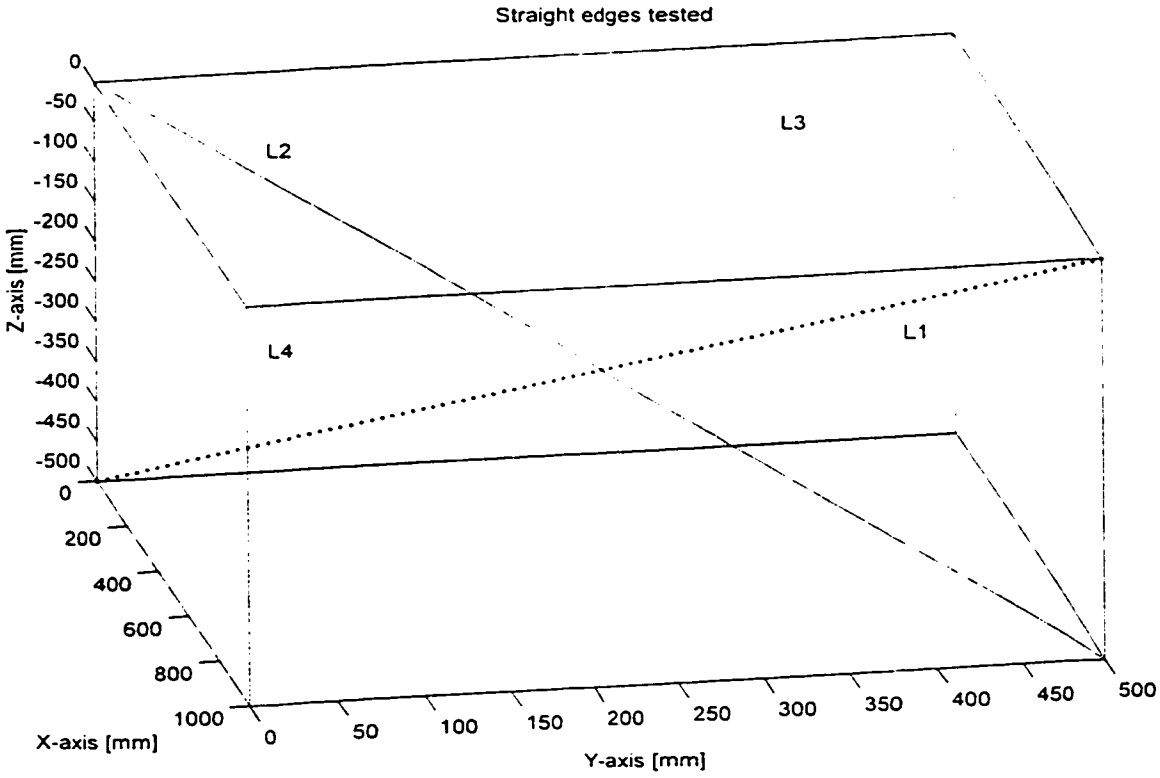


**Figure 39** Oblique trajectories suggested to test the CMM performance.

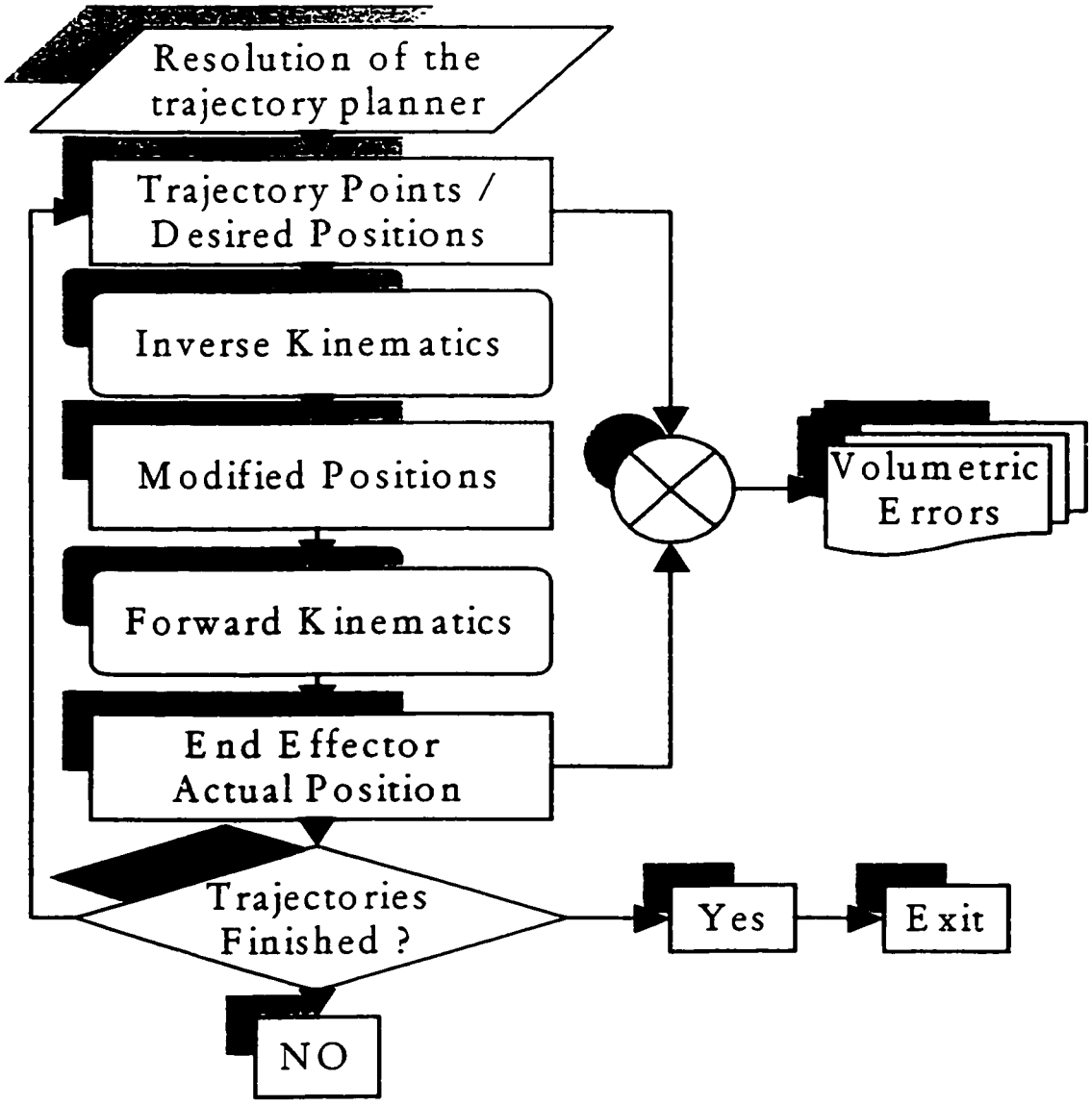


**Figure 40** Contouring tests steps.

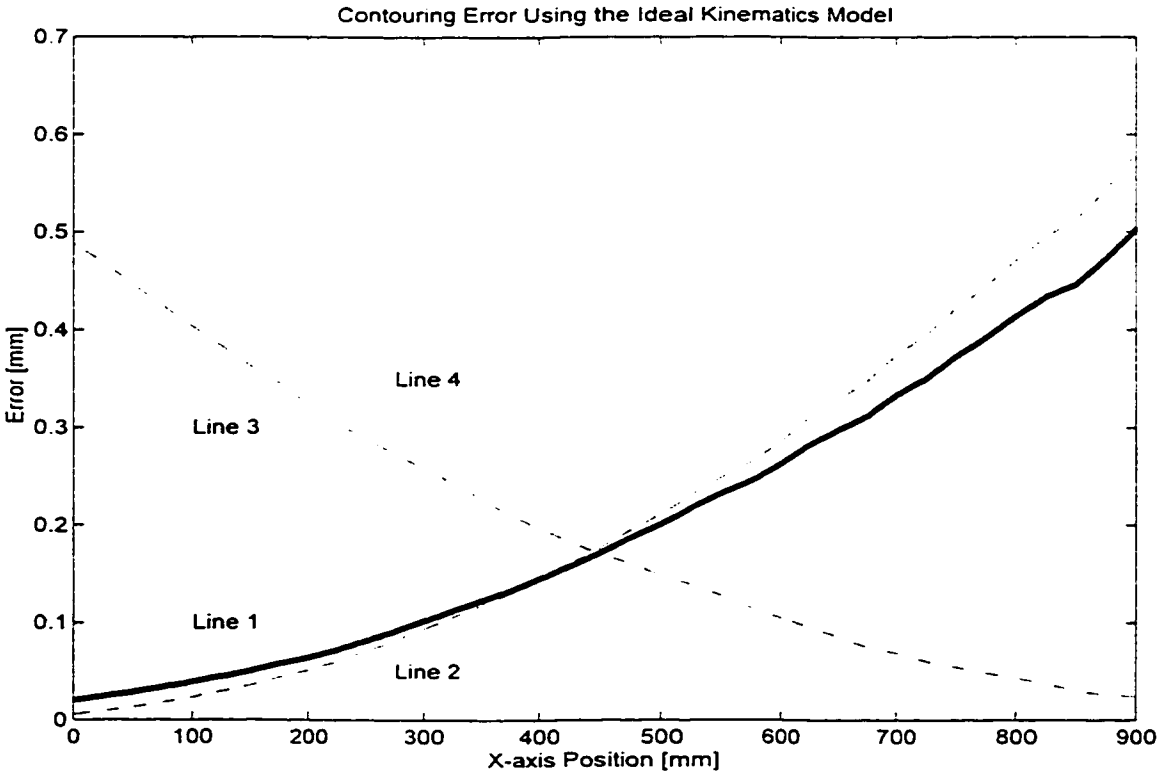


**Figure 41** CMM contouring errors using ideal models.

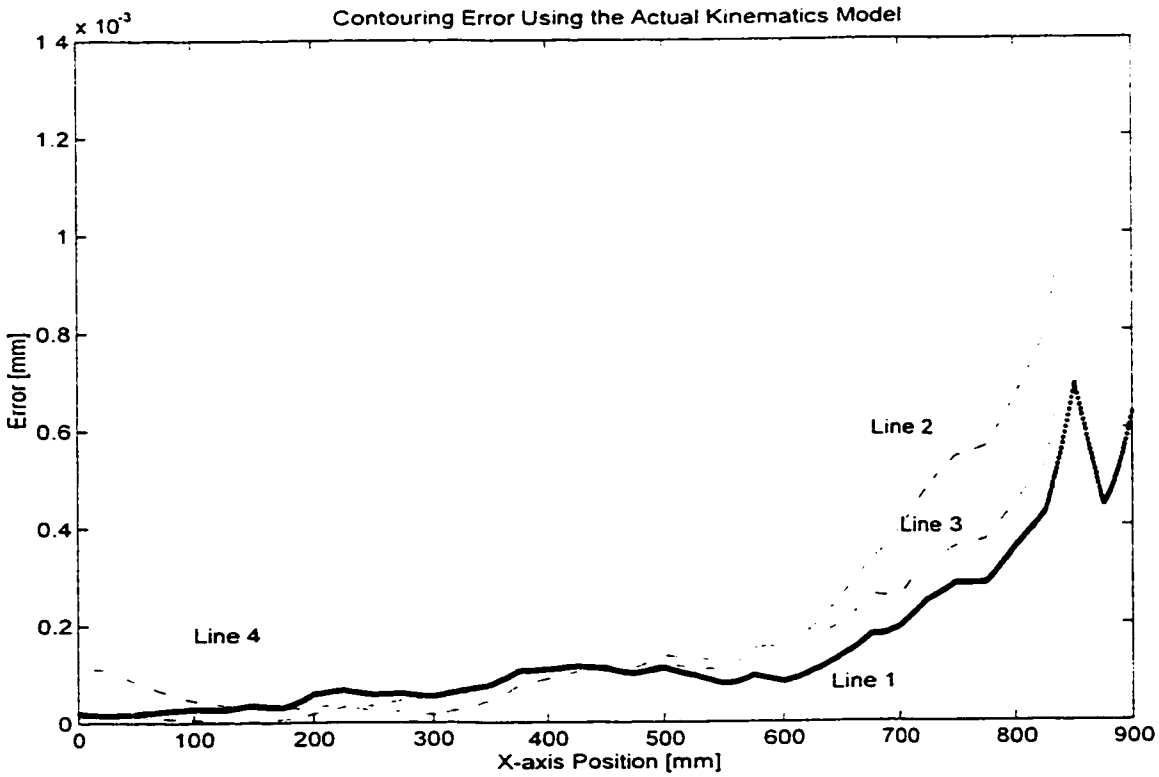


**Figure 42** CMM contouring errors using the proposed strategy and models.

The result of applying the modelling and compensation strategy proposed was a reduction of this error to 1.2 μm. This is a percentage reduction in volumetric error of 99.99 %. More practical effect of these results can be seen by concentrating on the most used part of the machine work volume. This is usually the center lower part of the work volume. The volumetric error at this part have been reduced from almost 480 μm to 0.42 μm, which is less than one micrometer error. This is also a percentage reduction of more than 99.99 %. Knowing that the investigated machine encoder resolution is 1 μm, these simulation results show that a significant performance improvement of the CMM using the proposed methodology is evident. Moreover, these results serve to prove that the inversion of the kinematics model using the regression analysis method was successful. This, in turn, gives very solid grounds for the application of this methodology for error elimination in any intrinsic machine. More insight into the effectiveness of this methodology will be gained by the incorporation of the thermal effects in the following chapter.

## 5.5 Summary

This chapter presented the first part in the implementation of the proposed compensation strategy for CMM error correction, and its corresponding results. This part included the correction of geometric and kinematic errors of the CMM excluding the thermal effects, or in a constant thermal state. In addition, this part included the experimental evaluation of the ECTE to arrive at a realistic value. This value will be used in the compensation models of the following chapter. Following, error functions of the CMM

model were evaluated at a constant thermal state using two different methods for compensation. Consequently, the model was employed in measurement error compensation. The effectiveness of this compensation was actually measured by conducting a B.89 standard performance evaluation test for the machine.

Figure 38 represents the results as per the recommended presentation of results by the ASME B.89 (1990). Figure 39 represents the residual errors after application of the compensation strategy for volumetric error in the CMM measurements. The compensation strategy used have improved the performance of the CMM significantly. The volumetric working tolerance zone of the CMM was reduced from 670.07 microns to 47.41 microns. This is almost 93% reduction. Based on these findings, a considerable amount of the CMM error was compensated for by the proposed strategy.

Finally, the contouring error was also compensated by employing the fitted inverse kinematic model of the machine. Simulations of the machine performance in tacking selected trajectories before and after the application of the compensation strategy was carried out. A reduction in contouring error of more than 99% was presented.

Chapter Six

# Implementation and Results Analysis (II):

## Varying Thermal State

The previous chapter presented the details of the experimental procedure and the analysis of the results obtained in applying the proposed solution for the CMM error correction by compensation. The experiments were carried throughout in a constant thermal state. In the present chapter, the thermal conditions are incorporated in the modelling and compensation for the errors of the CMM. The thermal state is being changed by changing the ambient temperature of the CMM as well as the spatial temperature gradient affecting the CMM. This chapter presents the details of the experimental implementation of this stage as well as the analysis of the obtained results.

## 6.1 Experimentation plan

The plan for this part was very similar to the plan set in chapter 5. It included the two parts which are: error functions identification and models testing and validation of the proposed strategy for CMM error compensation. This is in reference to both cases of measurement and contouring. The difference in this chapter is in the introduction of thermal effects to the CMM environment. A combination of simulations and experimental methods was carried out for verification, depending on equipment availability. Based on the results obtained in the previous chapter, error functions of the CMM were measured by laser interferometry, in different thermal conditions for this stage. In chapter 5, the performance of the CMM was evaluated based on the ASME B.89 test. However, this test was set to be carried out at constant thermal conditions. Therefore, up to the time of reporting the results of this thesis, there was no standard performance evaluation test available that can be used to evaluate the CMM performance in a thermally varying environment. Consequently, a performance evaluation test was needed and this led to the introduction of a modified version of the B.89 test to evaluate the machine performance changes before and after the proposed compensation strategy was employed. For the contouring performance testing of the machine, a simulation of the machine in tracking trajectories in its work volume was carried out.

The CMM was placed in a thermally insulated room. A heating device was built to raise the temperature of the room and introduce thermal gradients. In conjunction with the air conditioning and circulation system of the building, cooling and stabilization of thermal

states was achieved. For stable states, the CMM and the room were allowed enough time for soaking. The tests were carried out for different thermal states and the results are presented next.

## 6.2 Error functions identification

Error functions are the components that make up the 21 errors modelled. Error functions were measured by laser interferometry at different thermal states and positions of the CMM work volume. The measurements were carried out based on an input matrix of parameters resulting from a design of the experiments. The results of these experimental measurements are presented next.

### 6.2.1 Linear errors

This is the error resulting from the deviation between the machine encoder reading of displacement and the real displacement value. It is also known as the positioning error. This error can be measured by laser interferometry and the machine reading can be compared to the real value using the laser measurements. Each axis of the CMM has one error of this category associated with it. Extensive measurements of this error have been carried out for the investigated CMM for all axes at different thermal states. These states included different temperatures and gradients. It has been found that this particular category of error is a direct function of the temperature of the scale measuring the axis. Moreover, gradients have a relatively insignificant effect on the linear error. A sample of the measurements results are

presented by figure 43. A simulation of this result using theoretical models and the ECTE which was determined in chapter 5, was carried out. The result is presented by figure 44. A full set of experimental results showing detailed results for this error function are included in Appendix H. These figures represent the actual measurements results as opposed to simulated estimates based on the theoretical models and the experimentally determined ECTE. These results also confirm the theoretical assumptions made to estimate them at different temperatures and positions using the thermo-mechanical model represented by equation(11), and reproduced here:

$$\Delta L = L.\alpha.\Delta T \qquad \textbf{(33)}$$

The theoretical models for each of these errors were re-calibrated based on the experimental findings. Moreover, the experimental results were used to back calculate the ECTE. A comparison showing the deviations between measured and theoretical values is explained by table (1). The table shows that the worst case deviation was 13 %, which confirms that the estimation models are reasonably close to the real physical behaviour of the machine. This also confirms the experimentally verified fact that temperature difference affects this error and as opposed to gradients which has no effect on it. The final error functions are direct functions of the position and temperature profile. These error functions are included as part of the general kinematic model.

Table (6) Deviation of Experimentally obtained value for coefficient of thermal expansion from model value (9.5 ppm/°K).

| Alpha Exp. | Mean | Std Dev. | Percent Error |
|---|---|---|---|
| X | 9.8717e-6 | 1.1725e-6 | 3.91 % |
| Y | 8.5652e-6 | 1.6121e-6 | 9.84 % |
| Z | 8.2614 e-6 | 1.2638 e-6 | 13.04 % |

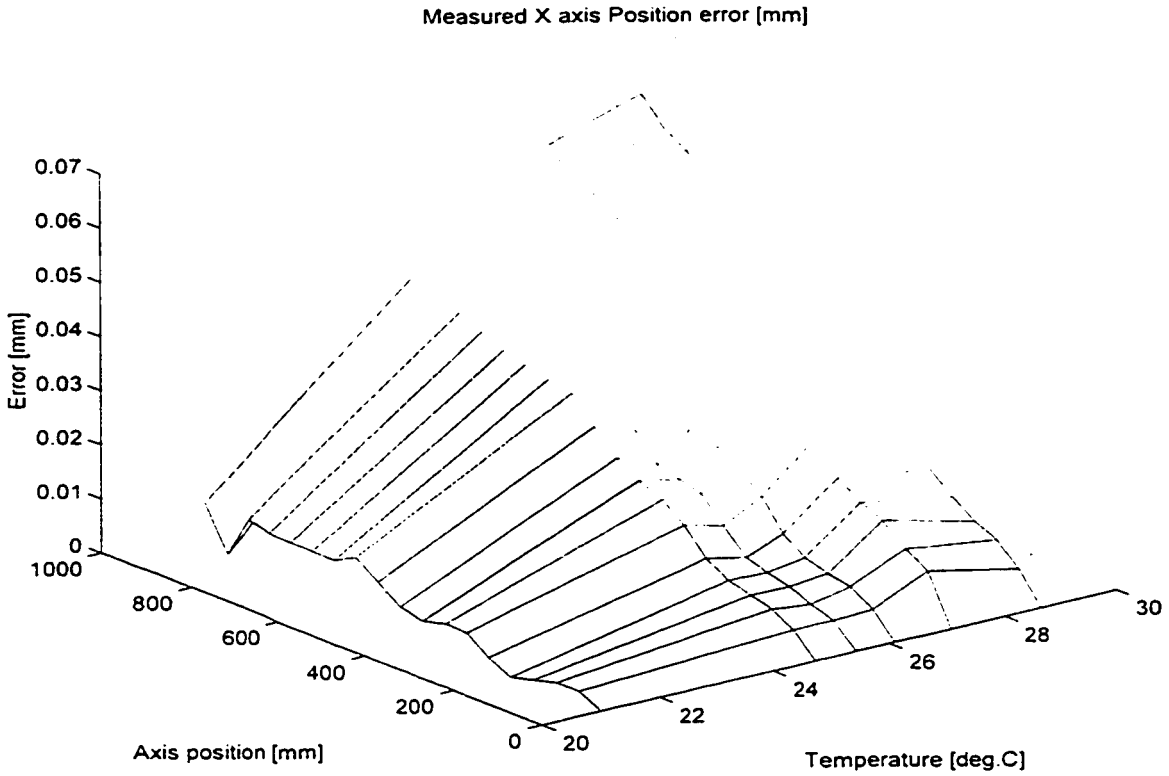


**Figure 43** Measured linear error along the X-axis at different temperatures.

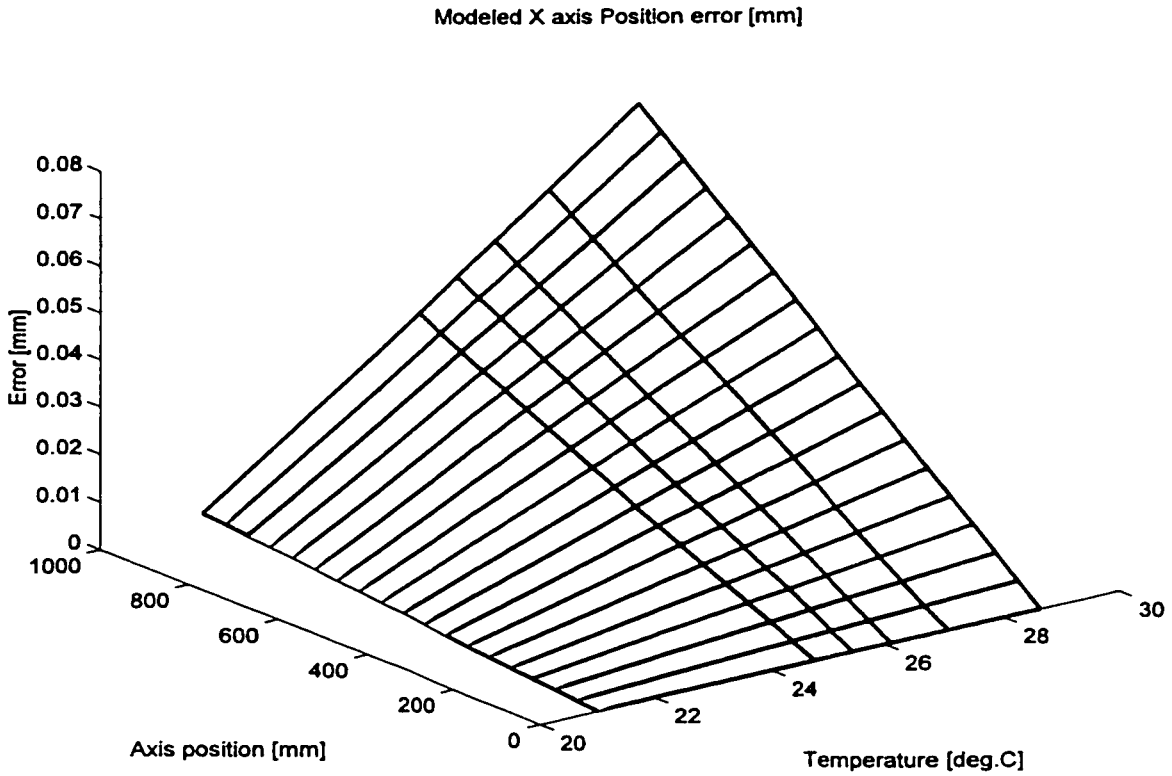


**Figure 2** Estimated linear error along the X-axis at different temperatures.

### 6.2.2 Straightness error

This is the error resulting from deviations of proper positioning of the end effector along a straight path. It is not to be confused with other errors like the angular error. Figure 45 illustrates the difference between these different error functions. Two errors of this category are associated with each axis of motion. The direction of these errors would be always in the direction of the two other perpendicular axes. A total of six sets of measurements for these errors were obtained. Figures 46 and 47 represent samples of the laser measured straightness errors. This error was measured as a function of position at six different temperature states. The figures represent the two straightness errors associated with the X-axis. The full set of results is included in Appendix I. The experimental results showed that the machine thermal state has a remarkably insignificant effect on this category of errors. Therefore, to incorporate this error function in the general error model, piecewise bilinear interpolation was used where the independent variables of position and temperature are input to obtain corresponding values of this error. These errors seem to be inherent in the machine.

### 6.2.3 Angular error

This is the error resulting from the deviation in motion along an axis by an angle of rotation around one of the three axes (figure 45). Three errors of this category are associated with each axis of motion and are known in the literature as: roll, pitch, and yaw errors.

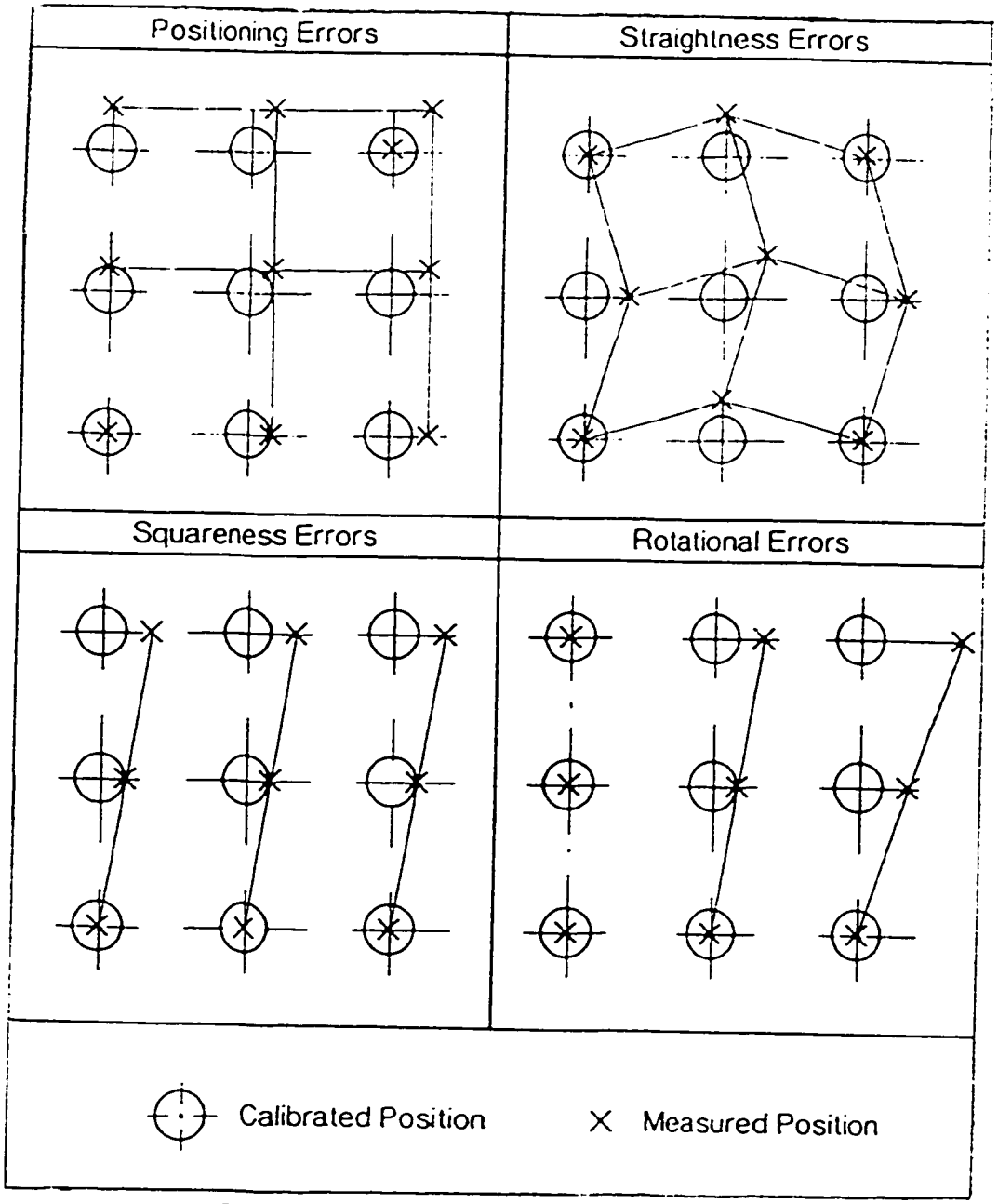


**Figure 45** Error functions of the CMM (Bosch, 1995).

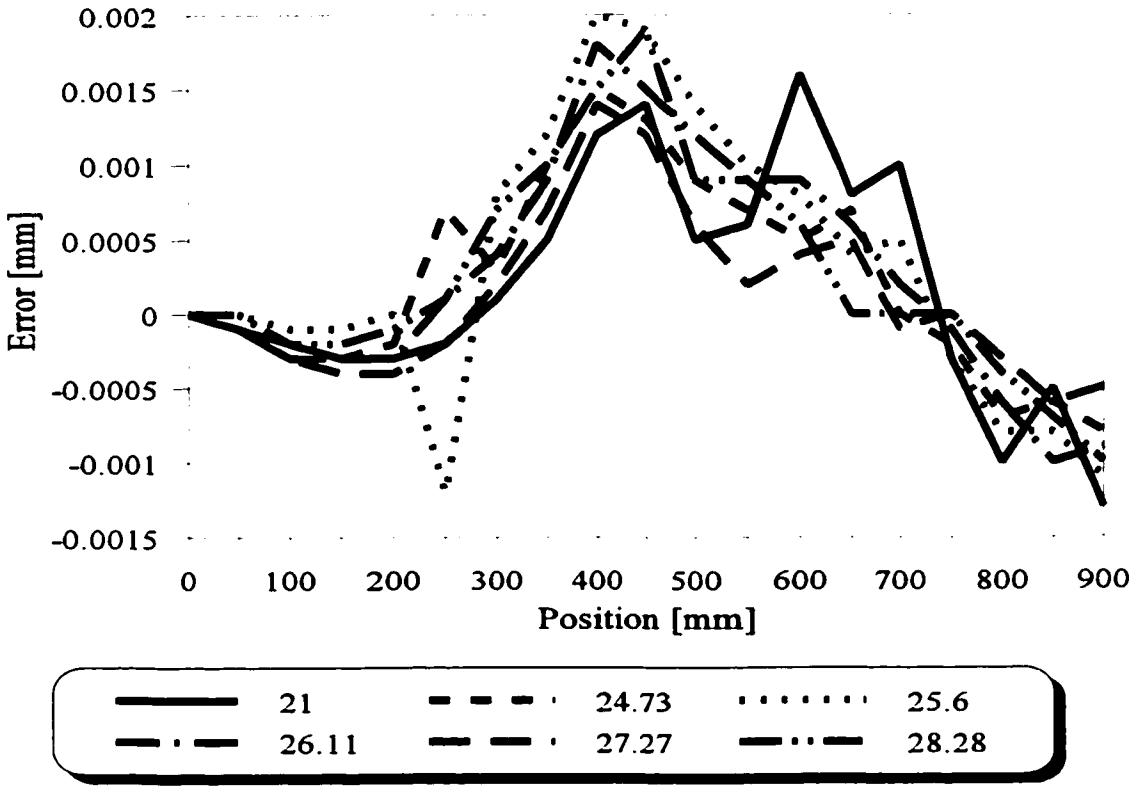


**Figure 4** Straightness error of X-axis in the Y-axis direction at different temperatures.

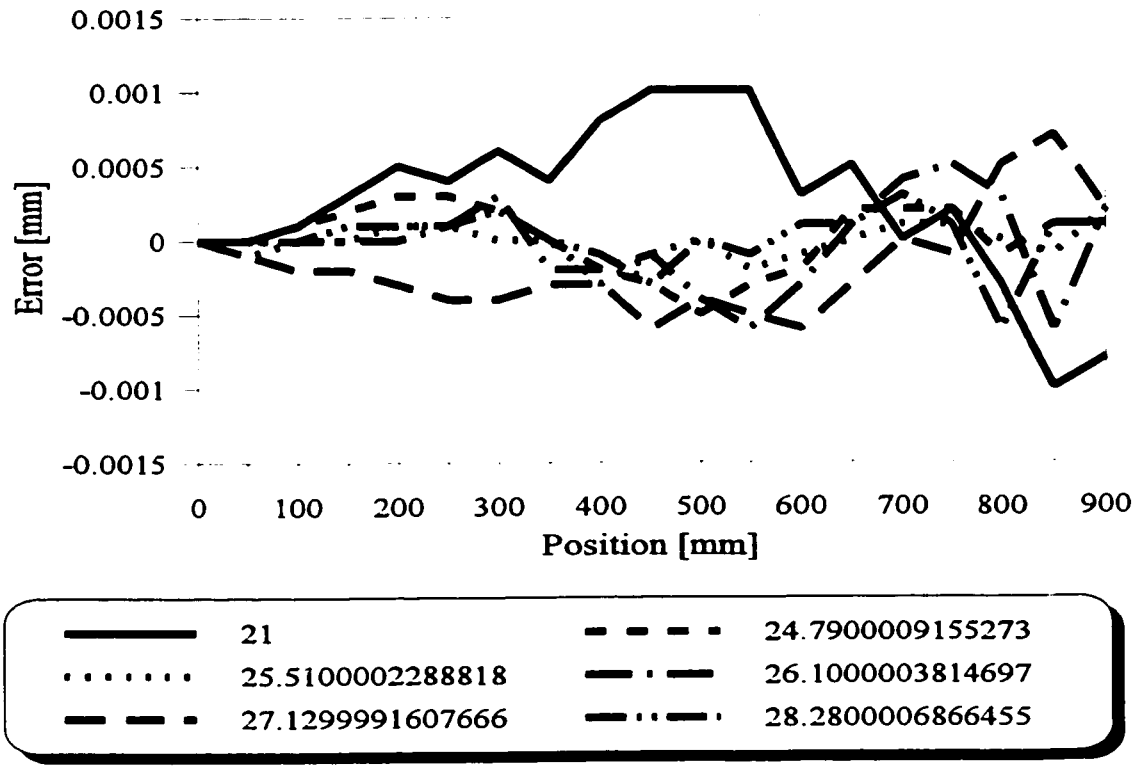


**Figure 5** Straightness error of X-axis in the Z-axis direction at different temperatures.

As a result of the experimental measurements, the three roll angles around the individual axes were found to be almost zero. This reduced the total of angular errors to six sets. Figures 48 and 49 represent samples of the laser measurements results of these errors at different thermal states. The figures represent the CMM end effector positioning deviation or error, as a function of position along the X-axis, as well as, a function of the thermal gradient across the same axis. Notice that there are two options to choose a direction perpendicular to the X-axis to measure this error. Since the error is measured along the Y-axis, the gradient is also measured along the same axis. A full set of measurements results are presented by figures which are included in Appendix J. These figures also include the estimated values and the fitted values for the measurements, as well as the actual measurement values. Fitted values are values of the error resulting from attempting to fit a proper model to the actual measured values. The estimated values are based on using the thermo-mechanical model presented in chapter 3 for a second order effect on the machine produced by a thermal gradient. Investigation of the experimental results also revealed that these angles are direct functions of the thermal gradients and not the average ambient temperatures. Figure 50 depicts the effect of a spacial gradient on the CMM. This relation is not linear in position. These errors are linear functions of the gradients but quadratic functions of the end effector position, and therefore, produce a linear function relating the angles to the rate of change of the square of the position. This is if the error resulting from the angles is considered. These results agree in full with the modelled assumptions characterized by the thermo-mechanical models represented in chapter 3 and equation (34).

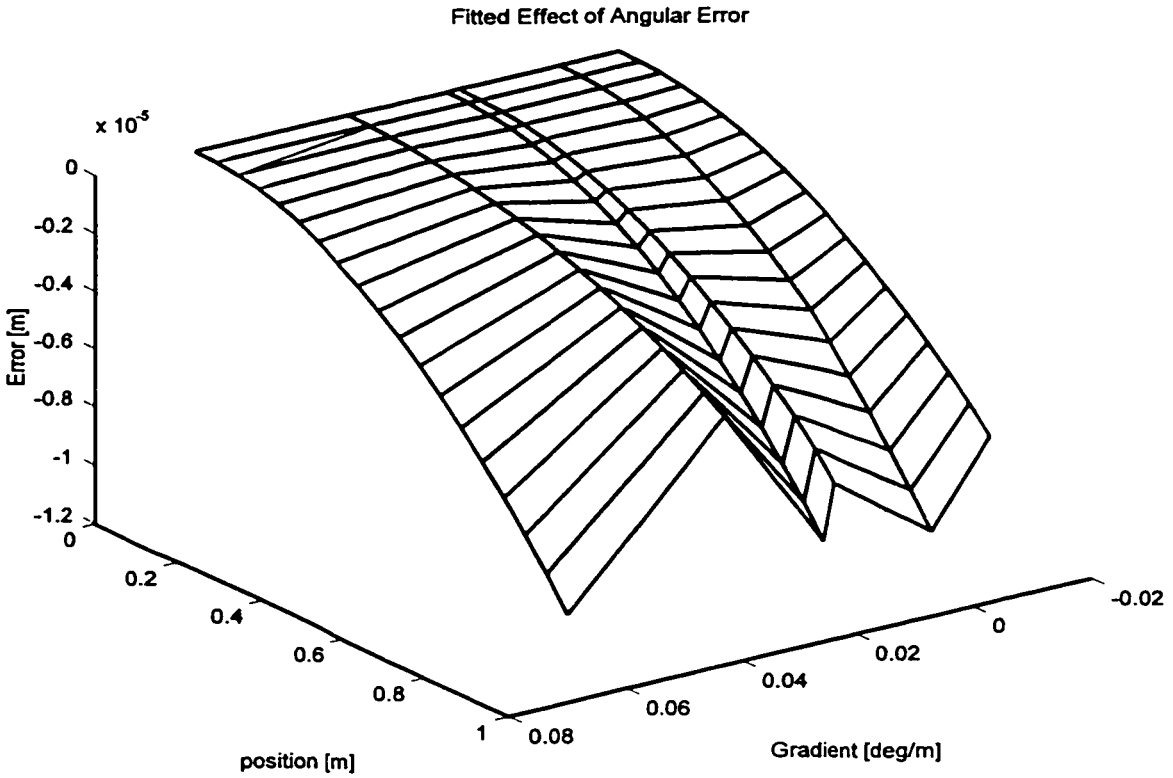


**Figure 6** Measured error resulting from X yaw angle γ in Y.

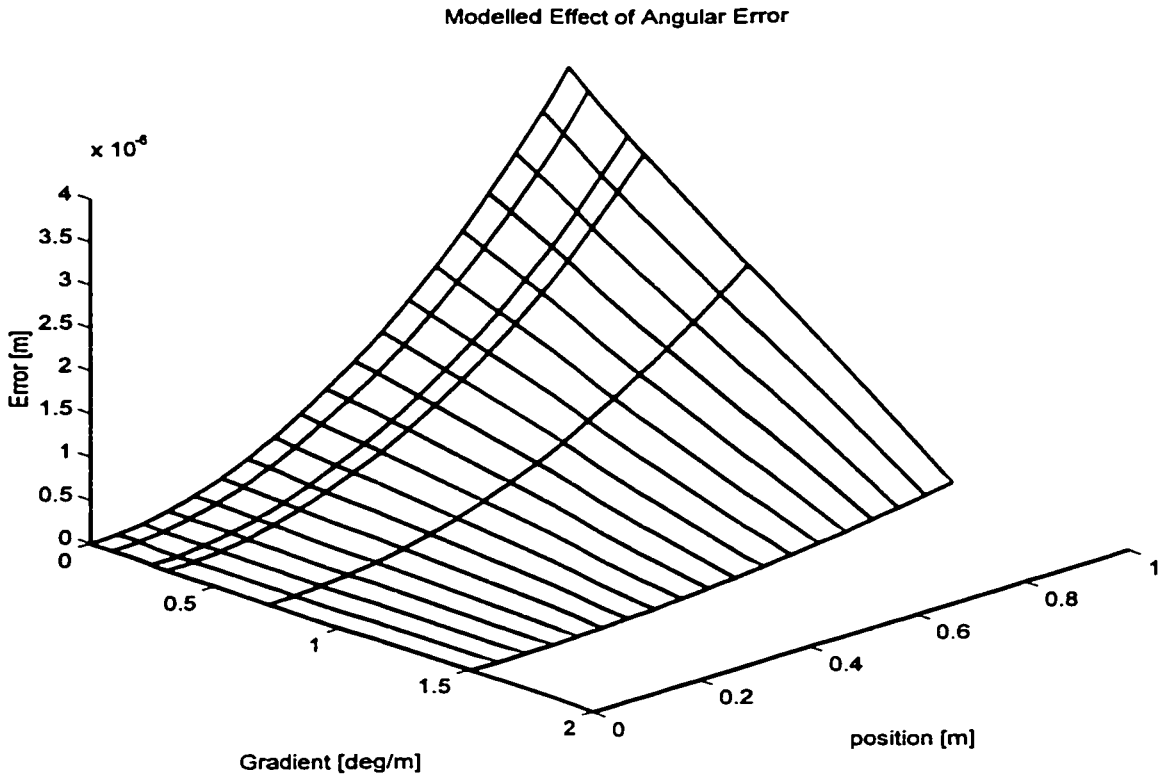


**Figure 7** Modelled error resulting from X Pitch angle β in Z.

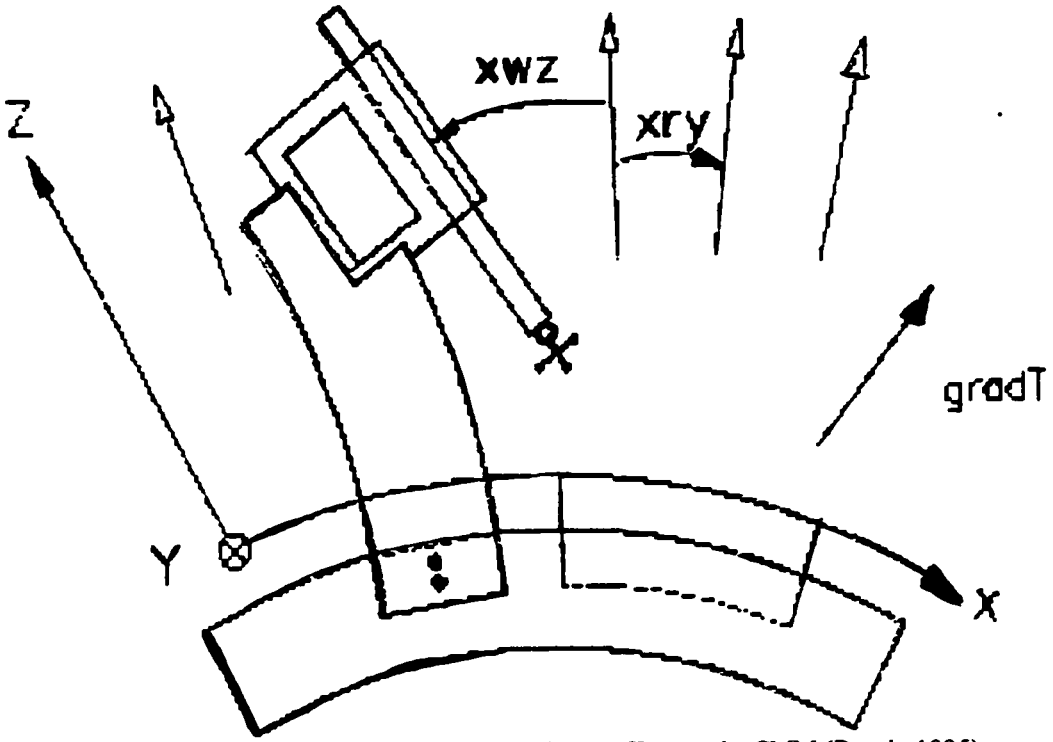


**Figure 50** A visualization of thermal gradients effect on the CMM (Bosch, 1995)

$$\Delta Z = -\frac{1}{2}.\alpha.grad(Z).X^2 \quad \textbf{(34)}$$

The error function models were re-calibrated using the experimentally measured values and used to find the angular errors of the machine at different temperatures and positions.

### 6.2.4 Squareness error

These are three errors of angles between the three axes. No clear relation was found between squareness angles and the thermal state. A slightly better relation can be established between squareness angles and gradients. The models to be used in the correction model are fitted using the experimental data through applying regression analysis.

## 6.3 Measurement error correction

Experimental evaluation of the CMM performance including the compensation and control strategy proposed was carried out. The ambient thermal state of the CMM was disturbed by introducing thermal gradients and random temperature changes. The average temperature state sensed by the thermocouples while performing each of the ball bar measurements is represented by figure 51. The B.89 test was carried out with the modifications introduced which consisted of varying the thermal states for each individual ball bar position measured. As expected, the machine performance degraded by introducing these thermal changes. The work tolerance increased from 670.07 micron at the constant

thermal state to 782.9 micron at this stage. Compensation was applied at these thermal states for the ball bar measurements. The compensation strategy implemented improved the CMM performance and reduced its work zone tolerance to 18.7 microns. Figure 52 represents these final results. The percentage reduction of errors is almost 97.6 %. Figure 53 represents the results of performance evaluation before compensation. Figure 54 represents the residual errors after application of the proposed methodology for compensation. A considerable amount of the CMM error covering most of its volume was eliminated by introducing the proposed compensation strategy. The results also show the robustness of the models used in adapting to the thermal state changes during the test. At this point residual errors can be explained by the involvement of manual operations, human factor, and data averaging. It is to be mentioned here that compensation for errors provides effective results in a small range of errors. In the present case, the error range was remarkably large. Nevertheless, the proposed compensation strategy effectively reduced this error.

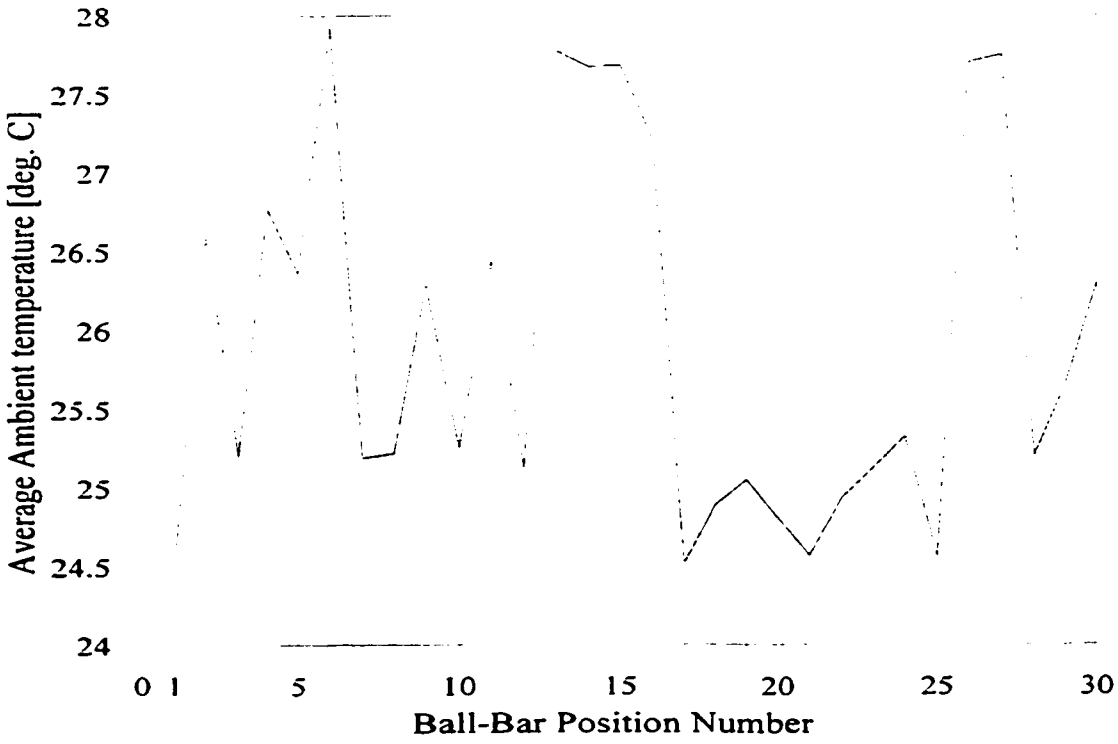


**Figure 51** Average ambient temperature for each measurement of the ball bar.

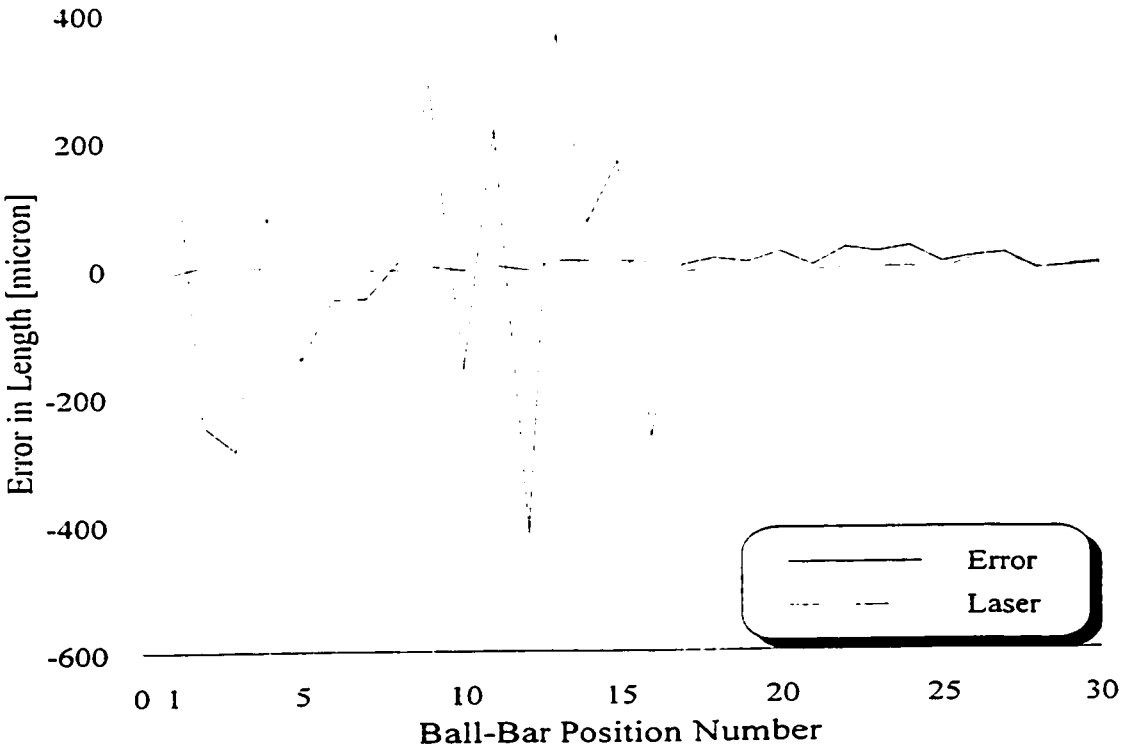


**Figure 52** Error residuals using the laser calibrated model compensation vs. original error.

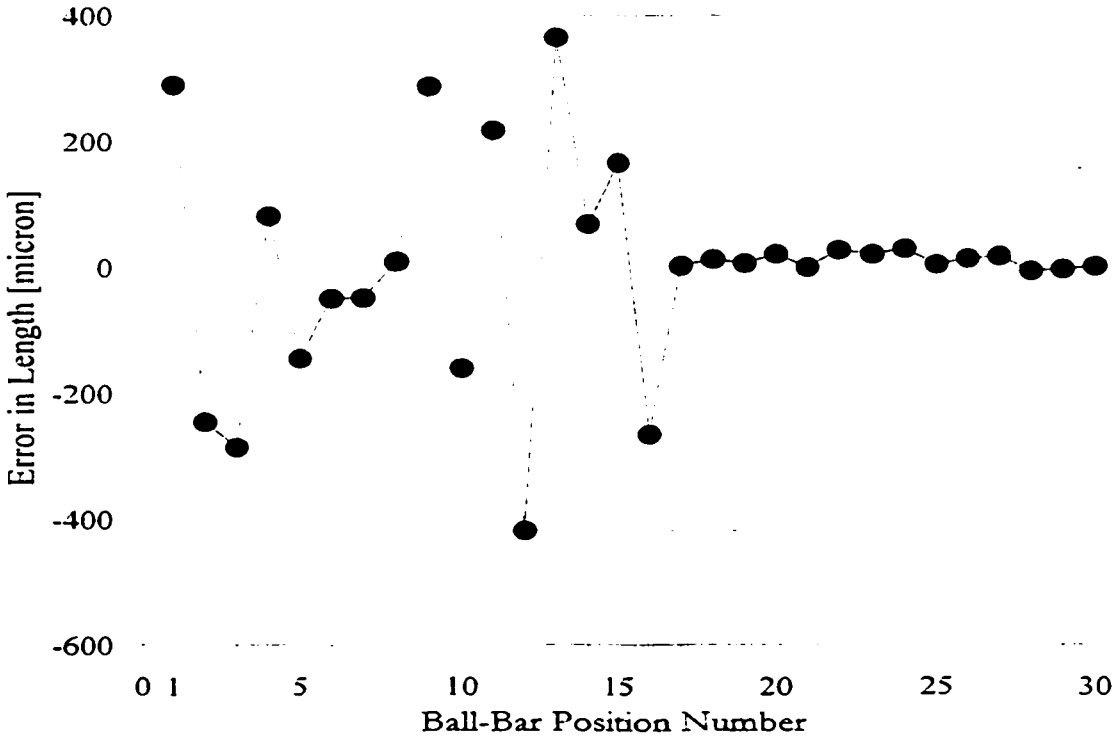


**Figure 53** Error in ball bar length measurement at ASME standard positions.

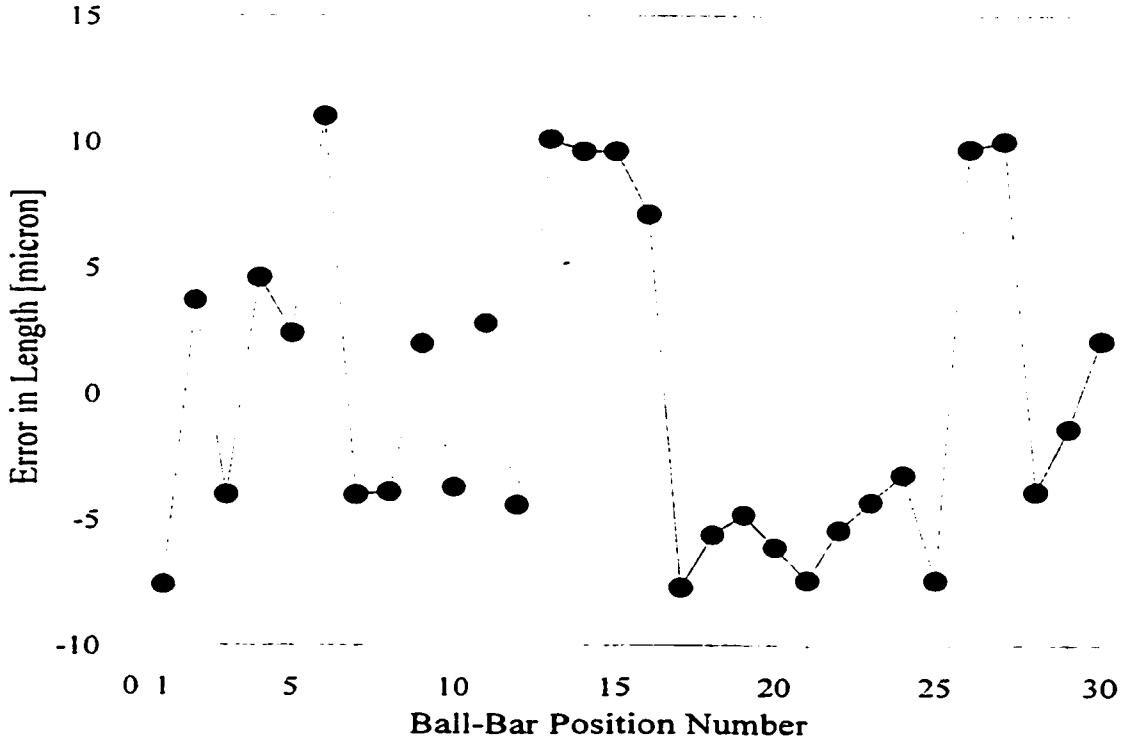


**Figure 54** Residual errors of the ball bar ASME measurements after compensation using the proposed strategy.

## 6.4 Contouring error correction

Simulation tests were carried out using the proposed compensation and control strategies, as well as, the models for the CMM performance including changes in the thermal state. These tests were analogous to the ones described in section 5.4. The results of these test to track the four diagonal trajectories suggested in figure 39 of chapter 5, were plotted before and after compensation using the corrected inverse kinematics. The technique is illustrated in figure 55. PD is the desired position input from the trajectory planner and PC is the corrected command position to be fed forward to the CMM servo controller. To properly quantify and model the thermal state changes, the CMM structure was divided into macro elements. The effect of changes in the thermal state was calculated for these elements individually using the thermo-mechanical models described in chapter 3. Following, the principle of superposition was applied to find the final error resulting at the end effector. The changes in the thermal state were calculated by the state observer and fed back to modify the inverse kinematics model coefficients state. Meanwhile, the actual forward kinematics error model simulating the machine behaviour including errors, was also modified based on the machine macro-elements change of state.

The simulations covered a range of 30° C, including the reference temperature state of 20°C in the middle of the range. A sample of the model effectiveness in predicting the modifications to the commanded positions are presented by figure 56. The rest of the figures is included in Appendix K. The volumetric errors in tracking line 1 before and after application of the proposed methodology are presented by figures 56 and 57 respectively.

A reduction in error to under 1 micrometer has been achieved. The error resulting from thermal state changes has more impact at the positions further away in the work volume from the home position of the machine. This is because the CMM will, in all circumstances, start at the home position and consider all other measurements as relative to it. Further away from the home position, more material is included in the axes and so more thermal effect will be experienced as accumulative errors. This is in agreement with thermo-mechanical models suggested in equation (11) and (12). Investigating the contours of errors resulting after compensation, a trace of second order curvature can be seen. This is due to the fact that the regression model performing the correction is a second order polynomial. The performance improvement of the CMM as a result of the proposed methodology including modelling and compensation, is very significant. The machine volumetric error has been reduced from an average maximum error of 500 μm for all lines to less than 1 μm. This is a percentage reduction of 99.99 %. This is also very close to the resolution of the CMM encoder, which is 1 μm, and therefore provides very firm grounds to use the methodology with great confidence.

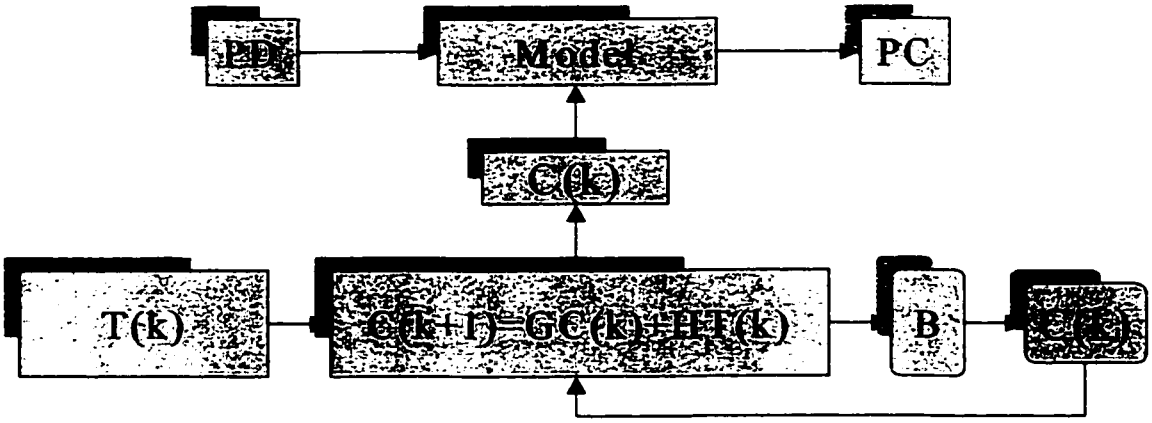


**Figure 55** State observation integration for contouring error correction.

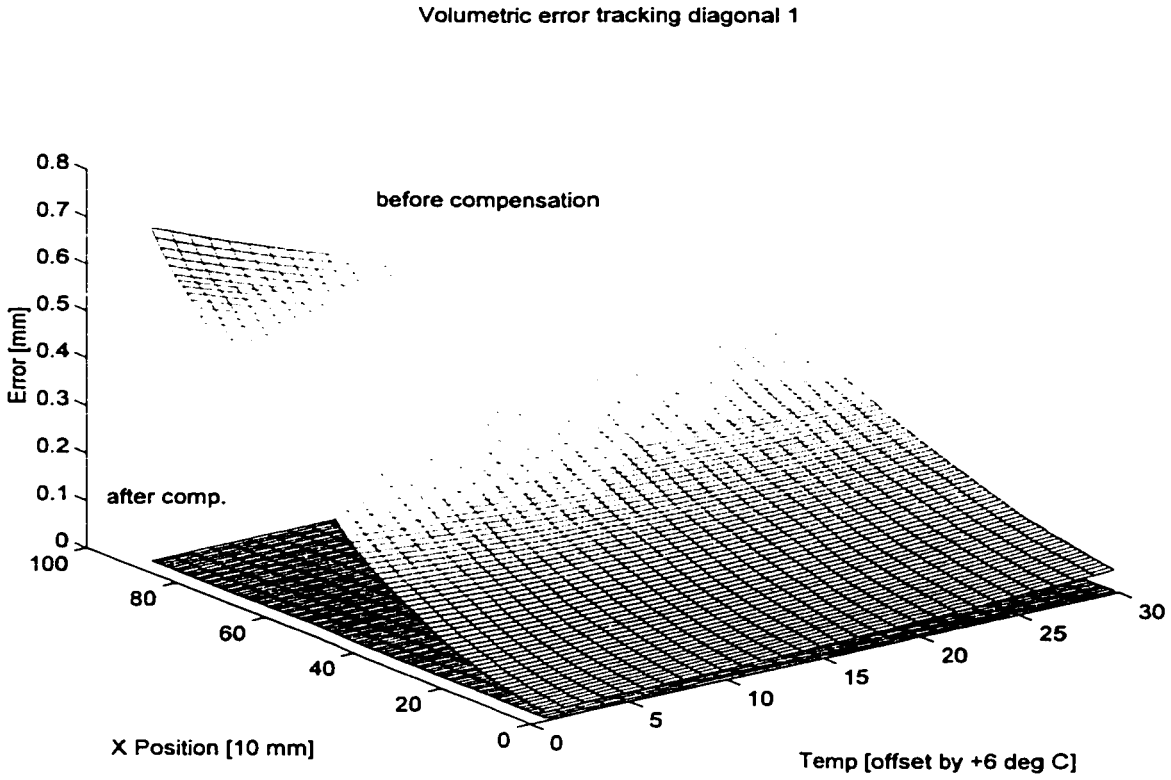


**Figure 14** Line 1 contouring error before and after correction, at different temperatures.

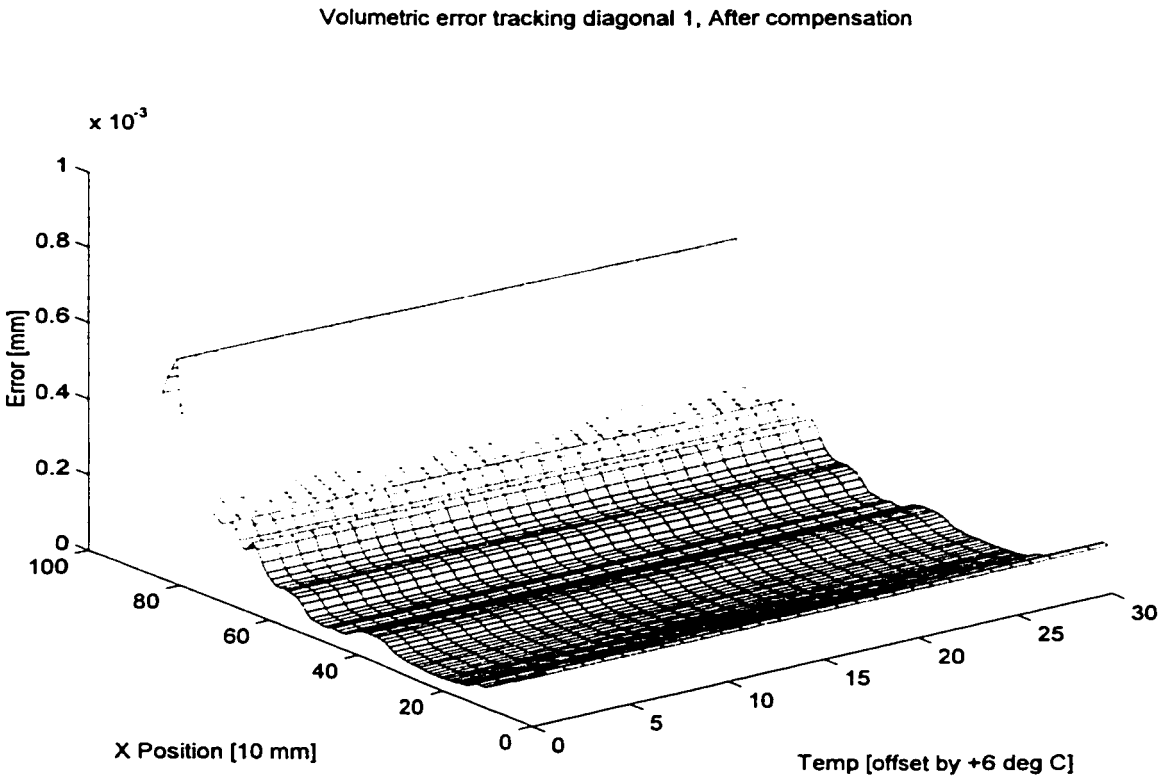


**Figure 15** Line 1 contouring error after correction.

## 6.5 Summary

This chapter completed the detailed description of implementation results that was started in chapter 5. The experimental results for CMM quasi-static errors compensation, including the thermal errors, were presented here. The experimental plan was analogous to the previous chapter where model error functions were actually measured by laser as a function of position and at different thermal states. These error functions were theoretically predicted using known thermo-mechanical models. The total of these error functions have been measured, analyzed and plotted as functions of position and temperature or gradient relatively. This also involved using different thermocouple sensors readings distributed around the machine to obtain the actual thermal state. These findings came out in agreement with the underlying physics of the previously discussed model. Furthermore, these models were updated using actual measurements, making the final model a hybrid between analytical and empirical methods. Error functions that were not thermally influenced were empirically modelled. Consequently, the kinematic models were applied in compensation for both measurement and contouring errors.

A novel performance evaluation test based on the standard B.89 with modification was proposed and tested. This is due to the unavailability of a standard evaluation test to measure the CMM performance in a thermally changing environment.

Chapter Seven

# Conclusions and Recommendations

In conclusion, a methodology for modelling and compensation of CMM quasi-static errors, including thermally induced ones, was proposed and applied. The influence of these errors on the performance of a CMM in both measuring and contouring operations, was dramatically reduced by applying the compensation strategy proposed in this thesis.

## 7.1 Concluding remarks

The high quality and precision demands by industry formed the motivation for this research. A CMM was chosen because of its ability to perform both measurement and contouring operations. These two categories of operations are the most common operations

performed by both machine tools and CMMs. Moreover, a CMM was chosen because of its critical importance as the instrument based on which the final quality of products can be decided. Since the quasi static error constitutes almost 70 % of the error affecting these machines, the correcting of this error established a remarkable improvement in the performance of these machines in general, and the CMM at hand in specific. It is to be mentioned here that the chosen CMM represents an intrinsic machine. The majority of available machines belong to this kinematic arrangement unless they are made for a very specific purpose.

The objective of this thesis was to develop a cost effective and systematic method for CMM quasi-static error correction by compensation. A CMM was selected as the test bed for this research. The standard ASME B.89 performance evaluation test was carried out to characterize the machine performance. In spite of the fact that the volumetric errors observed had values which are by far higher than those specified by the manufacturer, the machine was left as it is without physical adjustments. This is also contrary to the literature reports that compensation works only for small ranges of error and the larger errors have to be corrected at the design, assembly, and maintenance stages. The reason for this was to provide an actual evaluation of the effectiveness of compensation in correcting errors of larger than usual magnitudes. The result was surprisingly positive. The proposed methodology effectively reduced the volumetric error in the B.89 test of the machine by 97%.

This thesis proposed and tested a methodology for modelling and correction of errors in multi-axis machines. The kinematic model of the CMM was enhanced by upgrading it to

a hybrid of both analytical and empirical modelling. This allowed the incorporation of the tested CMM signature as each machine carries a slightly different signature. Systematic modelling of the machine was carried out in two stages; the first stage is based on physical modelling and consists of using the HTM's to model the machine kinematics in a reference thermal state and arrive at an error model. This model was used in conjunction with the proposed compensation strategy to correct for the machine measurement errors. The proposed strategy was tested using the ASME B.89.1.12.M standard CMM performance evaluation test and resulted in 93 % measurement error reduction. Error functions or coefficients of the model were calculated using two methods. The first method consisted of measuring a common artifact in a lattice of positions in the CMM work volume. This was accomplished through structured measurements of a ring gauge in the work space of the CMM. These measurements were conducted in a reference temperature and almost stable ambient conditions. Based on the results of these measurements, a model and a compensation strategy to improve the CMM volumetric performance was devised and applied. Some processing including statistical methods, in addition to interpolation, was employed to analyse these measurements and arrive at proper values to use for the model. The second method consisted of error functions measurement by laser interferometry. Compared to the first method, the laser data did not require any processing except interpolation for in-between points and gave values for each of the error functions individually. In addition, the performance of the compensation strategy based on the laser model surpassed the one based on the first method. This outcome confirmed the literature

prediction of the laser measurements being superior in evaluating the model error functions compared to all other models.

Before any compensation was carried out, a rapid, and cost effective test was proposed to be applied at shop floors for CMM error inspection. This test is using a ring gauge and would give a fast indication of the magnitude of CMM volumetric error so a proper decision between maintenance and compensation strategy modification can be made.

In the second stage of the thesis, ambient thermal changes were incorporated in the kinematics models through the use of basic theoretical models as a start. These error functions models were then verified and calibrated according to the actual laser measurements at varying thermal states. A performance evaluation test for the machine performance in thermally varying environment was proposed because of the lack of existence of a formal alternative. It was based on the B.89 standard test with modifications. The final kinematic models were tested through this modified version of the standard performance evaluation of the CMM, in conjunction with the proposed compensation strategy. The modification included the standard ASME B.89 performance evaluation of the CMM while having random variations in the machine and ambient thermal conditions. These changes were introduced using an experimental setup built for this purpose. As expected, the performance of the CMM deteriorated by the introduction of the thermal disturbances and instability. However, the application of the proposed compensation strategy improved the performance from its worst case by 97 %. The amount of work volume tolerance was reduced from 782.9 micron to 18.7 micron. This gave a solid proof of the correctness of the

proposed models to estimate the errors and the effectiveness of the proposed strategy to make the model capable of adapting to thermal changes.

Based on the error model developed, the inverse kinematics modelling was carried out for both stages using nonlinear regression analysis, due to the difficulty in inverting the forward kinematics of the machine. Choice of parameters of the analytical models was based on both the analysis-of-variance technique (ANOVA), and independent data testing. Inverse kinematics were necessary to carry out contouring error compensation. This compensation strategy proposed the incorporation of modifications in the feed forward path of the commanded positions to the machine motion commands. This strategy provides a viable alternative to attempting to modify the control loop of the machine which introduces different problems ranging from stability issues to controller accessibility.

The proposed methodology also provided an adaptive strategy to correct the quasi-static errors of the machine on-line using the state observer technique. The dynamic changes of machine thermal states were monitored by thermocouples. Based on data of these sensors, the state of the models error functions was updated using a state observer. Construction of the models and the state observer was carried out systematically to arrive at the final models. The proposed methodology including the models and the adaptive compensation strategy was tested by simulating the machine in contouring different trajectories. These trajectories were selected to be the diagonal straight lines in the CMM work volume because they provide coverage of a wide range in the work volume and extensive interaction between the machine elements. The machine reaction to thermal changes was calculated using an experimentally

determined effective coefficient of thermal expansion (ECTE). This also involved the use of a thermo-mechanical model derived from basic principles. The adaptive compensation strategy for contouring was applied while contouring the selected trajectories in a range of temperature close to shop floor environment. Results obtained show a significant error reduction to values below one micrometer.

## 7.2 Recommendations and future issues

Based on the literature recommendations and the results presented in this thesis, compensation for CMM errors can be an effective solution for errors. The condition is that these errors have to be restricted to a certain magnitude. Such errors can be the collection of errors left after all efforts have been exhausted for correction in the design, assembly, and maintenance stages. In addition, these errors can be the result of normal machine wear and tear as well as normal thermal state changes. This is in spite of the fact that in the particular case studied in this thesis, the error range was allowed to be of an extremely high magnitude. Although the compensation strategy proposed successfully improved the machine performance, the less the error left for compensation the better the results can be. In addition, it is recommended that a rapid test be applied to the machine before applying compensation to correct its error. Some errors can be corrected through regular maintenance. Other errors indicate defective parts or have an intermittent nature. The error magnitude might be too high to compensate for. These and other possibilities have to be considered and ruled out before considering compensation as a solution to the machine errors.

Once decided, a systematic approach and application of the modelling and compensation methodology have to be followed. Some hardware might be required like sensors and data processing systems.

Installing sensors and some other hardware, like a data acquisition system, for compensation to treat the thermally induced errors of the machine, introduces an extra cost to the machine capital investment. The premises of compensation as a solution for error elimination is the fact that it is a very cost effective solution. Once hardware and expertise are added, the cost of production of the machine becomes high to the point that it might become incompetent. Therefore, alternatives like having a thermally controlled room to preserve the machine would still hold some credit until something could be done about the cost of thermal compensation in the machine. A compromise justifying the extra machine cost can be argued based on the fact that the CMM now is closer to being installed on the shop floor right next to the production line. This will improve production cost, time, and quality through promotion of automation and cutting down on time and labour requirement. In addition, the rapid development in data processing hardware should gradually bring the cost of thermal compensation kits down to a competent level. The general knowledge gained through this research as well as these arguments should take the CMM steps closer to the production line.

This thesis investigated, modelled, and compensated thermal errors based on average temperature changes and spatial temperature gradients. This leaves an open research issue that is concerned with understanding other types of temperature effects as well as the

possibility of existence of a comprehensive model for the machine and thermal state relation in general. This also leaves another research issue open which is the effect of time gradients of thermal effects and cyclic thermal changes effects. This is specifically important for cycles of thermal changes that approach the natural machine thermal time constants.

The modelling methodology and compensation strategy proposed in this research were attempted as general as could possibly be. Still some specific models calibration had to be done to incorporate the signature of the machine at hand. For the proposed strategy to be generalized, a relation between the machine identifying parameters and the machine models have to be investigated. This will require carrying out research in two directions. The first direction is to investigate certain parameters of machines that identify them by having differences from one machine to the other. The second direction is the attempt to characterize the relation between the machine specific models and error functions and its identifying parameters. Such research issues will stay open for a while and propose a wide angle of investigation to be carried out.

# Appendix A

## ASME B.89 standard performance evaluation test for CMMs

Ball bar locations and orientations determined by the ASME B.89.1.12M 1990, and used for CMM performance evaluation are included in the enclosed figures. The Ball bar used in the tests is shown in figure A.1. The test locations and orientations are shown by figure A.2.

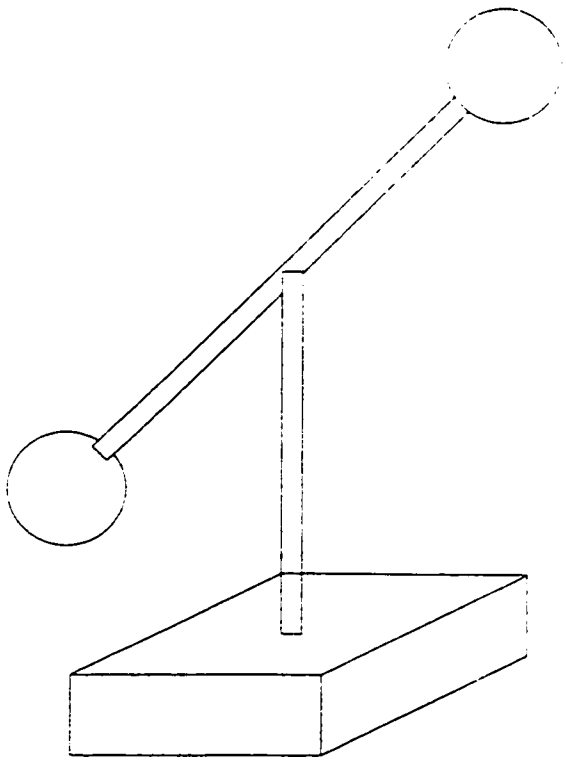

**Figure 58** Sketch of the ball bar used as an artifact in the ASME B.89 standard test.

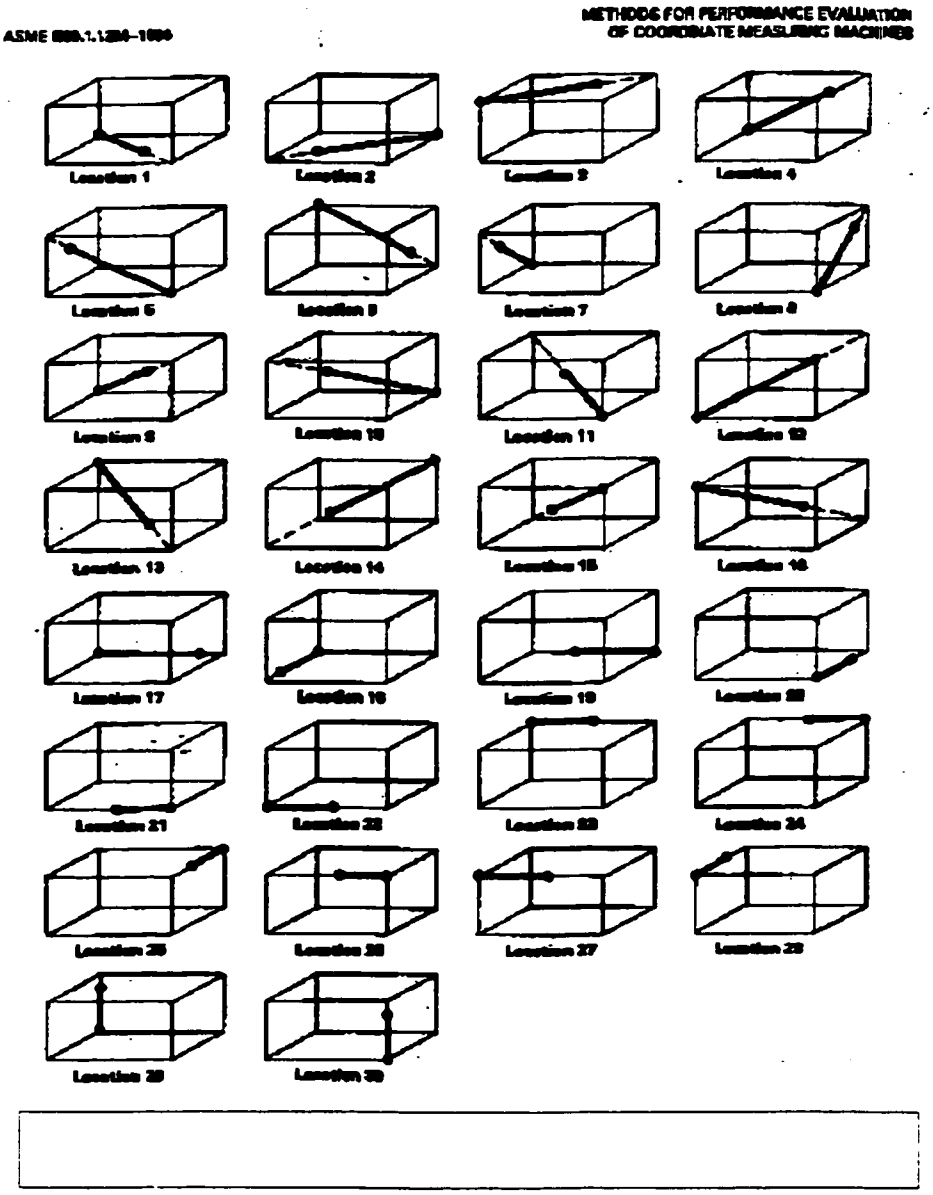

**Figure 59** Ball bar positions and orientations in the CMM work volume recommended by the ASME B.89 for conducting the performance evaluation test.

# Appendix B

## Individual matrices for each link and joint of the CMM and the final error model and compensation equations

Applying the Homogeneous Transformation Matrices (HTMs) method to model the CMM results in a set of matrices representing the kinematics of the parts of the machine and their interaction. Based on figure 12, the Individual links and joints transformation matrices with errors are as follows:

$$S_1 = \begin{bmatrix} 1 & -\gamma_1 & \beta_1 & a_1+\Delta a_1 \\ \gamma_1 & 1 & -\alpha_1 & \Delta b_1 \\ -\beta_1 & \alpha_1 & 1 & \Delta c_1 \\ 0 & 0 & 0 & 1 \end{bmatrix}$$

$$J_1 = \begin{bmatrix} 1 & -\gamma_{1x} & \beta_{1x} & x_1+\Delta x_1 \\ \gamma_{1x} & 1 & -\alpha_{1x} & \epsilon_{y1} \\ -\beta_{1x} & -\alpha_{1x} & 1 & \epsilon_{z1} \\ 0 & 0 & 0 & 1 \end{bmatrix} \qquad (1)$$

$$S_2 = \begin{bmatrix} 1 & -\gamma_2 & \beta_2 & \Delta a_2 \\ \gamma_2 & 1 & -\alpha_2 & b_2+\Delta b_2 \\ -\beta_2 & \alpha_2 & 1 & c_2+\Delta c_2 \\ 0 & 0 & 0 & 1 \end{bmatrix}$$

$$J_2 = \begin{bmatrix} 1 & -\gamma_{2y} & \beta_{2y} & \epsilon_{x2} \\ \gamma_{2y} & 1 & -\alpha_{2y} & y_2+\Delta y_2 \\ -\beta_{2y} & -\alpha_{2y} & 1 & \epsilon_{z2} \\ 0 & 0 & 0 & 1 \end{bmatrix} \quad (36)$$

$$S_3 = \begin{bmatrix} 1 & -\gamma_3 & \beta_3 & a3+\Delta a_3 \\ \gamma_3 & 1 & -\alpha_3 & \Delta b_3 \\ -\beta_3 & \alpha_3 & 1 & -c_3-\Delta c_3 \\ 0 & 0 & 0 & 1 \end{bmatrix}$$

$$J_3 = \begin{bmatrix} 1 & -\gamma_{3z} & \beta_{3z} & \epsilon_{x3} \\ \gamma_{3z} & 1 & -\alpha_{3z} & \epsilon_{y3} \\ -\beta_{3z} & -\alpha_{3z} & 1 & z_3+\Delta z_3 \\ 0 & 0 & 0 & 1 \end{bmatrix} \quad (37)$$

$$S_4 = \begin{bmatrix} 1 & -\gamma_4 & \beta_4 & \Delta a_4 \\ \gamma_4 & 1 & -\alpha_4 & \Delta b_4 \\ -\beta_4 & \alpha_4 & 1 & -c_4-\Delta c_4 \\ 0 & 0 & 0 & 1 \end{bmatrix} \quad (38)$$

$$
\begin{aligned}
\epsilon_{y1} &= \int_0^{x_1} \gamma\, dx \\
\epsilon_{z1} &= \int_0^{x_1} \beta\, dx \\
\epsilon_{x2} &= \int_0^{y_2} \gamma\, dy \\
\epsilon_{z2} &= \int_0^{y_2} \alpha\, dy \\
\epsilon_{x3} &= \int_0^{z_3} \beta\, dz \\
\epsilon_{y3} &= \int_0^{z_3} \alpha\, dz
\end{aligned}
\tag{39}
$$

Transformation matrices after multiplication for each combined link and joint.

$$
T_1 = \begin{bmatrix}
1 & -\gamma_1-\gamma_{1x} & \beta_1-\beta_{1x} & x_1+\Delta x_1+a_1+\Delta a_1 \\
\gamma_1+\gamma_{1x} & 1 & -\alpha_1-\alpha_{1x} & \Delta b_1+\epsilon_{y1}+\gamma_1 x_1 \\
-\beta_1-\beta_{1x} & \alpha_1+\alpha_{1x} & 1 & -\beta_1 x_1+\epsilon_{z1}+\Delta c_1 \\
0 & 0 & 0 & 1
\end{bmatrix}
\tag{40}
$$

$$
T_2 = \begin{bmatrix}
1 & -\gamma_2-\gamma_{2y} & \beta_2-\beta_{2y} & \epsilon_{x2}-\gamma_2 y_2+\Delta a_2 \\
\gamma_2+\gamma_{2y} & 1 & -\alpha_2-\alpha_{2y} & b_2+\Delta b_2+y_2+\Delta y_2 \\
-\beta_2-\beta_{2y} & \alpha_2+\alpha_{2y} & 1 & \alpha_2 y_2+\epsilon_{z2}+c_2+\Delta c_2 \\
0 & 0 & 0 & 1
\end{bmatrix}
\tag{41}
$$

$$T_3 = \begin{bmatrix} 1 & -\gamma_3-\gamma_{3z} & \beta_3-\beta_{3z} & \epsilon_{x3}+\beta_3 z_3+a3+\Delta a_3 \\ \gamma_3+\gamma_{3z} & 1 & -\alpha_3-\alpha_{3z} & \epsilon_{y3}-\alpha_3 z_3+\Delta b_3 \\ -\beta_3-\beta_{3z} & \alpha_3+\alpha_{3z} & 1 & z_3+\Delta z_3-c_3-\Delta c_3 \\ 0 & 0 & 0 & 1 \end{bmatrix} \quad (42)$$

$$T_4 = \begin{bmatrix} 1 & -\gamma_4 & \beta_4 & \Delta a_4 \\ \gamma_4 & 1 & -\alpha_4 & \Delta b_4 \\ -\beta_4 & \alpha_4 & 1 & -c_4-\Delta c_4 \\ 0 & 0 & 0 & 1 \end{bmatrix} \quad (43)$$

Final form of the transformation matrix (Kinematic Model).

$$ {}^{ref}T_{probe} = \begin{bmatrix} 1 & T12 & T13 & T14 \\ T21 & 1 & T23 & T24 \\ T31 & T32 & 1 & T34 \\ 0 & 0 & 0 & 1 \end{bmatrix} \quad (44)$$

$$T12 = -\gamma_1-\gamma_{1x}-\gamma_2-\gamma_{2y}-\gamma_3-\gamma_{3z}-\gamma_4$$

$$T13 = \beta_4+\beta_3-\beta_{3z}+\beta_2-\beta_{2y}+\beta_1-\beta_{1x}$$

$$T14 = \beta_3 z_3+\epsilon_{x2}+a_1+\Delta a_1+x_1+\Delta X_1+\epsilon_{x3}+\Delta a_3-\gamma_2 y_2+a_3+\Delta a_2+\Delta a_4-\gamma_{1x} y_2$$
$$-\gamma_{1x} b_2-\gamma_1 y_2-\gamma_1 b_2-\beta_{1x} c_2+\beta_1 c_2-\beta_{2y} z_3+\beta_{2y} c_3+\beta_2 z_3-\beta_2 c_3$$
$$-\beta_{1x} z_3+\beta_{1x} c_3+\beta_1 z_3-\beta_1 c_3-\beta_3 c_4-\beta_2 c_4+\beta_{1x} c_4+\beta_{2y} c_4-\beta_1 c_4+\beta_{3z} c_4$$

$$
\begin{aligned}
T21 &= \gamma_1+\gamma_{1x}+\gamma_2+\gamma_{2y}+\gamma_3+\gamma_{3z}+\gamma_4 \\
T23 &= -\alpha_4-\alpha_3-\alpha_{3z}-\alpha_2-\alpha_{2y}-\alpha_1-\alpha_{1x} \\
T24 &= \alpha_3c_4+\alpha_{1x}c_4+\alpha_{2y}c_4+\alpha_1c_4+\alpha_{3z}c_4+\alpha_2c_4-\alpha_3z_3+\Delta b_3+\epsilon_{y1}+\Delta b_1 \\
&\quad +\gamma_1x_1+\epsilon_{y3}+b_2+\Delta b_2+y_2+\Delta y_2+\Delta b_4-\alpha_{2y}z_3+\alpha_{2y}c_3-\alpha_2z_3 \\
&\quad +\alpha_2c_3-\alpha_{1x}z_3+\alpha_{1x}c_3-\alpha_1z_3+\alpha_1c_3+\gamma_1a_3+\gamma_2a_3+\gamma_{1x}a_3+\gamma_{2y}a_3-\alpha_{1x}c_2-\alpha_1c_2
\end{aligned}
\tag{45}
$$

$$
\begin{aligned}
T31 &= -\beta_1-\beta_{1x}-\beta_2-\beta_{2y}-\beta_3-\beta_{3z}-\beta_4 \\
T32 &= \alpha_4+\alpha_3+\alpha_{3z}+\alpha_2+\alpha_{2y}+\alpha_1+\alpha_{1x} \\
T34 &= z_3+\Delta z_3-\Delta c_3-c_3+\epsilon_{z1}+\epsilon_{z2}+\Delta c_1-\beta_1x_1+c_2+\Delta c_2+\alpha_2y_2-c_4 \\
&\quad -\Delta c_4-\beta_1a_3-\beta_{1x}a_3-\beta_2a_3-\beta_{2y}a_3-\alpha_1y_2+\alpha_1b_2+\alpha_{1x}y_2+\alpha_{1x}b_2
\end{aligned}
\tag{46}
$$

Compensation Terms :

$$\begin{aligned} E_x = {} & \beta_3 z_3 + \epsilon_{x2} + \Delta a_1 + \Delta X_1 + \epsilon_{x3} + \Delta a_3 - \gamma_2 y_2 + \Delta a_2 + \Delta a_4 - \gamma_{1x} y_2 \\ & - \gamma_{1x} b_2 - \gamma_1 y_2 - \gamma_1 b_2 - \beta_{1x} c_2 + \beta_1 c_2 - \beta_{2y} z_3 + \beta_{2y} c_3 + \beta_2 z_3 - \beta_2 c_3 \\ & - \beta_{1x} z_3 + \beta_{1x} c_3 + \beta_1 z_3 - \beta_1 c_3 - \beta_3 c_4 - \beta_2 c_4 + \beta_{1x} c_4 + \beta_{2y} c_4 - \beta_1 c_4 + \beta_{3z} c_4 \end{aligned} \quad (47)$$

$$\begin{aligned} E_y = {} & \alpha_3 c_4 + \alpha_{1x} c_4 + \alpha_{2y} c_4 + \alpha_1 c_4 + \alpha_{3z} c_4 + \alpha_2 c_4 - \alpha_3 z_3 + \Delta b_3 + \epsilon_{y1} + \Delta b_1 \\ & + \gamma_1 x_1 + \epsilon_{y3} + \Delta b_2 + \Delta y_2 + \Delta b_4 - \alpha_{2y} z_3 + \alpha_{2y} c_3 - \alpha_2 z_3 + \alpha_2 c_3 - \alpha_{1x} z_3 \\ & + \alpha_{1x} c_3 - \alpha_1 z_3 + \alpha_1 c_3 + \gamma_1 a_3 + \gamma_2 a_3 + \gamma_{1x} a_3 + \gamma_{2y} a_3 - \alpha_{1x} c_2 - \alpha_1 c_2 \end{aligned} \quad (48)$$

$$\begin{aligned} E_z = {} & \Delta z_3 - \Delta c_3 + \epsilon_{z1} + \epsilon_{z2} + \Delta c_1 - \beta_1 x_1 + \Delta c_2 + \alpha_2 y_2 - \Delta c_4 - \beta_1 a_3 \\ & - \beta_{1x} a_3 - \beta_2 a_3 - \beta_{2y} a_3 - \alpha_1 y_2 + \alpha_1 b_2 + \alpha_{1x} y_2 + \alpha_{1x} b_2 \end{aligned} \quad (49)$$

# Appendix C

## Thermal errors first and second order models derivation

The results of a thermal gradient affecting a structural element on the element dimension perpendicular to the gradient direction, can be calculated using the following equations.

1. For a cantilever element, shown by figure (60), the gradient in temperature between two ends along a dimension H, can be calculated as:

$$grad_Z = \frac{T_2 - T_1}{H} \tag{50}$$

The small change of angle can be approximated as:

$$d\beta = \alpha \cdot grad_Z \cdot dx \tag{51}$$

The angle value as a function of x can be calculated as:

$$\beta(x) = \int_0^x \alpha.grad_z.dx = \alpha.grad_z.x \tag{52}$$

The deflection caused by the gradient is then:

$$dZ = \beta \cdot dX \tag{53}$$

Which, finally is:

$$Z(x) = \int_0^x \beta(x)dx = \int_0^x \alpha.grad_z.xdx \tag{54}$$

The final form is:

$$Z(x) = \frac{1}{2}\alpha \cdot grad_Z \cdot x^2 \tag{55}$$

2. For a **simply supported beam**, of total length L, and free to rotate around the fixed points, x measured from the center of the elements,

$$d\beta = \alpha \cdot grad_Z \cdot dx \tag{56}$$

Therefore:

$$\beta(x) = \alpha \cdot grad_Z \cdot x \tag{57}$$

deflection in the Z direction is:

$$Z(x) = \frac{1}{2}\alpha \cdot grad_Z \cdot x^2 + c \tag{58}$$

However, deflection at x = 0.5 L, is equal to zero. Therefore, the constant c becomes:

$$c = -\frac{1}{8}\alpha \cdot grad_Z \cdot L^2 \tag{59}$$

and the equation resulting has the final form as follows:

$$Z(x) = \frac{1}{2}\beta.grad_z x^2 - \frac{L^2}{4} \quad (60)$$

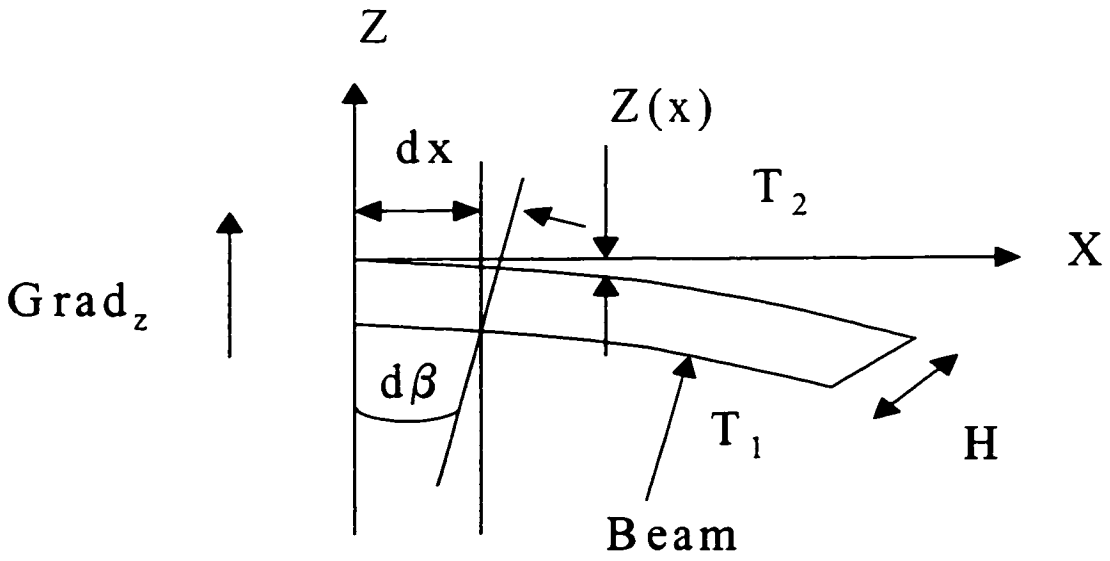


**Figure 60** Effect of thermal gradient perpendicular to the length direction of a cantilever beam.

# Appendix D

## Details of the circuit diagram and the schematics of the control box

The temperature profile of the room where the CMM is kept was controlled by introducing two commercial heaters of 1500 Watt power each. The circuitry of the two heaters was modified by introducing a relay in each to override the thermostats controlling them. These relays were connected to an external control box. The control box contains a sensitive thermal controller to the 0.1° C. The circuitry necessary to connect the controller and a thermocouple sensor of the E type were wired in the box according to the enclosed diagram. The room temperature profile was maintained at the desired values using this setup in conjunction with the building air conditioning and circulation system. In addition, two commercial de-humidifiers were also introduced to maintain the humidity of the room at a constant level. The controller of the heaters contains an advanced PID controller that maintains a steady state of the temperature sensed. Heaters were moved in different positions while monitoring the CMM sensors reading and the room sensors. By locating the heaters at different elevations and controlling the vents of the room, the desired temperatures and thermal gradients were arrived at.

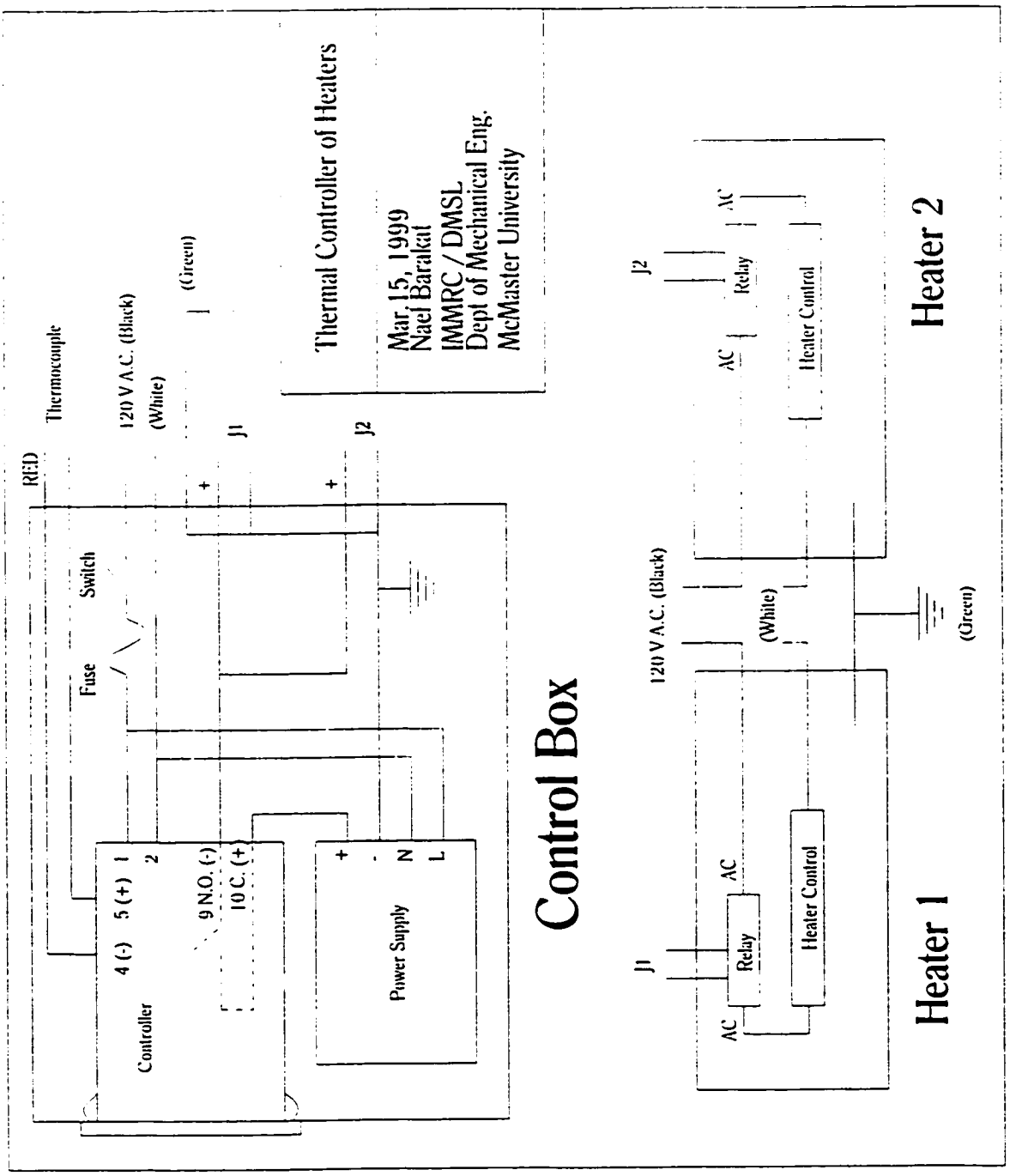


**Figure 61** Circuit diagram of the thermal control box used in the experiments.

# Appendix E

**The full set of measurement results of the error functions identified by the ring gauge**

Two methods were applied to identify the error functions of the CMM model. The results of one method are represented in this appendix. This method is based on carrying out measurements of a standard artifact (ring gauge in this case), in different locations forming a lattice covering the work volume of the CMM. The results of these measurements are presented in the coming figures. These results are processed and used in the kinematic model of the machine to predict its errors.

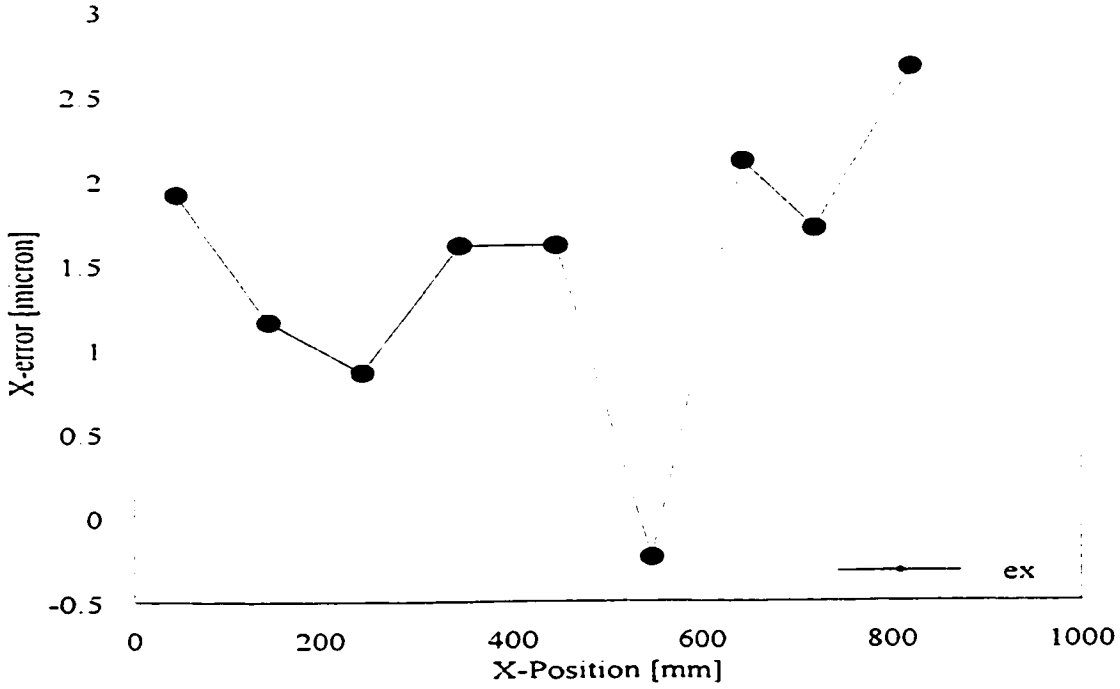


**Figure 62** Error in X-Direction as a Function of X-Position.

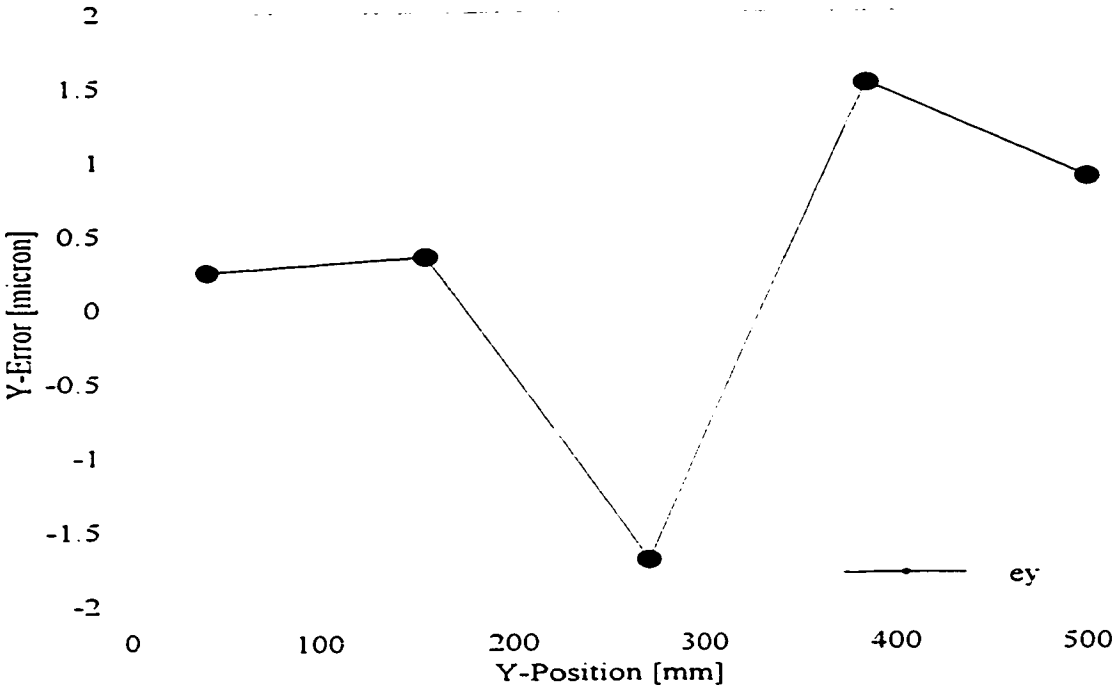


**Figure 63** Error in Y-Direction as a Function of Y-Position.

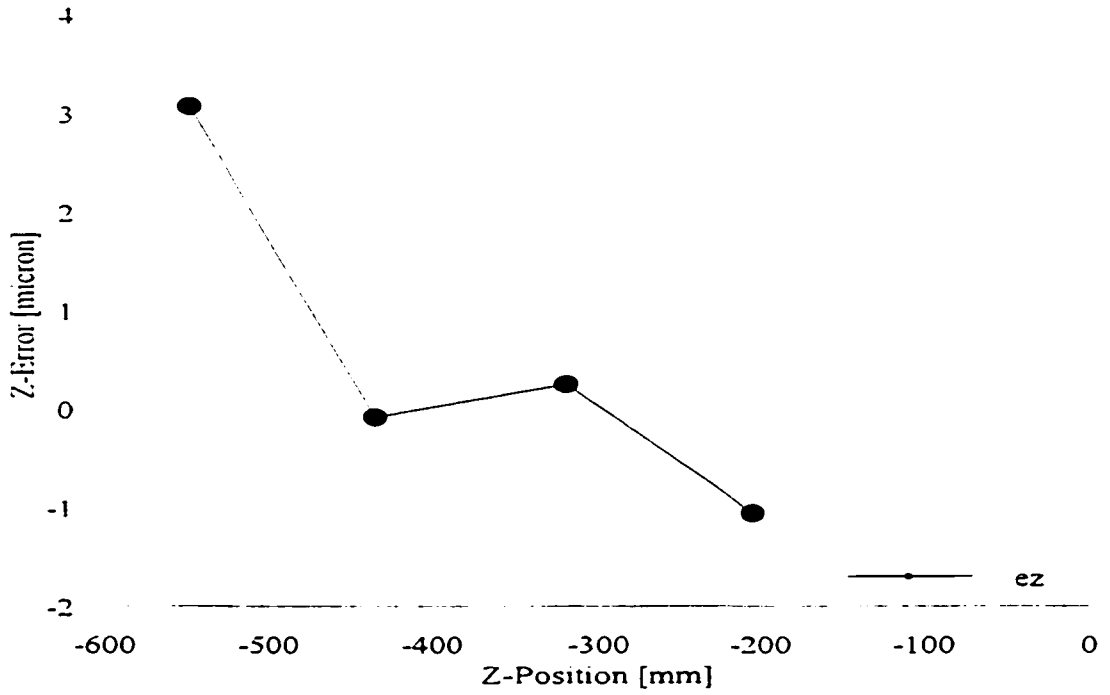


**Figure 64** Error in Z-Direction as a Function of Z-Position.

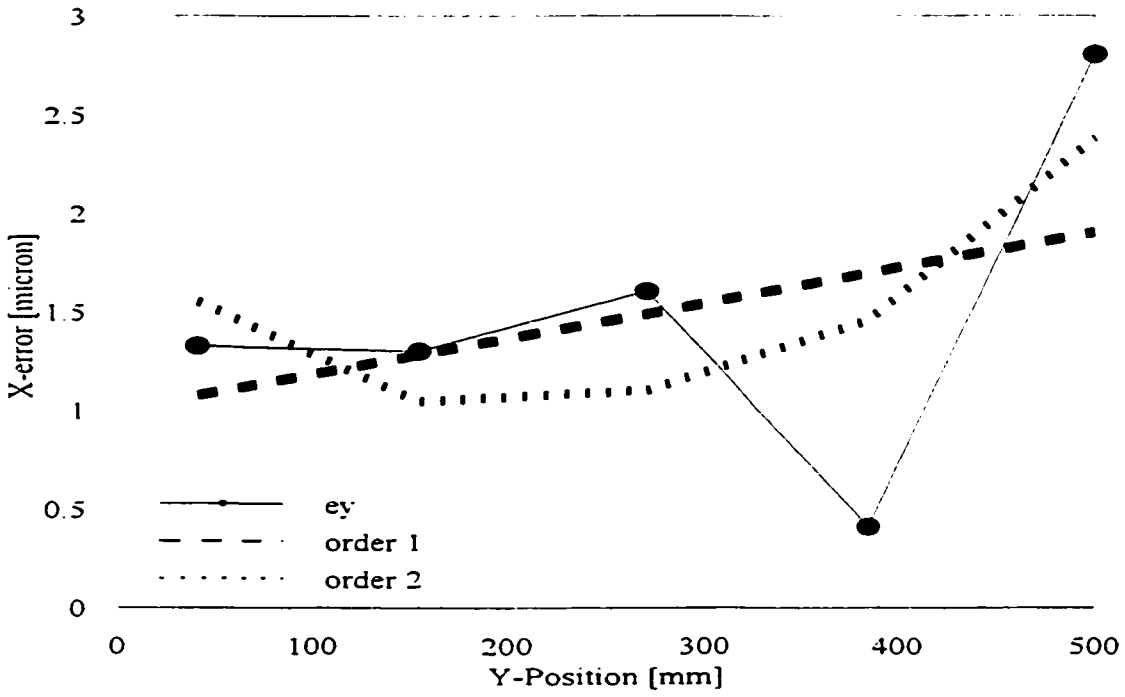


**Figure 65** Error in X-Direction as a Function of Y-Position.

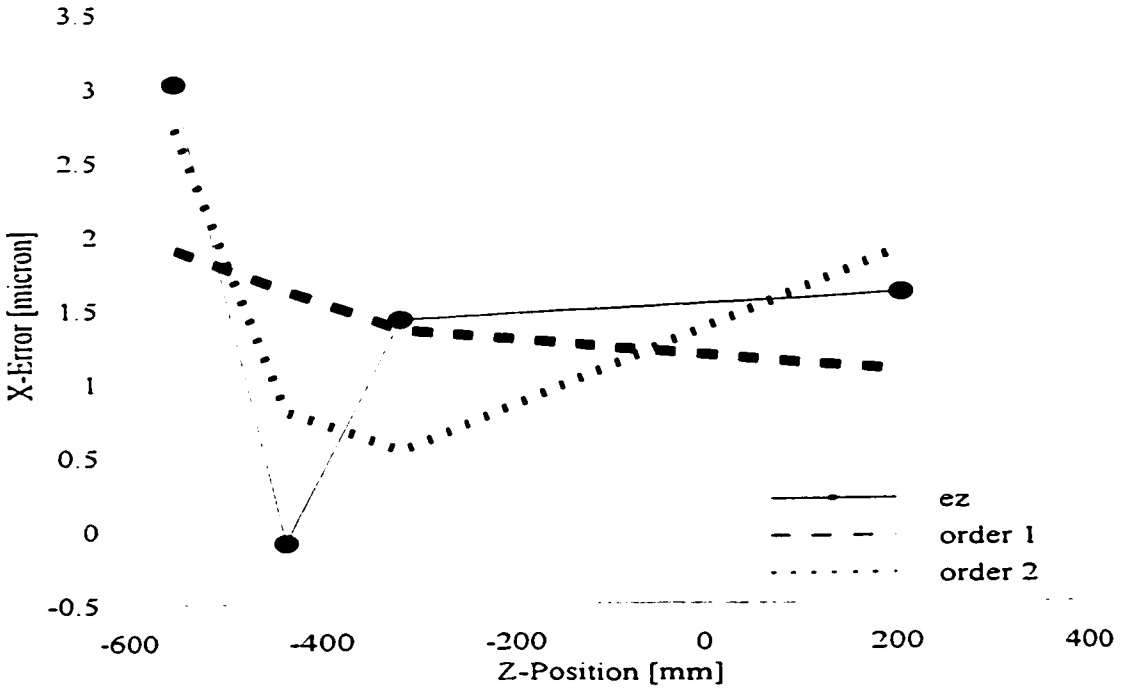


**Figure 66** Error in X-Direction as a Function of Z-Position.

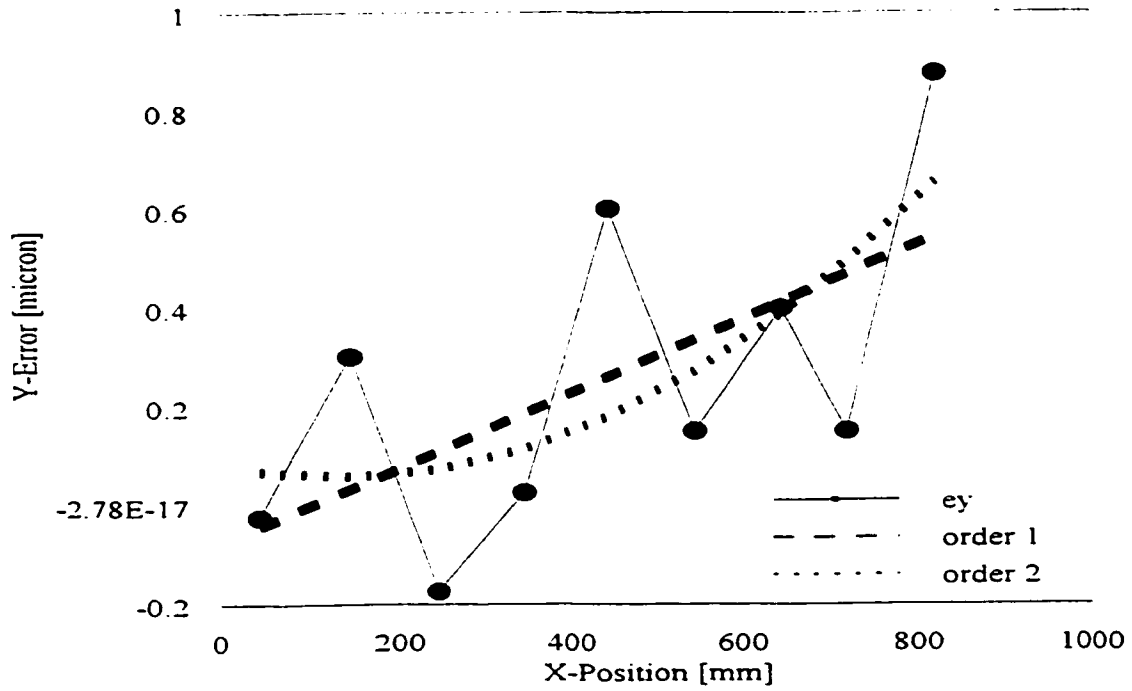


**Figure 67** Error in Y-Direction as a Function of X-Position.

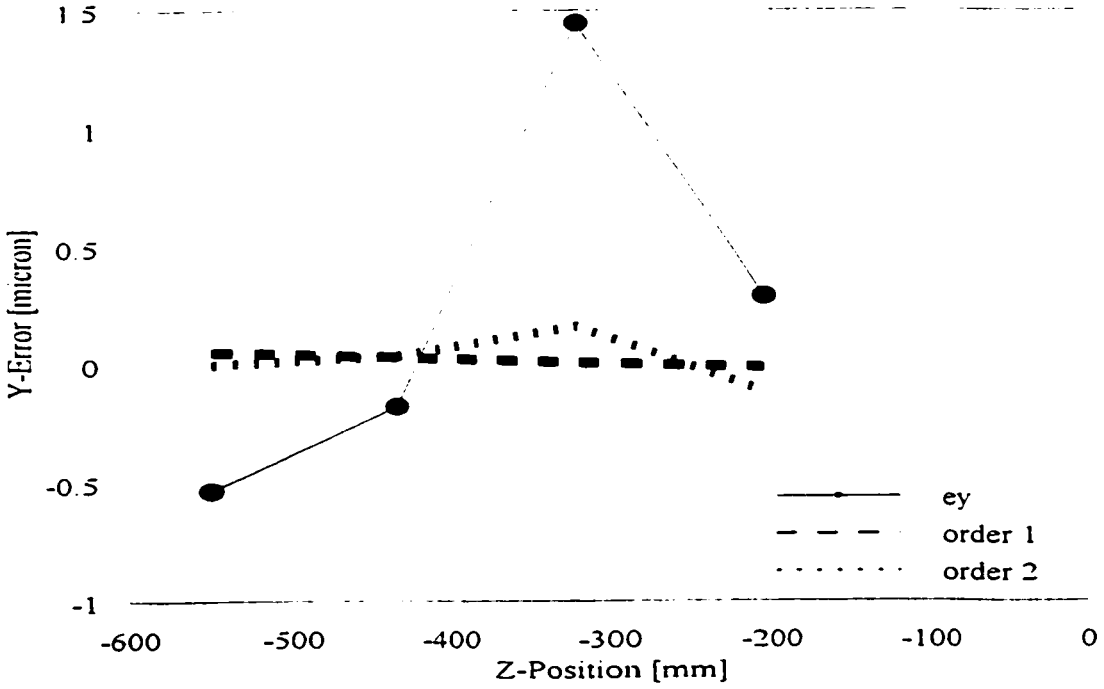


**Figure 68** Error in Y-Direction as a Function of Z- Position.

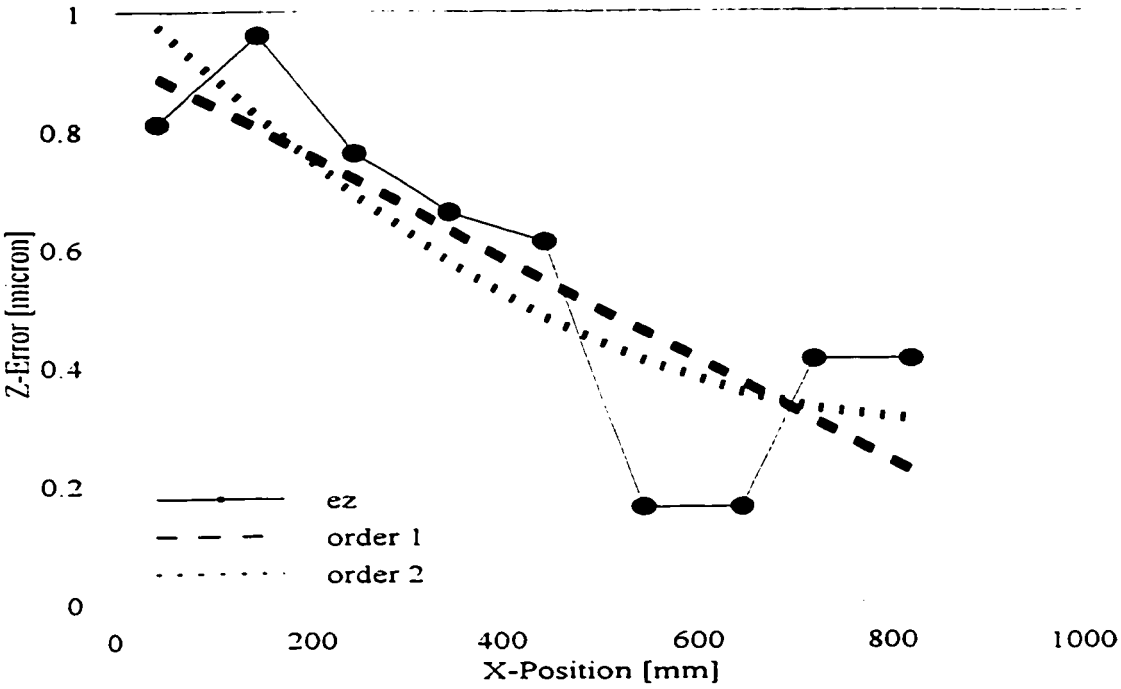


**Figure 69** Error in Z-Direction as a Function of X-Position.

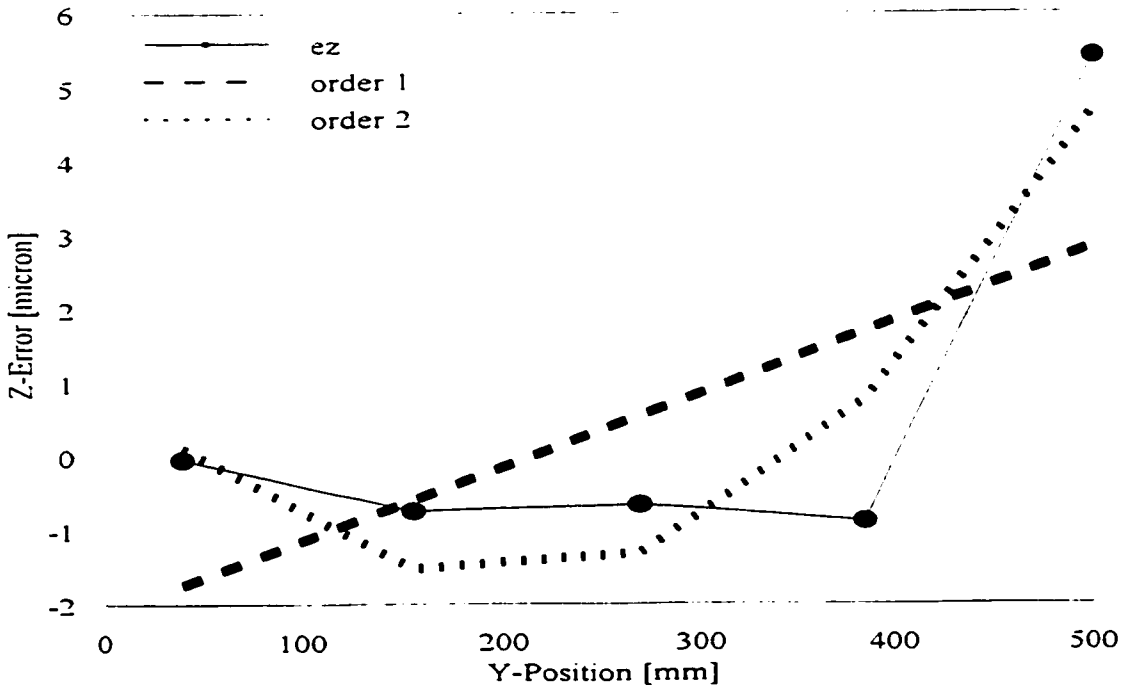


**Figure 70** Error in Z-Direction as a Function of Y-Position.

# Appendix F

**The full set of measurement results of the error functions identified by laser**

The second method applied to identify the error functions of the CMM model was direct laser measurement. The results of this method are represented in this appendix. This method is based on carrying out laser measurements of the error functions of the model directly in different locations in the work volume of the CMM. The results of these measurements are presented in the coming figures. These results are used in the kinematic model of the machine to predict its errors.

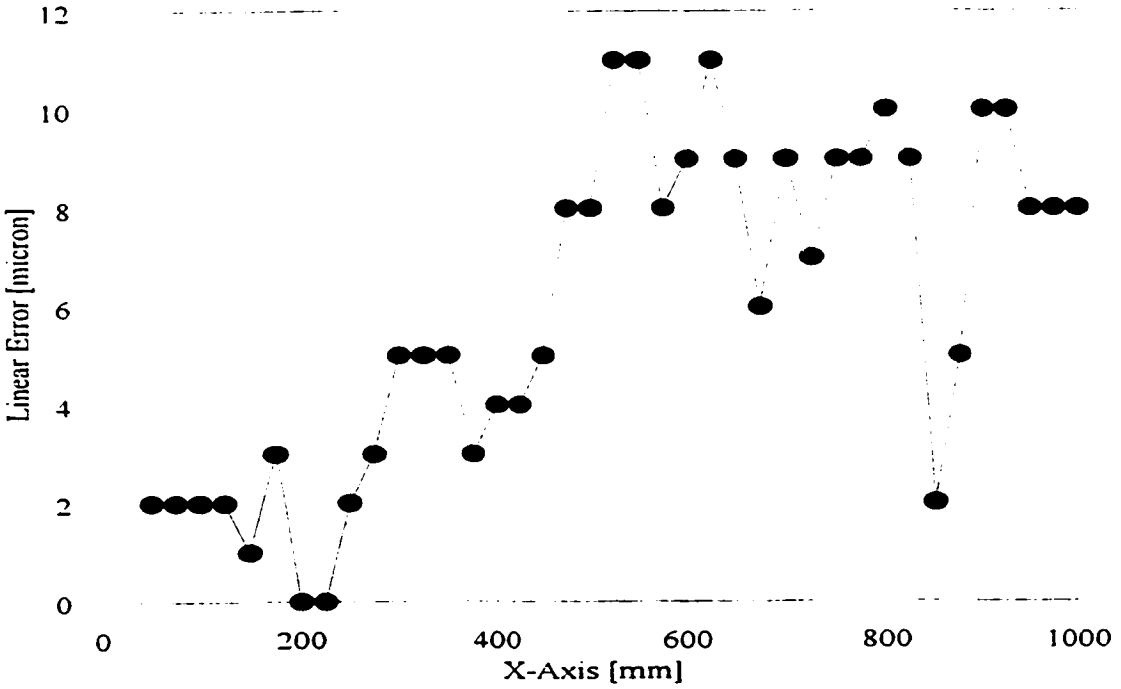


**Figure 71** Linear Error in X-axis Using Laser Measurements.

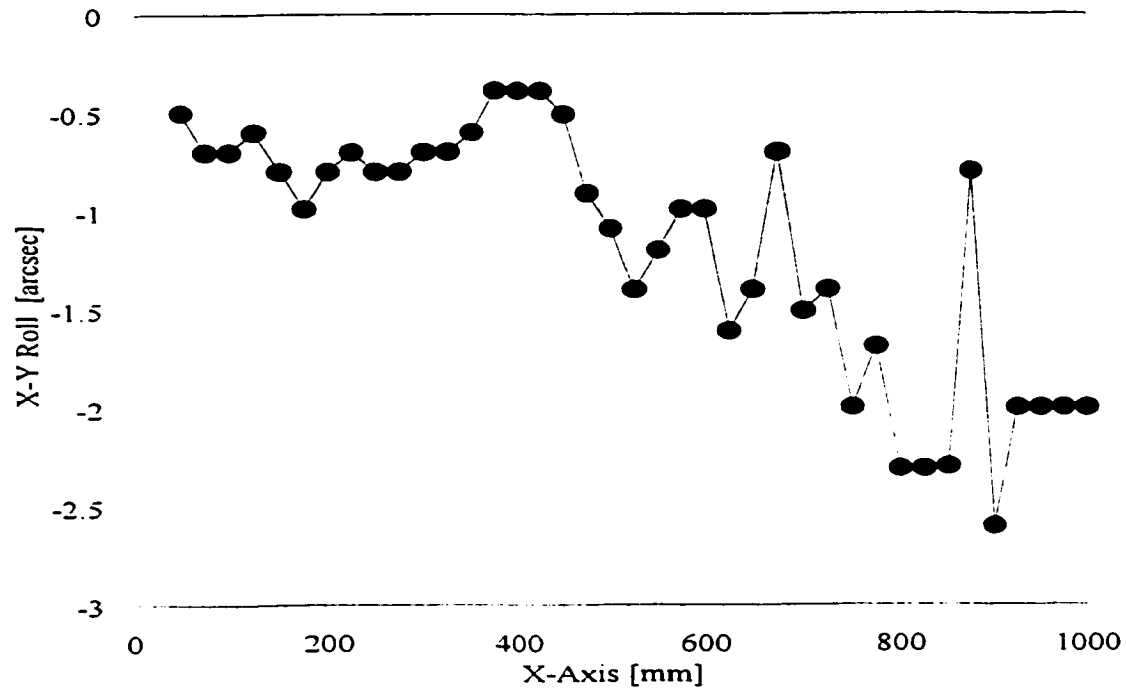


**Figure 72** X-Y Roll Angle Using Laser Measurements.

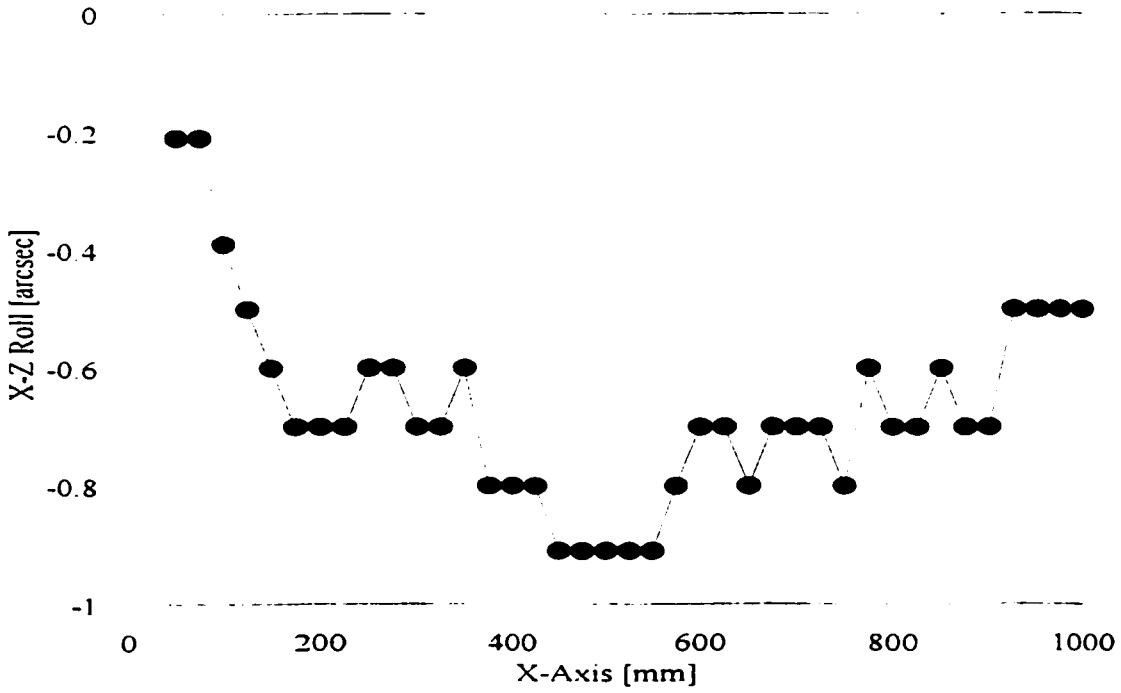


**Figure 73** X-Z Roll Angle Using Laser Measurements.

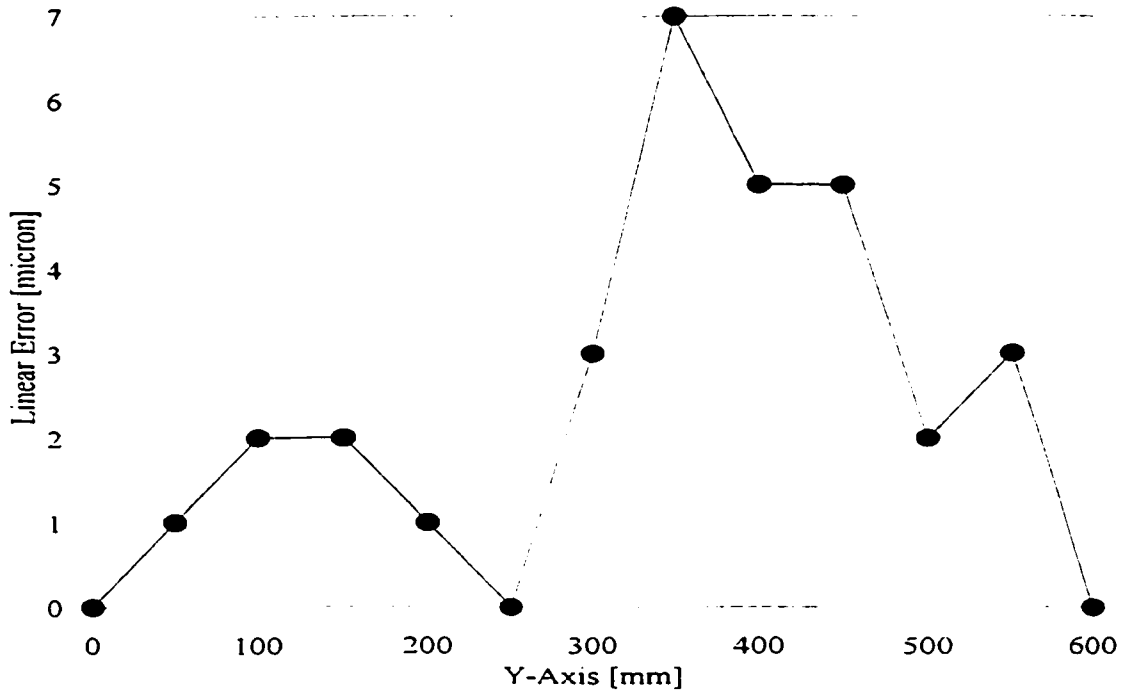


**Figure 74** Linear Error in Y-Axis Using Laser Measurements.

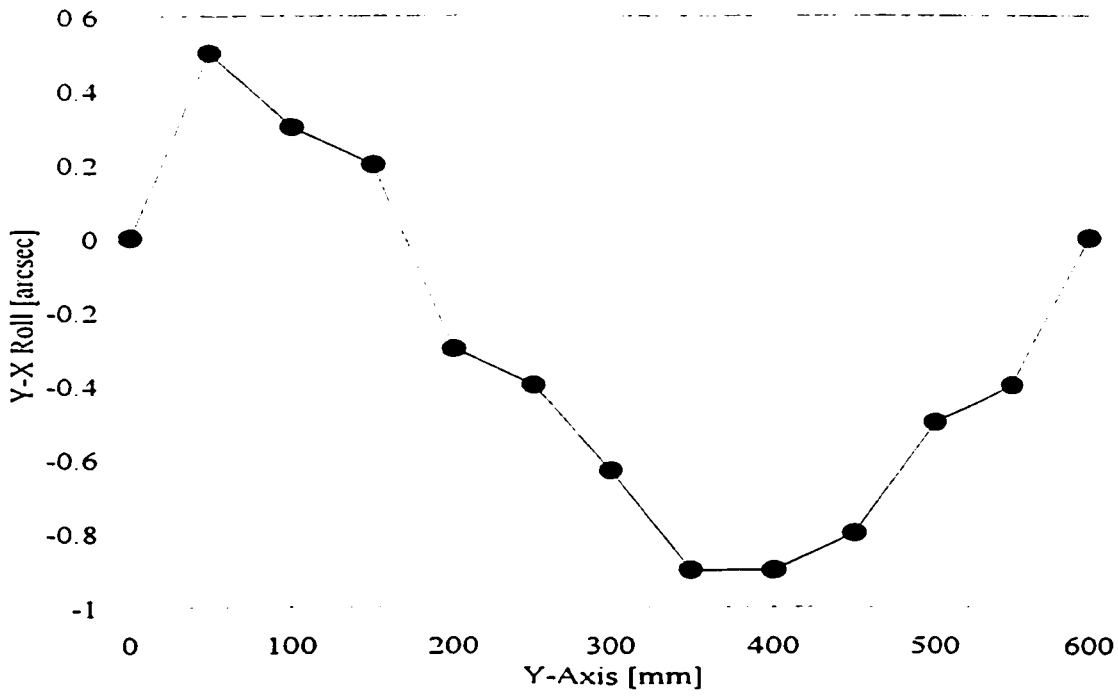


**Figure 75** Y-X Roll Angle Using Laser Measurements.

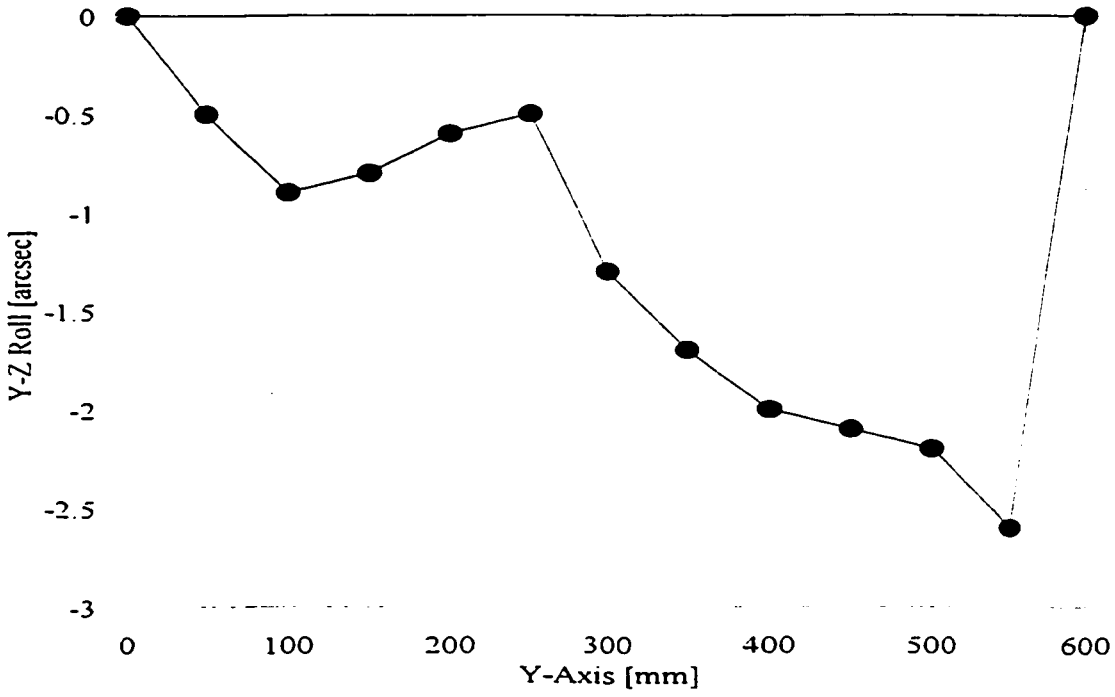


**Figure 76** Y-Z Roll Angle Using Laser Measurements.

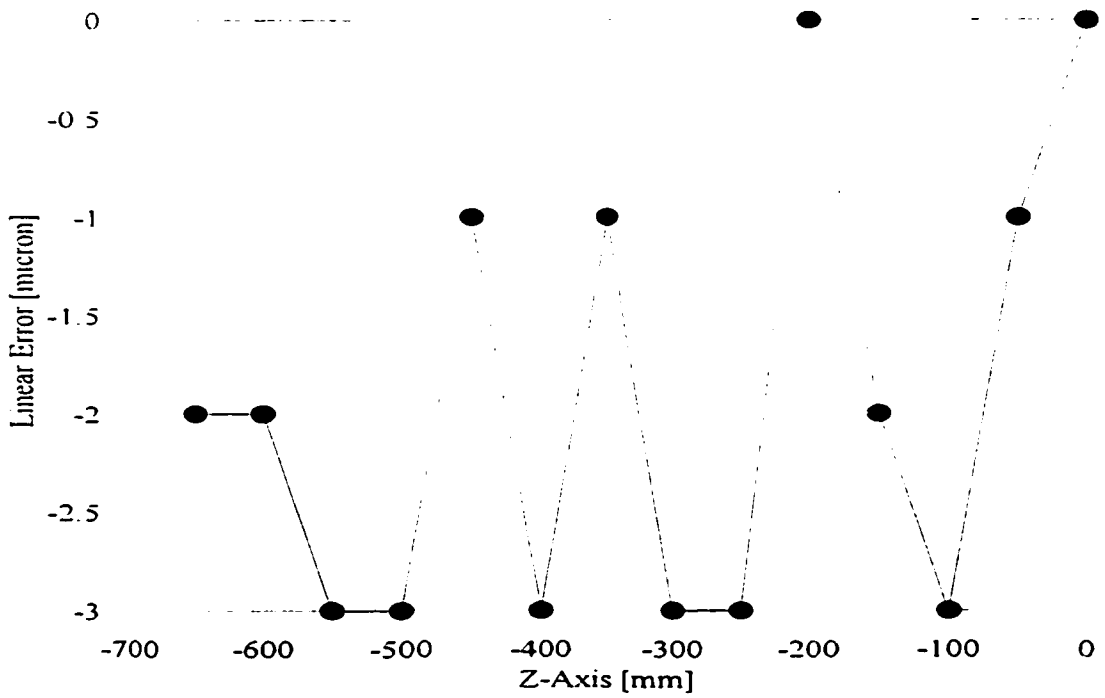


**Figure 77** Linear Error in Z-Axis Using Laser Measurements.

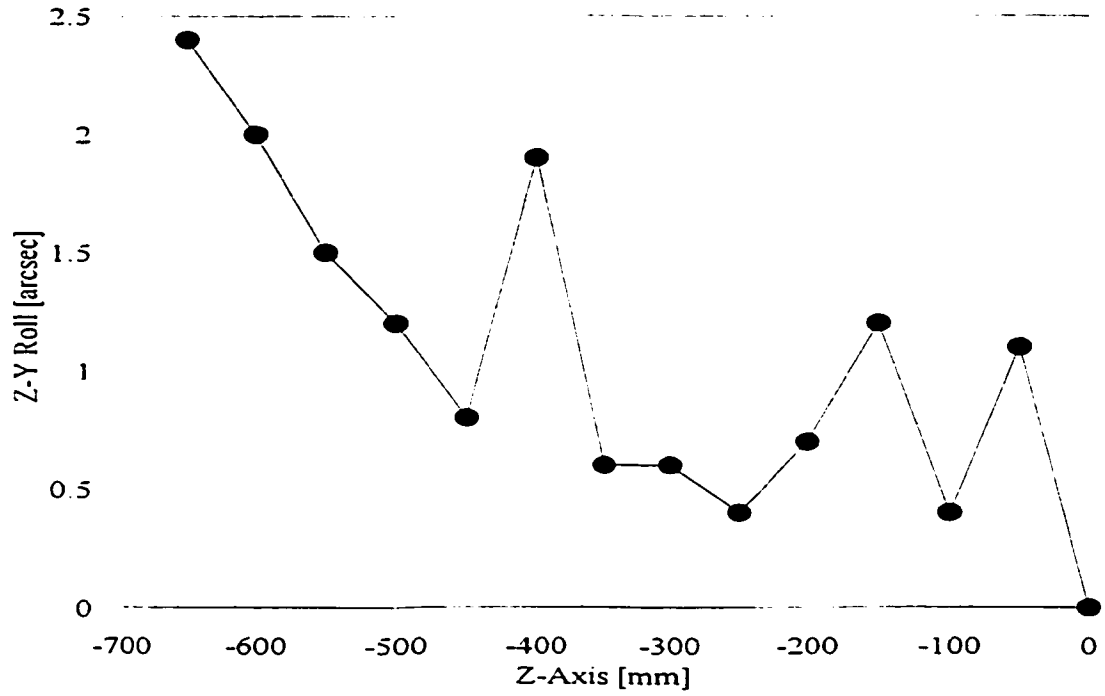


**Figure 78** Z-Y Roll Angle Using Laser Measurements.

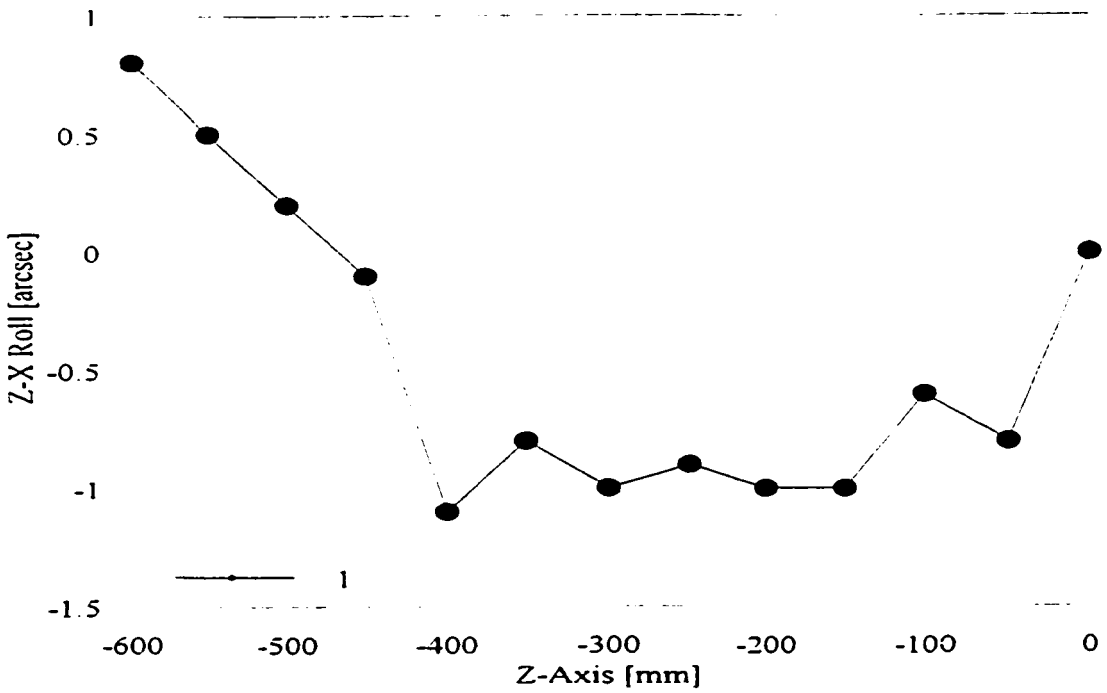


**Figure 79** Z-X Roll Angle Using Laser Measurements.

# Appendix G

## Statistical analysis and procedure for the evaluation and elimination of data outliers

Test for Outliers:

Suspicious pieces of information in a population of data are normally investigated by means of special tests in the literature of statistics (see Arnold, Balakrishnan, and Nagaraja, 1992). In order to check a suspicious outlier data point, the following quantity must be evaluated :

$$T = \frac{X_{1:n} - \bar{X}}{S} \qquad (61)$$

where S is the standard deviation, $X_{1:n}$ is the point under investigation, in a first order statistics arrangement, and $\bar{X}$ is the mean of the population. For a large T value in negative, $X_{1:n}$ is considered an outlier. This holds true under the hypothesis that this population of data is normally distributed with a mean of zero (i.e. $\mu = 0$). For the particular situation at hand, and upon application of equation 1 for $X_{1:n} = -121.1963$, the value T becomes as follows :

$$T = \frac{-121.1963 - 10.6584}{43.2994} = -3.0452 \qquad (62)$$

which is a large negative value compared to the t-table values with a 95 % significance level (Arnold et. al., 1992).

To verify this result, the hypothesis $H_o$ ($\mu = 0$) and the opposing hypothesis $H_1$ ($\mu$ not = 0) are tested. $H_o$ assumes that all values ($X_1$, $X_2$, .....,$X_n$) in a first order statistics form, are random samples from $N(\mu, \sigma^2)$ distribution. The opposing hypothesis $H_1$: assumes that one of the $X_i$'s is from $N(\mu + \delta, \sigma^2)$ where $\delta < 0$. Hence if T is a large negative value, $X_{1:n}$ is rejected from the data set or given less weight in subsequent statistical analysis. T value can be decided if large by checking it in tables given in (Arnold et. al.,, 1992).

This is done by evaluating the following statistic t :

$$t = \frac{\overline{X} - (\mu = 0)}{S/\sqrt{n}} \tag{63}$$

where it is found that t = 1.3484. This is less than the value for $\alpha = 0.1$, $t_{0.05,29} = 2.042$ (from t - tables (Arnold et. al., 1992) where evaluation is for 29 degrees of freedom and a 90% level of significance. Therefore, $H_o$ ($\mu = 0$) is sustained and $H_1$ ($\mu$ not = 0 ) is rejected.

Accordingly, for the particular point under investigation, the previous investigation confirms that it is an outlier. Position error of the CMM along its 3 axes was measured experimental by laser at different thermal states. Extensive measurements revealed that this error is a function of temperature change from the standard and not of the thermal gradients. The resulting measurements were plotted and are presented in full in this appendix.

# Appendix H

## The full set of linear errors measured by laser at different thermal states

The linear or position error of the CMM along its 3 axes was measured experimentally by laser at different thermal states. Extensive measurements revealed that this error is a function of temperature change from the standard and not of the thermal gradients. The resulting measurements were plotted and are presented in full in this appendix.

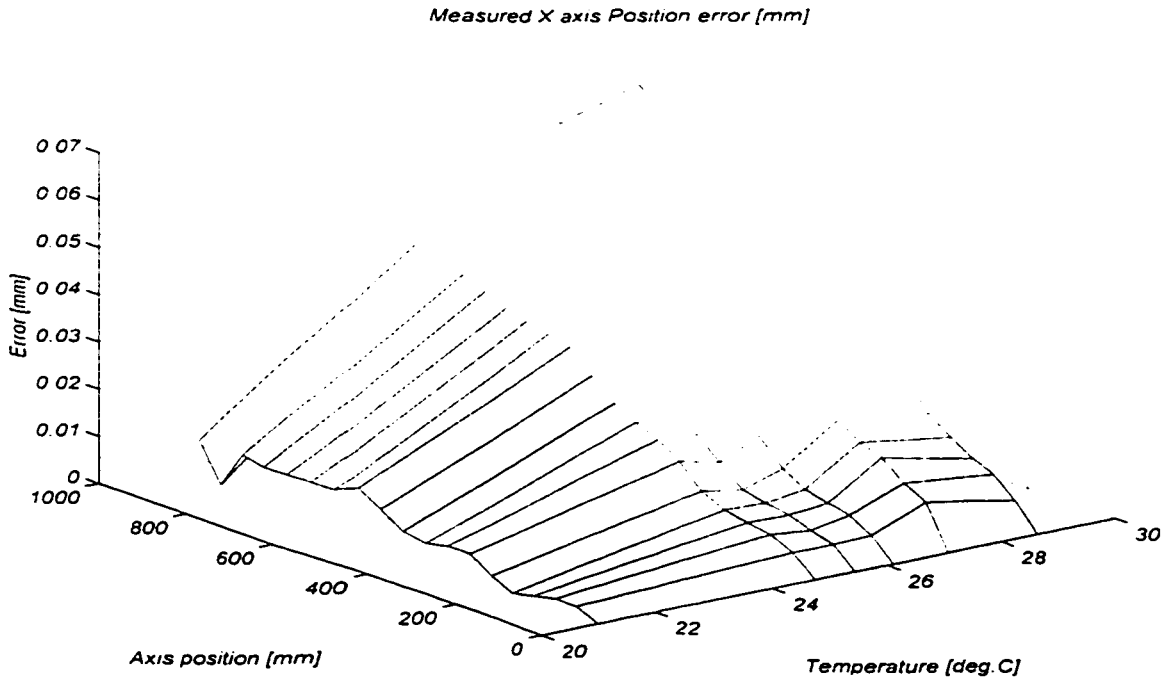


**Figure 80** Measured linear error along the X-axis at different temperatures.

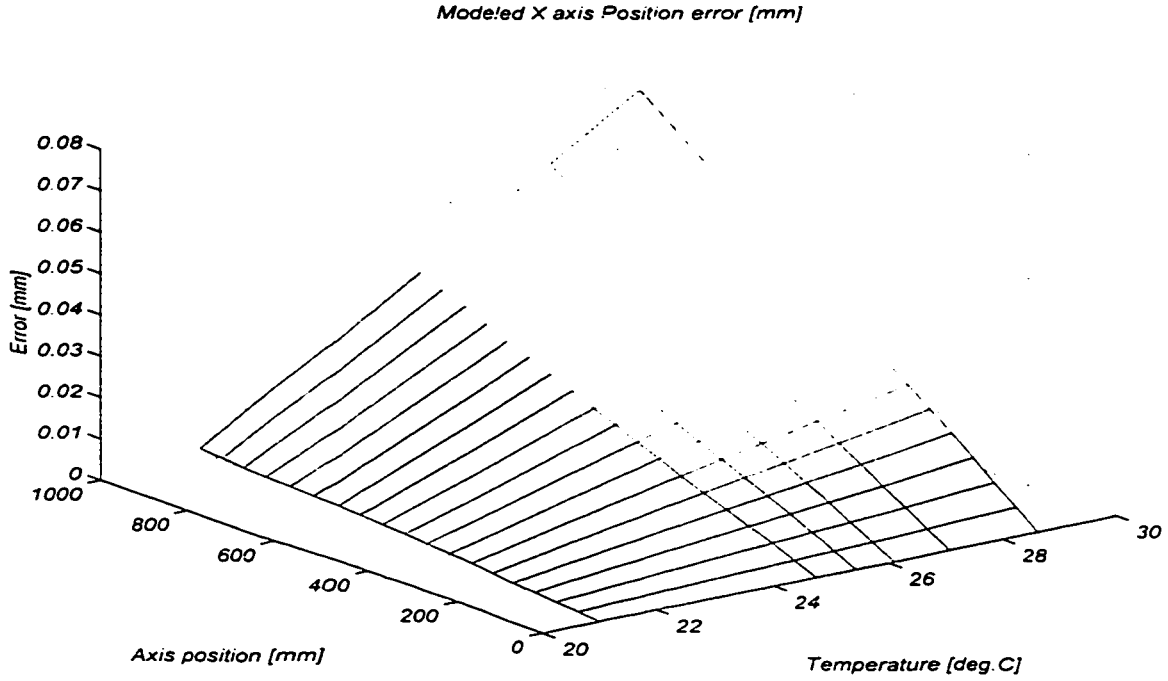


**Figure 81** Estimated linear error along the X-axis at different temperatures.

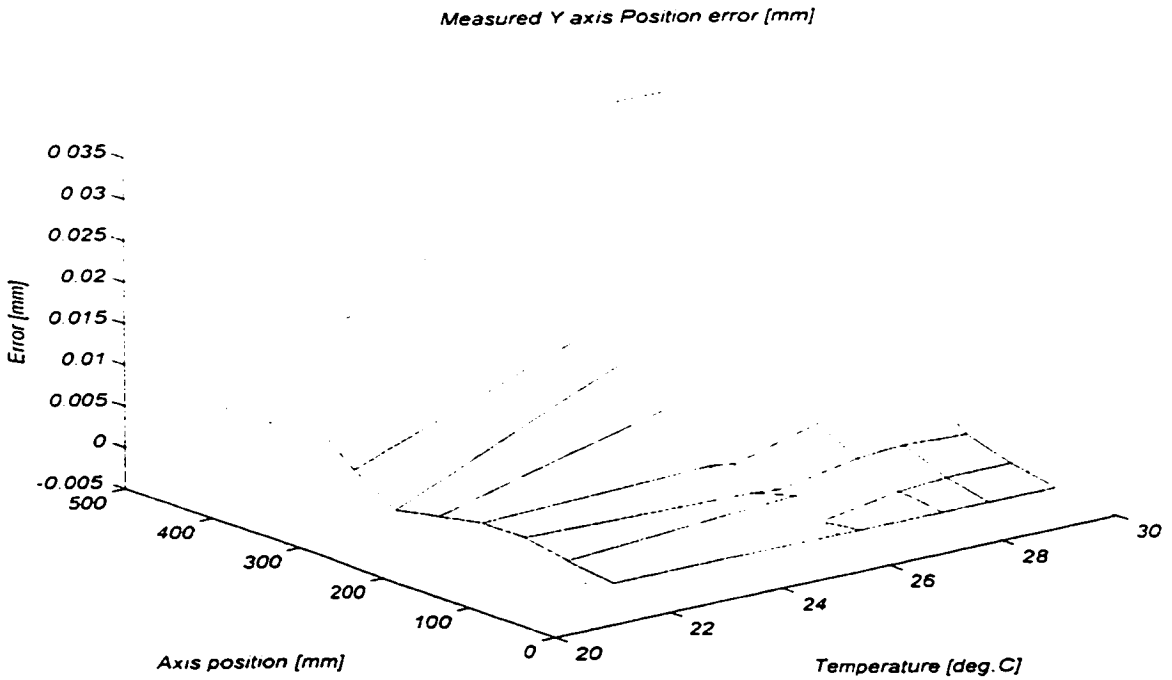


**Figure 82** Measured linear error along the Y-axis at different temperatures.

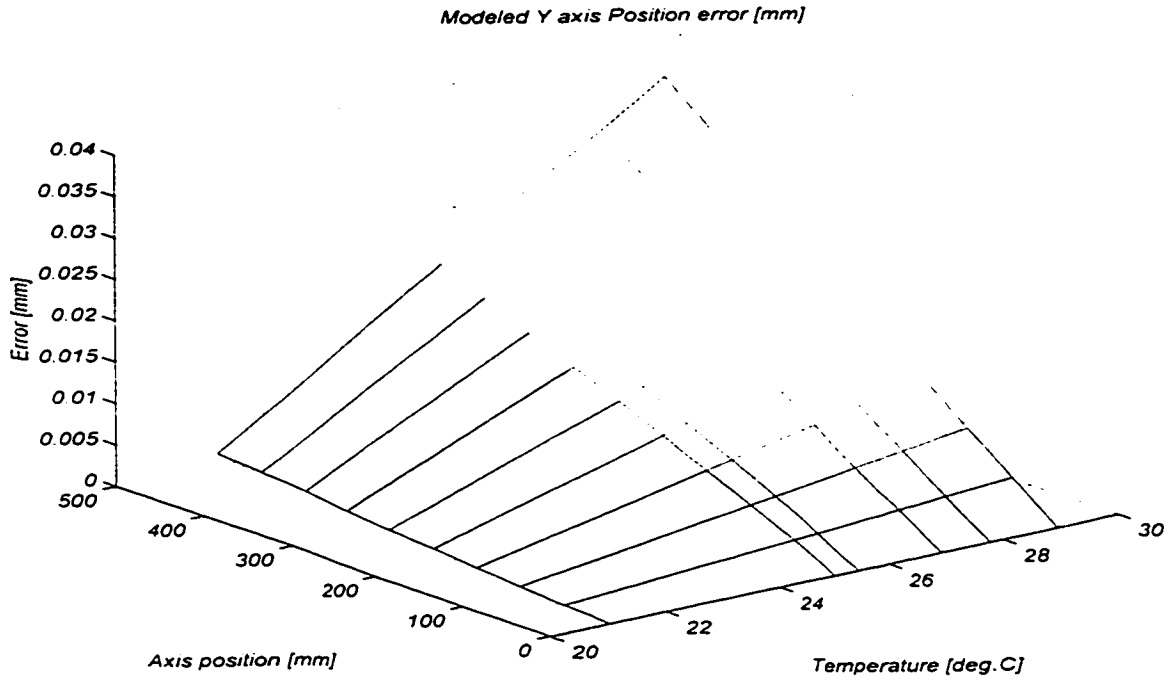


**Figure 83** Estimated linear error along the Y-axis at different temperatures.

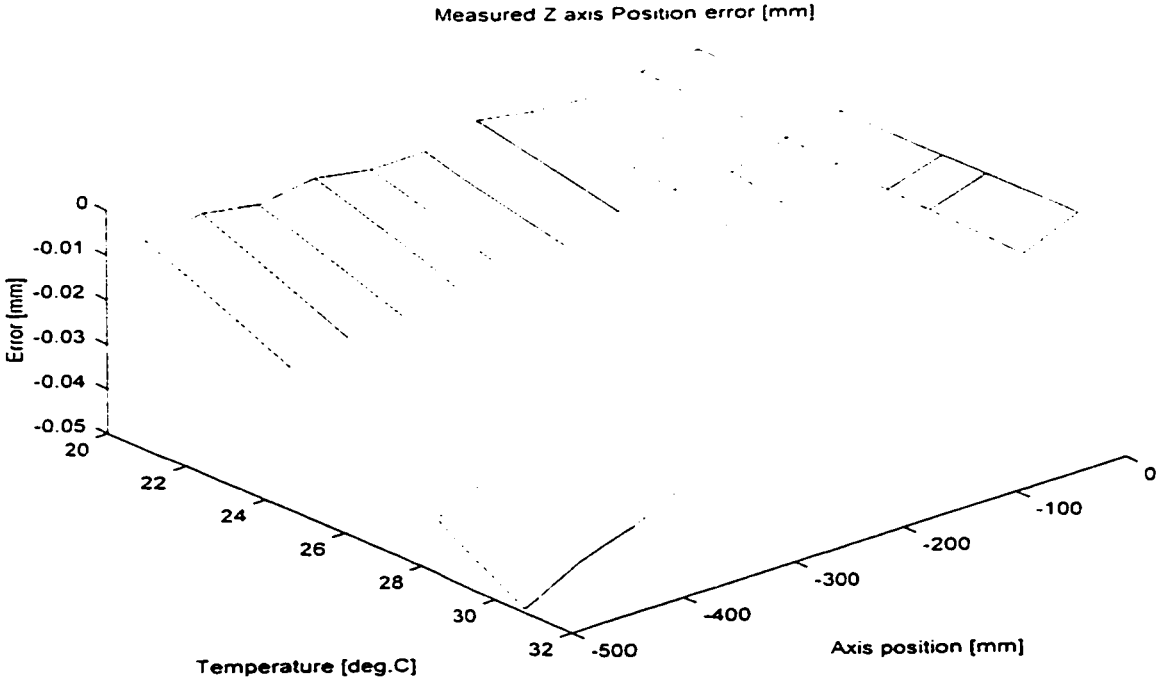


**Figure 84** Measured linear error along the Z-axis at different temperatures.

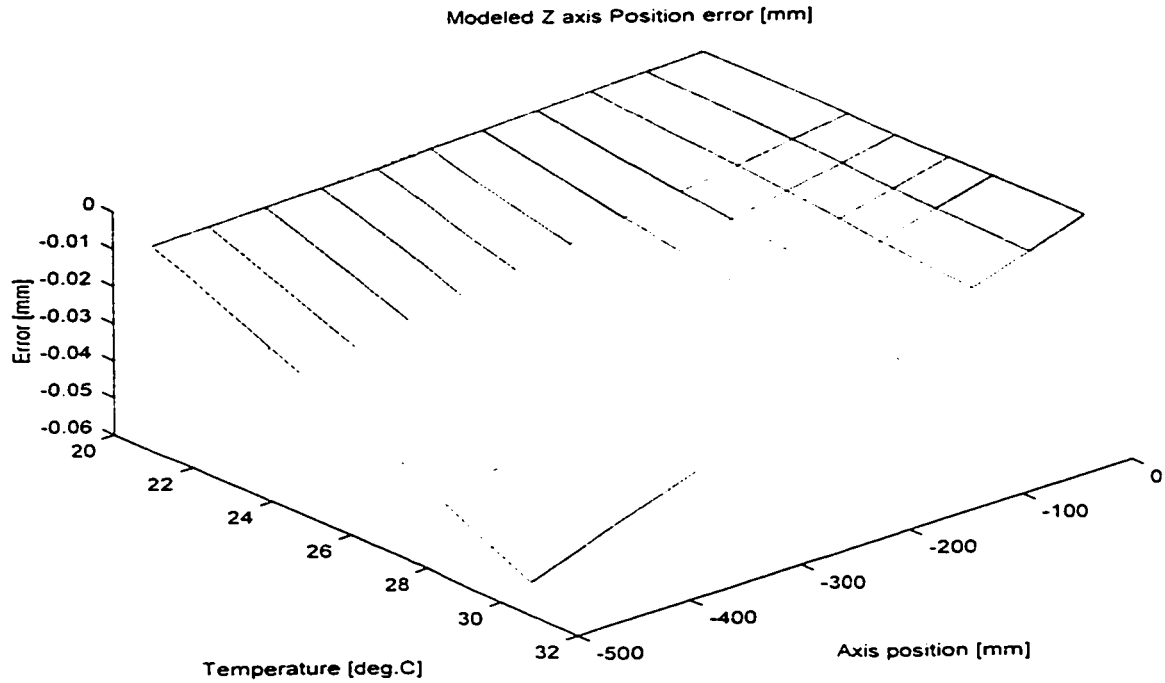


**Figure 85** Estimated linear error along the Z-axis at different temperatures.

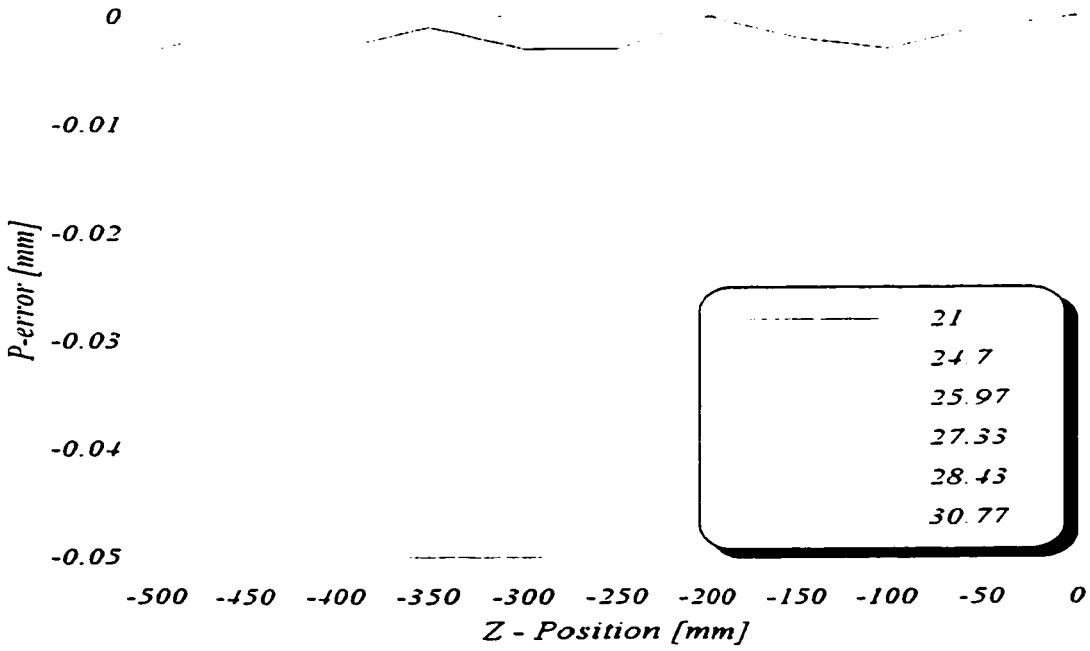


**Figure 86** Measured linear error along the Z-axis at different temperatures.

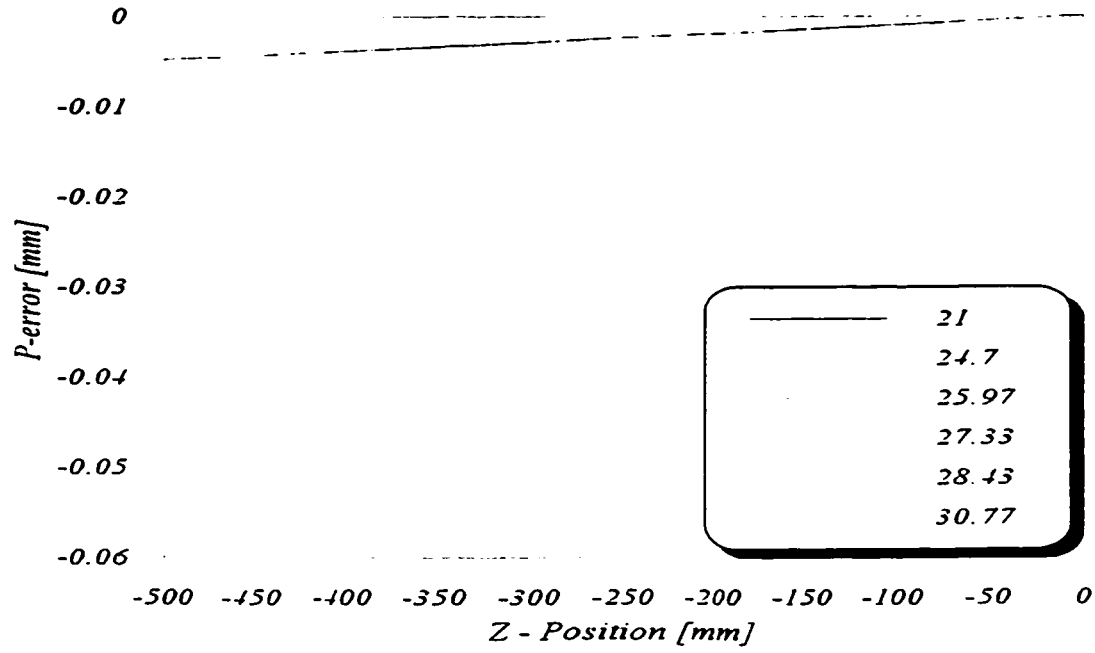


**Figure 87** Estimated Linear error along the Z-axis at different temperatures.

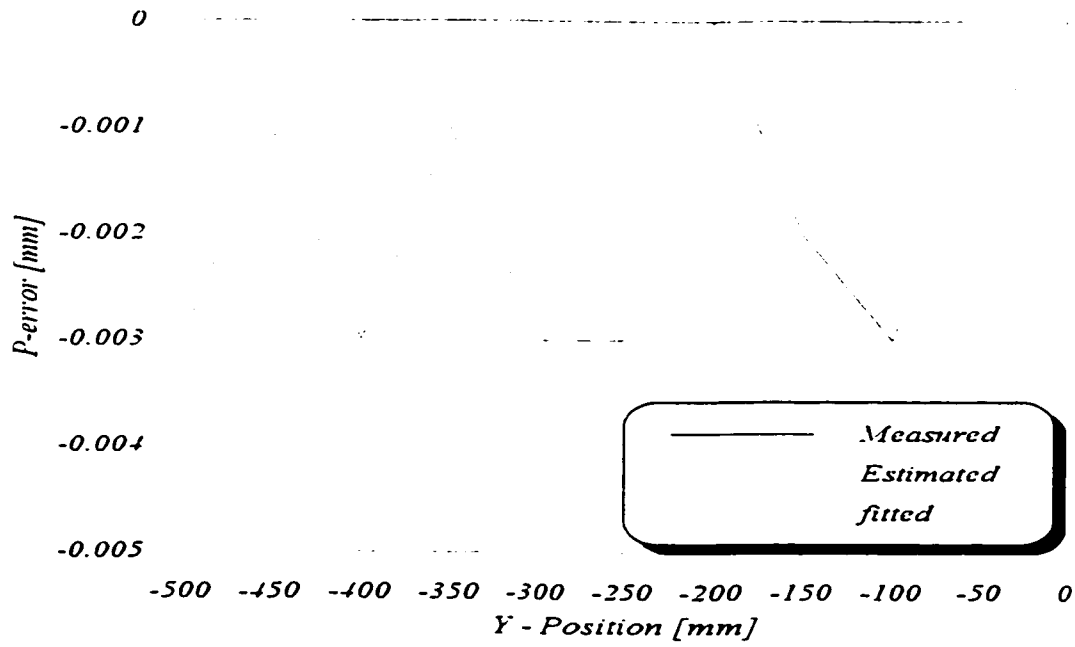


**Figure 88** Linear error along Z-axis at T = 21° C.

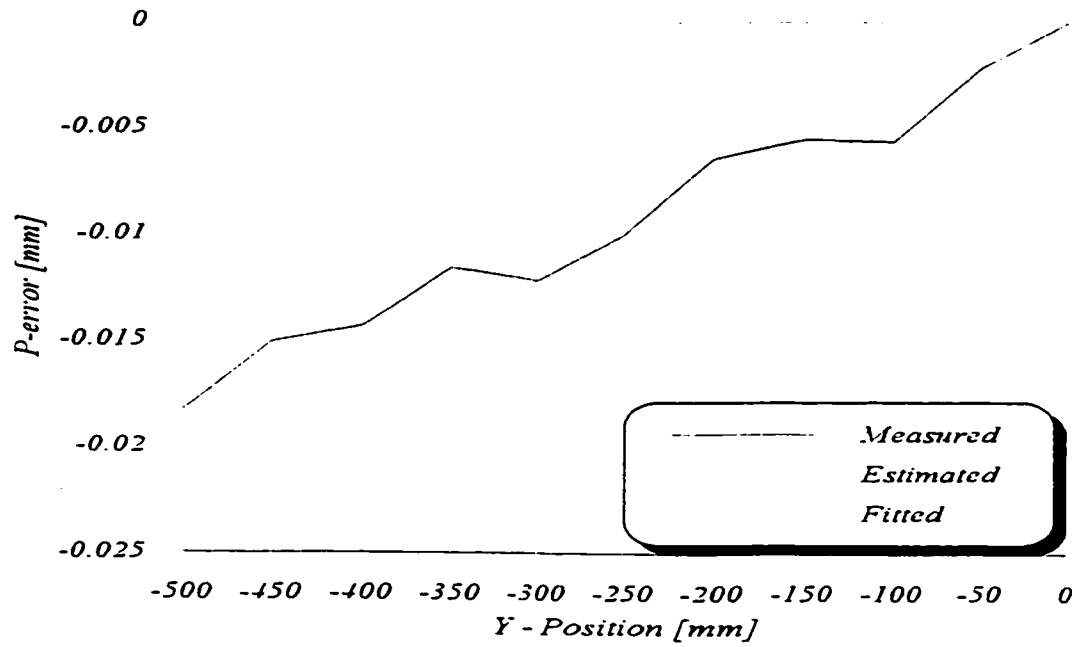


**Figure 89** Linear error along Z-axis at T = 24.7° C.

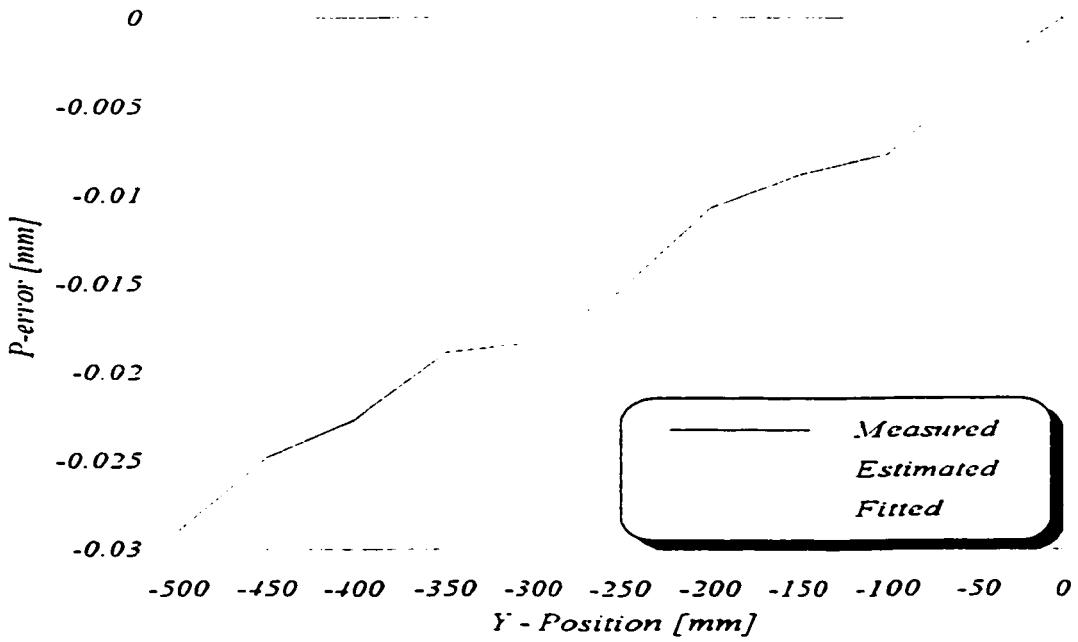


**Figure 90** Linear error along Z-axis at T = 25.97° C.

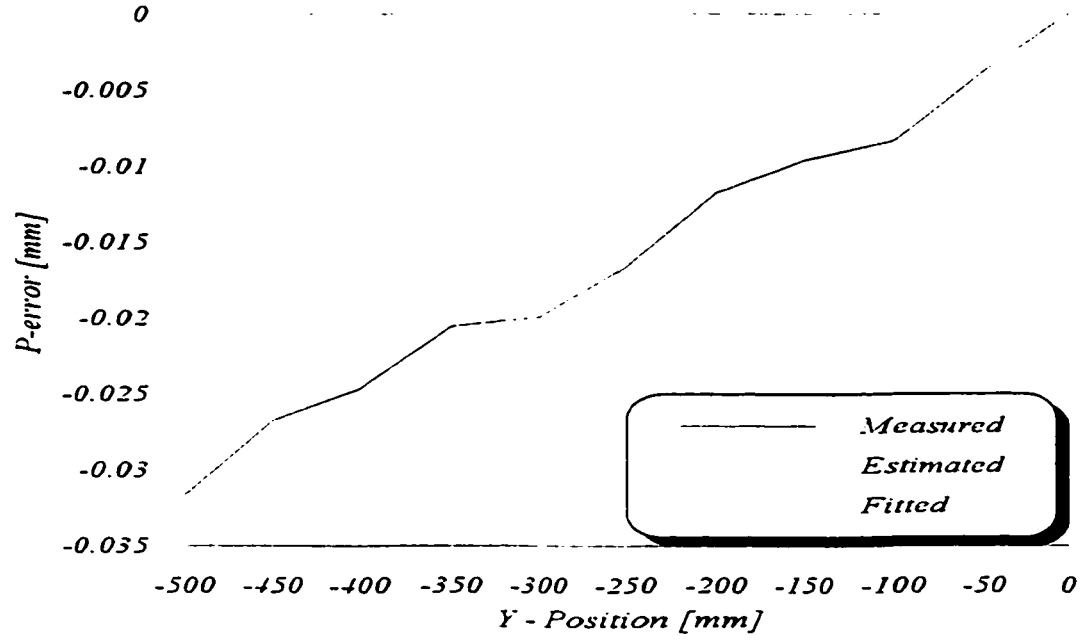


**Figure 91** Linear error along Z-axis at T = 27.33° C.

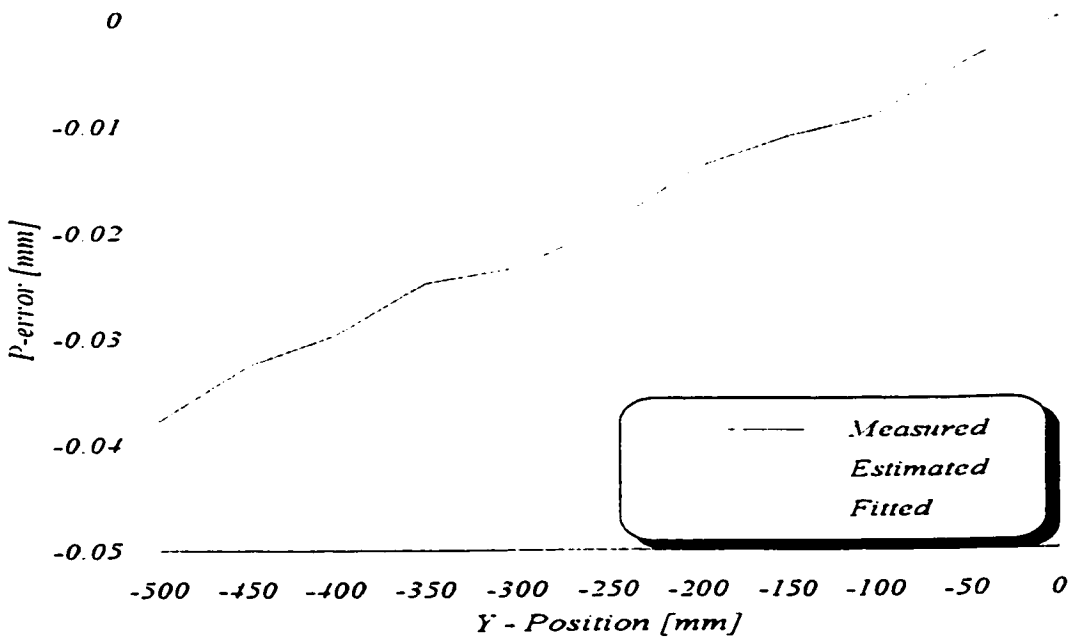


**Figure 92** Linear error along Z-axis at T = 28.43° C.

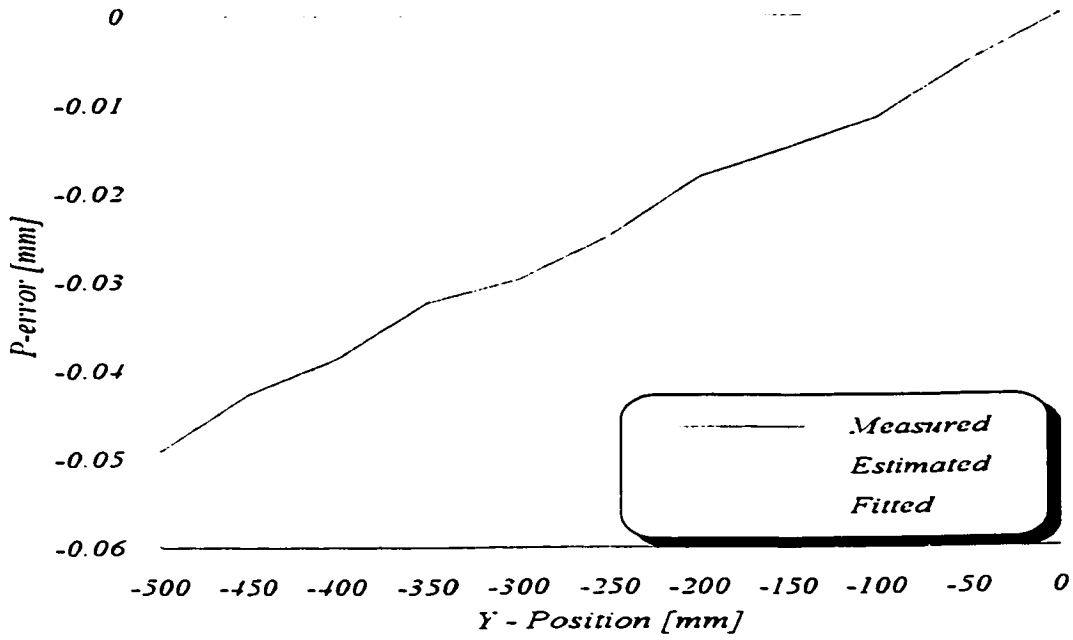


**Figure 93** Linear error along Z-axis at T = 30.77° C.

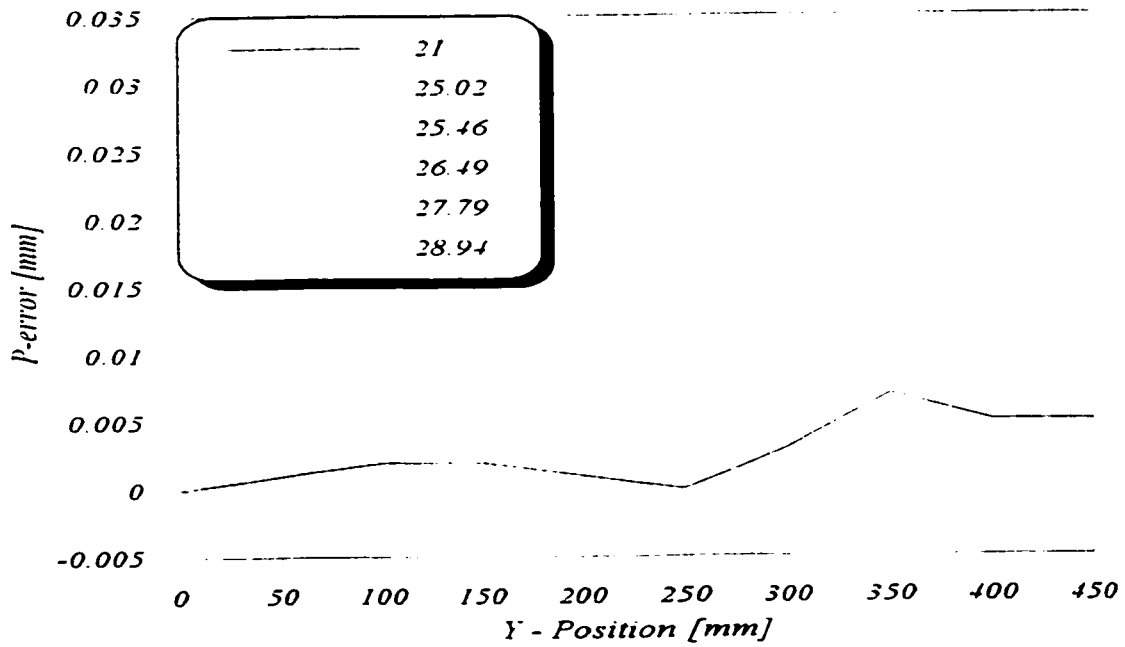


**Figure 94** Measured linear error along the Y-axis at different temperatures.

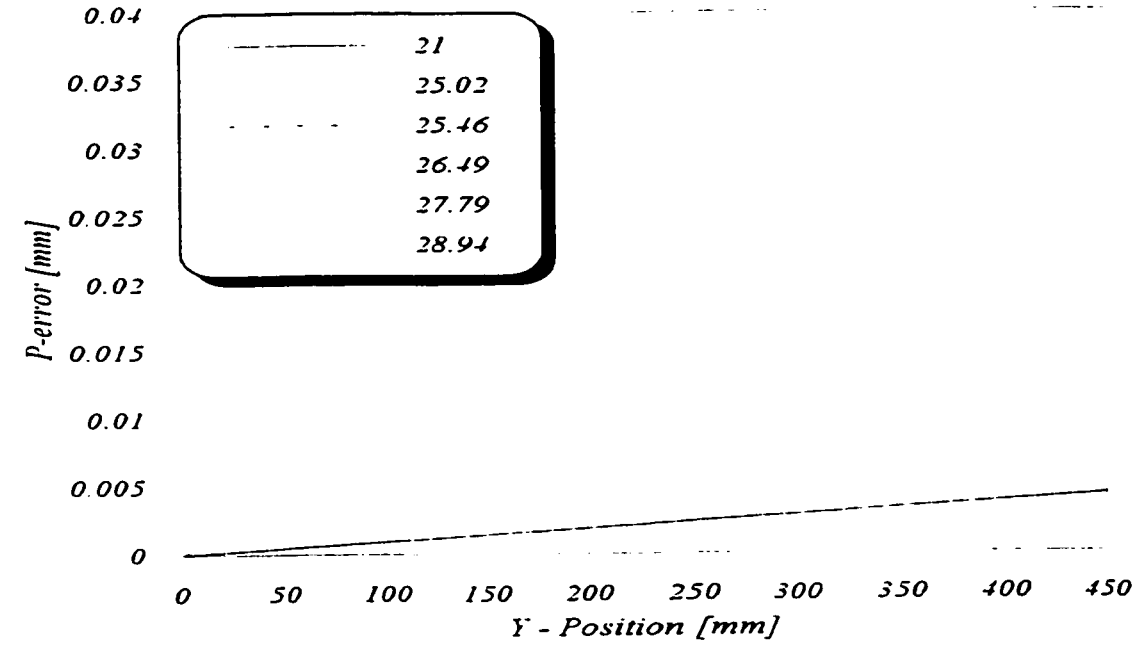


**Figure 95** Estimated linear error along the Y-axis at different temperatures.

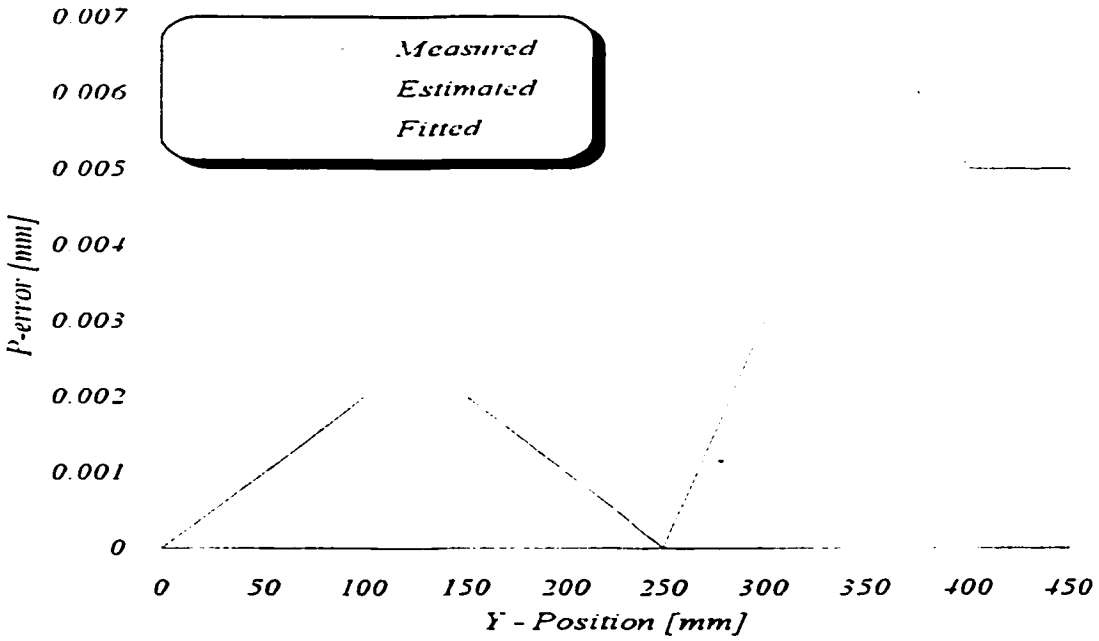


**Figure 96** Linear error along Y-axis at T = 21° C.

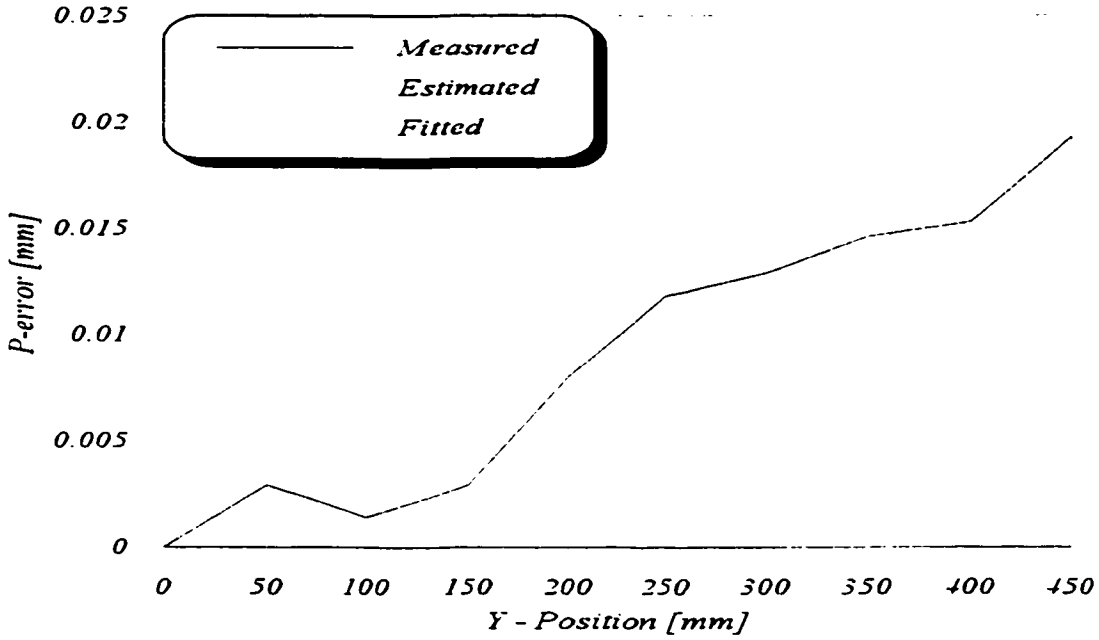


**Figure 97** Linear error along Y-axis at T = 25.02° C.

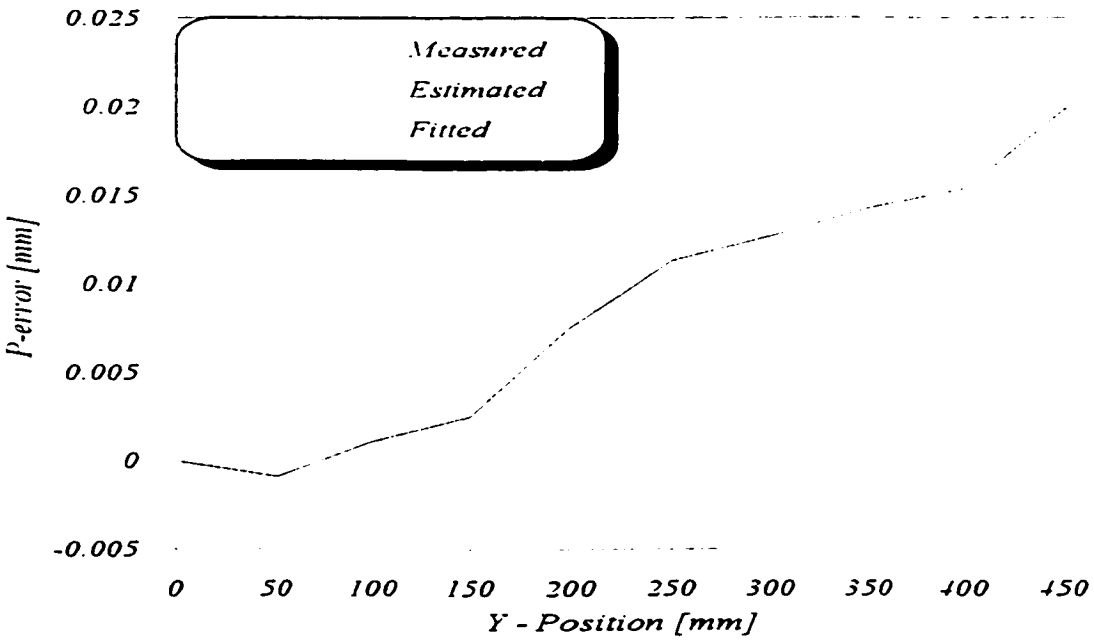


**Figure 98** Linear error along Y-axis at T = 25.46° C.

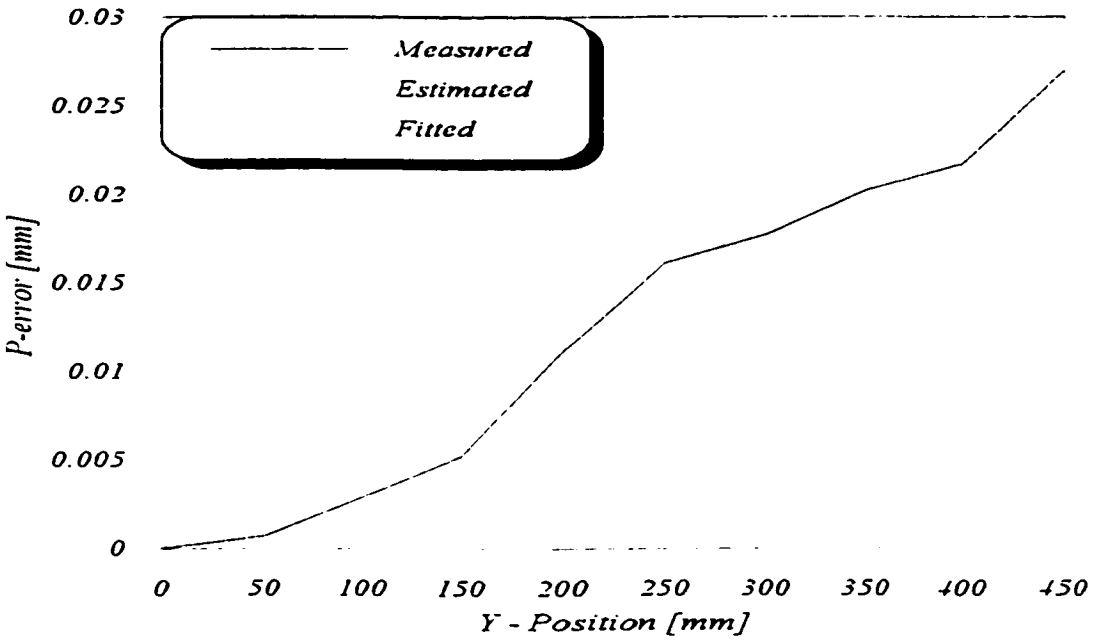


**Figure 99** Linear error along Y-axis at T = 26.49° C.

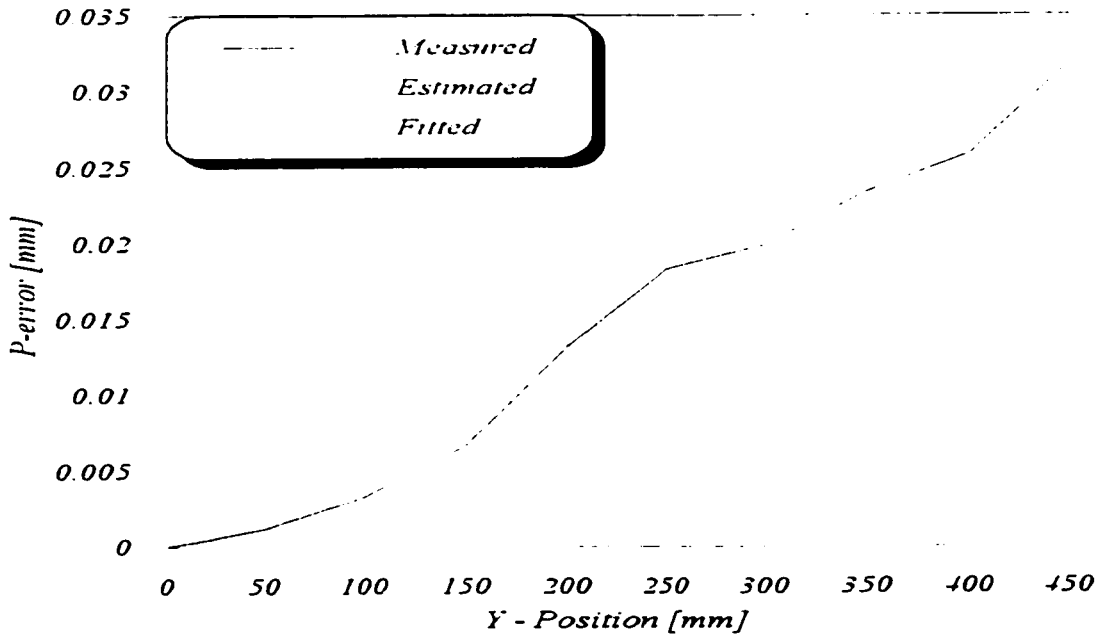


**Figure 100** Linear error along Y-axis at T = 27.79° C.

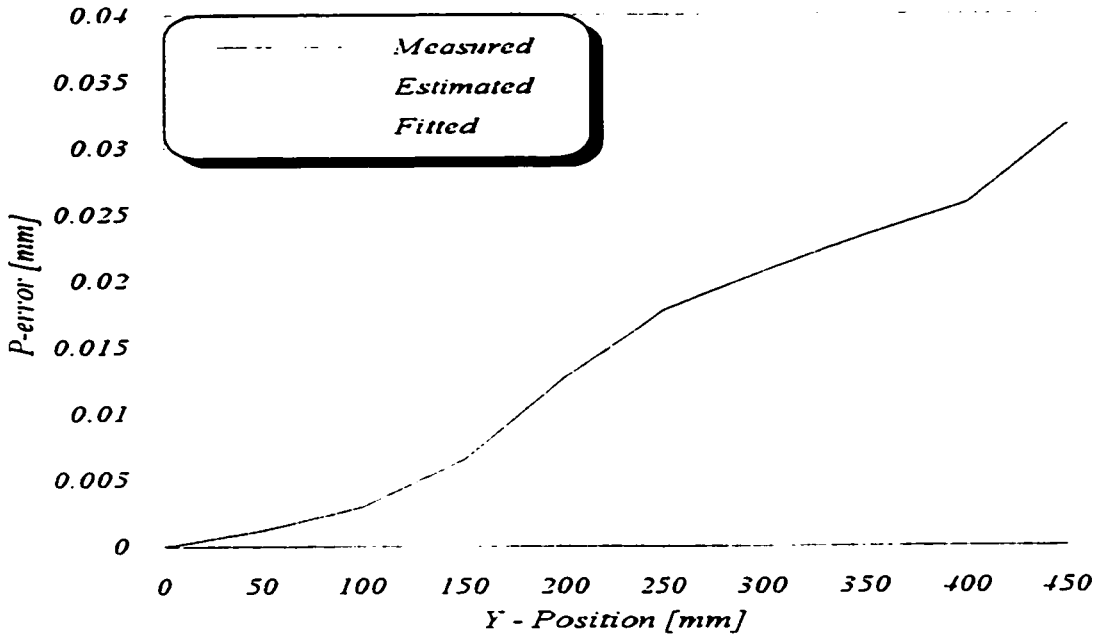


**Figure 101** Linear error along Y-axis at T = 28.94° C.

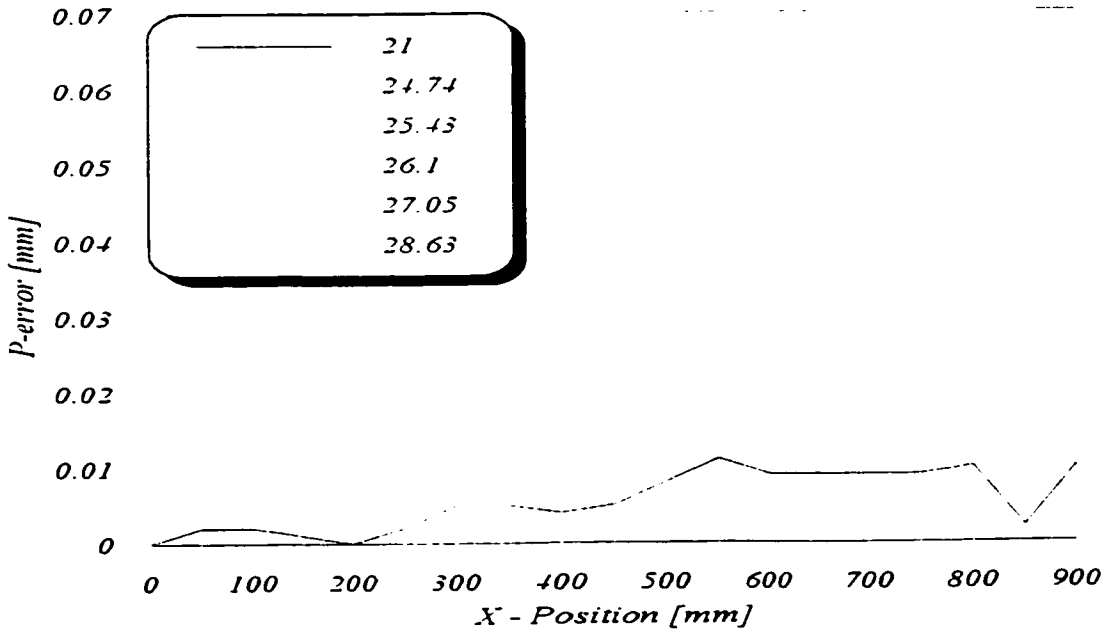


**Figure 102** Measured linear error along the X-Axis at different temperatures.

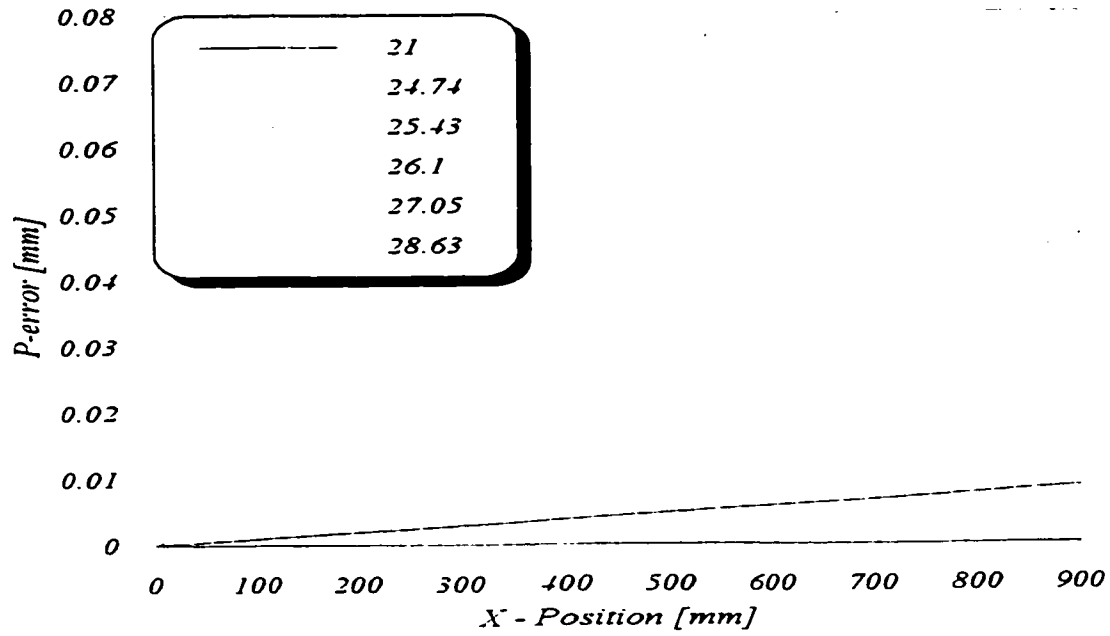


**Figure 103** Estimated linear error along the X-Axis at different temperatures.

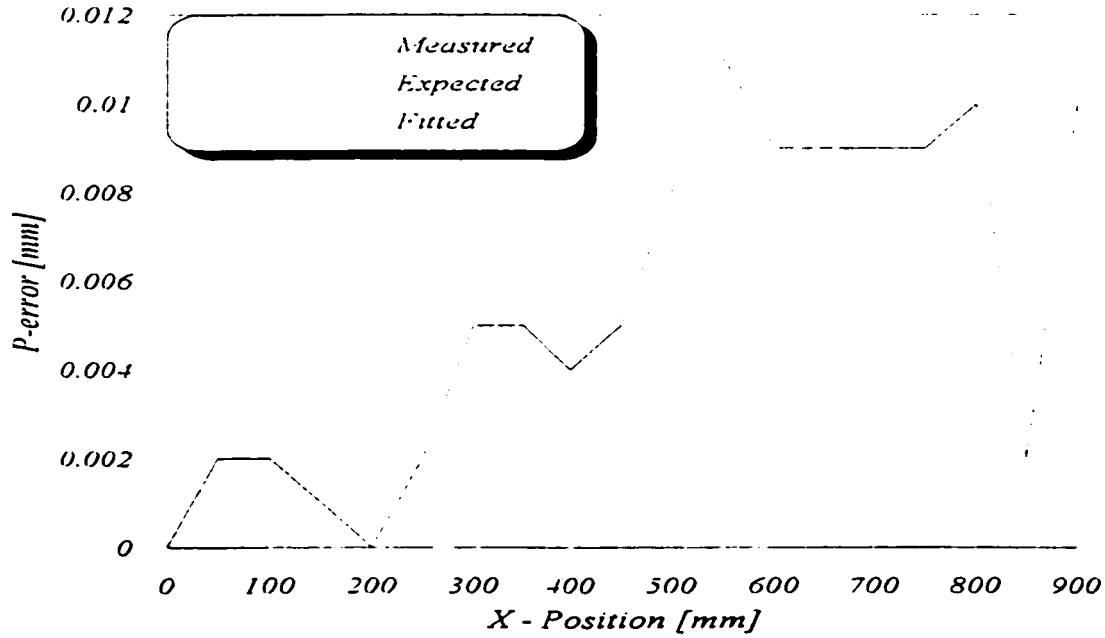


**Figure 104** Linear error along X-axis at $T_1$ =21° C.

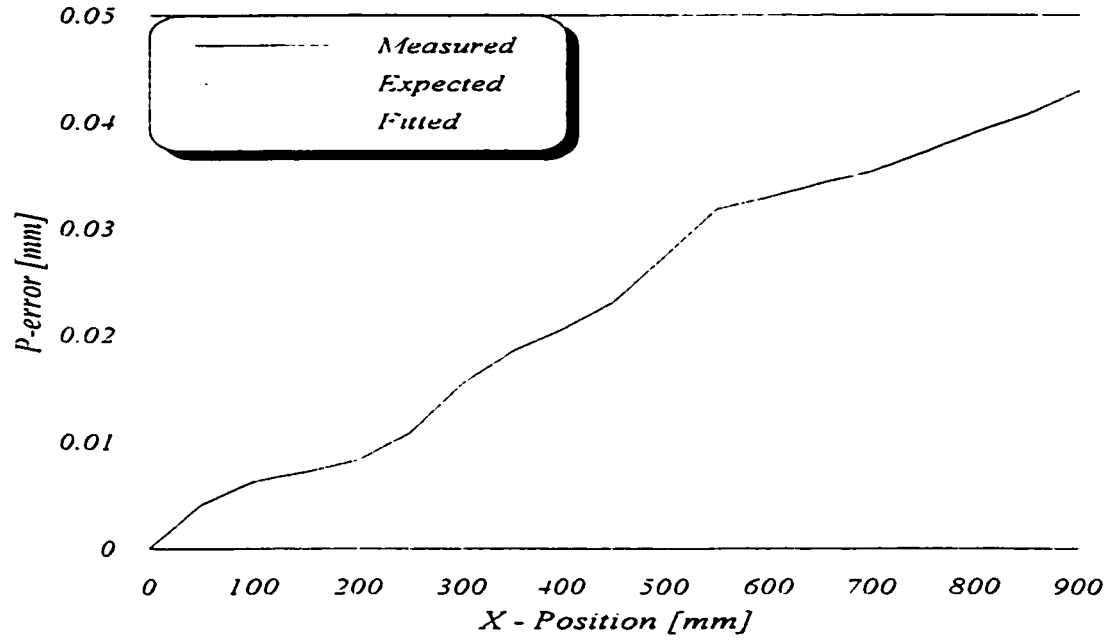


**Figure 105** Linear error along X-axis at $T_2$ = 24.74° C.

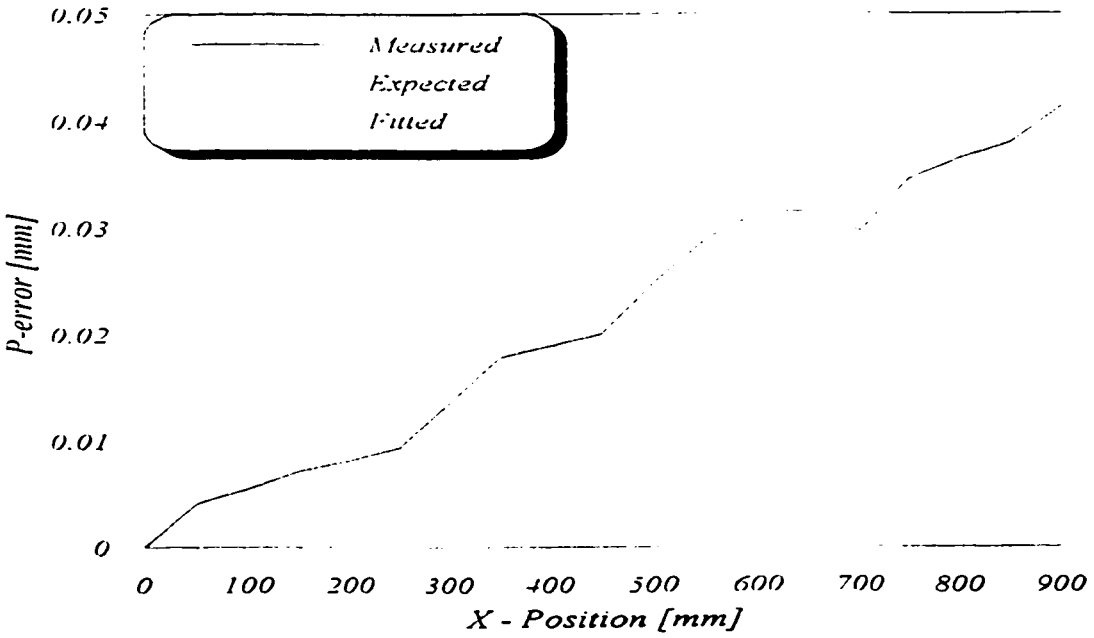


**Figure 106** Linear error along X-axis at $T_3$ = 25.43° C.

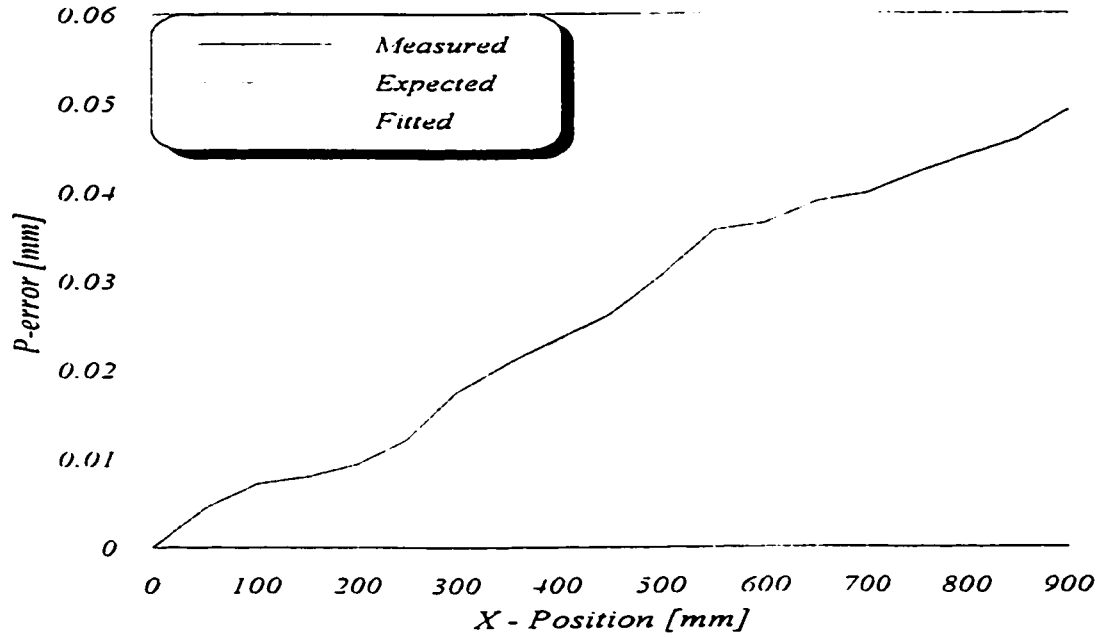


**Figure 107** Linear error along X-axis at $T_4$ = 26.1° C.

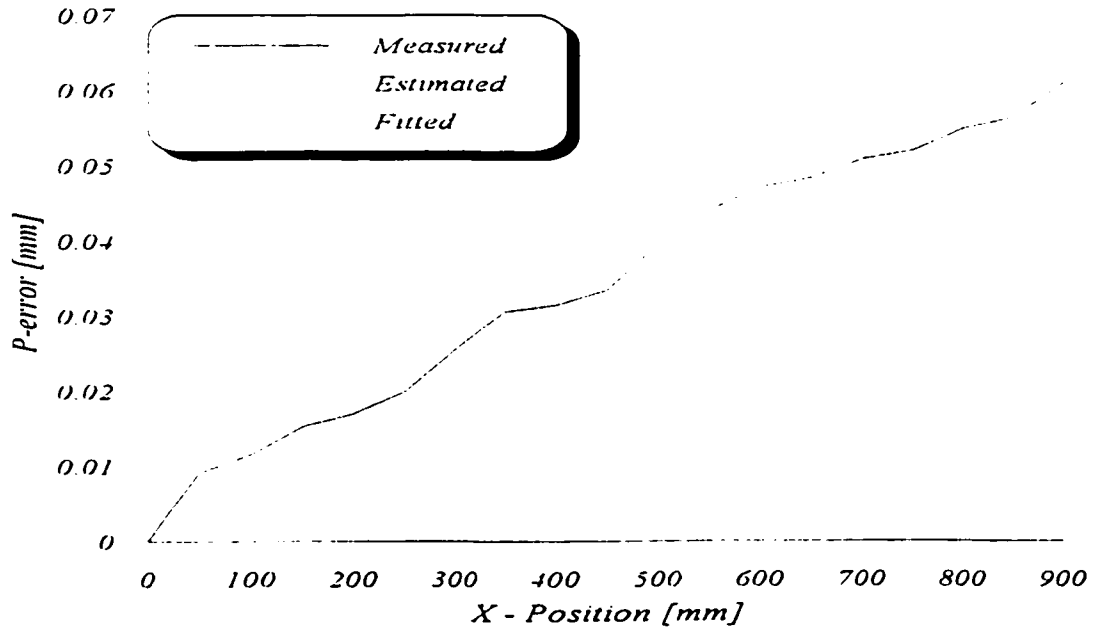


**Figure 108** Linear error along X-axis at $T_5$ = 27.05° C.

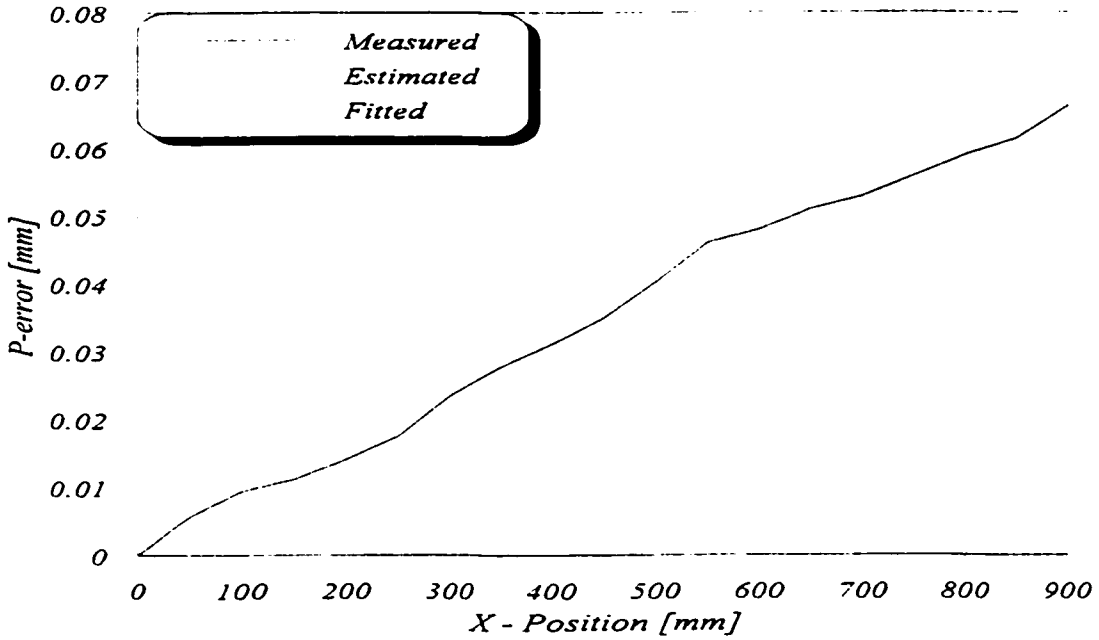


**Figure 109** Linear error along X-axis at $T_6$ = 28.63° C.

# Appendix I

## The full set of Straightness errors measured by laser at different thermal states

The straightness error of the CMM along its 3 axes was measured experimentally by laser at different thermal states. Extensive measurements revealed that this error is neither a function of temperature change from the standard nor the thermal gradients. The resulting measurements were plotted and are presented in full in this appendix.

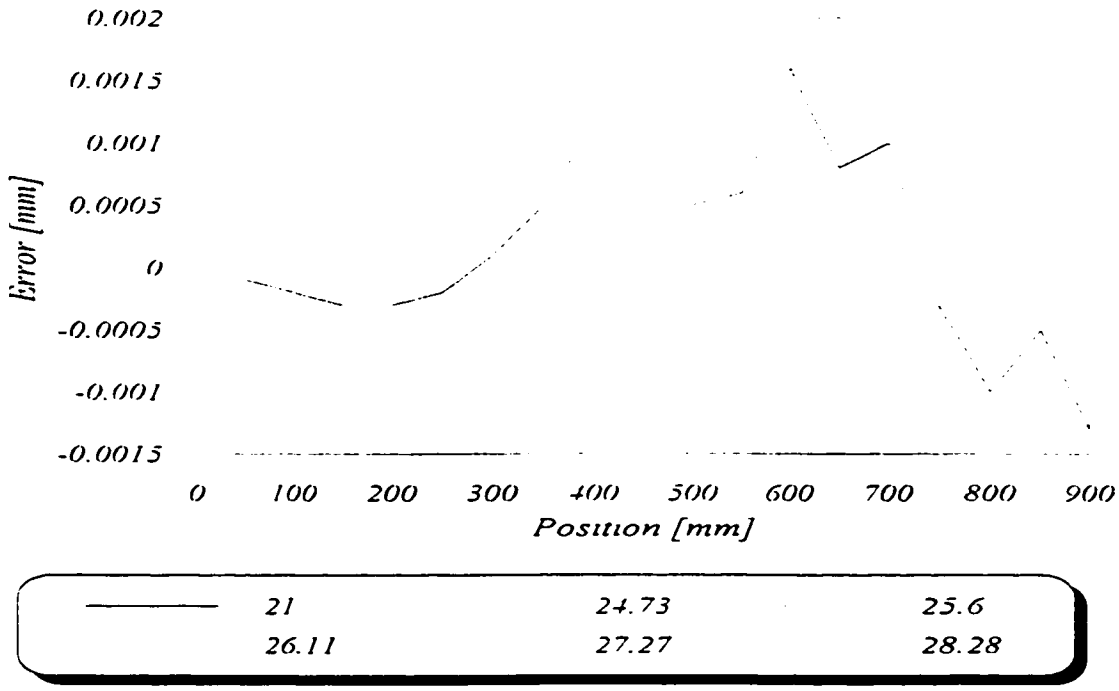


**Figure 110** Straightness error of X-axis in the Y-axis direction at different temperatures.

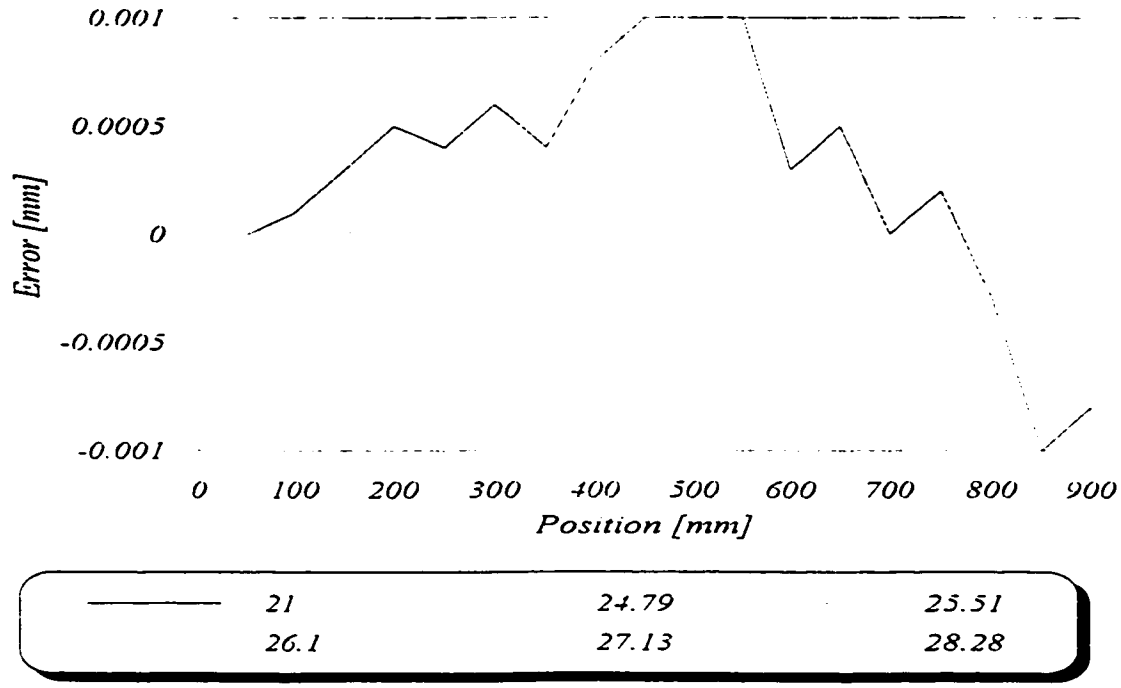


**Figure 111** Straightness error of X-axis in the Z-axis direction at different temperatures.

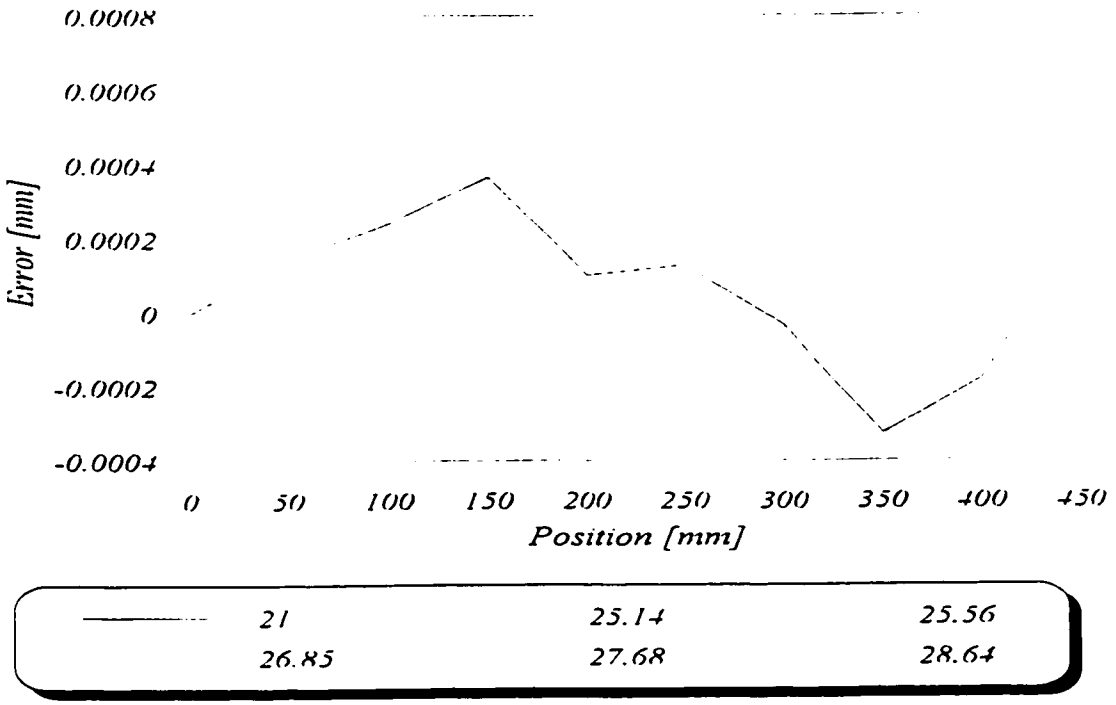


**Figure 112** Straightness error of Y-axis in the X-axis direction at different temperatures.

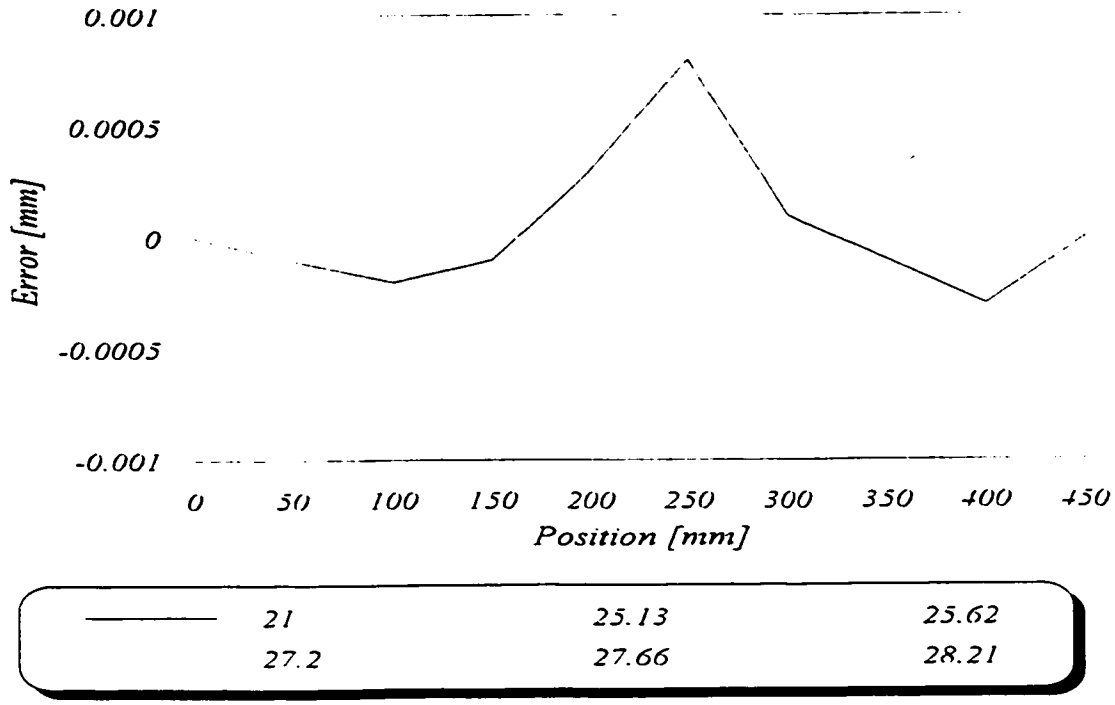


**Figure 113** Straightness error of Y-axis in the Z-axis direction at different temperatures.

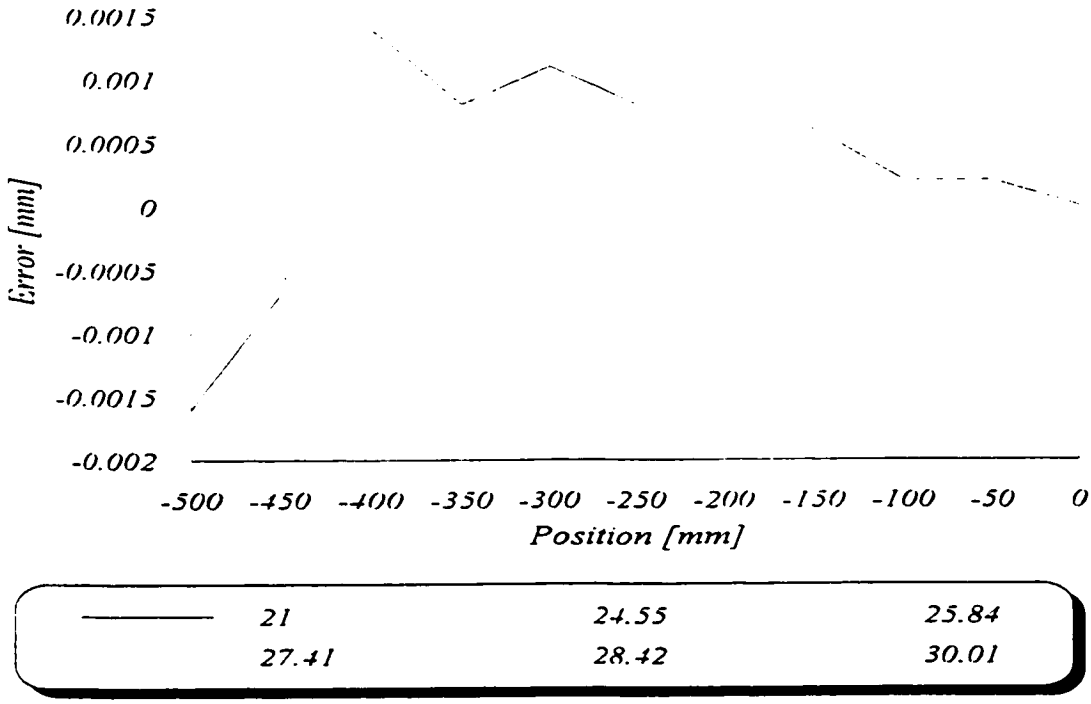


**Figure 114** Straightness error of Z-axis in the X-axis direction at different temperatures.

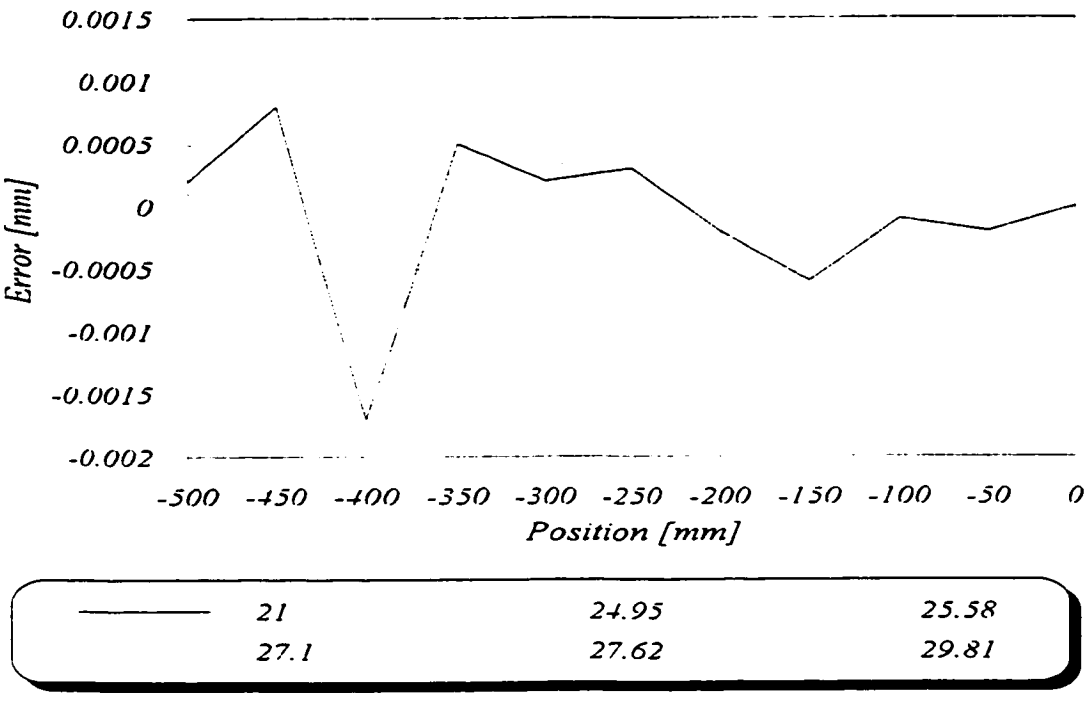


**Figure 115** Straightness error of Z-axis in the Y-axis direction at different temperatures.

# Appendix J

## The full set of angular errors measured by laser at different thermal states

The angular error of the CMM along its 3 axes was measured experimental by laser at different thermal states. Extensive measurements revealed that this error is a function of thermal gradients across the axis being measured. The resulting measurements were plotted and are presented in full in this appendix.

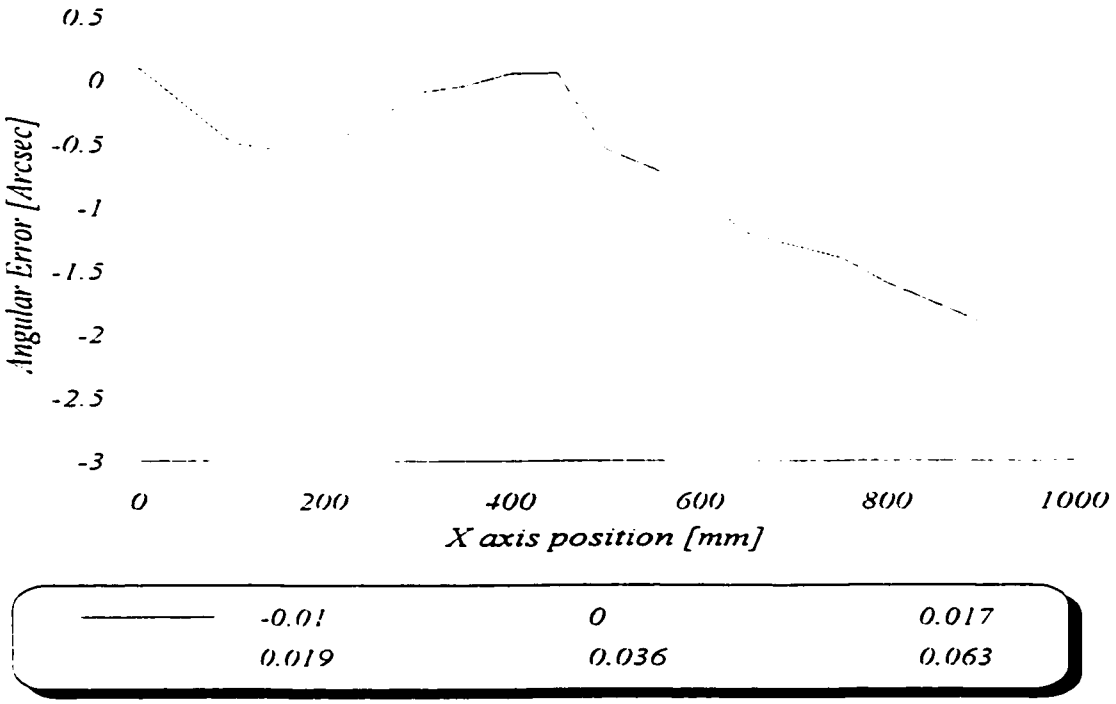


**Figure 116** $\gamma_{1x}$ Angular and Straightness error of X axis rotation around Z axis at different gradients [deg/m].

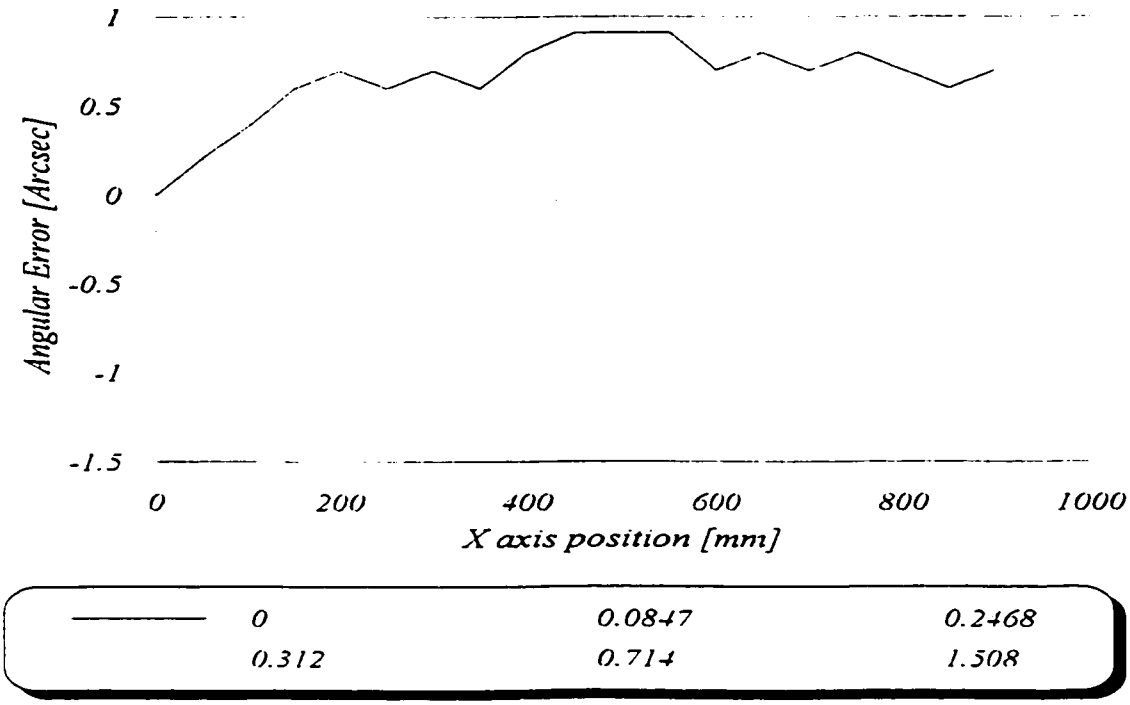


**Figure 117** $\beta_{1x}$ Angular and Straightness error of X axis rotation around Y axis at different gradients [deg/m].

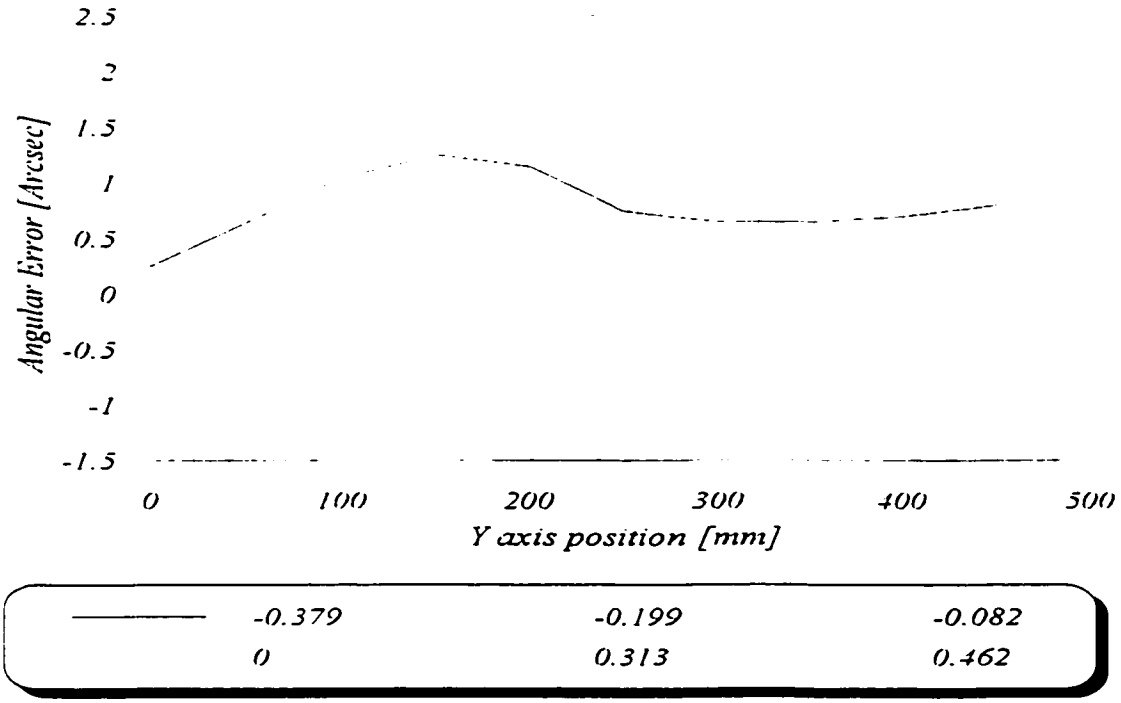


**Figure 118** $\gamma_{2y}$ Angular and Straightness error of Y axis rotation around Z axis at different gradients [deg/m].

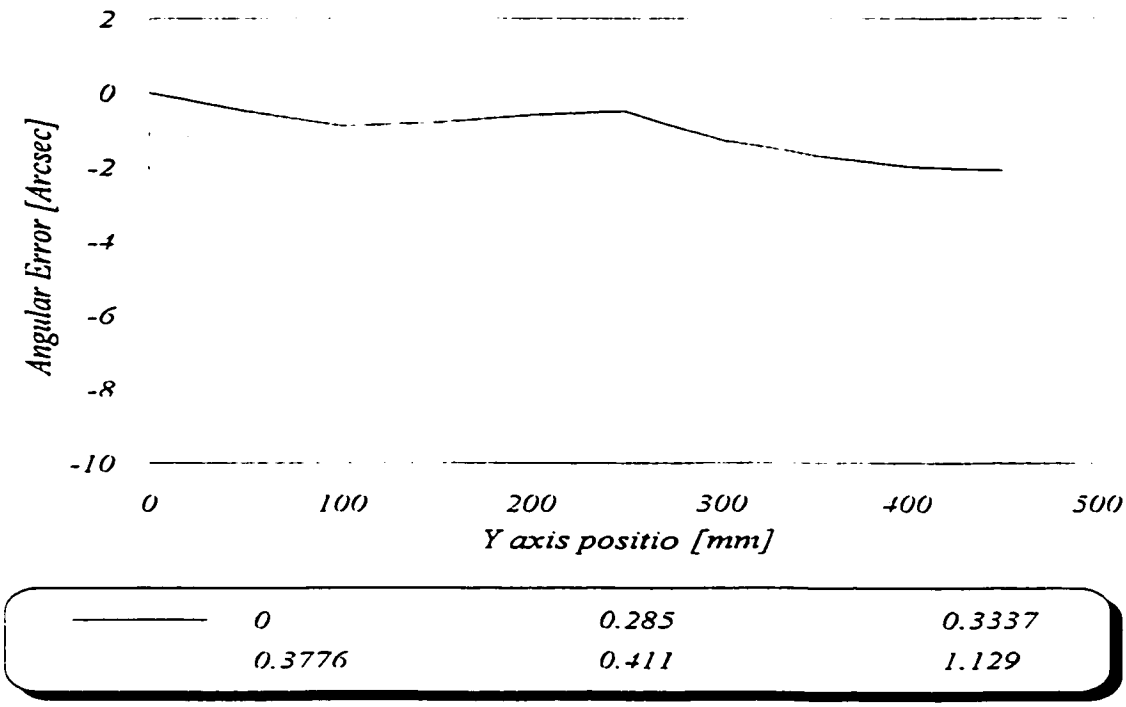


**Figure 119** $\alpha_{2y}$ Angular and Straightness error of Y axis rotation around X axis at different gradients [deg/m].

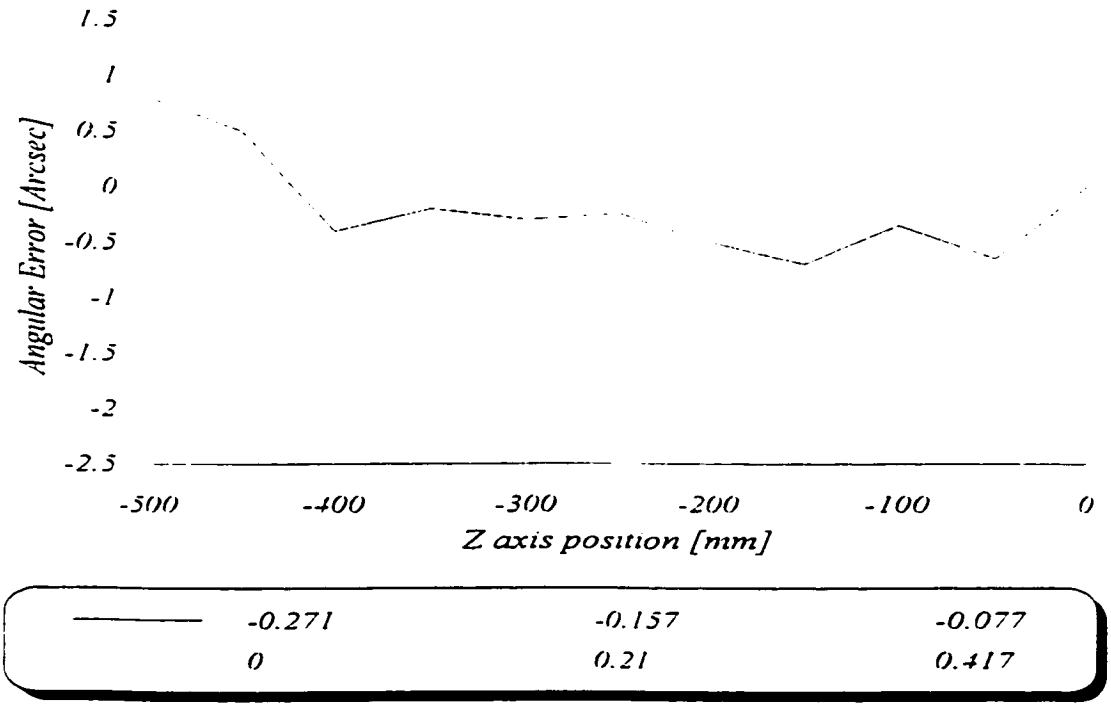


**Figure 120** $\beta_{3z}$ Angular and Straightness error of Z axis rotation around Y axis at different gradients [deg/m].

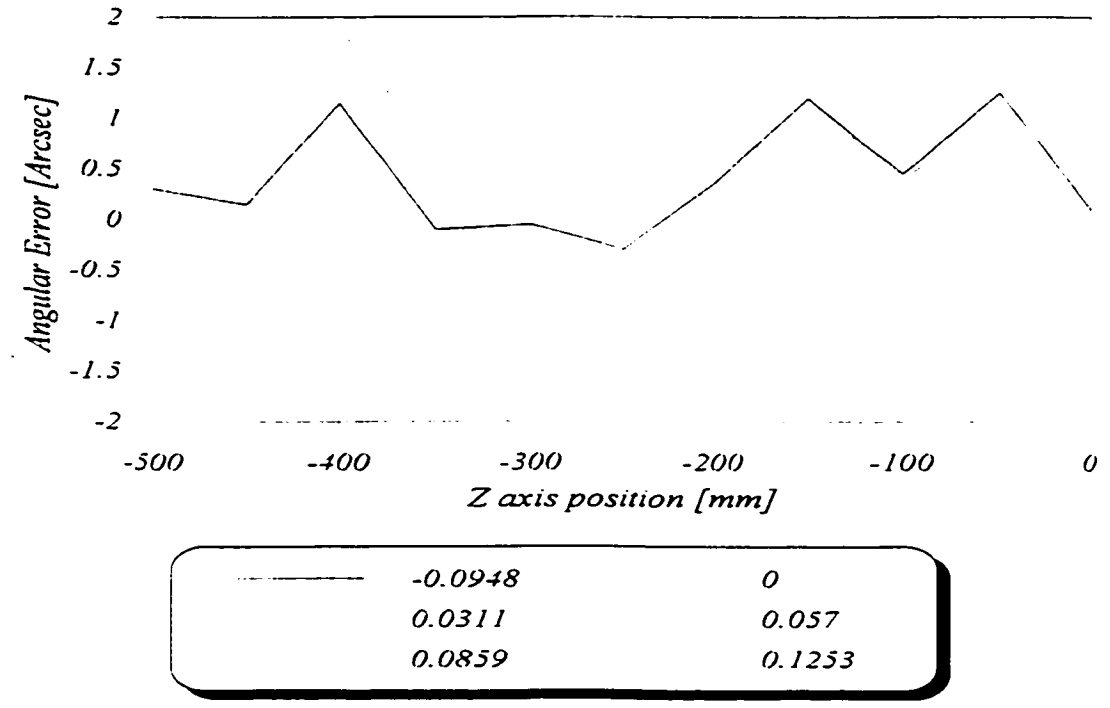


**Figure 121** $\alpha_{3z}$ Angular and Straightness error of Z axis rotation around X axis at different gradients [deg/m].

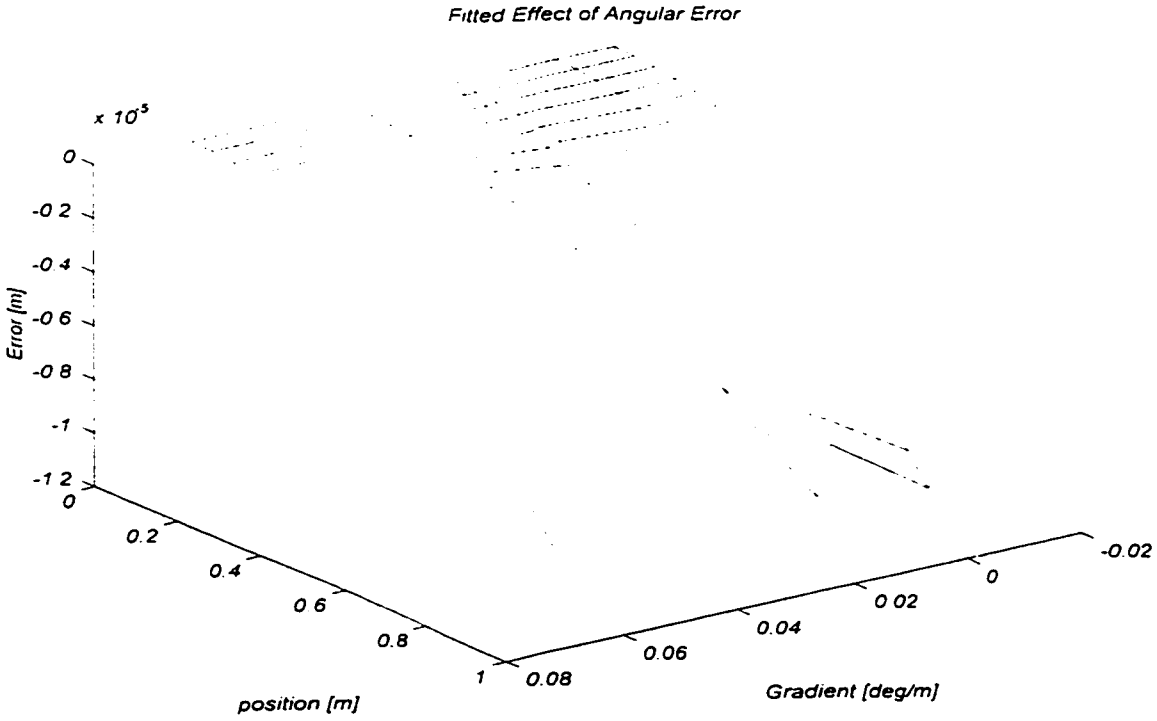


**Figure 122** Measured error resulting from X yaw angle γ in Y.

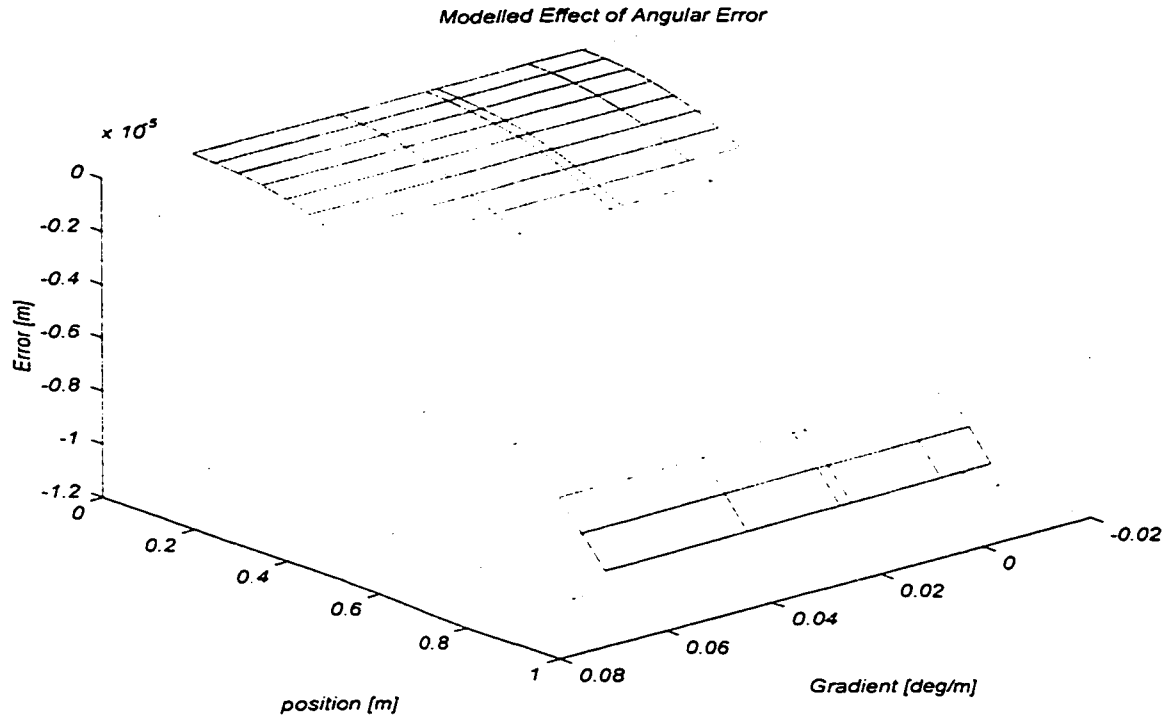


**Figure 123** Modelled error resulting from X yaw angle γ in Y.

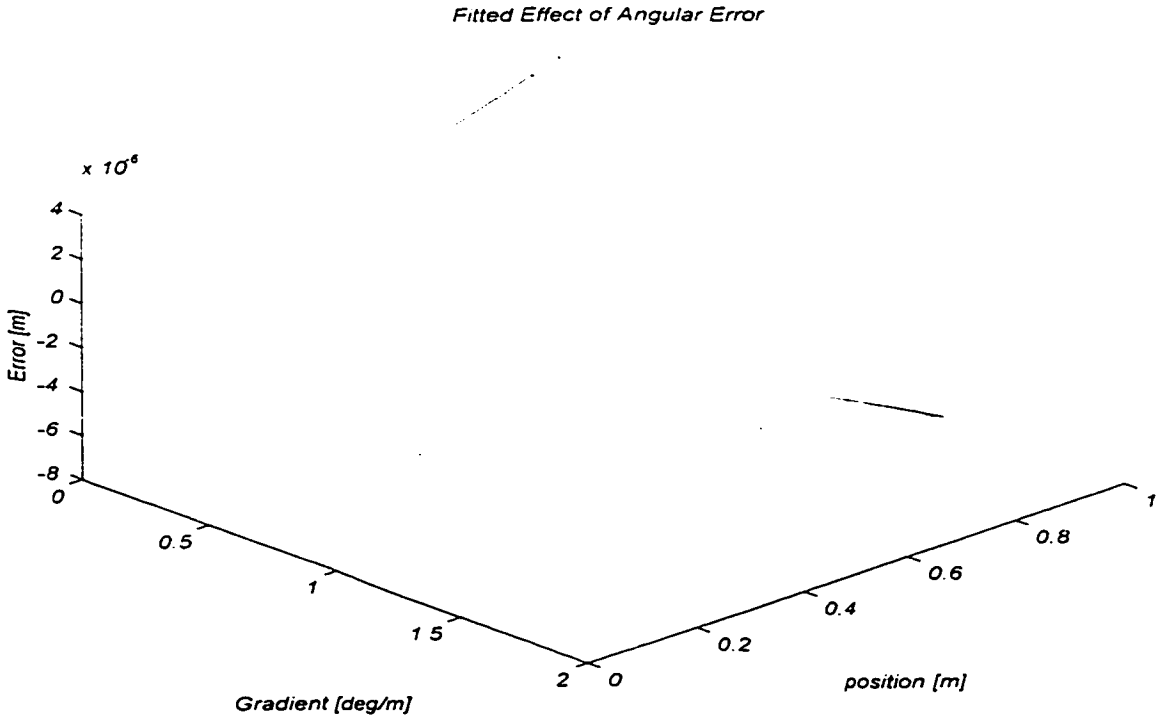


**Figure 124** Measured error resulting from X Pitch angle β in Z.

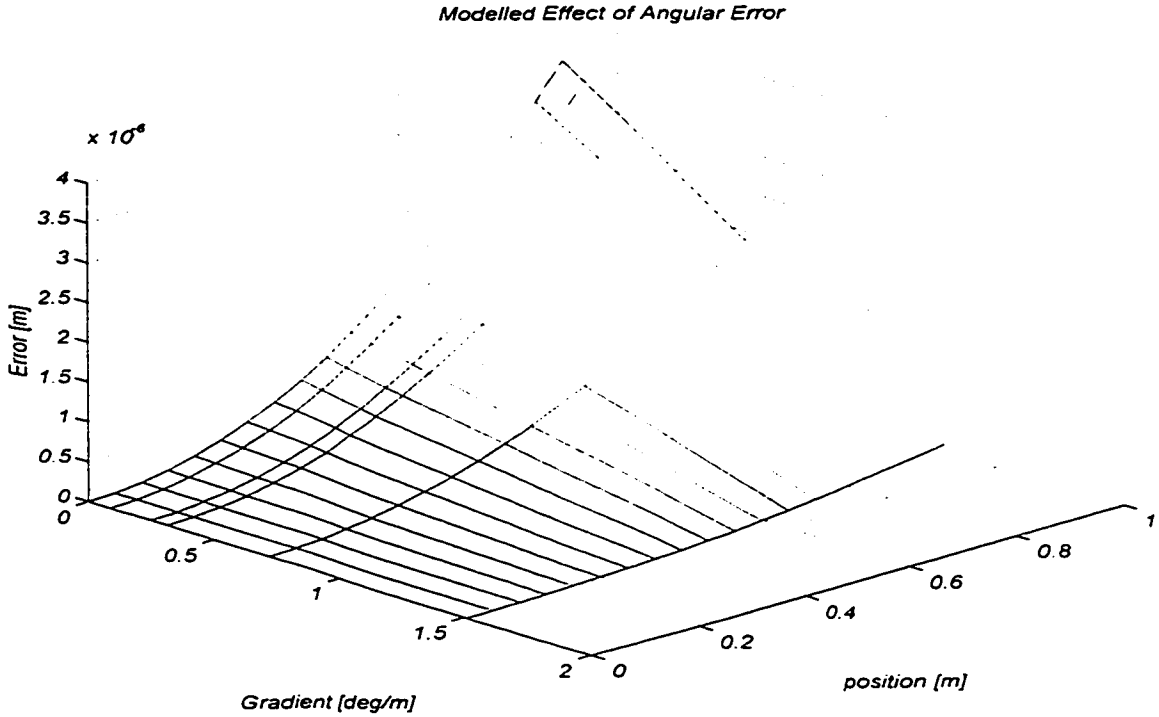


**Figure 125** Modelled error resulting from X Pitch angle β in Z.

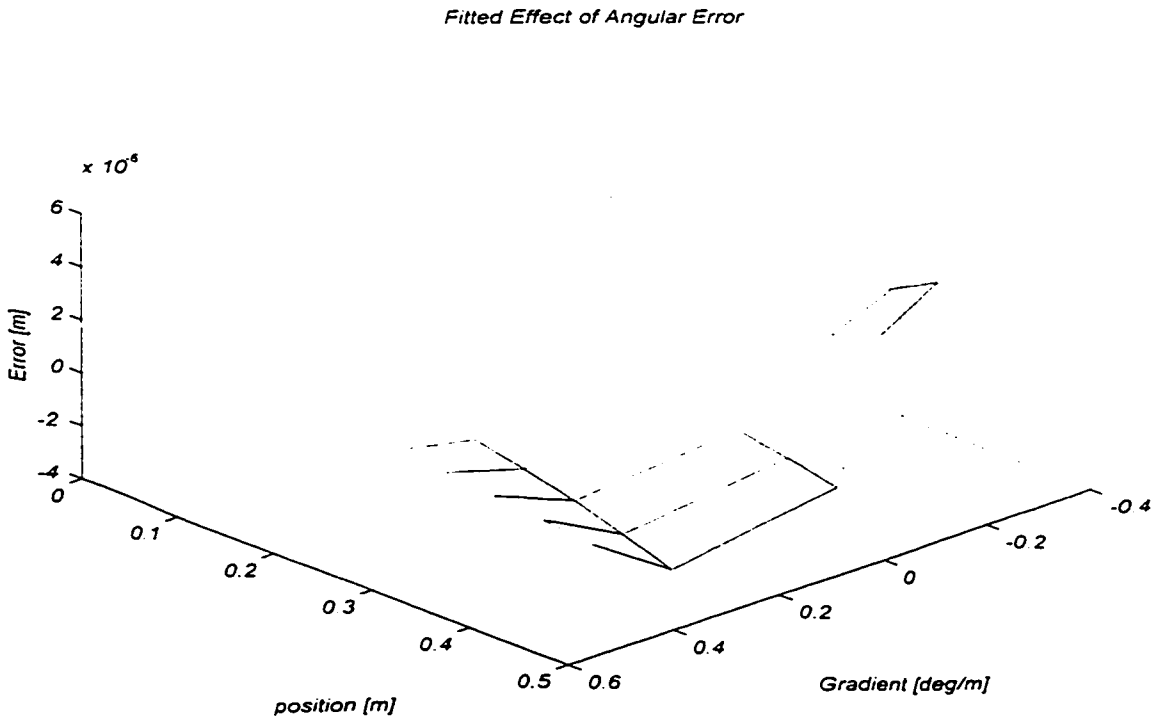


**Figure 126** Measured error resulting from Y Yaw angle γ in X.

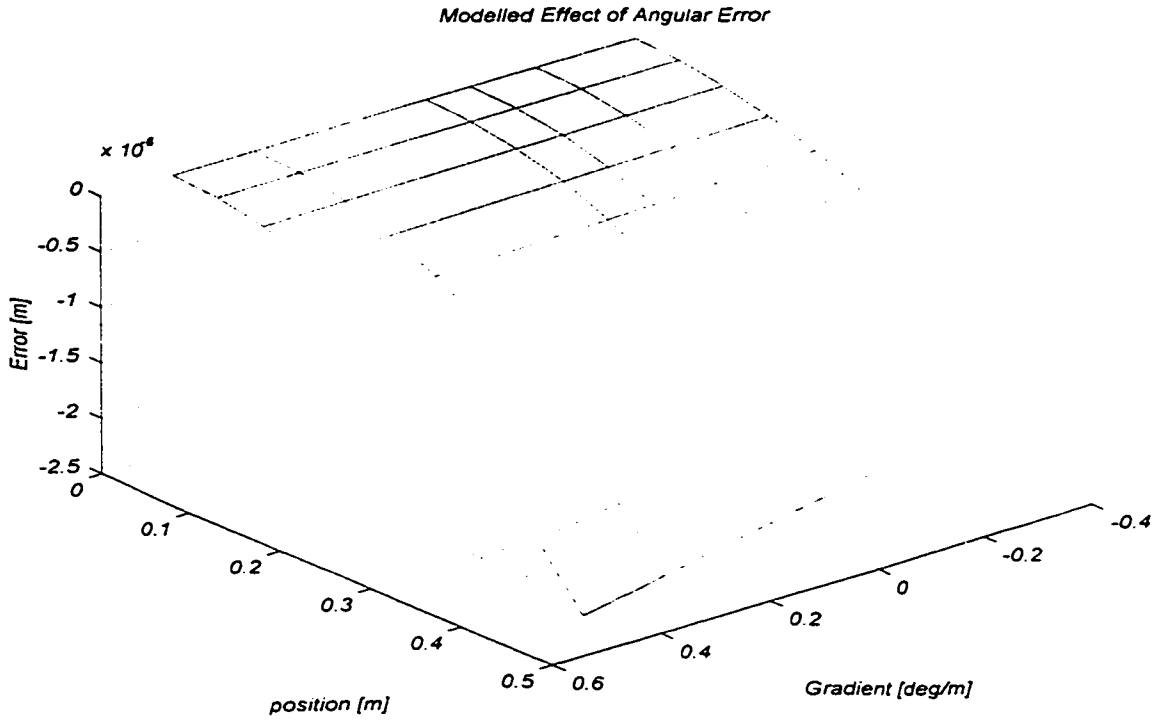


**Figure 127** Modelled error resulting from X Yaw angle γ in X.

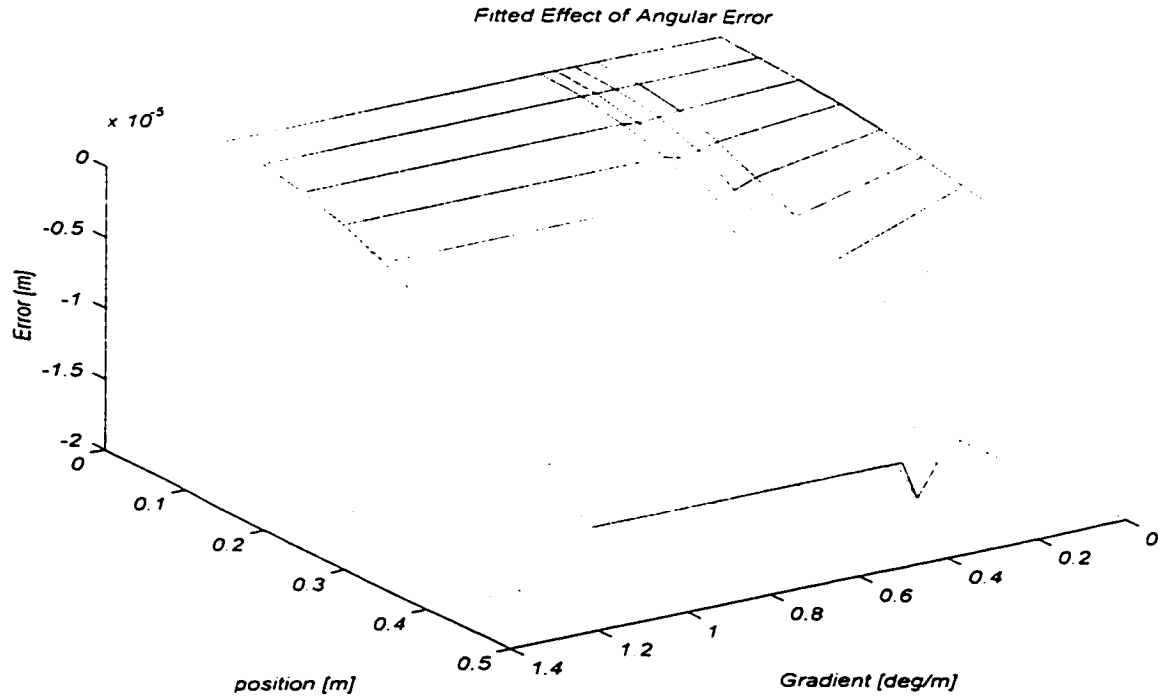


**Figure 128** Measured error resulting from Y Pitch angle α in Z.

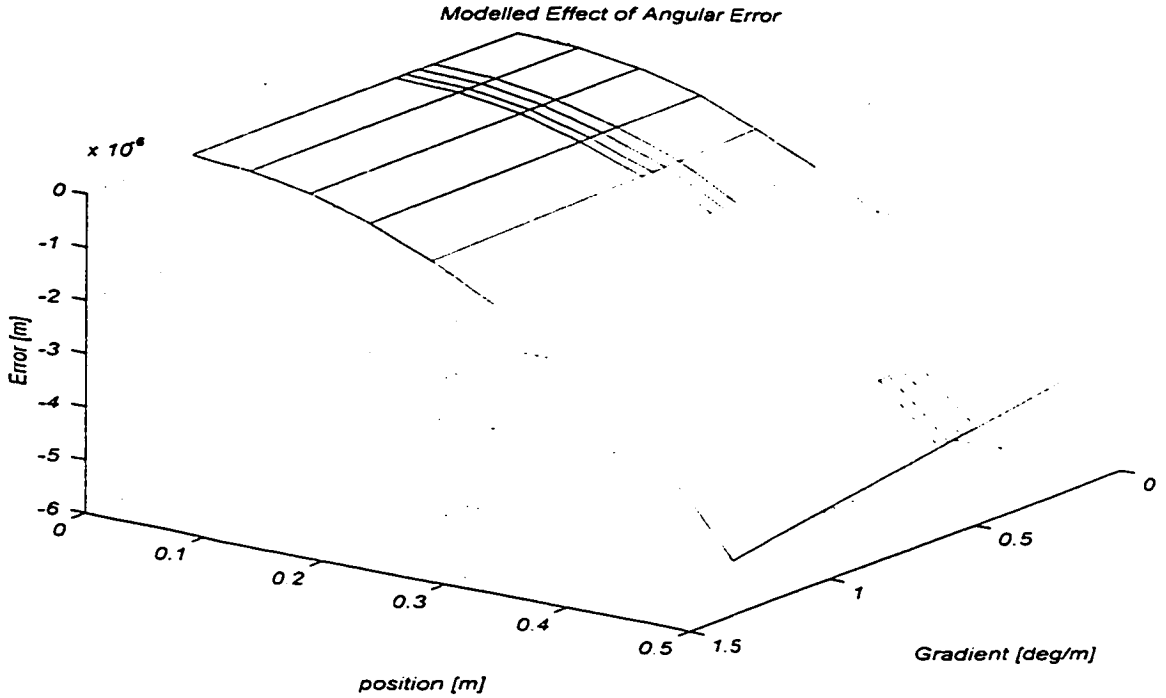


**Figure 129** Modelled error resulting from Y Pitch angle α in Z.

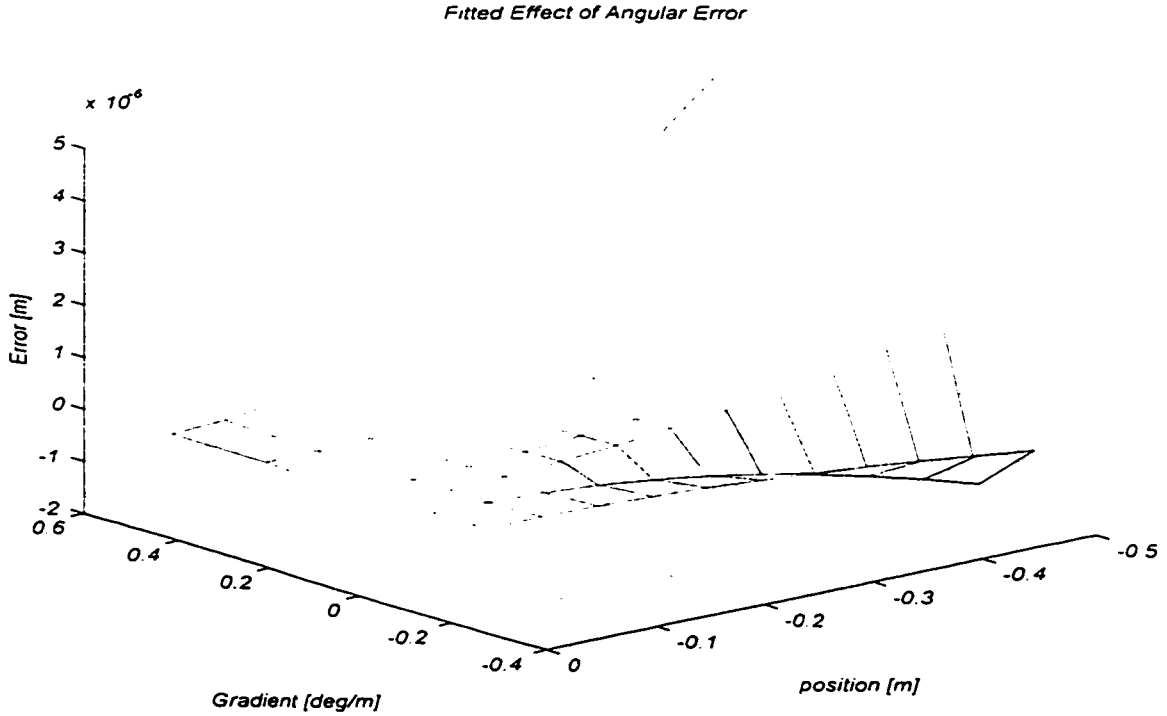


**Figure 130** Measured error resulting from Z Pitch angle β in X.

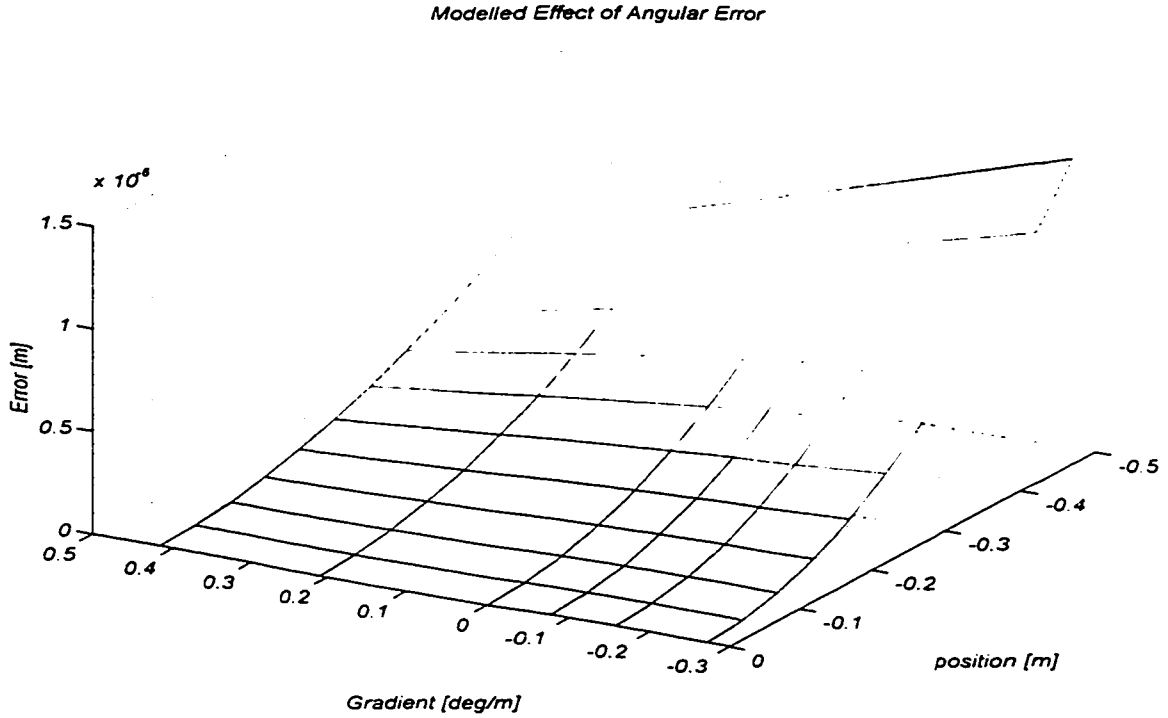


**Figure 131** Modelled error resulting from Z Pitch angle β in X.

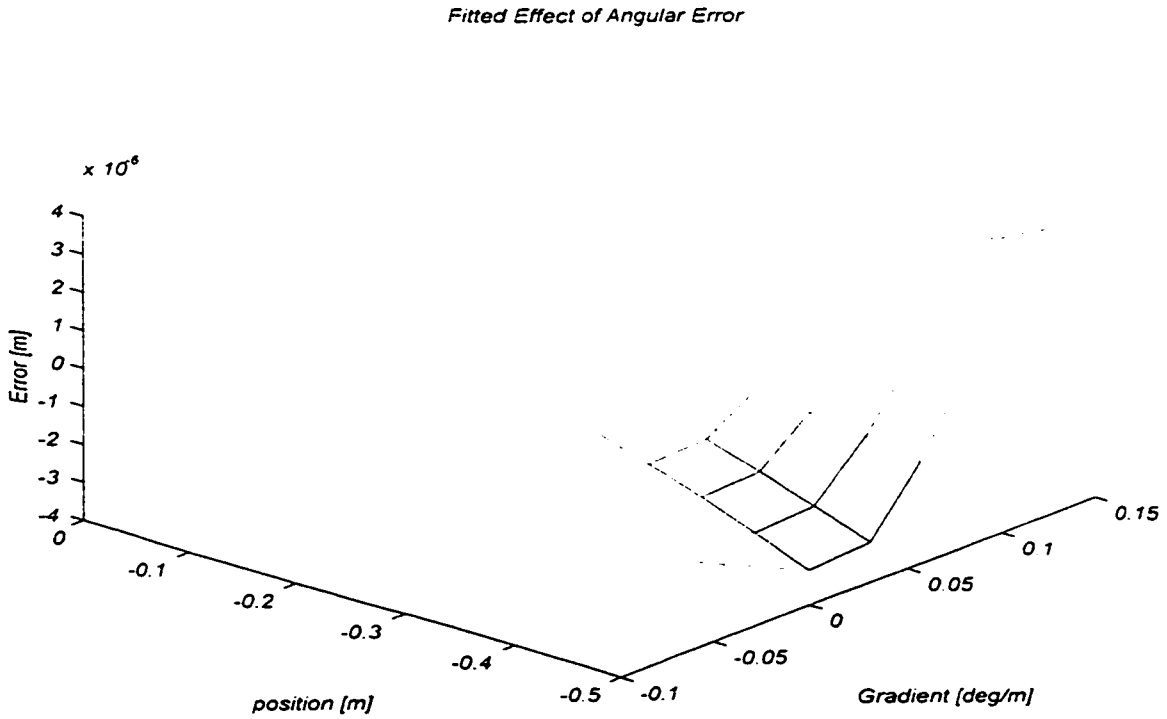


**Figure 132** Measured error resulting from Z Yaw angle α in Y.

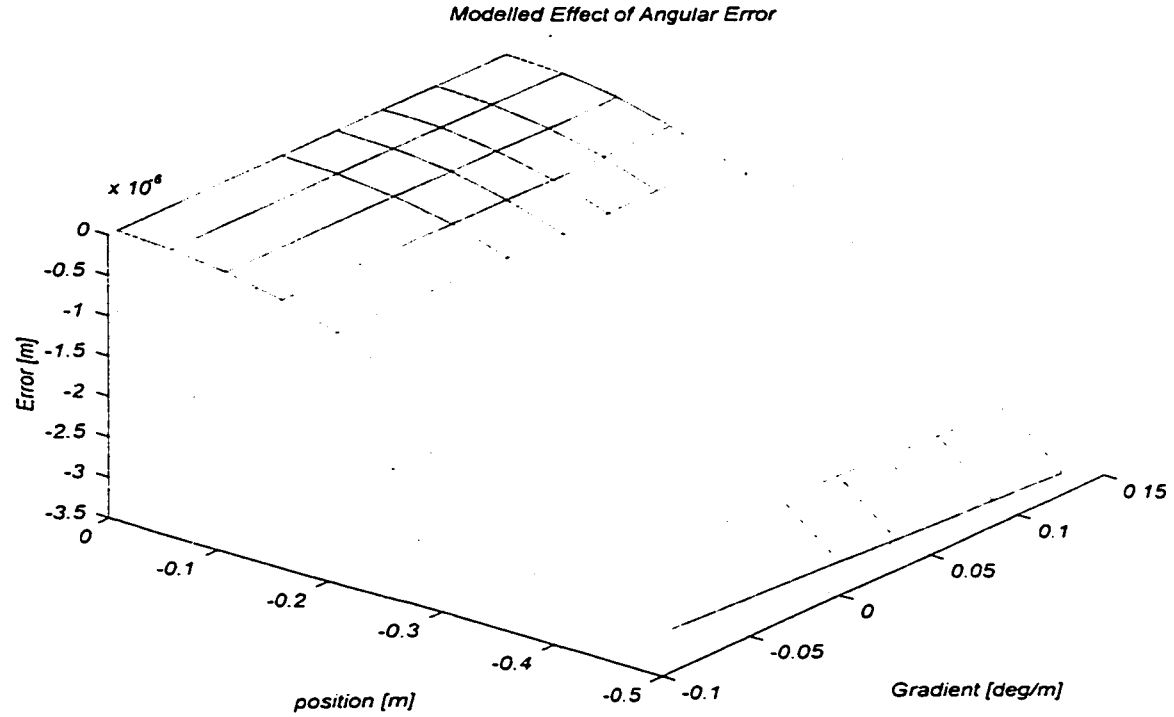


**Figure 133** Modelled error resulting from Z Yaw angle α in Y.

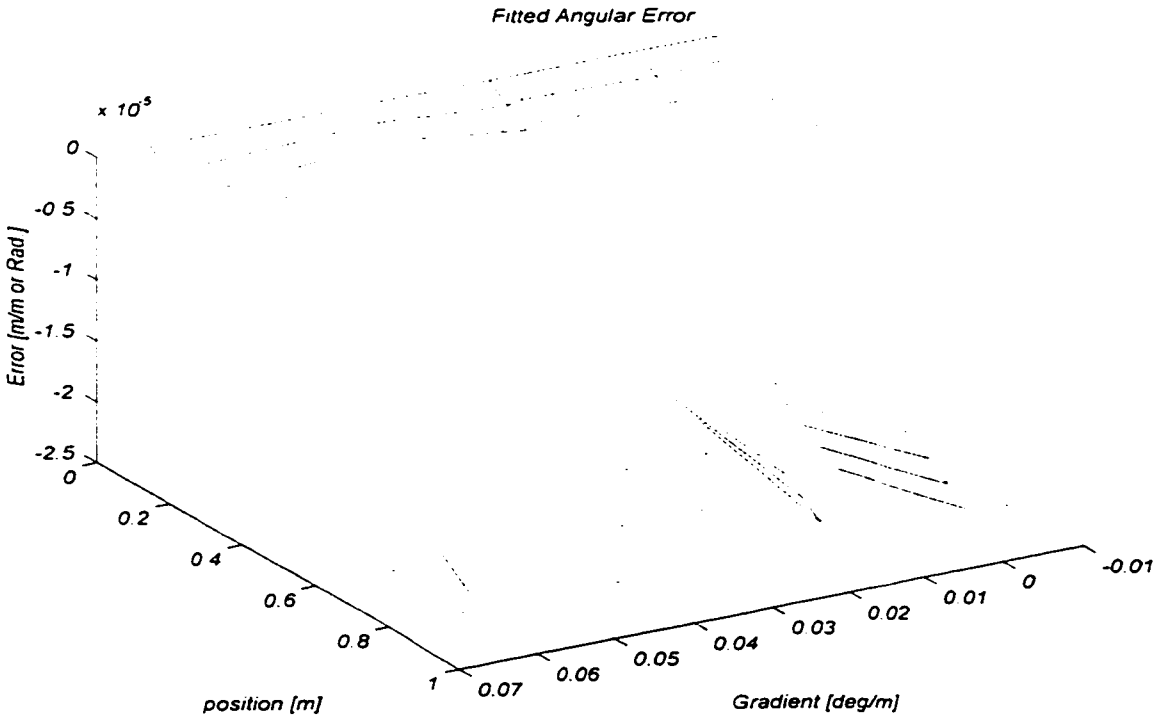


**Figure 134** Measured angular error γ of X motion in Y.

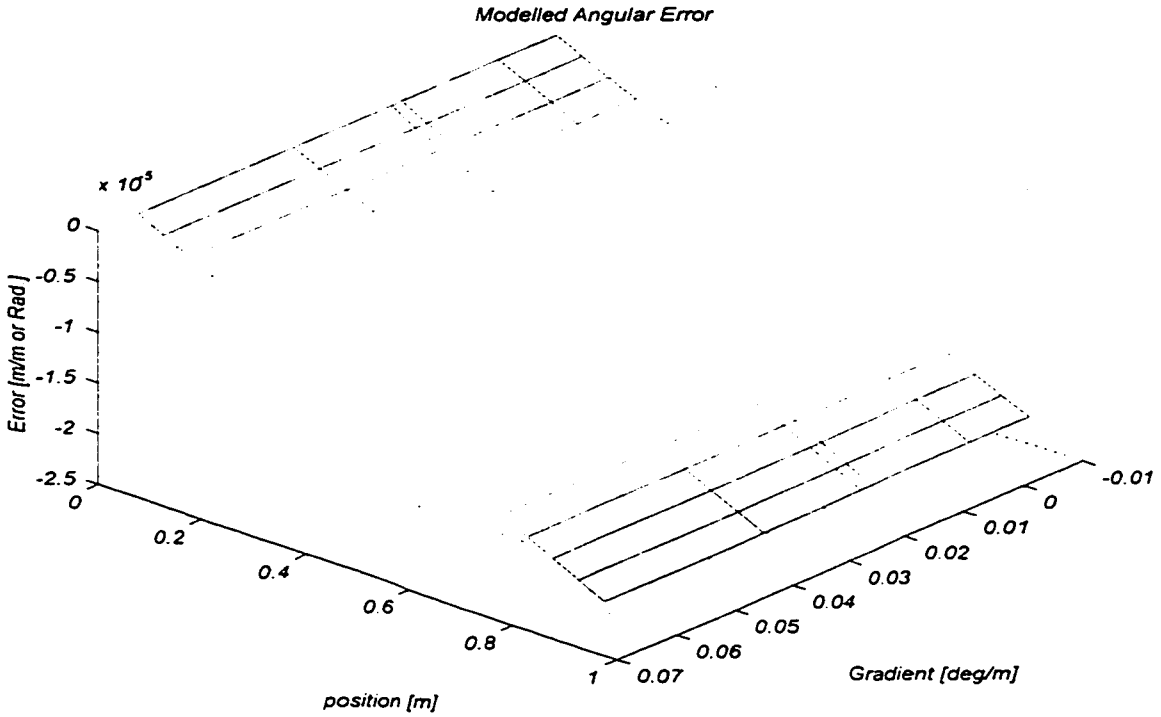


**Figure 135** Modelled angular error γ of X motion in Y.

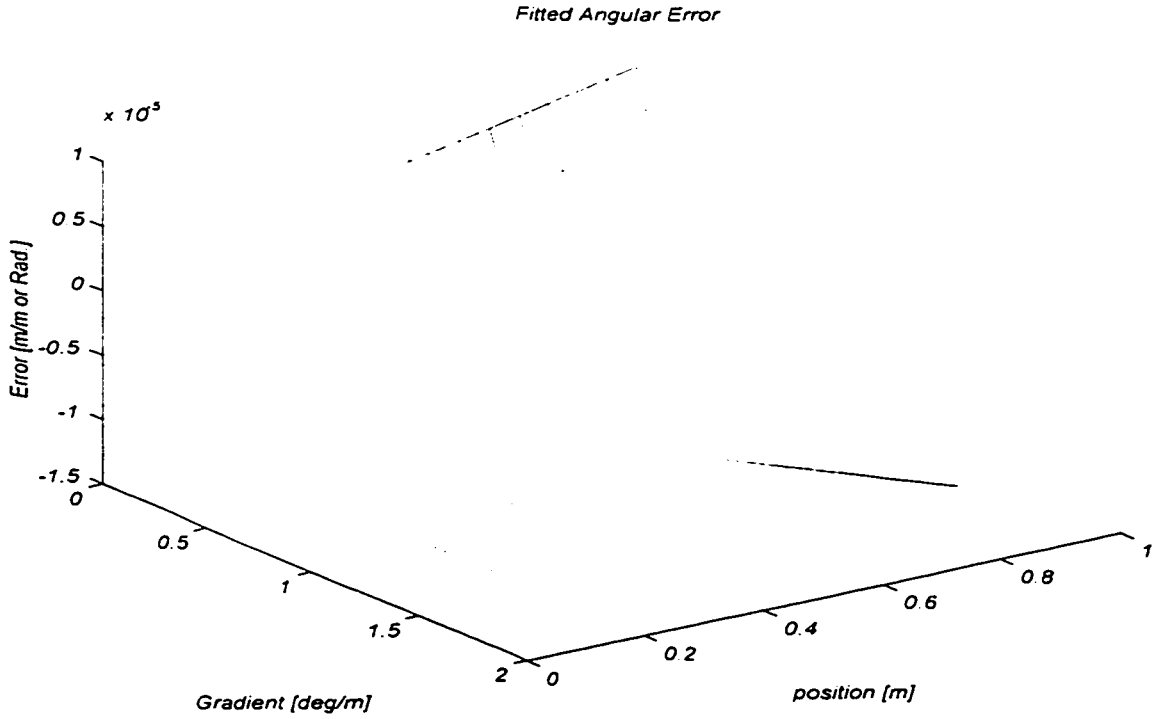


**Figure 136** Measured angular error β of X motion in Z.

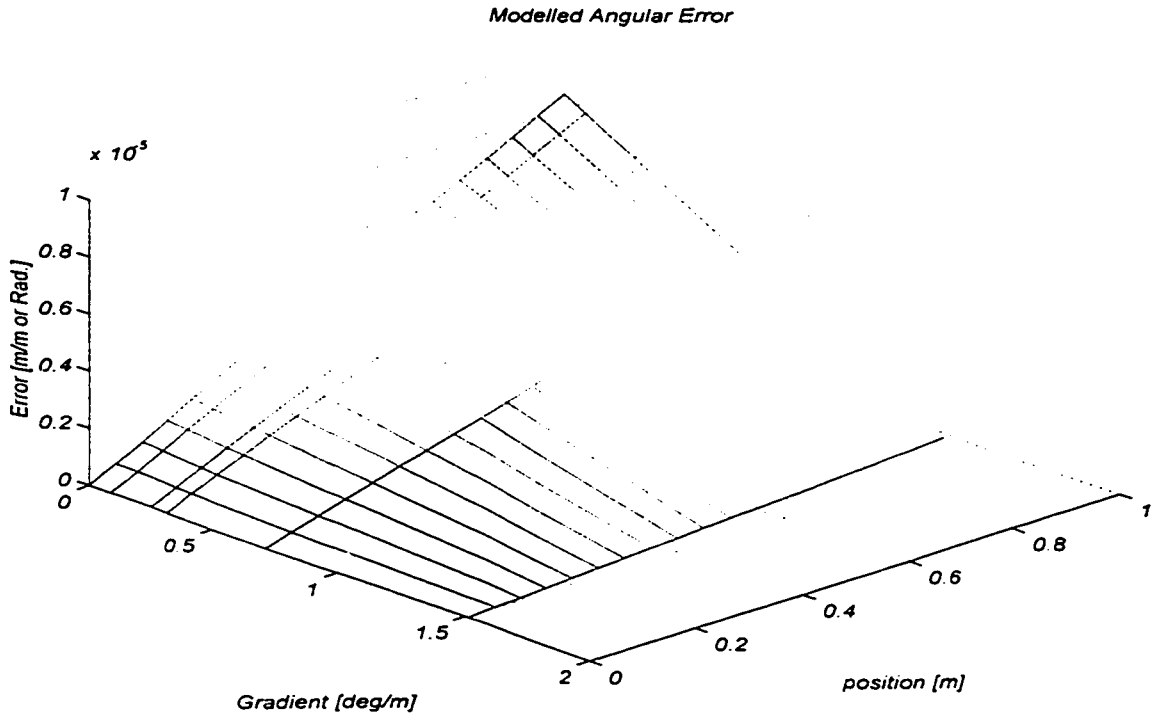


**Figure 137** Modelled angular error β of X motion in Z.

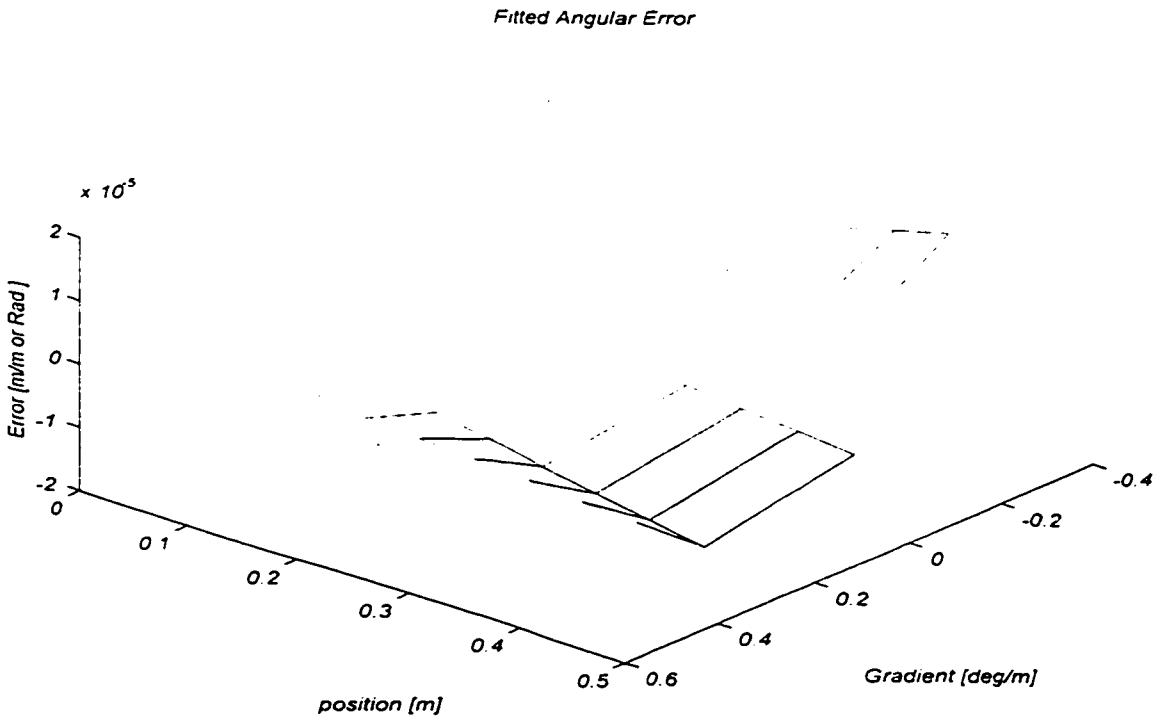


**Figure 138** Measured angular error γ of Y motion in X.

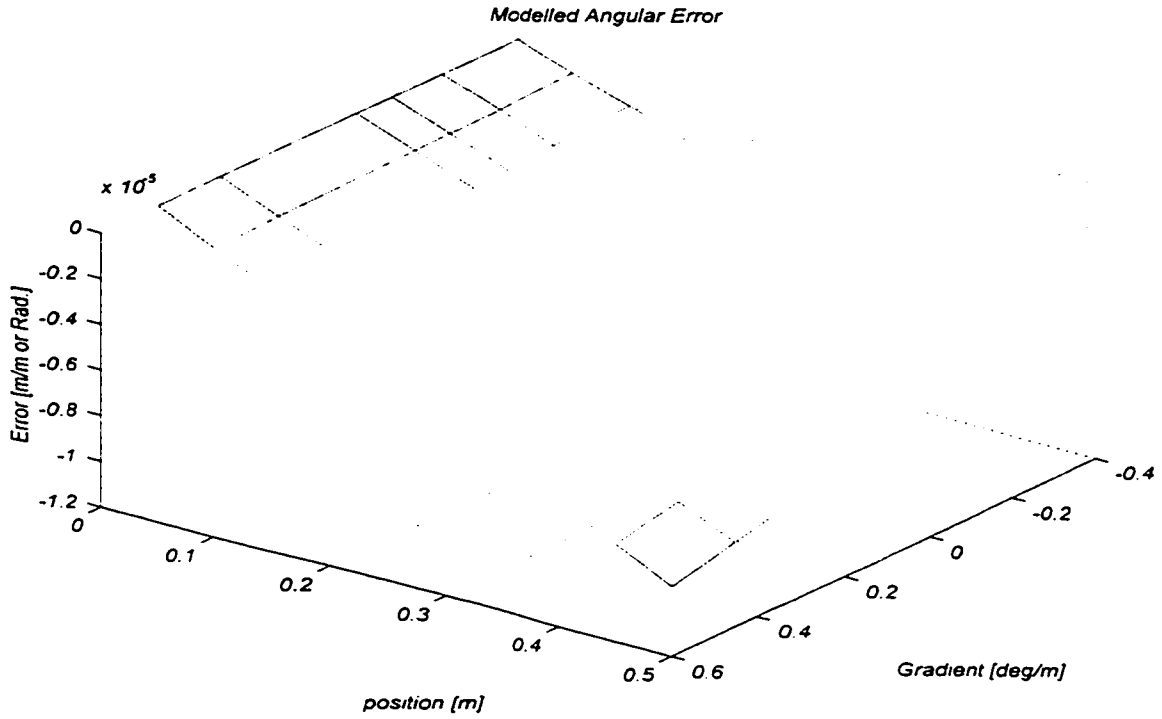


**Figure 139** Modelled angular error γ of Y motion in X.

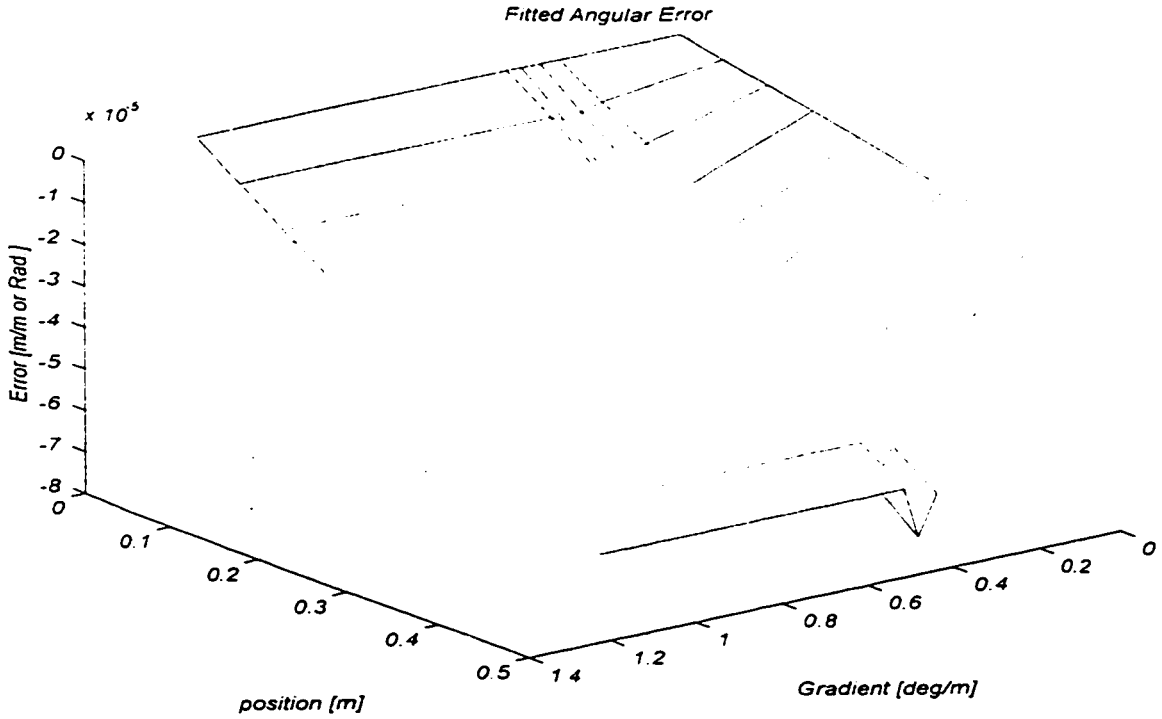


**Figure 140** Measured angular error αof Y motion in Z

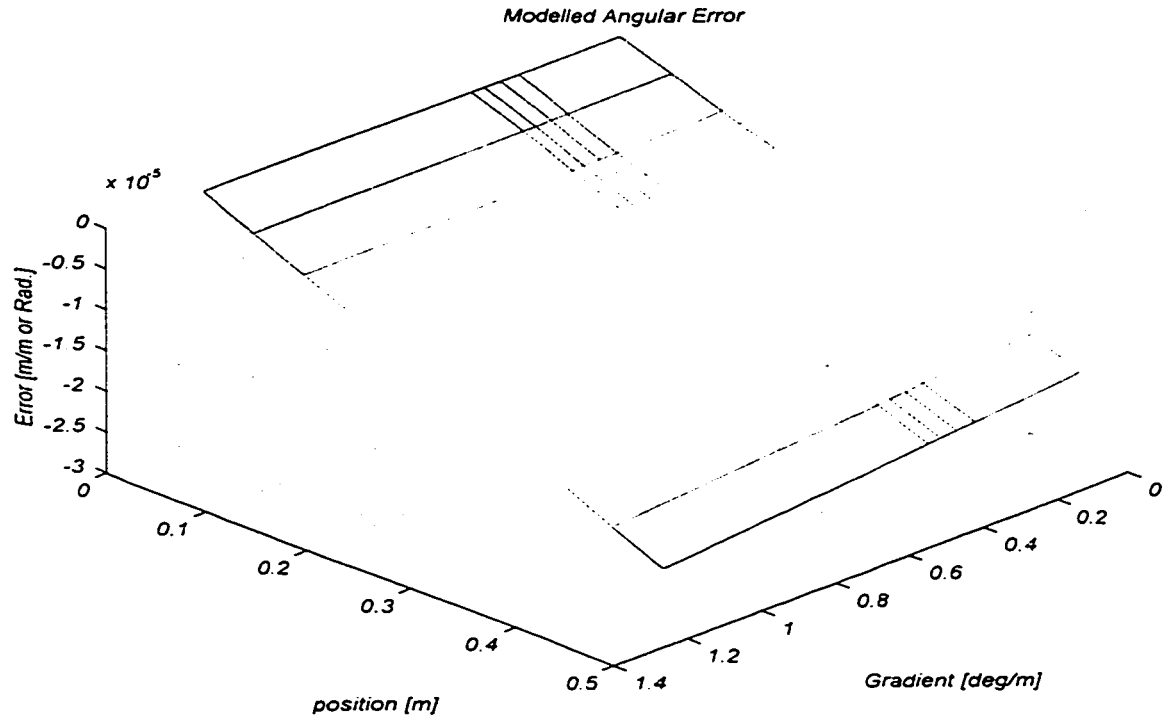


**Figure 141** Modelled angular error α of Y motion in Z

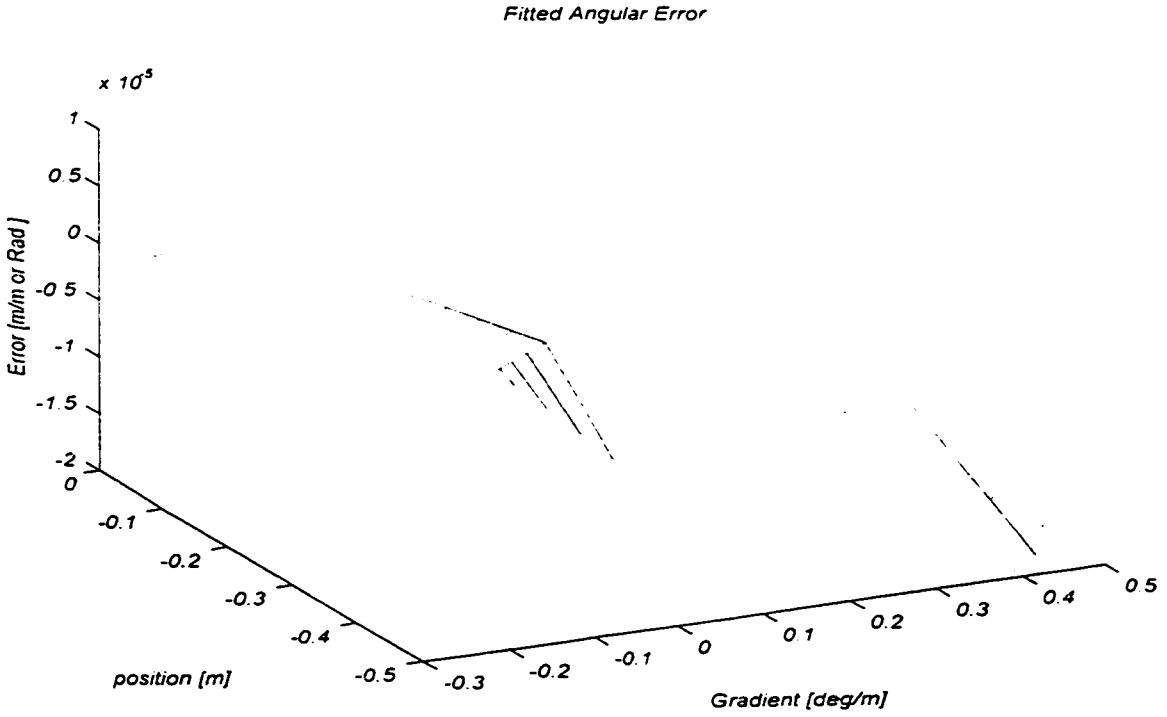


**Figure 142**Measured angular error β of Z motion in X

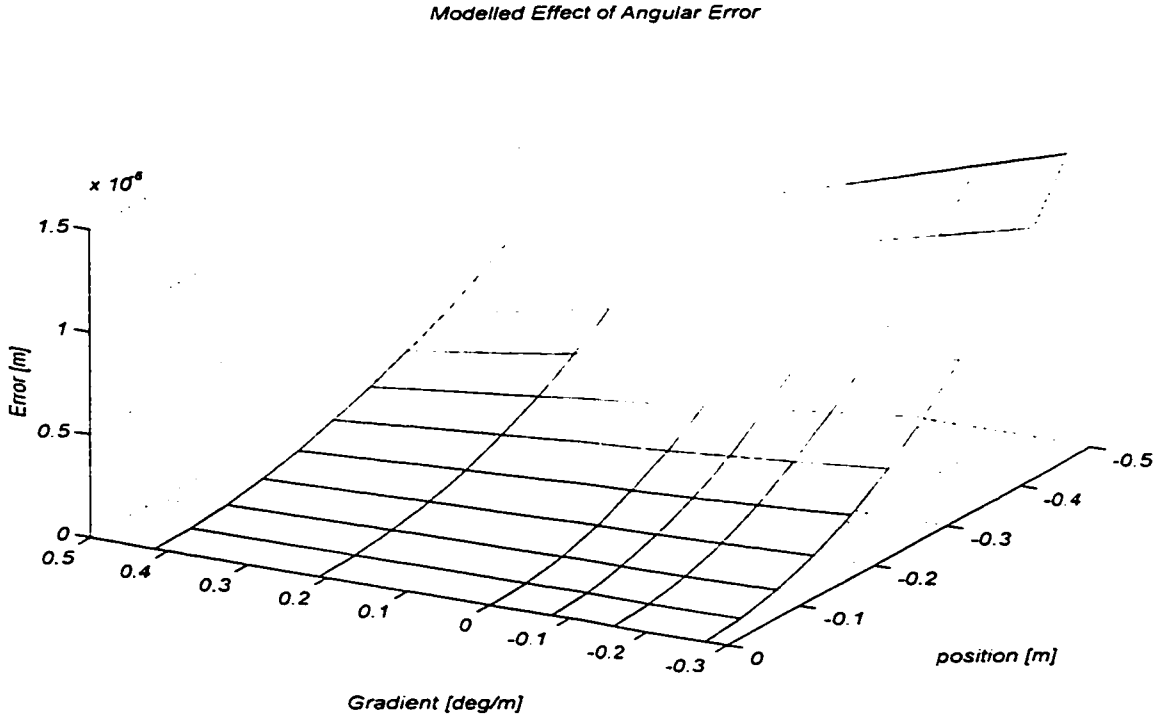


**Figure 143** Modelled angular error β of Z motion in X

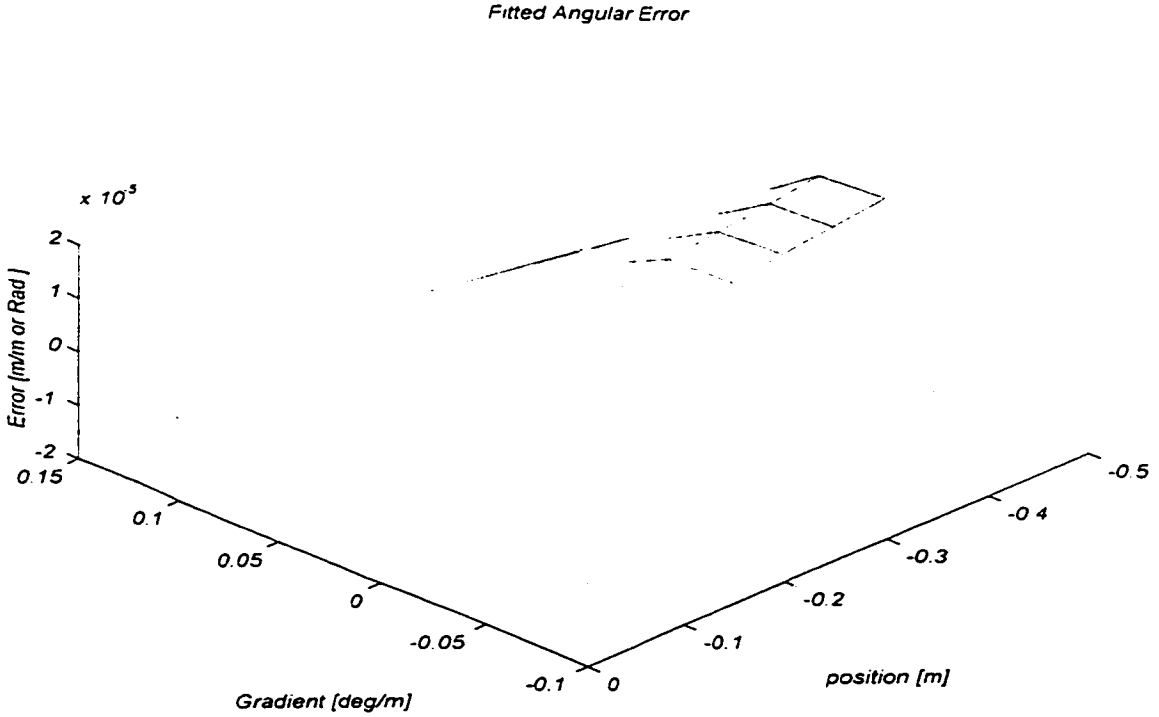


**Figure 144** Measured angular error αof Z motion in Y

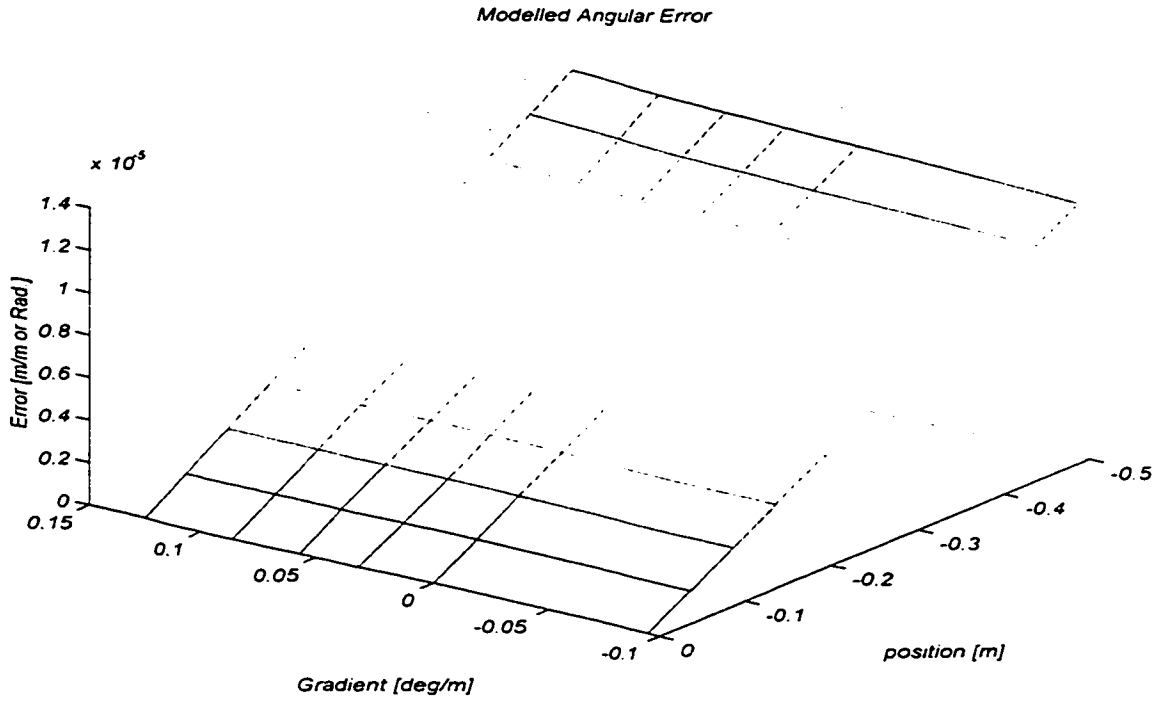


**Figure 145** Modelled angular error αof Z motion in Y

# Appendix K

**The full set of results of residual errors in contouring before and after applying the proposed compensation strategy**

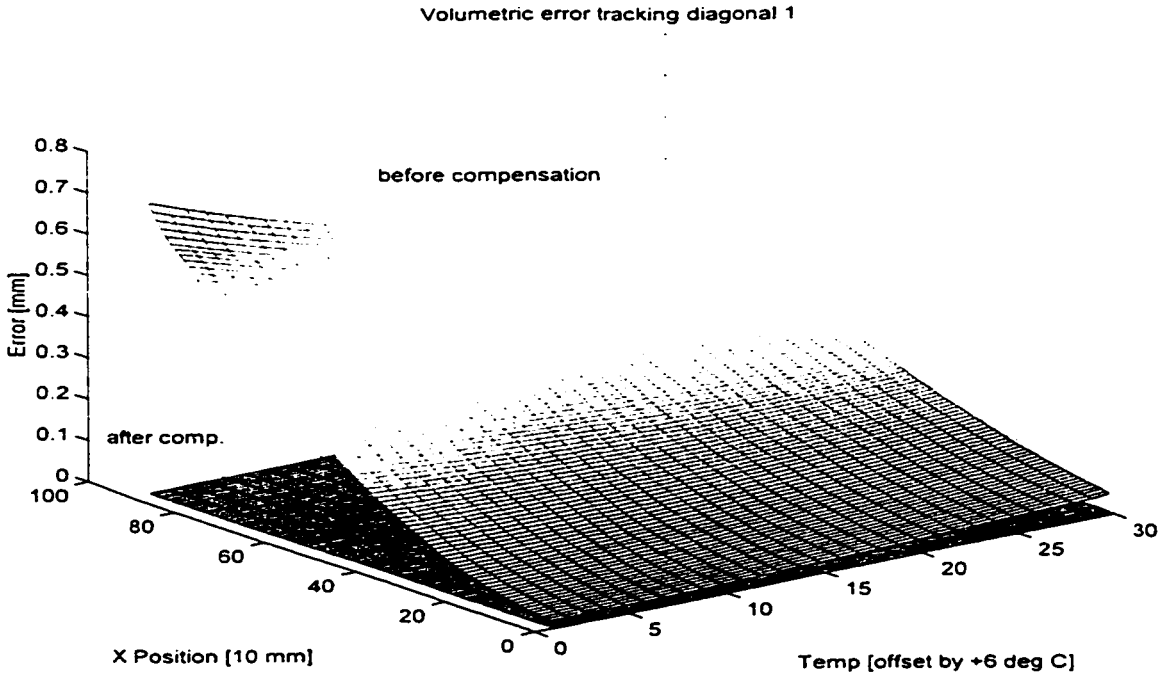


**Figure 1** Line 1 contouring error before and after correction, at different temperatures.

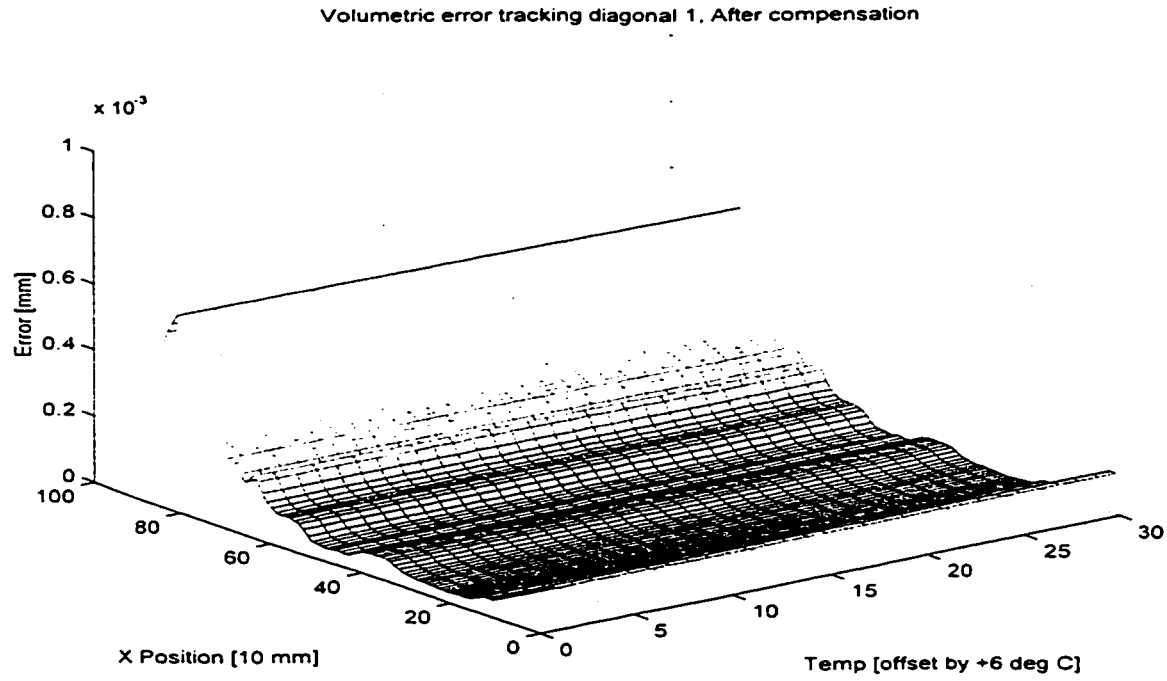


**Figure 2** Line 1 contouring error after correction.

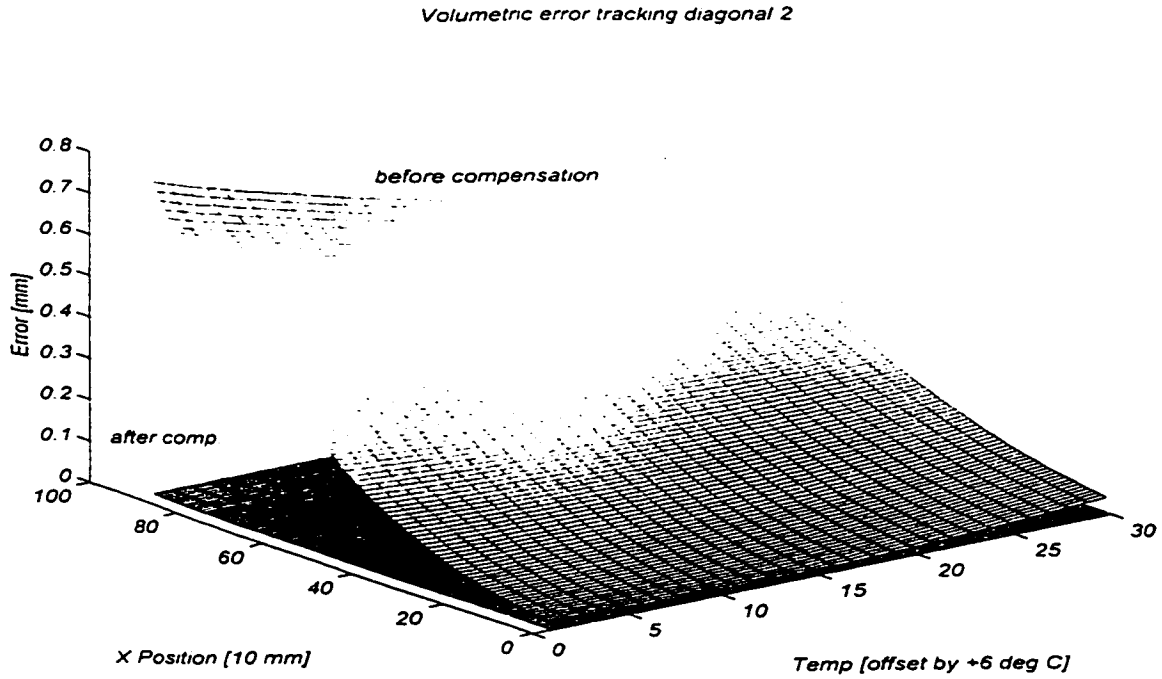


**Figure 149** Line 2 contouring error before and after correction, at different temperatures.

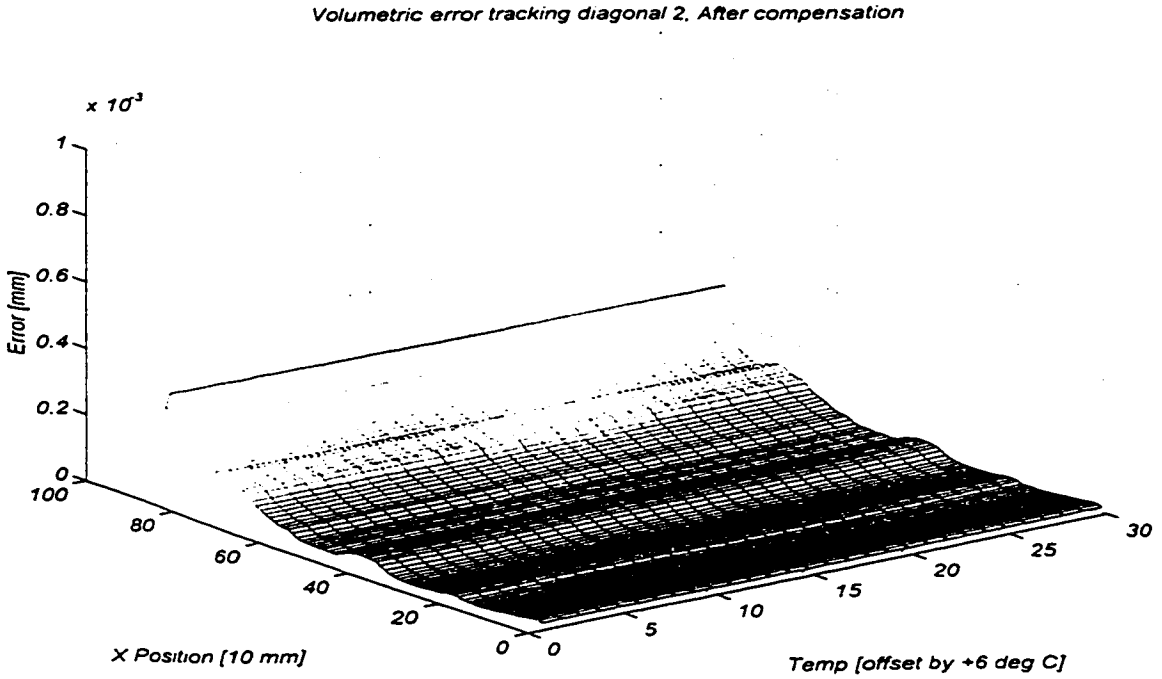


**Figure 148** Line 2 contouring error after compensation.

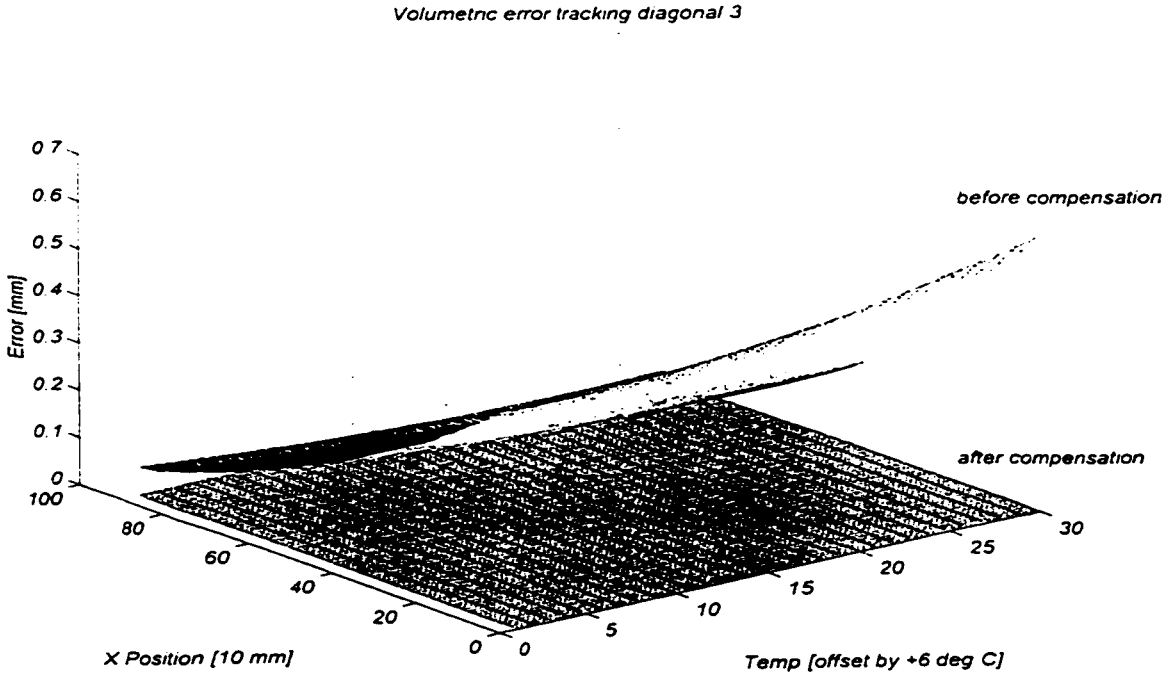


**Figure 150** Line 3 contouring error before and after compensation.

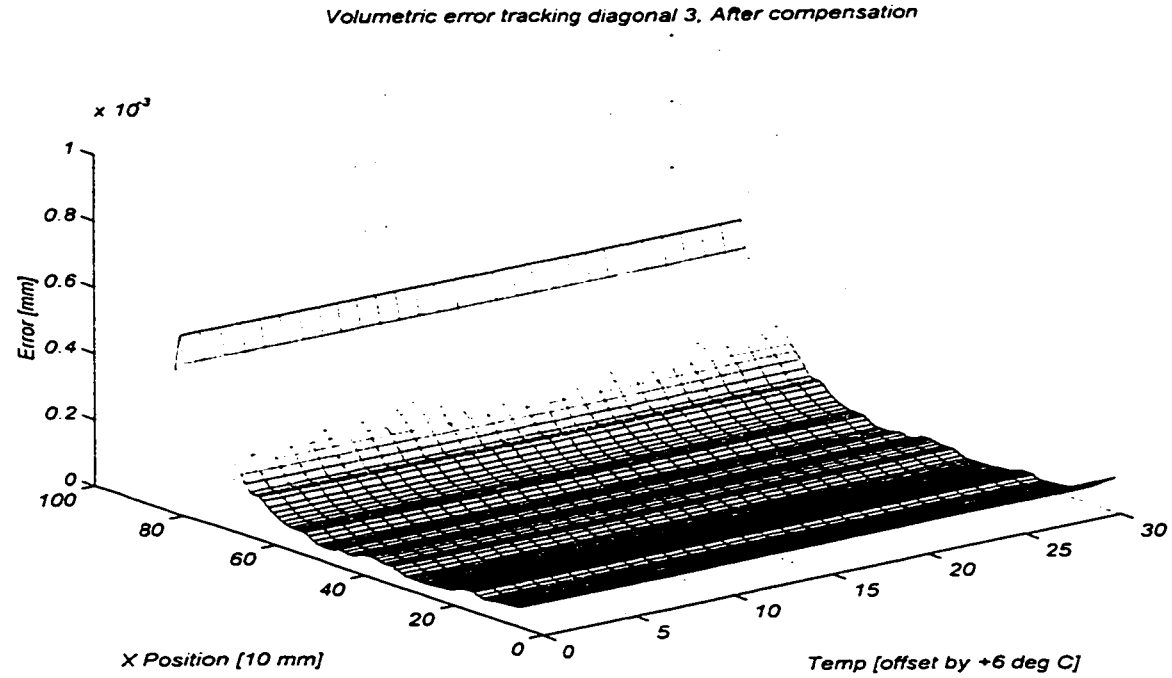


**Figure 151** Line 3 contouring error after compensation.

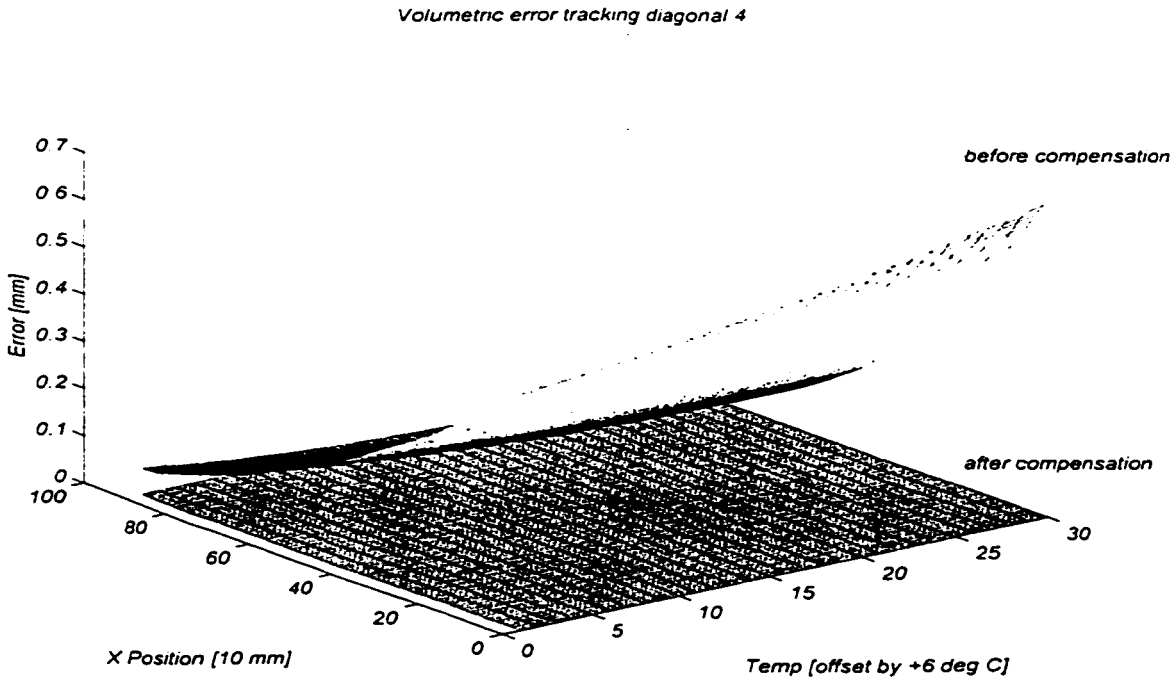


**Figure 152** Line 4 contouring error before and after compensation.

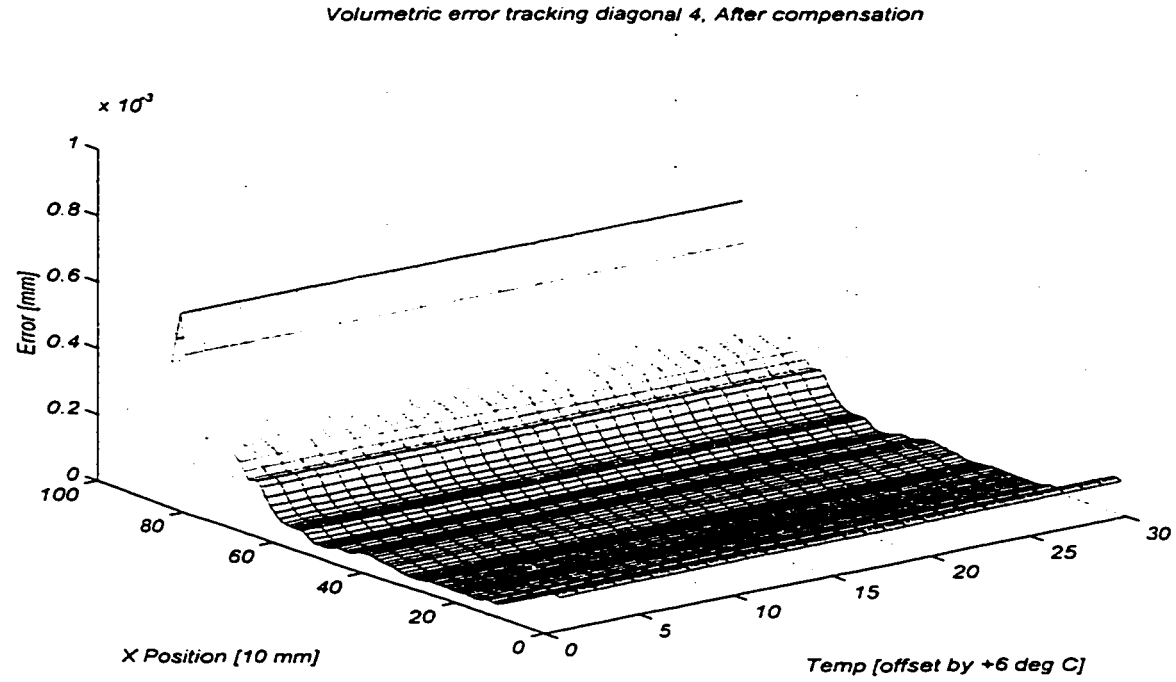


**Figure 153** Line 4 contouring error after compensation.

# References


1. B. Arnold, N. Balakrishnan, H. Nagaraj, 1992, "A first Course in Order Statistics", John Wiley and Sons, Inc.

2. M. H. Attia, L. Kops,1993, "Thermometric Design Considerations for Temperature Monitoring in Machine Tools and CMM Structures", Int. J. Adv. Manuf. Tech., Vol. 8, pp. 311-319.

3. ASME B89.1.12M - 1990, "Methods for Performance Evaluation of Coordinate Measuring Machines", An American National Standard.

4. A. Balsamo, 1995, "Effect of Arbitrary Coefficients of CMM Error Maps on Probe Qualification", Annals of CIRP, Vol. 44/1/1995.

5. A. Balsamo, D. Marques, S. Sartori, 1990, "A Method for Thermal - Deformation Correction of CMMs", Annals of CIRP, Vol. 39/1/1990.

6. N. Barakat, 1998, "Calibration of Coordinate Measuring Machines Using Ball Bars and Laser Interferometers," ACMC Annual Meeting, McMaster University, Hamilton, Ontario, Canada, June 4, 5, 1998, (Invited session lecture and paper).

7. N.A. Barakat and M.A. Elbestawi, 1998, "Detection, Modelling, and Compensation of Geometric Errors in Coordinate Measuring Machines," ASME - WAM., CA. MED-8:597-603.

8. N.A. Barakat, M.A. Elbestawi, A.D. Spence, 2000, "Kinematic and geometric error compensation of a coordinate measuring machine", International Journal of Machine Tools and Manufacture 40 (6) (2000) pp. 833-850.

9. Nael A. Barakat, Mohamed A. Elbestawi, Allan D. Spence, 2000, " Error Compensation for an Intrinsic Machine", CSME May.16-19, 2000, Montreal, Canada.

10. Barakat, N.A., Elbestawi, M.A., and Spence, A.D., 2000, "Adaptive Compensation for Errors in an Intrinsic Machine", Int. J. Mach. Tools and Manufacture., to appear.

11. G. Belforte, B. Bona, E. Canuto, F. Ferraris, I. Gorini, S, Morei, M. Peisino, S. Sartori, 1987, "Coordinate Measuring Machines and Machine Tools Selfcalibration and Error Correction", Annals of CIRP, Vol. 36/1/1987.

12. J. A. Bosch , 1995, "Coordinate Measuring Machines and Systems", Marcel Dekker, Inc.

13. R. Brook and G. Arnold, 1985, "Applied Regression Analysis and Experimental Design", Marcel Dekker Inc.

14. Jim Bryan, 1990, "International Status of Thermal Error Research," Annals of CIRP, vol. 39/2.

15. Alex Chan, 1997, "Improving the Accuracy of a Coordinate Measuring Machine," Master Degree Thesis, Dept. of Mech. Eng., McMaster University, Hamilton,

Ontario, Canada.

16. J. Craig, 1989, "Introduction to Robotics and Mechanics Control", Addison Wesley Publishing Company.

17. H. Danzer, H. Kunzmann, 1987, "Application of 3-Dimentional Coordinae Measuring Machines for Problem Investigation and Upstream quality assurance", Annals of CIRP, Vol. 36/1/1987.

18. R. Decarlo, 1989, "Linear Systems", Prentice Hall, NJ, USA.

19. N. Duffie, S. Malmberg, 1987, "Error Diagnosis and Compensation Using Kinematic Models and Position Error data", Annals of CIRP, Vol. 36/1/1987.

20. N. Duffie, S. Yang, 1985, "Generation of Parametric Kinematic Error-Correction Functions from Volumetric Error Measurements", Annals of CIRP, Vol. 34/1/1985.

21. K. Eman, B. Wu, M. DeVries, 1987, "A Generalized Geometric Error Model for Multi-axis Machines," Annals of CIRP, Vol. 36/1.

22. P. Ferreira, C. Liu, 1986, "A Contribution to the Analysis and Compensation of The Geometric Error of a Machining Centre", Annals of CIRP, Vol. 35/1/1986.

23. Chris Garcia, 1999, "Software Advancement for CMMs", ACMC Annual Meeting, National Research Council of Canada, London, Ontario, Canada, June, 1999.

24. International Organization for Standards. ISO, 1993, "Internation Vocabulary of Basic and general Terms in Metrology", ISO.

25. K. Iwata, T. Moriwaki, S. Ueno, 1982, "Development of a Modular-Type Measuring System for Evaluation of Machining Accuracy", Annals of CIRP, Vol. 31/1/1982.

26. L. Jie-Chi, N. Duffie, J. Bollinger, 1982, "Two Dimentional Tracing and

Measurement Using Touch Trigger Probes", Annals of CIRP, Vol. 31/1/1982.

27. W. Knapp, 1983, "Test of The Three-Dimentional Uncertainty of Machine Tools and Measuring Machines and its Relation to the Machine Errors", Annals of CIRP, Vol. 32/1/1983.

28. W. Knapp, 1988, "Accuracy of Length Measurement and Positioning : Statical Measurement and Contouring Mode", Annals of CIRP, Vol. 37/1/1988.

29. H. Kunzmann, E. Trapet, F. Waldele, 1990, "A Uniform Concept for Calibration, Acceptance Test, and Periodic Inspection of Coordinate Measuring Machines Using Reference Objects", Annals of CIRP, Vol. 39/1/1990.

30. H. Kunzmann, E. Trapet, F. Waldele, 1995, "Results of The International Comparison of Ball Plate Measurements in CIRP and WECC", Annals of CIRP, Vol. 44/1/1995.

31. H. Kunzmann, F Waldele, 1983, "On Testing Coordinate Measuring Machines (CMM) with Kinemaic Reference Standards (KRS)", Annals of CIRP, Vol. 32/1/1983.

32. H. Kunzmann, F. Waldele, 1988, "Performance of CMMs", Annals of CIRP, Vol. 37/2/1988.

33. K. Lau, R. Hocken, 1984, "A Survey of Current Robot Metrology Methods", Annals of CIRP, Vol. 33/2/1984.

34. P. Lingard, M. Purss, C. Sona, E. Thwaite, 1991, "Length-Bar and Step-Guage Calibration Using a Laser Measurement System with a COOrdinate Measuring Machine", Annals of CIRP, Vol. 40/1/1991.

35. L. Ljung and T. Soderstrom, 1983, "Theory and Practice of Recursive Identification", The MIT Press, Cambridge, MA.

36. P.A. McKeown, 1987, "The Role of Precision Engineering in Manufacturing of the future", Annals of CIRP, Vol. 36/2/1987.

37. P. Mckeown, M. Weck, R. Bonse, 1995, "Reduction and Compensation of Thermal Errors in Machine Tools", Annals of CIRP, Vol. 44/2/1995.

38. T. Moriwaki, 1988, "Thermal Deformation and its On-Line Compensation of Hydrostatically Supported Precision Spindle", Annals of CIRP, Vol. 37/1/1988.

39. J. Mou, C. Liu, 1993, "A Methodology for Machine Tool Error Correction - An Adaptive Approach", Ped-Vol. 64, Manufacturing Science and Engineering, ASME Winter Annual Meeting 1993.

40. O. Nakamura, M. Goto, K. Toyoda, Y. Tanimura, 1991, "Development of a Coordinate Measuring System with Tracking Laser Inferometers", Annals of CIRP, Vol. 40/1/1991.

41. L. Nawara, M. Kowalski, 1981, "Investigations on The Variability of Measurements Realized by Multicoordinate Measuring Machines on Circular Sections with Determined Types of Roudness Errors", Annals of CIRP, Vol. 30/1/1981.

42. L. Nawara, M. Kowalski, 1984, "The Investigations on Selected Dynamical Phenomena in The Heads of Multi-Coordinate Measuring Devices", Annals of CIRP, Vol. 33/1/1984.

43. H. L. Nawara, M. Kowalski, 1987, "Analysis of The Random Component of Multicoordinate Measuring Machines and Metrological Robots Position Error",

Annals of CIRP, Vol. 36/1/1987.

44. L. Nawara, M. Kowalski, J. Sladik, 1989, "The Influence of Kinematic Errors on The Profile Shapes by Means of CMM", Annals of CIRP, Vol. 38/1/1989.

45. J. Nijs, M. Lammers, P. Shellekens, A. Van der Wolf, 1988, "Modelling of a Coordinate Measuring Mchine for Analysis of its Dynamic Behaviour", Annals of CIRP, Vol. 37/1/1988.

46. H. Pahk, and J. Kim, 1995, "Application of Microcomputer for Assessing the Probe Lobing Error and Geometric Errors of CMM's Using Commercial Ring Gauges," Int. J. Adv. Manuf. Technol. 10:208-218.

47. R. Paul, 1982, "Robot Manipulators - Mathematics, Programming and Control", MIT Press, Cambridge, Mass.

48. G. Peggs, P. McKeown, 1989, "Creating a Standard Infrastructure for Coordinate Measurement Technology in the U.K.", Annals of CIRP, Vol. 38/1/1989.

49. Jaspal Riarh, 1994, "Inspect Your Machinee not Your Parts", Modern Machine Shop Magazine, July 1994.

50. S. Sartori, (1995), "Geometric Error Measurement and Compensation of Machines," Annals of the CIRP, Vol. 44/2.

51. Y. Shen, N. Duffie, 1991, "Uncertainties in the Acquisition and Utilization of Coordinate Frames in Manufacturing Systems", Annals of CIRP, Vol. 40/1/1991.

52. A. Slocum, 1992, "Precision Machine Design", Prentice Hall Inc.

53. A. Srivastava, S. Veldhuis, M. A. Elbestawi, 1995, "Modelling Geometric and Thermal Errors in a Five-Axes CNC Machine Tool," Int. J. Mach. Tools Manufact.

Vol. 35, No. 9.

54. Sydney Clark Jr., 1966, "Handbook of Physical Constants", Publication of the Geological Society of America.

55. Y. Takeuchi, H. Shimizu, I. Mukai, 1990, "Automatic Measurement of 3-Dimensional Coordinate Measuring Machine by Means of CAD and Image Data", Annals of CIRP, Vol. 39/1/1990.

56. Y. Tani, K. Katsuki, H. Sato, Y. Kamimura, 1995, "Development of High-Speed and High-Accuracy Straightness Measurement of a Granite Base of a CMM", Annals of CIRP, Vol. 44/1/1995.

57. J. Teeuwsen, J. Soons, P. Schellekens 1989, "A General Method for Error Description of CMMs Using Polynomial Fitting Procedures," Annals of CIRP, Vol. 38/1.

58. T. Treib, 1987, "Error Budgeting - Applied to The Calculation and Optimixation of The Volumetric Error Field of Multiaxis Systems", Annals of CIRP, Vol. 36/1/1987.

59. Stephen Veldhuis, 1998, "Modelling and Compensation of Errors in Five-Axis Machining", PhD Degree Thesis, Dept. of Mech. Eng., McMaster University, Hamilton, Ontario, Canada.

60. S. Veldhuis, and M. Elbestawi 1995, "A Strategy for the Compensation of Errors in Five-axis Machining," Annals of CIRP 44/1:373-377.

61. R. Venugopal, M. Barash, 1986, "Thermal Effect on The Accuracy of Numerically Controlled Machine Tools", Annals of CIRP, Vol. 35/1/1986.

62. W. Weekers, P. Schellekens, 1995, "Assessment of Dynamic Errors of CMMs for

Fast Probing", Annals of CIRP, Vol.44/1/1995.

63. H. Yonezawa, Y. Hirata, H. Sasai, 1990, "Positioning Table with High Accuracy and High Speed", Annals of CIRP, Vol. 39/1/1990.

64. G. Zhang, 1989, "A Study on The Abbe Priciple and Abbe Error", Annals of CIRP, Vol. 38/1/1989.

65. G. Zhang, Y. Fang, 1991, "A Method for Machine Geometry Calibration Using 1-D Ball Array", Annals of CIRP, Vol. 40/1/1991.

66. G. Zhang, R. Veale, T. Charlton, B. Borchardt, R. Hocken, 1985, "Error Compensation of Coordinate Measuring Machines", Annals of CIRP, Vol. 34/1/1985.